



2023-2 Tagungsbericht

Conference Proceedings
C1 Building Blocks for Future Chemistry

October 11 - 13, 2023 | Dresden



DGMK und Autor(en) haben alle Sorgfalt walten lassen, um vollständige und akkurate Informationen in diesem Buch zu publizieren. Der Verlag übernimmt weder Garantie noch die juristische Verantwortung oder irgendeine Haftung für die Nutzung dieser Informationen, für deren Wirtschaftlichkeit oder fehlerfreie Funktion für einen bestimmten Zweck. Die DGMK übernimmt keine Gewähr dafür, dass die beschriebenen Verfahren, Programme usw. frei von Schutzrechten Dritter sind.

Alle Rechte vorbehalten

© DGMK e.V., Hamburg, 2023

Für Copyright in Bezug auf das verwendete Bildmaterial siehe Quellenangaben in den Abbildungsunterschriften. Abbildungen ohne Quellenangabe sind von den Autoren.

Das Werk einschließlich aller seiner Teile ist urheberrechtlich geschützt. Jede Verwertung außerhalb der engen Grenzen des Urheberrechtsgesetzes ist ohne Zustimmung der DGMK unzulässig und strafbar. Das gilt insbesondere für Vervielfältigungen, Übersetzungen, Mikroverfilmungen und die Einspeicherung und Verarbeitung in elektronischen Systemen.

The work including all its parts is protected by copyright. Any use outside the narrow limits of the German Copyright Law without the consent of the DGMK is prohibited and punishable by law. This applies in particular to reproduction, translation, microfilming and storage and processing in electronic systems.

Umschlaggestaltung: DIE NEUDENKER®, Darmstadt | DGMK e.V., Hamburg

Titelfotografie: Copyright (c) 2017 Zolnierrek/Shutterstock.

ISSN 1433-9013

ISBN 978-3-947716-54-8

<https://www.dgmk.de>

C O N T E N T S	Page
A Comprehensive Strategy Towards Structure Elucidation of Hydroformylation Bottoms <i>C. Loeschel, R. Fels-Brendel, K.-H. Gunzelmann, R. Doetzer</i>	1
Optimisation of Platinum-based Catalysts for the Dehydrogenation of Perhydro Benzyltoluene as LOHC <i>E. Herzinger, D. Strauch, P. Wasserscheid, M. Wolf</i>	2
Valorisation of CO₂ from Biogas Plants: Circularity in Agro-economy <i>I. Rossetti, M. Tommasi, S. Naz Degerli, G. Ramis</i>	3
Decarbonization of Syngas and Hydrogen Production: A Zero-Carbon Puzzle? <i>M. Marchionna</i>	18
Joule-heated Structured Catalytic Reactors for CO₂ Valorization <i>L. Zheng, M. Ambrosetti, A. Beretta, G. Groppi, E. Tronconi</i>	27
Electrically Heated Reactor for Steam Methane Reforming <i>H. Malburg, M. Baumgärtl, S. Guffanti, G. Pauletto, J. Lercher</i>	28
Syngas Production from Secondary Feedstock as a Key Element for a Circular Carbon Economy– Gasification Performance Enhancement via Plasma Integration <i>A. Helf, F. Keller, M. Gräbner</i>	42
But-1-ene Hydroformylation in a Continuous Gas-phase Membrane Reactor: Road to Industrial Application <i>A. Al-Shaibani, M. Schörner, I. W. Panjikkaran, C. Nentwich, F. Weigelt, T. Brinkmann, F. Stenger, R. Franke, M. Haumann</i>	59
Continuous Processes for the Rh-catalyzed Carbonylation of Olefins and Unsaturated Esters Enabled by Cyclodextrin-mediated Aqueous Biphasic Systems <i>T. Roth, K. Künnemann, D. Vogt, T. Seidensticker</i>	60
Carbon Chain Building Reactions from Synthesis Gas to Hydrocarbons via a Three-Step Reaction Cycle with Increased Selectivity <i>J. T. Vossen, A. J. Vorholt, W. Leitner</i>	61
Continuously Operated Hydroaminomethylation in Advanced Multiphase Systems for Efficient Recycling <i>T. B. Riemer, A. Kampwerth, T. Sinnhoffer, D. Vogt, T. Seidensticker</i>	62
Co-electrolysis and its Integration into Power-to-X Concepts as a Key Step in a Renewable Energy System <i>E. Reichelt, P. Adam, R. Näke, G. Herz, S. Megel</i>	63
Combining Fischer Tropsch and Hydroformylation for Long Chain Alcohols from Syngas <i>K. Jeske, T. Rösler, M. Belleflamme, W. Leitner, A. J. Vorholt, G. Prieto</i>	74

Promotor Effect on Fe-based Catalysts for CO₂-FTS: A XAS Study <i>E. Saraçı, Q. Yang, E. Fedorova, D. Doronkin, E. Kondratenko</i>	75
Controlling the Complex Reaction Network of the Hydrogenation of CO to Higher Alcohols Using Co-based Catalysts Derived from Prussian Blue Analogues <i>P. Diehl, P. Telaar, M. Muhler</i>	76
About the Art to Prepare Mixed SAPO-CHA/MFI Catalyst Materials for Methanol-to-olefins Reaction <i>M. Seifert, L.A. Haufe, R. Shiyanova, F. Ahmadi, H. Rahimi, J.J. Weigand</i>	77
Process Intensification Strategy Demonstrated by Innovative DME Synthesis <i>M. Semmel, O. Salem, A. Schaad</i>	85
Directly Coupled Production of Methanol and Formaldehyde Based on CO₂ <i>P. Münzer, U. Arnold, J. Sauer</i>	86

Postersession

Mobile Small-Scale Methanol Synthesis Pilot-Plant with Internal Recycle Operated with CO_x from Waste Gasification	87
<i>J. Reisch, T. Nowak, M. Siodlaczek, B. Eppler, A. Drochner, B. J.M. Etzold</i>	
An In-Depth Investigation: Surprising Effect of the Second Liquid Phase in Homogeneously Ru-Catalyzed CO₂ Hydrogenation to Formic Acid	88
<i>K. R. Ehmman, K. Dinsing, C. Ribeiro Maier, A. J. Vorholt, W. Leitner</i>	
A Review of the Fischer-Tropsch and Methanol Pathways for the Production of Jet Fuel	89
<i>R. Ali, L. Edenhofer, A. Schaadt, O. Salem</i>	
Liquid-phase Co-Reagent Free Hydrogenation of Carbon Monoxide to Methanol Using Molecular Manganese Catalysts	90
<i>S. Stahl, A. J. Vorholt, W. Leitner</i>	
Biogenic Residues as Potential Feedstock for Green Energy Carriers in Urban Areas – Gasification and Synthesis Demonstration in Vienna	91
<i>T. Schubert, P. Krobath, S. Egger, M. Höller</i>	
The Influence of the Support on Pd-based Catalysts in direct DME Synthesis	102
<i>B. Wang, M. Zimmermann, S. Behrens</i>	
Multiphasic Hydroformylations of Long Chain Alkenes and the Liquid-liquid Interface	103
<i>K. E. Naße, M. Schrimpf, F. S. Heinen, N. Pawlowsky, Andreas J. Vorholt, W. Leitner</i>	
Different Exfoliation Procedure of Carbon Nitride-Based Catalysts for CO₂ Photoreduction	104
<i>I. Rossetti, Simge Naz Degerli, M. Tommasi, G. Ramis</i>	
The Change of Product Selectivity in the Electrochemical Methanol Oxidation Reaction with Decreasing Water Content in the Nafion Membrane	116
<i>S. Lechler, M. Deitermann, Z. Huang, W. Schuhmann, M. Muhler</i>	
Operando ATR-IR Assisted Mechanistic Study of the Electrocatalytic Methanol Oxidation over a Platinum Catalyst in Acidic Medium	117
<i>Z. Huang, S. Lechler, S. Cychy, M. Muhler</i>	
Improving the Selectivity to Liquefied Petroleum Gas by Combining Fischer-Tropsch Synthesis with Zeolite Cracking	118
<i>N. Oppmann, A. Jess</i>	
Development and Enhancement of Iron-Based Catalysts to Boost the Conversion of CO₂ via Fischer-Tropsch-Synthesis	119
<i>F. Mai, A. Jess</i>	
Hydrogen Production from Biomass via Formic Acid and Methyl Formate: An Economic Comparison of Different Process Routes	120
<i>F. Kroll, M. Schörner, P. Schühle</i>	

Efficient Long Distance Hydrogen Transport Including DME as Hydrogen Vector and CO₂ Back-shipment	121
<i>P. Schühle, R. Stöber, M. Semmel, A. Schaadt, R. Szolak, S. Thill, M. Alders, C. Hebling, P. Wasserscheid, O. Salem</i>	
Photo-selective Methanol Synthesis over Supported Cu Catalysts	122
<i>J. Huang, M. Klahn, J. Strunk</i>	
Fine-Tuning Texture of Highly Acidic HZSM-5 Zeolite for Efficient Ethanol Dehydration	123
<i>P. Pornsetmetakul, S. Klinyod, C. Rodaum, S. Salakhum, P. Iadrat, E. J. M. Hensen, C. Wattanakit</i>	
Photocatalytic Conversion of Methanol to Formaldehyde in a Continuous Laboratory Plant	124
<i>F. Stubenrauch, M. Schörner, Y. Mahayni, A. Bösmann, P. Schühle, P. Wasserscheid</i>	
About the Dehydrogenation of Diformamides to Diisocyanates – A Greener Pathway for the Production of Polyurethanes	125
<i>P. P. Kossmann, A. J. Vorholt, W. Leitner</i>	

A Comprehensive Strategy Towards Structure Elucidation of Hydroformylation Bottoms

C. Loeschel, R. Fels-Brendel, K.-H. Gunzelmann, R. Doetzer
BASF

Abstract

While the desired product in hydroformylation chemistry is often well defined and isolated with high specificity and yield, the byproducts formed in the oxo-process still contains a large amount of functionalized hydrocarbons with a variety of uses. These include applications as solvents in leather and textile processing, in metal processing, in industrial water treatment, and as surface tension modifiers. Due to the high complexity of these mixtures, full characterization, which is a significant hurdle for regulatory approval of such streams, presents a challenge; this challenge results in many potentially useful streams to be incinerated rather than being utilized as a product.

Herein, we present a comprehensive analytical approach to characterization of the hydroformylation bottoms of 1-octene. At its core stands the grouping of isomeric compounds into peak clusters using a combination of mass spectrometry approaches, particularly by means of combination of a soft (FI) and hard (EI) ionization technique. Separation of isomers is further achieved by comprehensive GC separations and ion mobility techniques. We also highlight the utility of field ionization over chemical ionization in the characterization of UVCB substances.

Optimisation of Platinum-based Catalysts for the Dehydrogenation of Perhydro Benzyltoluene as LOHC

E. Herzinger¹, D. Strauch^{2,3}, P. Wasserscheid^{2,3}, M. Wolf¹

¹Karlsruhe Institute of Technology (KIT), Institute of Catalysis Research and Technology (IKFT), Eggenstein-Leopoldshafen, Germany

²Forschungszentrum Jülich, Helmholtz-Institut Erlangen-Nürnberg (IEK-11), Erlangen, Germany

³Friedrich-Alexander-Universität Erlangen-Nürnberg (FAU), Lehrstuhl für Chemische Reaktionstechnik, Erlangen, Germany

Abstract

Hydrogen as an energy carrier offers many benefits for the environment, energy security, economy and end users [1]. Cost-effective, compact, safe and convenient storage of hydrogen are essential for large-scale implementation. However, the volumetric energy density of molecular hydrogen is low compared to other energy carriers [2]. One approach to address this challenge is the use of liquid organic hydrogen carriers (LOHCs) for chemical hydrogen storage. LOHCs are organic liquids that can chemically bind hydrogen in a reversible manner, which allows for long-term storage and safe transportation of hydrogen under ambient conditions [2]. Benzyltoluene/perhydro benzyltoluene (H0-BT/H12-BT) is a technical LOHC system that is thermally stable, has low toxicity, and has a wide liquid range. It has a hydrogen storage capacity of 6.2 wt.%, which is equivalent to 2.1 kWh kg⁻¹ or 1.9 kWh L⁻¹ [3]. However, to maximize the hydrogen storage capacity and the number of repeated loading and unloading cycles via catalytic hydrogenation and dehydrogenation, respectively, a superior catalyst selectivity and high conversions are of utmost importance.

In this study, the influence of promoters and the properties of the support material on the dehydrogenation activity of platinum-based catalyst systems are investigated. Therefore, bimetallic catalysts were prepared and a range of support materials was tested. The catalyst activity was mostly evaluated in semi-batch laboratory-scale dehydrogenation experiments to compare key performance indicators, such as the degree of dehydrogenation (DoDH) of perhydro benzyltoluene and the platinum-based productivity of the catalysts. Further, continuous testing in fixed-bed reactors and cyclic testing, that is consecutive hydrogenation and dehydrogenation of the LOHC, elucidated the commercial suitability of the developed catalysts.

Key results from the present study include the successful development of a bimetallic Pt-Re/Al₂O₃ catalyst and the identification of optimized support properties to prohibit pore diffusion limitation and strengthen interaction. The results indicate that the composition, structure, and morphology of the support may dictate the catalyst activity. Lastly, the new catalyst design was transferred to the preparation using shaped carrier pellets for bridging the gap between laboratory research and catalytic application in large-scale fixed-bed reactors for efficient H₂ release from perhydro benzyltoluene.

References

[1] J.O. Abe, A.P.I. Popoola, E. Ajenifuja, O.M. Popoola, *Int. J. Hydrog. Energy* **44** (2019) 15072.

[2] P. Preuster, C. Papp and P. Wasserscheid, *Acc. Chem. Res.* **50** (2017) 74.

[3] T. Rüde, S. Dürr, P. Preuster, M. Wolf, P. Wasserscheid, *Sustain. Energy Fuels* **6** (2022) 1541.

Valorisation of CO₂ from Biogas Plants: Circularity in Agro-economy

Ilenia Rossetti¹, Matteo Tommasi¹, Simge Naz Degerli¹, Gianguido Ramis²

¹Chemical Plants and Industrial Chemistry Group, Dip. Chimica, Università degli Studi di Milano, CNR-SCITEC and INSTM Unit Milano-Università, Milan, Italy; ² Dip. Ing. Chimica, Civile ed Ambientale, Università degli Studi di Genova and INSTM Unit Genova, Genoa, Italy

Abstract

As methane has been establishing as a primary energy source, to obtain it from renewable carbon feedstock rather than to extract it as natural gas is by far more appealing: biomass-generated methane is an efficient power generation mean with a virtually closed CO₂ cycle, accompanying the transition towards a zero-carbon energy future. Biogas however contains large amounts of CO₂, to be at least separated to exploit biomethane, and possibly valorised. A first option is CO₂ hydrogenation to methane, also promising to transform an energy vector that is uneasy to handle (green H₂) into a valuable and worldwide-distributed fuel and feedstock (CH₄). A “power-to-gas” framework could then help to overcome the drawbacks of H₂ as an energy storage medium and to increase the continuity and general availability of different intermittent renewable energy sources. This flexibility offers also additional possibilities for the downstream use of biogas, which may be richer in hydrogen or methane according to the process operation, even if these conditions might not fit the distribution networks nearer to the biomass-treating site.

Different options for the efficient direct conversion of CO₂ and H₂ into CH₄ (Sabatier reaction) are here explored through process design and briefly summarised. A key issue is the strong exothermicity of the reaction. Our research explores the use of water vapour, added on purpose to the reactor as a thermal vector and later condensed. The simplest reactor arrangement is composed of a certain number of adiabatic beds (up to five) with intercooling. Some options propose cooled stages, but they are more complex and likely expensive. Alternatives may be fluidized-bed reactors that allow better temperature control, but they lead to incomplete conversion and are more difficult to scale-up. The possibility to use the methane already present in biogas as diluent (i.e. thermal vector to control the exothermicity) is also considered, offering the additional advantage to eliminate the otherwise needed and expensive CO₂ capture step.

Introduction

Biogas is a type of renewable product that is produced through anaerobic digestion. It is generated by the decomposition of organic matter, such as animal waste, food scraps, agricultural residues and sewage. During anaerobic digestion, bacteria break down the organic matter in the absence of oxygen, resulting in the production of biogas. In addition, the anaerobic digestion process also results in the production of a nutrient-rich residue called digestate, which can be used as fertilizer. This makes this process very attractive to convert agricultural residua or zootechnical wastes, to recover circularly both the gaseous biofuel and the fertiliser.

The primary component of biogas is methane, in a concentration between 50 and 80%, which can be valorised energetically through combustion. However, biogas also contains other gases: mainly carbon dioxide, but also few % of nitrogen, ammonia, hydrogen sulfide. Methane in biogas can be purified by removal of other components either by scrubbing or adsorption

(e.g. by pressure swing adsorption, PSA). Biogas purification is an important step in the production of biomethane. One approach is through biological biogas purification technologies. Biofiltration systems, for example, can efficiently remove gases like H₂S, NH₃ and VOCs from biogas. Suitable feedstock and process optimization in anaerobic digestion can also significantly reduce biogas impurities [1].

Another method used for biomethane purification is PSA. This technology selectively removes CO₂ from biogas using adsorbents. PSA offers advantages such as low energy requirements, low cost and safe operation. Alternatively, water scrubbing, membrane separation, cryogenic processes, chemical absorption can be considered [2,3].

Global biogas production in 2020 had an equivalent energy content of 1.46 EJ. This indicates a significant increase in biogas production since 2000 when the total biogas production was equivalent to 0.29 EJ [4].

Specifically, in Italy the production is estimated to reach 10 billion m³ by 2030. The presence of more than 500 plants is reported, with a current capacity of 250,000 m³/h and an annual production of 1.5 billion m³ of biomethane [5,6].

Therefore, if on one hand biogas must be upgraded to be effectively exploited as a fuel, on the other hand this offers a range of opportunities to valorise its main impurity, i.e. CO₂. In this work we examine, from a conceptual design point of view, a route for the valorisation of CO₂ from biogas in form of upgraded biomethane.

Models and methods

The basic design of plant was carried out with Aspen Plus[®] V12 and Aspen Adsorption[®] by Aspen Technology Inc. (Bedford, MA, US). Vapour Liquid Equilibria were treated by the Redlich-Kwong equation of state (EOS) or the PSRK model, depending on the blocks considered and selected after validation of experimental data, while the ENRTL model has been used instead of the NRTL one to compute the activity coefficients due to the possible existence of dissolved electrolytes. Gases dissolved in liquid phase were computed through the Henry equation.

For the CO₂ methanation reaction, according to the literature, it was divided into two steps [7–10]:



or treated with the lumped stoichiometry:



The following kinetics has been adapted to simulate the methanation packed bed reactor, as better detailed elsewhere [10]:

$$r_{\chi < 0.1} = 3550 \left[\frac{\text{mol/s}}{\text{kg} \times \text{kPa}^{0.88}} \right] e^{-7950 \text{ K}/T} \left(\frac{P_{\text{CO}_2}^{0.34} P_{\text{H}_2}^{0.88}}{P_{\text{CH}_4}^{0.11} P_{\text{H}_2\text{O}}^{0.23}} \right) \quad (4)$$

$$r_{\chi > 0.1} = 11.2 \left[\frac{\text{mol/s}}{\text{kg} \times \text{bar}^{1.5}} \right] e^{-2490 \text{ K}/T} \left(P_{\text{CO}_2}^{0.3} P_{\text{H}_2}^{1.2} - \frac{1}{K} P_{\text{CH}_4}^{0.3} P_{\text{H}_2\text{O}}^{0.6} \right) \quad (5)$$

The steady-state mass and energy balances for the 1-D reacting system yielded:

$$0 = -u' \frac{\partial n_i}{\partial z} + r v_i \left[\frac{\text{mol/s}}{\text{kg}} \right] \quad (6)$$

$$0 = -u'' \frac{\partial h}{\partial z} + r \Delta h \left[\frac{\text{J/s}}{\text{kg}} \right] - U(T_r - T_c) \quad (7)$$

where n are the moles of the i -th species, r is the reaction rate based on the catalyst load, v_i the stoichiometric coefficients and u' is the local molar flow expressed as a function of the molar flowrate at the reactor inlet \dot{n} and the actual concentration at the reactor conditions $C(P,T)$, hydraulic section A and catalysts load w , h represents the molar specific enthalpy and u'' is calculated as detailed in the cited reference. T_r, T_c are the reactants and coolant temperatures and U the overall heat transfer coefficient. The momentum balance is also included in the calculations.

The reactor was designed with a multistage configuration to allow efficient heat removal and so enhancing the yield for this highly exothermal reaction. Two different strategies were also considered to slow down the reaction for a better thermal control, in particular steam addition [10], which thermodynamically unfavours the reaction, and the direct methanation of biogas (purified from S- and N-containing compounds).

Figure 1 exemplifies one of the plant layouts tested. Different options including preliminary CO₂ separation or direct feed of biogas to the methanator were tested.

For operating conditions leading to incomplete CO₂ conversion, a separation unit was conceived including a carbonate based scrubbing to eliminate residual CO₂ and a PSA unit containing zeolites to dehydrate the upgraded biomethane before injection into the grid or supply to the dealer.

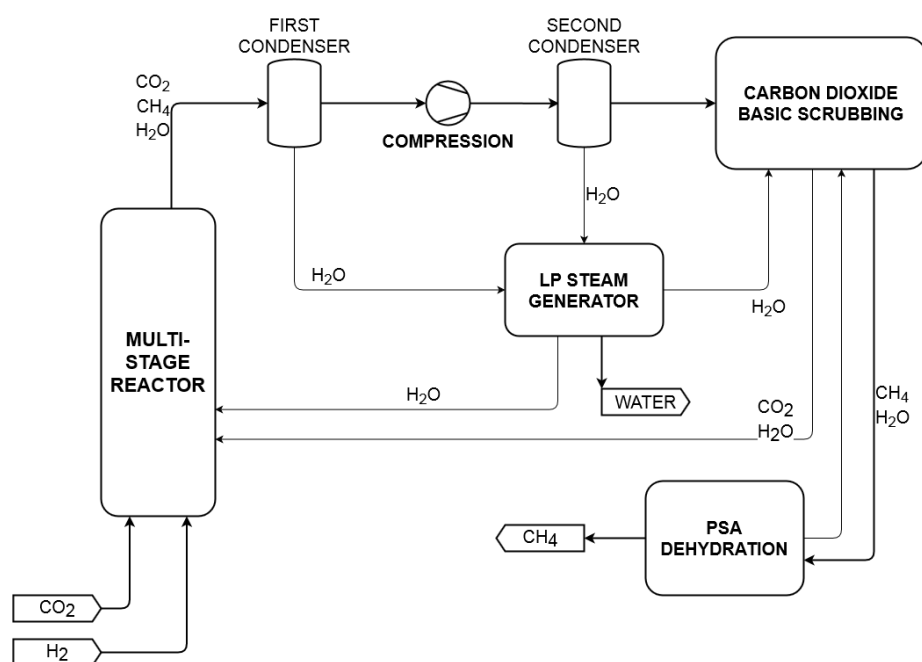
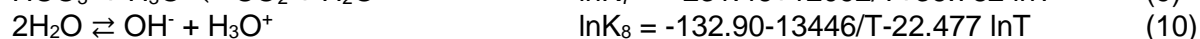
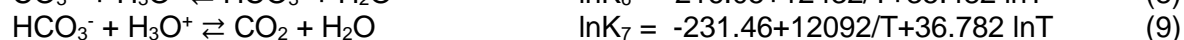


Figure 1: Scheme of the methanation process. Reproduced from [10] in the frame of CC-BY 4.0 open access licence by ACS.

The carbonate/bicarbonate equilibria in water were considered as follows:



The Henry constants for CO₂ and CH₄ in presence of the electrolytes have been reviewed [11,12] and corrected if necessary based on the validation with experimental data. Gas solubility changes when a dissolved salt is present and a variation of the ionic strength of the solution is expected which affects the activity coefficients. The amount of unreacted H₂

remaining in the biomethane stream has been also calculated [10,13].

Gas solubility in water has been considered in the 15-20 atm pressure interval, while CH₄ and H₂O adsorption was considered over different zeolites and modelled according to the Langmuir isotherm at 20°C and 25°C:

$$w_{CH_4} \left[\frac{kmol}{kg} \right] = \frac{0.001 \left[\frac{kmol/kg}{bar} \right] P_{CH_4}}{1 + 2.2 \left[\frac{kmol/kg}{bar} \right] P_{CH_4}} \quad (11)$$

$$w_{H_2O} \left[\frac{kmol}{kg} \right] = \frac{3.5 \left[\frac{kmol/kg}{bar} \right] P_{H_2O}}{1 + 2500 \left[\frac{kmol/kg}{bar} \right] P_{H_2O}} \quad (12)$$

Results and discussion

Selected results are discussed for the sake of brevity.

In order to study the effect of different parameters (pressure, temperature, feed composition) on the CO₂ conversion, the methanation reaction has been simulated in Aspen Plus using a Gibbs reactor that simulates a situation in which equilibrium conditions are achieved.

In this simulation a sensitivity analysis of the parameters was performed from 150 to 500 °C and from 1 to 20 atm at different CO₂ / H₂ / H₂O molar ratios.

Examples of results are plotted in Figures 2 and 3. As expected conversion decreases with temperature and increases with pressure. The presence of steam also unfavours the reaction from a thermodynamic point of view.

Water and methane can be considered viable tools to control the exothermicity of the reactor, though decreasing the achievable conversion. Water removal has a positive effect on CO₂ conversion, because for each pressure and fractional conversion considered, the conversion remains in a higher range of values referred to the same conditions with the presence of water. Another effect of the removal is that higher temperatures in the Gibbs reactor were required to achieve the same conversions, this is good, from a thermodynamic point of view, because the temperature needs to be less tightly controlled.

Similar considerations are done also in case of CH₄ addition to the reactor, which limits the conversion, but opens the way to the direct use of biogas without the preliminary CO₂ separation step, provided that the conversion penalty and consequent resizing of the reactor are economically feasible.

By implementing the reaction kinetics in a plug flow reactor block, different trials have been done to identify the best configuration of a multitube system with 4 blocks that allow intercooling and water discharge as additional option. After optimal sizing each of them the following results have been achieved (Table 1 and Figure 4).

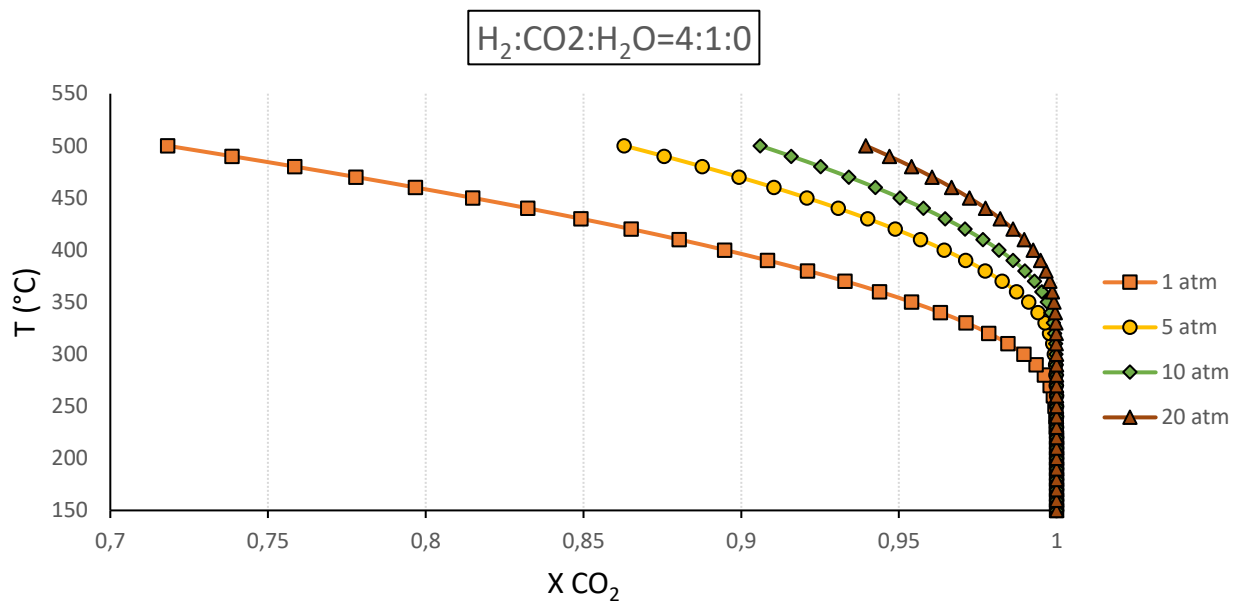


Figure 2: Equilibrium CO_2 conversion at different pressure, temperature and with a feed composition $H_2 : CO_2 = 4:1$ (mol/mol)

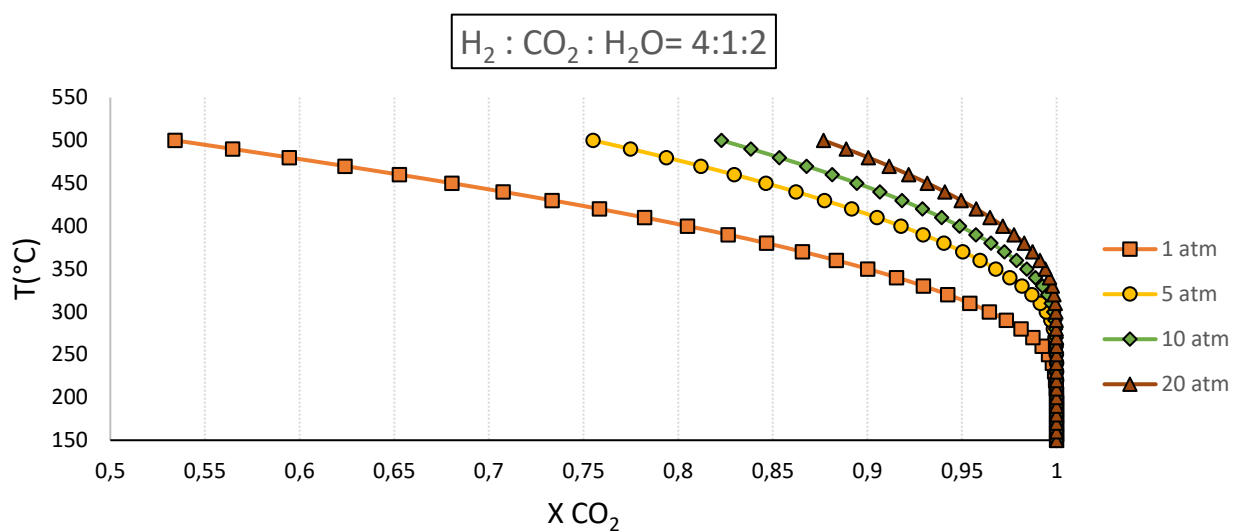


Figure 3: Equilibrium CO_2 conversion at different pressure, temperature and with a feed composition $H_2:CO_2:H_2O = 4:1:2$ (mol/mol)

Table 1: Methanation reactors final specifications.

<i>Reactors specification</i>	<i>MET1</i>	<i>MET2</i>	<i>MET3</i>	<i>MET4</i>
Catalyst [kg]	7800	7800	7800	5000
Particle diameter [mm]	3	3	3	3
Shape factor	0,8	0,8	0,8	0,8
U [$W/m^2 K$]	300	300	300	300

The conversion achieved per pass, calculated on the CO₂ amount present in the fresh feed and the working temperature range of each reactor stage is reported in Figure 4, where the corresponding Gibbs reactors are also depicted. The four stages are able to almost fully convert CO₂ with optimum selectivity to methane.

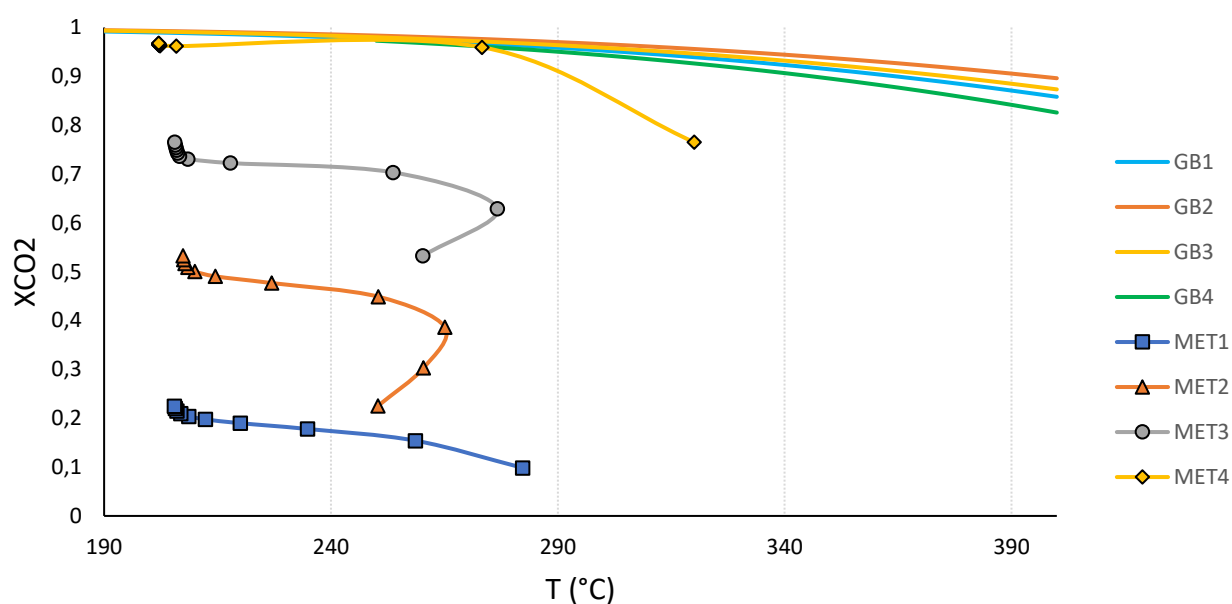


Figure 4: CO₂ conversion per pass calculated on the CO₂ amount in the fresh feed and the equilibrium curve per pass.

The scheme of the full plant for the methanation of CO₂ is represented in Figure 5 [10]. It includes a multi-tubular Plug-Flow Reactor where the product is cooled after each stage and the shell is also cooled with the fresh feed. This configuration saves 340 kW_{th} per ton of fresh CO₂ with respect to a simpler layout of adiabatic beds with intercooling, tested as a first alternative.

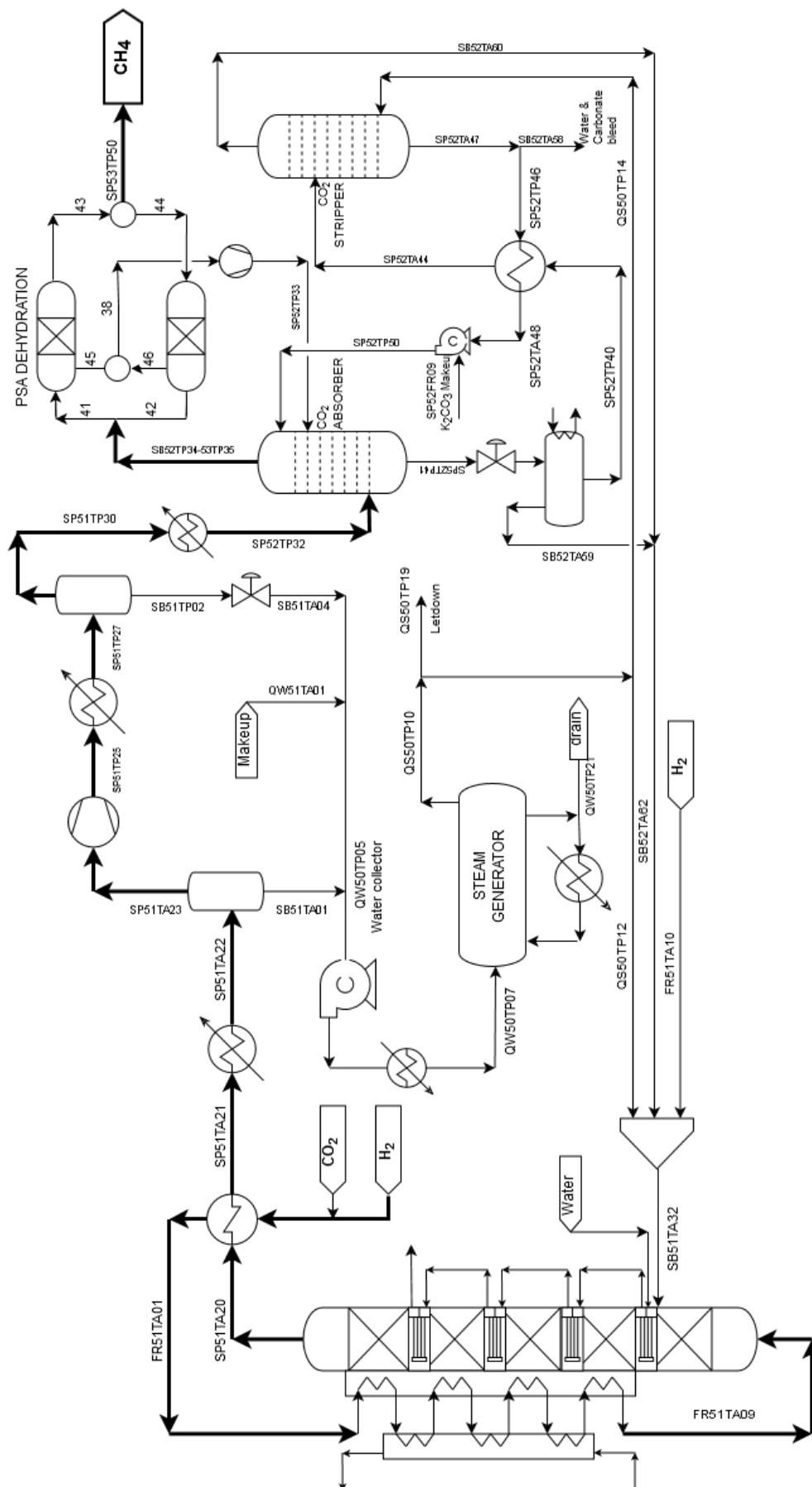


Figure 5: Scheme of the CO₂ methanation plant. Reproduced from [10] thanks to CC-BY 4.0 open access licence by ACS.

In order to meet the specifications for biomethane injection into the natural gas grid, local purity settings are differently indicated. Typically, a CH₄ minimum concentration of 96% is prescribed, but deviations may occur in countries that specifically favour biomethane usage. For instance the Netherlands let biomethane with methane content only 85 % be injected, but Switzerland and Sweden require 96 % and 97 % of methane content [14]. The allowed CO₂ content admitted in pipelines is usually of the order of 2 mol%. The maximum allowed water content in natural gas is stated in the national gas quality regulations as 200 mg/m³ at low-pressure (< 10 bar) and as 50 mg/m³ in high-pressure pipelines (> 10 bar). In order to achieve these values multiple flash and a PSA column were designed in the present flowsheet.

Five steps of water removal were simulated with dedicated flash units. The stream exiting from each reactor was cooled to 80 °C and sent to a flash block that was specified, every time, with pressure of 5 atm and duty of 0 cal/sec. The fourth step was followed by another flash, in which the pressure was raised to 10 atm and the separation was made at 30 °C. In this way, the water contained in the produced gas was reduced from 9 % to 0.4%.

To further purify the stream, a PSA unit was designed considering Zeolite 13 X as adsorbent, selected after comparison with different materials [15,16].

The general PSA scheme, simulated in Aspen Adsorption, is shown in Figures 6-9. As an attempt, hydrogen was used as purge gas to recover all the purged stream in the methanator.

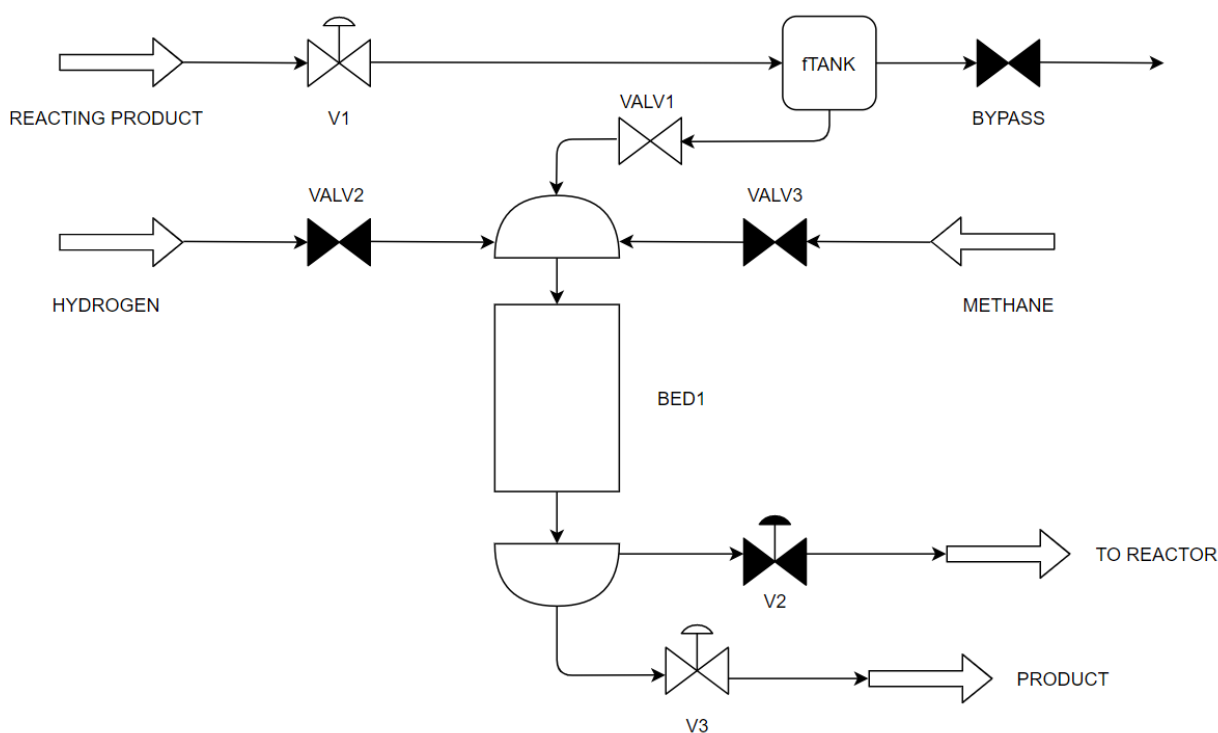


Figure 6: The scheme shows the PSA during the working step, the white valves are open, and the black ones are closed. The valve V1 controls the flowrate of the reacting product sent to the PSA.

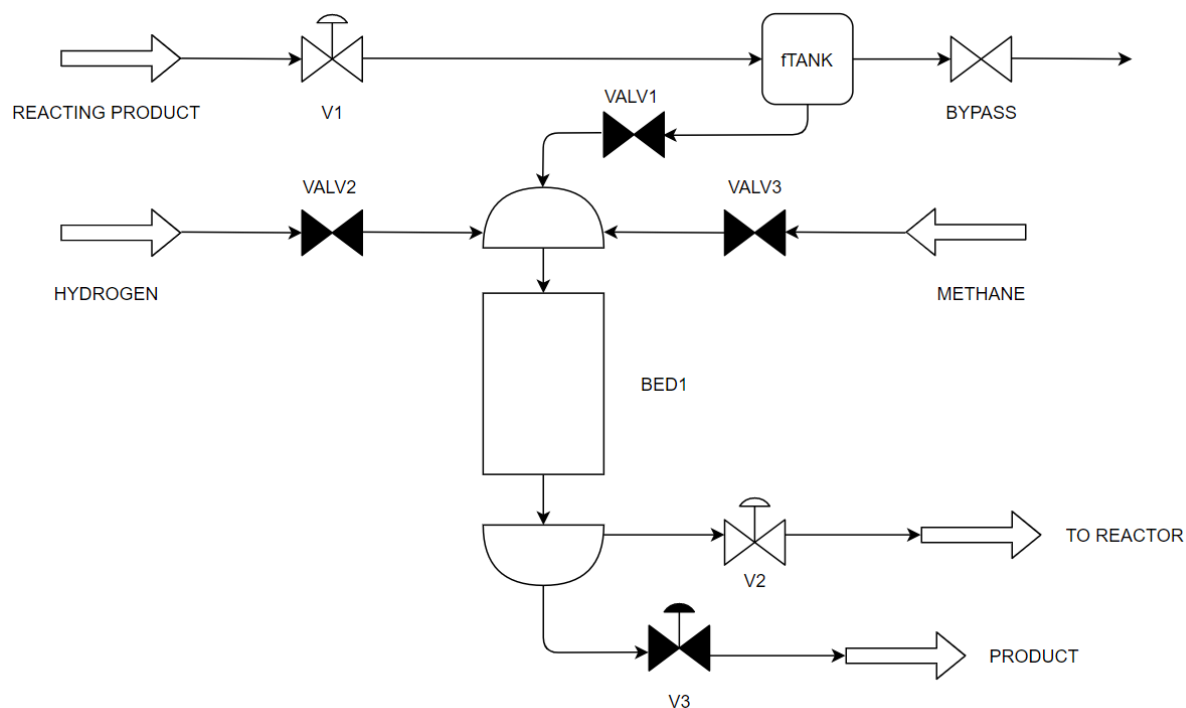


Figure 7: Discharge step. The valve V3 is closed, but as the flow from valve V1 does not stop, the bypass valve is opened to avoid flooding of the column. Also, the V2 is opened at this point, it maintains pressure greater than 9 bar. The valve that leads the reacting product to the BED1 is closed.

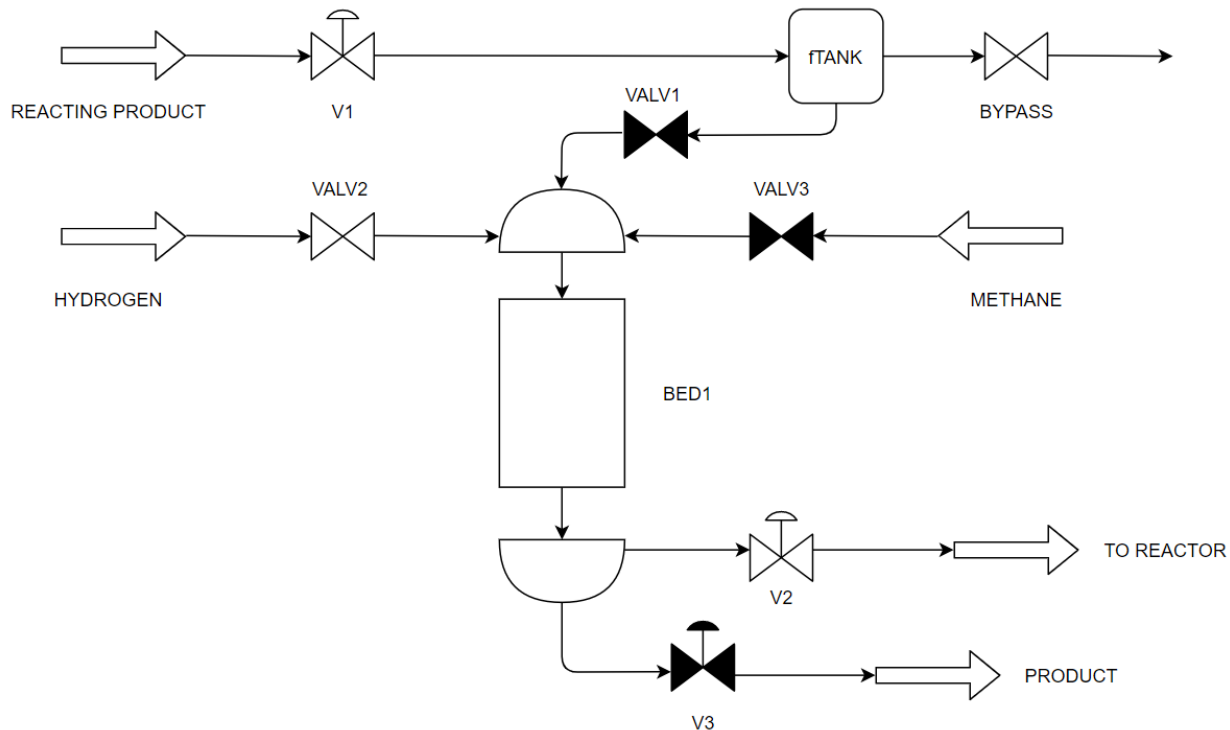


Figure 8: Purge step; the valve of hydrogen is opened, in order to clear the bed.

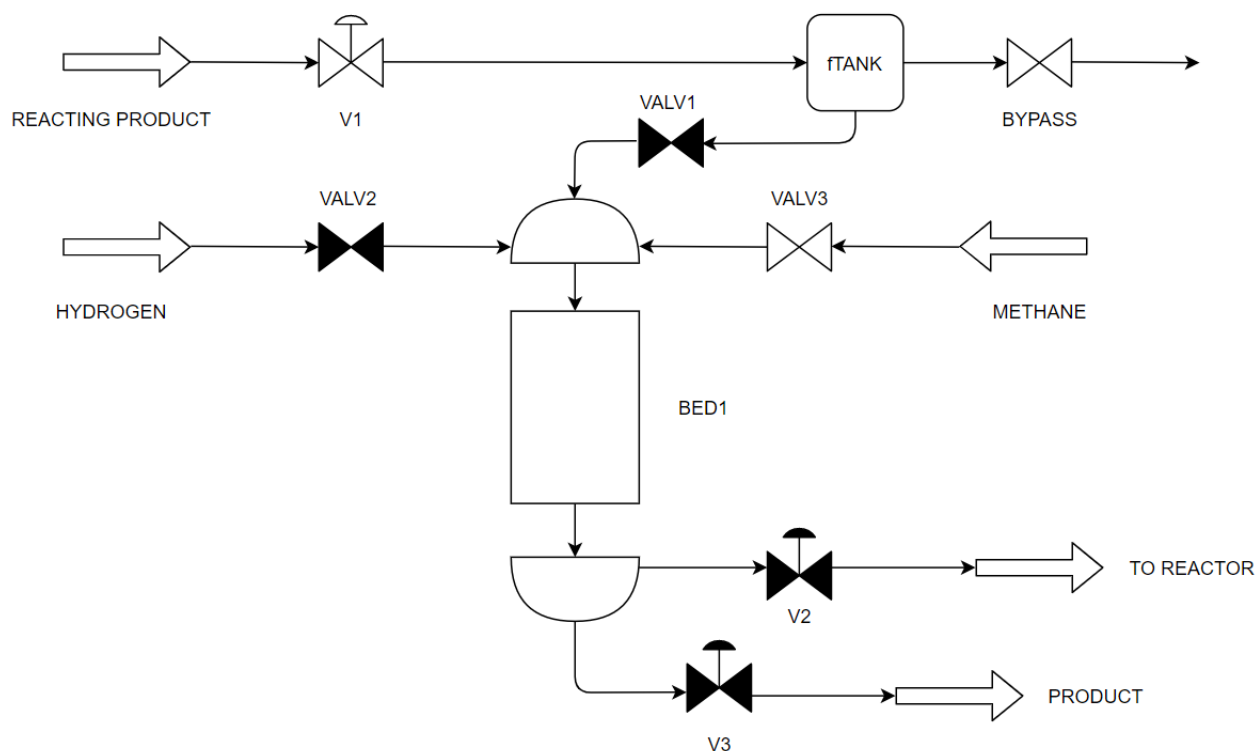


Figure 9: The reload step; the bed is pressurized again with methane.

The adsorption parameters were calculated for the different species through the fitting of the equilibrium adsorption isotherms retrieved from the literature for Zeolite 13 X, as exemplified in Figures 10-12.

Then, the results were used in the Langmuir-Freundlich model. This isotherm is a function of temperature and of the partial pressure or concentration as in Eq. 13:

$$\omega_i = \frac{IP_1IP_2P_i^{IP_3}e^{IP_4/T_8}}{1+IP_5P_i^{IP_3}e^{IP_6/T_8}} \quad (13)$$

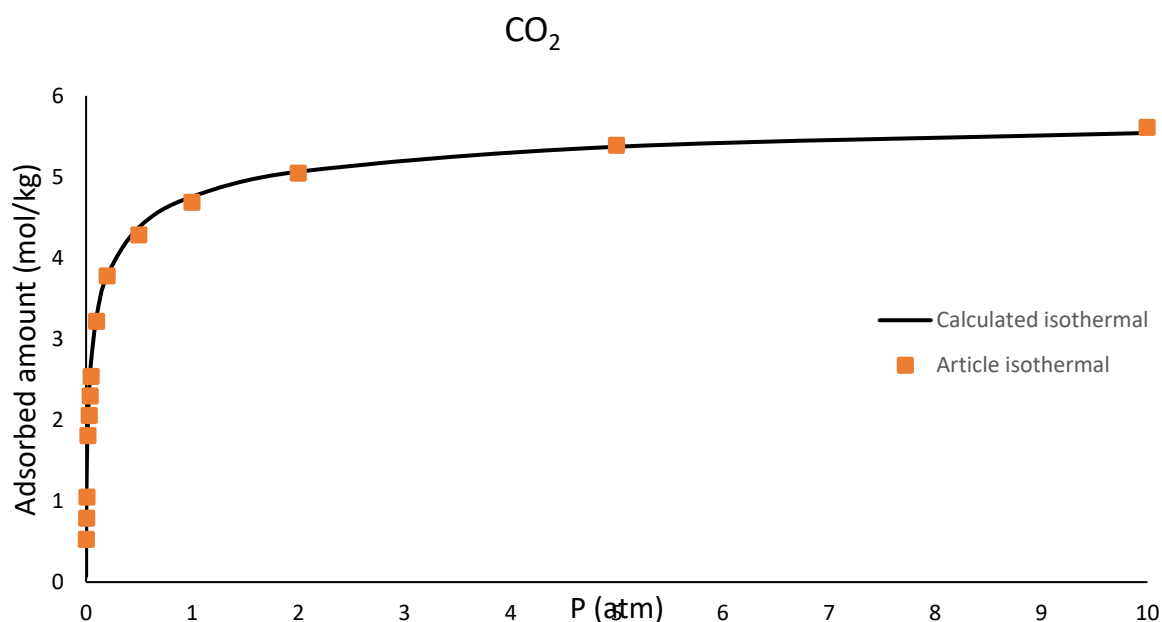


Figure 10: Adsorption isotherm for CO₂ on zeolite 13 X, reproducing literature data [17], at a

temperature of 293 K.

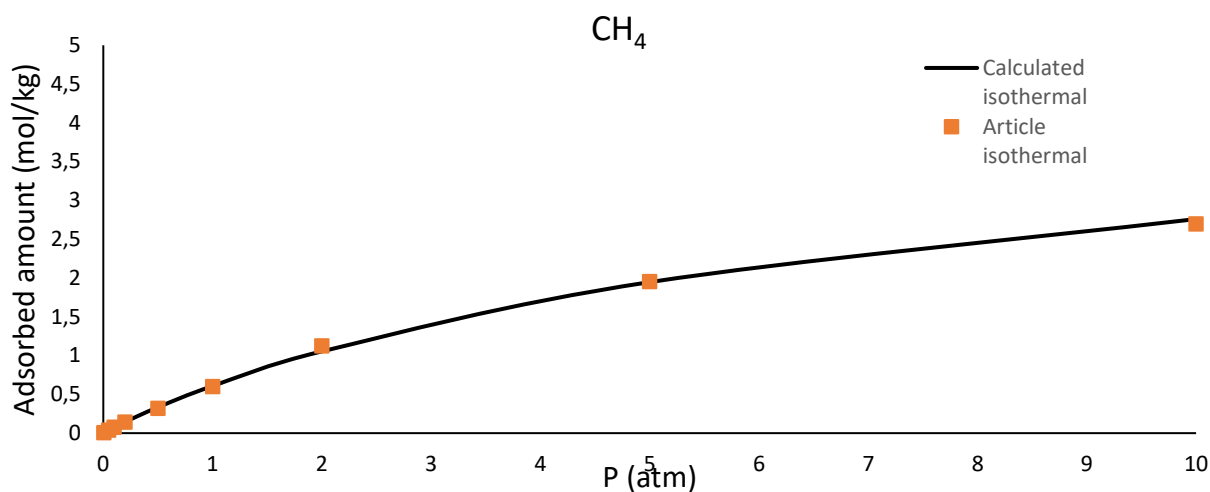


Figure 11: Adsorption isotherm for CH_4 on zeolite 13 X, reproducing the literature data [17], at a temperature of 293 K.

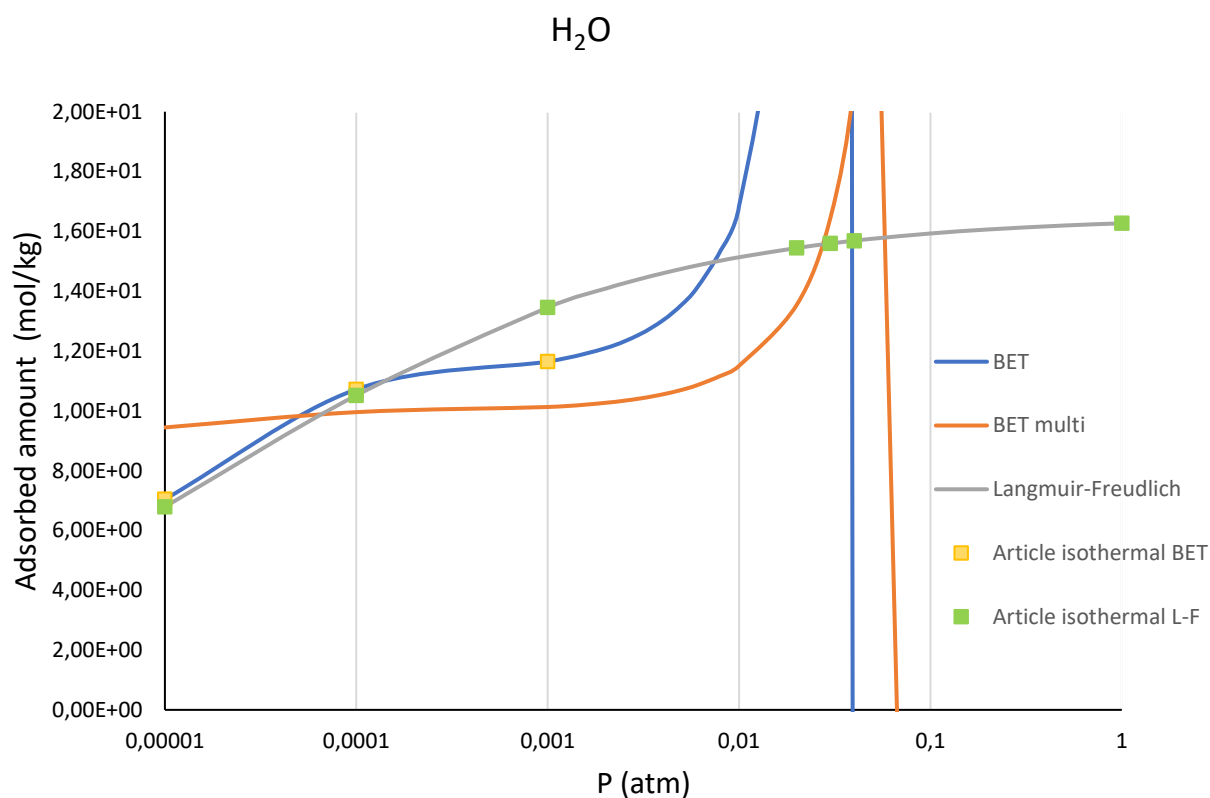


Figure 12: Adsorption isotherms for H_2O on zeolite 13 X, reproducing literature data [16], at a temperature of 293 K. Interpolation with different models.

The columns characteristics are reported in the following Table 2, while Table 3 collects the parameters of the isotherms to be used for columns modelling.

Table 2: Main features of the PSA adsorption columns.

Column height [m]	1.5
Column diameter [m]	0.5
Bed porosity ε_i [m^3void/m^3bed]	0.5
Solid density [kg/m^3]	1300
Particle radius [m]	0.02

Table 3: Langmuir-Freundlich adsorption isotherm fitted parameters of CO₂, H₂, H₂O and CH₄ for Zeolite 13X, at the pressure of 10 bar.

Species	IP₁	IP₂	IP₃	IP₄	IP₅	IP₆
CH₄	0.005	1.5E-4	0.95	2000	1.5E-4	2000
CO₂	0.006	0.0035	0.5	2050	0.0035	2050
H₂	0.0071	1E-4	1	1000	1E-4	1000
H₂O	0.0165	0.0025	0.4	3000	0.0025	3000

The gas stream exiting from the last flash block and feeding the PSA unit is reported in Table 4.

Table 4: Steams specifications entering the PSA unit.

Species	Mole Flows [mol/min]	Molar Fractions	Total Flows [mol/min]	Temperature [°C]	Pressure [atm]
CH₄	2579	0.85	3026	30	10
CO₂	85	0.028			
H₂	348	0.115			
H₂O	14	0.0046			

The PSA has been designed for 1/2 of the feed to avoid too high pressure drops and too large beds. In the real design two PSA modules are envisaged working in parallel. The working bed works for 1/3 (600 s) of the total cycle time (1800 s).

The product obtained from this PSA was composed as in Table 5.

Table 5: Steams specifications exiting the PSA unit and after the cryogenic separation.

<i>Species</i>	<i>Molar fractions</i>	
<i>CH₄</i>	0.88	
<i>CO₂</i>	4.2E-4	
<i>H₂</i>	0.12	
<i>H₂O</i>	1.58E-4	

<i>After cryogenic separation</i>		
<i>Species</i>	<i>Mole flows [kmol/hr]</i>	<i>Mole fractions</i>
<i>CH₄</i>	120.0	0.99
<i>CO₂</i>	0.068	0.00056
<i>H₂</i>	0.038	0.0003
<i>H₂O</i>	0.035	0.0002

As it can be seen, the amount of water in the product respected the fixed standards so the aim of this work was achieved. Also, the CO₂ in the product was well within the specifications, thanks to the high adsorption capacity of the selected zeolites. The main problem lies in the amount of H₂, which accounted for the 12% of our product, while its content could not exceed given limits, broadly varying for national regulations, in average 5% [18].

To bring the hydrogen value below 5% within the product, a cryogenic separation was developed as a first option. From the CH₄ phase diagram, it could be seen that the temperature had to decrease to around -160 °C to have a suitable separation at 1 bar. The specifications for composition of the biomethane produced are also reported in the bottom of Table 5. This fits the most restrictive regulations.

As an alternative, in order to avoid the presence of excessive residual hydrogen, the 3rd and 4th stages of the reactor have been redesigned to improve conversion and the final product specifications were as in Table 6, which were compliant with the conditions for grid injection also regarding hydrogen in the case of 5% limit, without the need of a cryogenic unit. Final economic assessment will identify the most economic option between resizing the reactor or adding a further separator for H₂.

Table 6: Steams specifications exiting the PSA unit with optimised reactors configuration.

<i>Species</i>	<i>Mole flows [kmol/h]</i>	<i>Mole fractions</i>
<i>CH₄</i>	134.06	0.96
<i>CO₂</i>	0.15	0.0010
<i>H₂</i>	5.08	0.036
<i>H₂O</i>	0.0038	2.7e-5

Conclusions

In this work different layouts of a CO₂ methanation plant using green hydrogen were set up and compared. Biogas was the source and the methanator was fed either with previously separated CO₂ or with direct injection of biogas purified from S. and N- containing compounds. After retrieval and validation against experimental data of the pertinent kinetic and thermodynamic models, a reactor design based on four catalytic layers was conceived, comparing a simpler adiabatic multibed system with intercooling, with a more complex but efficient configuration in which cooling and water separation are achieved between all the beds and a multitubular layout is used, to allow cooling with the fresh feed. In both configurations a CO₂ conversion of 99.9% was obtained.

Biomethane purification was accomplished discarding most water through cooling and flash separation and a final PSA stage. Finally, the water content in the product was $3 \cdot 10^{-5}$ g/g, H_2 was reduced below 5% and CO_2 was well below the admissible concentration.

Acknowledgements

I. Rossetti gratefully acknowledges the financial contribution of Fondazione Cariplo through the grant 2021-0855 – “SCORE - Solar Energy for Circular CO_2 Photoconversion and Chemicals Regeneration”, funded in the frame of the Circular Economy call 2021.

This study was carried out within the Agritech National Research Center and received funding from the European Union Next-GenerationEU (PIANO NAZIONALE DI RIPRESA E RESILIENZA (PNRR) – MISSIONE 4 COMPONENTE 2, INVESTIMENTO 1.4 – D.D. 1032 17/06/2022, CN00000022). This manuscript reflects only the authors' views and opinions, neither the European Union nor the European Commission can be considered responsible for them. I. Rossetti and M. Tommasi acknowledge specifically the participation and funding of Tasks 8.2.3, 8.3.2 and 8.4.1.

I. Rossetti acknowledges Università degli Studi di Milano for support through the grant PSR 2021 - GSA - Linea 6 “One Health Action Hub: University Task Force for the resilience of territorial ecosystems”.

References

- [1] J. Das, H. Ravishankar, P.N.L. Lens, Biological biogas purification: Recent developments, challenges and future prospects, *J. Environ. Manage.* 304 (2022) 114198. <https://doi.org/10.1016/j.jenvman.2021.114198>.
- [2] N. Chouikhi, F. Brandani, P. Pullumbi, P. Perre, F. Puel, Biomethane production by adsorption technology: new cycle development, adsorbent selection and process optimization, *Adsorption*. 26 (2020) 1275–1289. <https://doi.org/10.1007/s10450-020-00250-3>.
- [3] D. Haldar, N. Bhattacharjee, A.M. Shabbirahmed, G.S. Anisha, A.K. Patel, J.-S. Chang, C.-D. Dong, R.R. Singhanian, Purification of biogas for methane enrichment using biomass-based adsorbents: A review, *Biomass and Bioenergy*. 173 (2023) 106804. <https://doi.org/10.1016/j.biombioe.2023.106804>.
- [4] <https://www.iea.org/reports/renewables-2021/biofuels?mode=transport®ion=World&publication=2021&flow=Consumption&product=Ethanol>, (n.d.).
- [5] <https://www.biogasworld.com/news/development-biomethane-italy-present-situation-prospects/>, (n.d.).
- [6] M. Gustafsson, S. Anderberg, Biogas policies and production development in Europe: a comparative analysis of eight countries, *Biofuels*. 13 (2022) 931–944. <https://doi.org/10.1080/17597269.2022.2034380>.
- [7] M.S. Duyar, A. Ramachandran, C. Wang, R.J. Farrauto, Kinetics of CO_2 methanation over $Ru/\gamma-Al_2O_3$ and implications for renewable energy storage applications, *J. CO₂ Util.* 12 (2015) 27–33. <https://doi.org/10.1016/j.jcou.2015.10.003>.
- [8] K.P. Brooks, J. Hu, H. Zhu, R.J. Kee, Methanation of carbon dioxide by hydrogen reduction using the Sabatier process in microchannel reactors, *Chem. Eng. Sci.* 62 (2007) 1161–1170. <https://doi.org/10.1016/j.ces.2006.11.020>.
- [9] K. Ghaib, K. Nitz, F.-Z. Ben-Fares, Chemical Methanation of CO_2 : A Review, *ChemBioEng Rev.* 3 (2016) 266–275. <https://doi.org/10.1002/cben.201600022>.
- [10] A. Tripodi, F. Conte, I. Rossetti, Carbon Dioxide Methanation: Design of a Fully Integrated Plant, *Energy & Fuels*. 34 (2020) 7242–7256. <https://doi.org/10.1021/acs.energyfuels.0c00580>.
- [11] Á. Pérez-Salado Kamps, E. Meyer, B. Rumpf, G. Maurer, Solubility of CO_2 in Aqueous Solutions of KCl and in Aqueous Solutions of K_2CO_3 , *J. Chem. Eng. Data*. 52 (2007) 817–832. <https://doi.org/10.1021/je060430q>.
- [12] R.K. Stoessell, P.A. Byrne, Salting-out of methane in single-salt solutions at 25°C and

- below 800 psia, *Geochim. Cosmochim. Acta.* 46 (1982) 1327–1332.
[https://doi.org/10.1016/0016-7037\(82\)90268-X](https://doi.org/10.1016/0016-7037(82)90268-X).
- [13] H. Sagara, Y. Arai, S. Saito, Vapor-liquid equilibria of binary and ternary systems containing hydrogen and light hydrocarbons, *J. Chem. Eng. Japan.* 5 (1972) 339–348.
<https://doi.org/10.1252/jcej.5.339>.
- [14] J. Savickis, L. Zemite, N. Zeltins, I. Bode, L. Jansons, E. Dzelzitis, A. Kuposovs, A. Selickis, A. Ansons, The biomethane injection into the natural gas networks: The EU's gas synergy path, *Latv. J. Phys. Tech. Sci.* 57 (2020) 34–50.
<https://doi.org/10.2478/lpts-2020-0020>.
- [15] J.A. Delgado, V.I. Águeda, M.A. Uguina, J.L. Sotelo, P. Brea, A. Carlos, C.A. Grande, Adsorption and diffusion of H₂, CO, CH₄, and CO₂ in BPL activated carbon and 13X zeolite: Evaluation of performance in pressure swing adsorption hydrogen purification by simulation, *Ind. Eng. Chem. Res.* 53 (2014) 15414–15426.
<https://doi.org/10.1021/ie403744u>.
- [16] K.N. Son, T.M.J. Richardson, G.E. Cmarik, Equilibrium Adsorption Isotherms for H₂ O on Zeolite 13X, *J. Chem. Eng. Data.* 64 (2019) 1063–1071.
<https://doi.org/10.1021/acs.jced.8b00961>.
- [17] Y. Park, Y. Ju, D. Park, C.H. Lee, Adsorption equilibria and kinetics of six pure gases on pelletized zeolite 13X up to 1.0 MPa: CO₂, CO, N₂, CH₄, Ar and H₂, *Chem. Eng. J.* 292 (2016) 348–365. <https://doi.org/10.1016/j.cej.2016.02.046>.
- [18] <https://www.iea.org/data-and-statistics/charts/current-limits-on-hydrogen-blending-in-natural-gas-networks-and-gas-demand-per-capita-in-selected-locations>, (n.d.).

Decarbonization of Syngas and Hydrogen Production: A Zero-Carbon Puzzle?

M. Marchionna

Saipem SpA, Milano, Italy

Abstract

Hydrogen is currently used as an intermediate product in the chemical (mainly ammonia and methanol) and refining industries. It is produced mostly from Natural Gas in large scale plants using Steam Methane Reforming, a very mature technology. Hydrogen produced from Natural Gas has a high carbon footprint, considering that about 6-9 tons of CO₂ are co-produced (and emitted to the atmosphere) per ton of produced hydrogen, depending on Natural Gas composition. For this reason, Hydrogen produced from fossil fuels is nowadays named as “Grey” Hydrogen. The current production of Hydrogen is responsible of about 2.5% of CO₂ emissions worldwide.

For Hydrogen remaining in business, and then becoming a factor in the energy transition period and later, decarbonizing its production is a must.

Partially decarbonized hydrogen produced from fossil fuels, through CO₂ Capture, is named “Blue” Hydrogen. A completely different path is followed for the production of fully decarbonized, or “Green” Hydrogen. This path is already commercially available, though on a smaller scale than required for wide industrial application. It is the electrolysis of water, i.e. the use of electric power from renewable sources to break the water molecule into its constituent Hydrogen and Oxygen.

Pros & Cons of these two options will be critically examined with also some look to the application of Hydrogen in the so-called “Hard to Abate” sector.

Introduction

Synthesis Gas can be produced from many sources, including natural gas, coal, biomass, or virtually any hydrocarbon feedstock, by reaction with steam and oxygen. This versatility made it as one of the most attractive building blocks for different industries (petrochemistry, refinery, natural gas conversion, power, alternative sources exploitation) and, as shown in Figure 1, many different products are industrially produced through this building block [1].

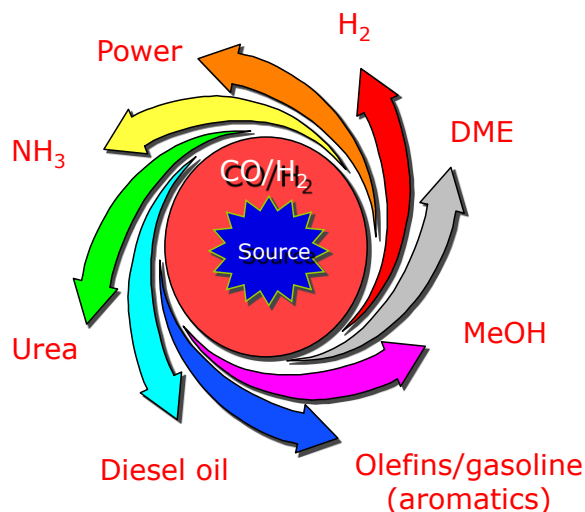


Fig. 1: Synthesis Gas to products

However, in the energy transition context, decarbonization of its production is now a must, considering the relevant impact on the related CO₂ emissions. In this article, and in this respect, attention is mostly paid to hydrogen production, maybe the most important intermediate, considering also the related production of ammonia and methanol, and their derivatives.

Hydrogen today

Though hydrogen is the most abundant element in the universe, mostly it does not exist naturally on our planet. Hydrogen cannot therefore be considered as an energy source, but as an energy vector that must be produced from an energy source.

Today hydrogen is used as a chemical intermediate in the production of chemicals (mainly ammonia and methanol) and in oil refining processes [2]. Fossil fuels (natural gas, but also coal and oil) are the sources for producing hydrogen, mostly via Steam Methane Reforming (SMR), a very mature technology, in production lines with capacity of 50,000-150,000 Nm³/hr of hydrogen [3]. As a consequence, the production of hydrogen is associated to a high carbon footprint. About 6-9 tons of CO₂ are co-produced (and emitted to the atmosphere) per ton of produced hydrogen when Natural Gas is used as the raw material. For this reason, hydrogen produced from fossil fuels is named as “grey” hydrogen (even “black” when coal is the raw material – in this case the carbon footprint increases to about 20 tons per ton of hydrogen [4]. The production of hydrogen is responsible of about 2.5% of CO₂ emissions worldwide (almost 1 billion tons of CO₂ yearly [5]). For hydrogen remaining in business, even before becoming a positive factor in the energy transition period and later, decarbonizing its production is a must.

The two largest uses are bulk chemicals production such as ammonia, mostly for the fertilizer market, or methanol production, mostly an intermediate for the chemical industry and fossil fuel processing (e.g., hydrotreating/hydrocracking), as shown in Fig.2 [6].

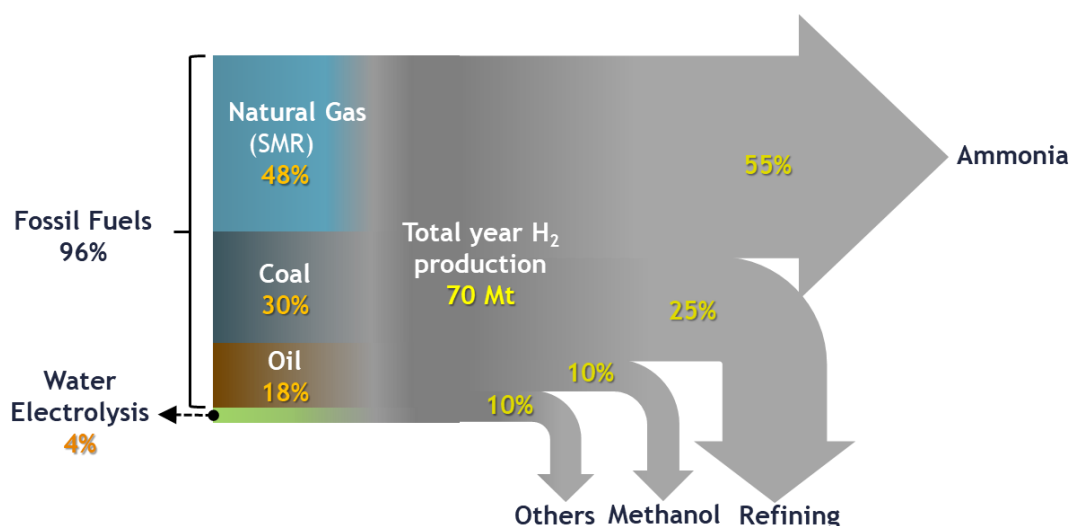


Fig. 2: Hydrogen from Renewable Power Technology (Outlook for the energy transition September 2018; IEA 2019 The Future of Hydrogen)

Most hydrogen is used near the site of its production, and as it is produced, is consumed without intermediated operation of storage; furthermore, these productions besides being characterized by very high scale are also characterized by a high operational continuity (more than 8000 h/y), this means that decarbonizing any of these uses should take into account all these aspects.

Blue Hydrogen

Partially decarbonized hydrogen produced from fossil fuels is named “blue” hydrogen. Of course, hydrogen will be “blue” if captured CO₂ is either geologically stored or sustainably used. The deployment of blue hydrogen will therefore proceed in parallel to the development of the infrastructure needed for Carbon Capture, Storage and Utilization (CCUS).

More specifically, three main criteria have to be followed for the Blue Hydrogen option:

- Availability of affordable or cheap gas
- Existing pipeline infrastructure
- CO₂ sequestration potential (its absence could limit this option, although CO₂ reuse could be another possibility)

A few geographical areas are particularly suited for this scope: US, Canada, North Sea, Middle East, Russia, Australia, ...

On the other side, this option is well suited for retrofitting operations and displays a good synergy when CO₂ is requested as a co-reactant such as in the production of fertilizers (urea) or of methanol.

Capturing about 90% CO₂ from the steam reformer effluent at the current scale of deployment is already done today in some petrochemical plants and refineries [7-8], particularly in urea production schemes where captured CO₂ is used to increase the production rate. Mature technologies, based on selective absorption of CO₂ in aqueous solutions of amines, are used to this purpose [9].

Considering blue hydrogen, the current scale of production would remain the same also in the possible extension of its use to other sectors. For instance, simple calculations show that a world scale steel mill will need about 50000 Nm³/h of hydrogen. SMR plants may be equipped with carbon capture facilities, also as a retrofit of existing units, and the required scale is commercially available and industrially referenced.

The production of blue hydrogen entails proper management of captured CO₂. CO₂ must be transported to a storage site for geological storage. An infrastructure for pipeline transportation of CO₂ is today existing only in specific areas (e.g. Texas), while geological storage, though considered as a key element of every decarbonization strategy, is still far from a widespread acceptance, particularly in onshore locations. A quick development is however expected in Northern Europe, where Norway, The Netherlands and UK are preparing the infrastructure for transporting CO₂ from industrial sites north of the Alpes for storage in offshore reservoirs in the North Sea. The development of blue hydrogen projects must go in parallel to this infrastructural development. As an alternative, captured CO₂ could be sustainably re-used. Sustainable re-use however means that the products obtained from CO₂ should not generate new CO₂ when used, unless carbon is of biogenic origin. This is a strong limitation to all plans of CO₂ utilization, since the range of durable products obtainable from CO₂ is quite limited (plastics, construction materials) [10].

Green Hydrogen

A completely different path is followed for the production of fully decarbonized, or “green” hydrogen. This path is already commercially available, though on a smaller scale than required for wide industrial application. It is the electrolysis of water, i.e. the use of electric power from renewable sources to break the water molecule into its base element hydrogen and oxygen [11].

Water electrolysis is a modular technology; current standard modules have a capacity of about 1 MW, i.e. each module accepts an electric input of 1 MW, producing about 200 Nm³/hr of hydrogen, with a transformation efficiency of 70-75%. This means that about 500 modules in parallel would be needed to produce 100,000 Nm³/h of hydrogen.

Taking into account the typical utilization factors of renewable energy, the continued production of 100,000 Nm³/hr of green hydrogen would need dedicated parks of:

- about 2000 MW for solar photovoltaic (25% utilization factor considered);
- about 1000 MW for wind (50% utilization factor considered).

However, water electrolysis is much behind SMR in the maturity curve, so that substantial improvements are expected in the next decade of technology development. The achievement of a transformation efficiency of 80-85% [12], as well as the increase in size of the standard modules up to 10 MW [13], are feasible targets of ongoing activity in a 2030 scenario.

Emerging technologies such as Solid Oxide Electrolyzers will improve the efficiency (up to +20%) which is essential considering the strong impact of electrolyser power consumption in the overall green hydrogen/ammonia scheme.

One peculiar feature of the electrolysis of water, often very neglected, is the co-production of pure oxygen. For a hydrogen production of 100,000 Nm³/h, 50,000 Nm³/h of oxygen are co-produced. Considering the current market value of oxygen, the co-production of green oxygen may improve the economics of water electrolysis plants to an extent which may be negligible today but might give a decisive push to green hydrogen vs. blue in a 2030 prospect. In a 2050 scenario, water electrolysis may even become the preferred way for the production of oxygen, “greening” also this energy intensive industrial sector.

Low Carbon Ammonia and recent related projects

Ammonia is one of the most important chemicals (one of the top-five mostly produced while methanol is the tenth of this special ranking [14], for its use as feedstock in the fertilizer industry; it is produced in many countries and traded across the world. The current production of ammonia is energy-intensive, and it is responsible for more than 1% of the global carbon dioxide and overall Green House Gases, considering that for each ton of ammonia nearly 2 tons of CO₂ are generated. It is therefore imperative to change to a more sustainable way to produce ammonia to replace grey ammonia and provide a sustainable alternative to ensure world's food production.

Clean ammonia is expected to become a solution to tackle the climate change also in other ways: ammonia could be also an attractive molecule for transportation of hydrogen and thus energy. Already relatively simple infrastructure for ammonia liquefaction, storage and shipping exists making ammonia the perfect choice for H₂ transportation. In addition to the use of ammonia as hydrogen carrier, which is expected to be widely developed in the short term, the use of ammonia as direct fuel (for example for marine engines and for electric power generation) may unlock further potential of clean ammonia market [15].

Amongst different ways to produce clean ammonia, the so-called blue ammonia, which is based on reforming of natural gas coupled with carbon capture and storage, offers immediate advantages since it is based on the process schemes already adopted by the current industry and minimizes the cost especially in areas where it is possible to safely store CO₂.

Blue ammonia concept is based on the well-consolidated process scheme for production of ammonia which expands the CO₂ capture already included in the syngas purification to the full Carbon Capture Utilization and Storage (CCUS) value chain. The concept is essentially made of end-of-pipe blocks that do not affect the main process; however, minor adjustments may be required to improve the CO₂ capture rate. Despite the lack of a standard, it is generally recognized as a “blue” concept if most of the CO₂ (typically > 80%) is captured.

The main project, Saipem is recently carrying over together Horisont Energi, is the Barents Blue Ammonia Project characterized by very high carbon capture rate target, high degree of modularization, winterization, infrastructure for ammonia and CO₂ management and provision for future expansion. Actually, Horisont Energi is planning to develop a large-scale blue ammonia complex in Finnmark, Norway, exploiting the favorable combination of feedstock gas

availability, cold climate conditions which allow higher process efficiency, and proximity to offshore CO₂ storage [16].

The Barents Blue Ammonia Project represent a milestone in the large-scale low carbon ammonia production industry, the first world scale blue ammonia plant in Europe, a reference for the optimized solutions identified to address the many challenges posed by the stringent requirements.

The integration of the utilities with the ammonia plant, and in particular the optimization of the steam and power network, is a key element in the design of the overall complex.

Barents Blue Ammonia Project captures and permanently stores approximately 2 million tons per annum of CO₂ per each ammonia train, which corresponds to the CO₂ emissions generated from more than 400.000 cars.

It is possible to achieve 99% CO₂ capture target with proper design (Fig. 3) aimed at minimizing the CO₂ emissions taking into consideration the whole life of the project.

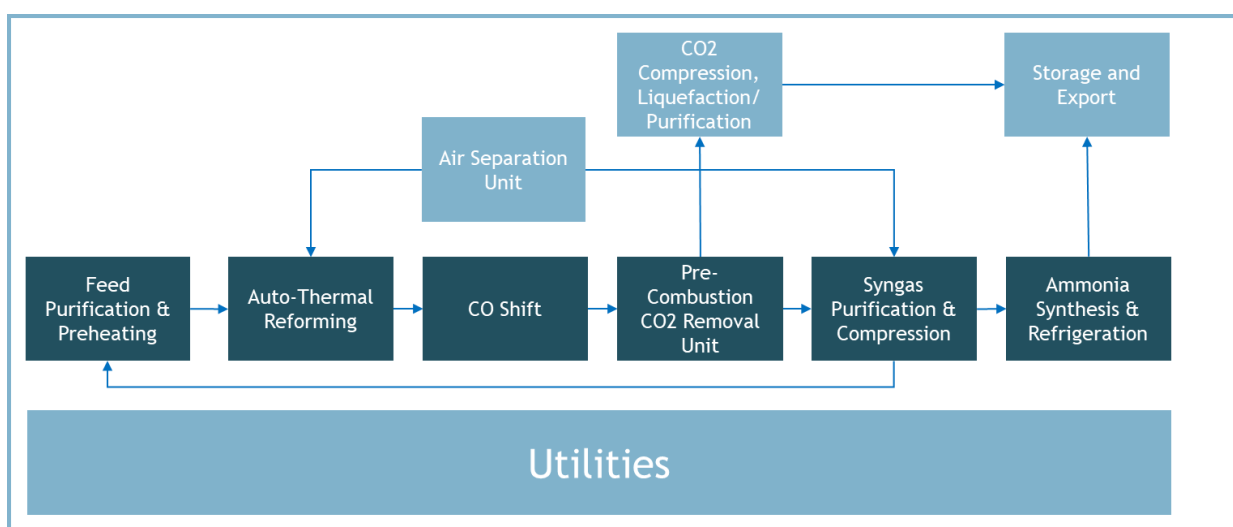


Fig. 3: Barents Blue Ammonia Plant scheme

As regards Green Ammonia, derived by Green Hydrogen, several case studies have been developed by Saipem for hybridization/stand-alone ammonia plant and ammonia-urea complexes for undisclosed Clients (Fig.4).

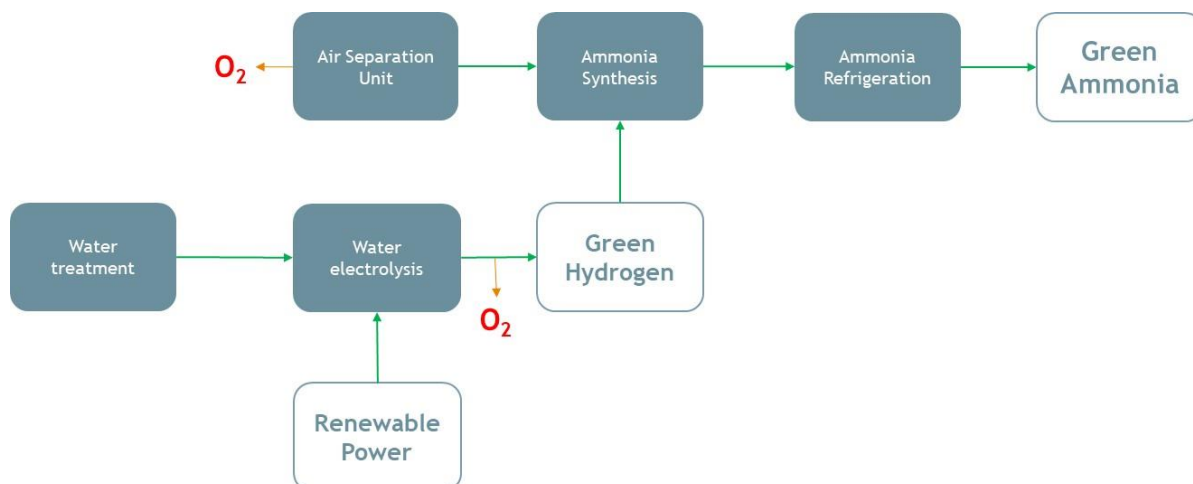


Fig. 4: Green Ammonia Plant scheme

Each studies included a business model for hydrogen production cost estimation ($\pm 40\%$). The capacity of the PV plant has been optimized through a business model in order to have the minimum value of the cost of hydrogen (LCOH), i.e. a ratio 1,75 :1 between the PV plant peak capacity and the capacity of the electrolysis plant, and a LCOH = 8,8 €/kgH₂ has been carried out.

The installation areas are particularly significant; for example, a PV plant of 140 MWp corresponds notably to 160 ha of soil occupied, and additional areas are to be booked for electrolysers and storage, although definitely lower with respect to the PV plants.

Futhermore, Saipem and Alboran have collaborated since 2021 to develop green hydrogen initiatives in the Mediterranean region, focusing also on a green ammonia plant in Morocco. A large scale electrolyzer plant (450 MW) fed by renewable plants (wind farm with a total power of about 1000 MW) has been engineered to produce green hydrogen and oxygen; the produced hydrogen is converted into 1000 TPD green ammonia that will be transferred to the potential off-taker and final user.

A few considerations for “Low Carbon” Hydrogen to Chemicals (including Refinery)

Both Green and Blue Hydrogen have the potential for gradually replacing grey hydrogen in current uses, to achieve decarbonization of the whole hydrogen sector, although the use of non-dedicated renewable energy sources will be limited to very small capacities.

In the short term, when possible, the Blue Hydrogen option will be the easiest applicable, especially for large scale productions.

In the mid term, Green Hydrogen could be more competitive in terms of production cost with Grey H₂ and may be produced at scale closer to that of fossil Hydrogen, provided that electricity produced from dedicated renewable parks located in favorable geographic areas is available at production cost.

Co-production of pure Oxygen can contribute to the deployment of Green Hydrogen and, in the long run, water electrolysis might become the main production route of pure oxygen.

However, the goal of a total decarbonization of the sector does not present an easy and immediate solution and the related “zero-carbon puzzle” is still far to be completely solved.

Otherwise, in perspective, the use of “low-carbon” hydrogen might not be limited only to the current use of chemical intermediate but could be advantageously extended well beside the current perimeter to “Hard to Abate” sectors.

Extending the use of hydrogen: from Chemicals to “Hard to Abate” sector

Enlarging the landscape to the overall energy transition frame, not the power sector only is involved in this process, for sure it is the main actor being responsible for about 40% of the anthropic CO₂ emissions, but the industrial sector is sufficiently close with 25-30% of the emissions.

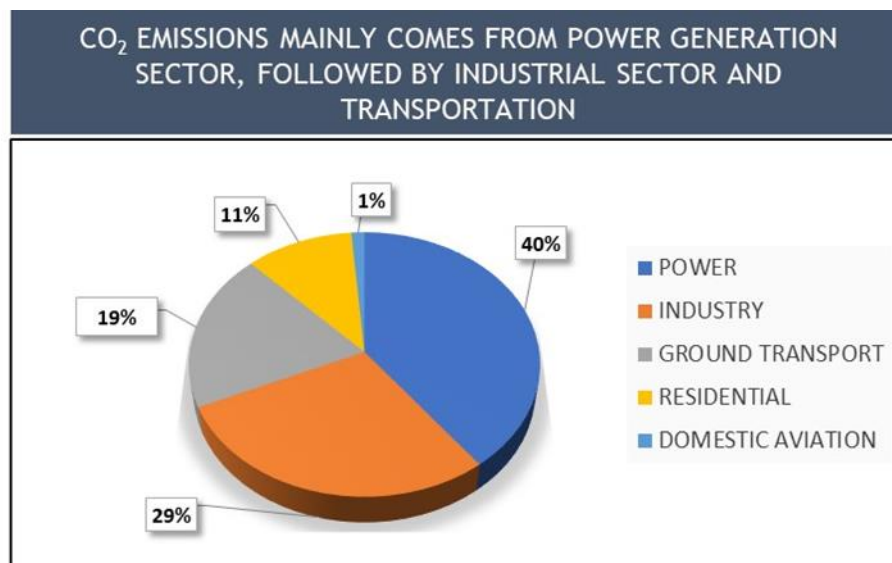


Fig. 5: Anthropogenic CO₂ emissions

While there are several alternatives for decarbonizing power production (renewables first), much more complex is the situation with regard to the so-called hard-to-abate industry, which is responsible for the main fraction of the industrial sector. By hard-to-abate we refer both to Oil & Gas industries, such as refinery and petrochemicals, and to very intensive industries such as steel, cement, paper mills, metal production (especially aluminum), ceramics, glass, waste treatment, etc.

Indeed, these industries are energy-intensive (often requiring very high temperatures) and may have carbon at the very core of their product. The reference is mainly to the petrochemical and steel industries, but CO₂ also plays an important role in the cement production cycle (although in a negative direction). Therefore, our goal – by no means trivial – is twofold: on the one hand, we have to achieve total efficiency in order to manage only the residual carbon in the product, and, on the other, we have to avoid using it to generate the energy required for the process. We are just in front of a very challenging 'zero-carbon puzzle'.

The following Figure 6 [17-18] provides us a more quantitative idea of the related impact for the different industries. Indeed, the chemical industry ranks as the largest industrial energy consumer even if it is just the third largest industry subsector in terms of direct CO₂ emissions just because a substantial portion of the carbon (and the energy) of the feedstock remains locked into its products. Thus, the CO₂ emissions of the overall chemical industry are lower than it may be expected from its energy demand. Hydrogen, ammonia, methanol (all described before in the article) and light olefins are responsible of the majority of the sector's CO₂ emissions.

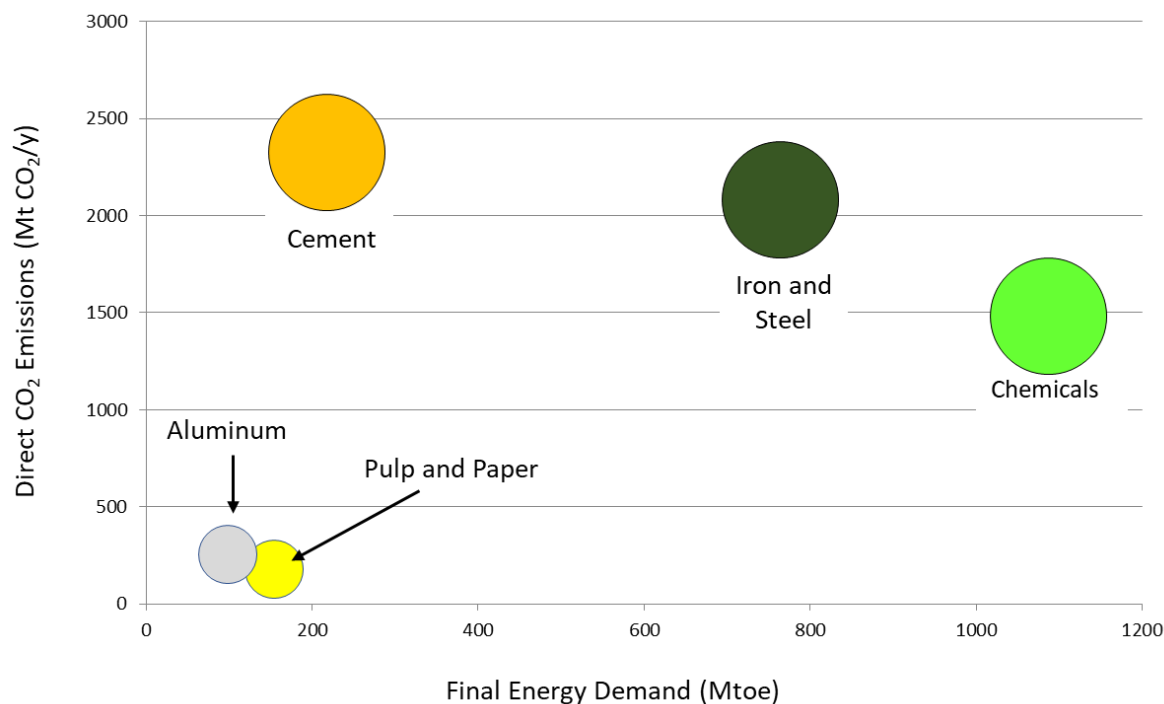


Fig. 6: Energy demand and CO₂ emissions for different industrial productions ([17, there adapted from [18]). Mtoe (Million Tonnes of Oil Equivalent).

The same rationale is in part applicable also to steel while the reverse happens for cement industry due to the net production of CO₂ by decomposition of calcium carbonate,

Focusing a bit more on the steel industrial sector, responsible for the emission of 2.6 billion tons of CO₂ per year (8% of world emissions and 1/4th of industrial emissions), it might need just hydrogen for its decarbonization [19].

The most advanced steel producers are targeting carbon neutrality of their production by 2050. Their selected decarbonization path involves replacement of coal in the reduction step of iron ores with green or blue hydrogen coupled to the use of an electric furnace for the melt. Hydrogen may consequently contribute to about at least 30% of the decarbonization of steel production (0.8 billion tons of CO₂), while direct renewable power and, when possible, carbon capture would do the remaining. If this has to become the standard route for production of steel, each mill will need deployment of a green (or blue) hydrogen plant with typical size in the 10,000-50,000 Nm³/hr, which can be a good intermediate scale in view of the 100,000 Nm³/hr, thus opening a novel attractive market for hydrogen.

References

- 1) Marchionna M., *Oil & Gas Eur. Mag.*, 2016, (2), 101.
- 2) Brown A., *Uses of Hydrogen in Industry. Chem. Eng.* 2019, 937.
- 3) Twigg M.W.; Dupont V., *Advances in Hydrogen Production, Storage and Distribution*; Woodhead Publishing: Cambridge, 2014.
- 4) Burmistrz P.; Chmielniak T.; Czepinski L.; Garda-Grzywacz M., *J. Clean. Prod.* 2016, **139**, 858.
- 5) *The Future of Hydrogen*, Report prepared by the Int. Energy Agency for the G20, 2019.
- 6) Iijima M., Takahiko E., Daisuke S., *CO₂ Capture Technology for mitigating Global Warming and Climate Change. Mitsubishi Heavy Ind. Tech. Rev.* 2010, (47), 37.
- 7) Rock L., O'Brien S., Tessarolo S., Duer J., Oropeza Bacci V., Hirst B., Randell D., Helmy M., Blackmore J., Duong C., Halladay A., Smith N., Dixit T., Kassam S., Yaychuk M., *The Quest CCS Project: 1st year review post start of injection. Energy Procedia* 2017, 114, 5320.

- 8) Roussanaly S., Anantharaman R., Fu C., Low Carbon Footprint Hydrogen Production from Natural Gas: A Techno-Economic Analysis of Carbon Capture and Storage from Steam Methane Reforming. *Che. Eng. Trans.* 2020, (81), 1015.
- 9) CO₂ Pipeline Infrastructure. Report by International Energy Agency, 2014.
- 10) Perego, C., *La Chimica & l'Industria*, 2022 (1), 50.
- 11) Millet P., Grigoryev, S., Water Electrolysis Technologies. Renewable Hydrogen Technologies; Elsevier: Amsterdam, 2013.
- 12) Schmidt O., Gambhir A., Staffell I., Hawkes A., Nelson J., Few S., *Int. J. Hydrog. Energy*, 2017, (42), 30470.
- 13) Bailey M.P., *Chem. Eng.*, 2020, Apr. 15th
- 14) Danner J., *Common Science*, 2016, Mar. 6. (<https://chapelboro.com/town-square/columns/common-science/the-highest-volume-chemical-produced-in-the-world-is>)
- 15) Tullo A., *Chemical & Engineering News*, 2021, March 8, 20.
- 16) Haukelldsaeter Eidesen E., Zambianco A., Sala M., *Nitrogen+Syngas*, 2023, **364**, 43.
- 17) Perego C., Ricci M. *La Chimica & l'Industria*, 2023 (1), 14.
- 18) Holmes K. J., Zeitler E., Kerxhalli-Kleinfield M., DeBoer R., *Earth's Future*, 2021, (11), 9.
- 19) Peplow P., *Chemical & Engineering News*, 2021, June 14, 22.

Joule-heated Structured Catalytic Reactors for CO₂ Valorization

L. Zheng, M. Ambrosetti, A. Beretta, G. Groppi and E. Tronconi

Laboratory of Catalysis and Catalytic Processes, Politecnico di Milano, Italy

Abstract

The growing environmental concerns have driven the catalytic CO₂ valorization as a forward-looking solution to mitigate the carbon footprint of valuable chemical products. Processes for CO₂ conversion into synthesis gas, such as CO₂ reforming of methane or reverse water-gas shift, may have a strategic role for the future sustainable production of chemicals and energy carriers. However, fuel combustion to supply the heat of the associated endothermic reactions would result in unwanted CO₂ emissions, which strongly reduce the CO₂ valorization potential. Electrification of the endothermic processes may represent the technological solution to such an issue [1].

Here we report a promising approach for the direct electrification of both the CO₂ reforming of methane (eCRM) and the reverse water-gas shift (eRWGS) processes in washcoated structured reactors. Similar to a concept recently demonstrated for electrified stema reforming of methane [2], we employ catalytically activated open-cell foams that provide optimal heat and mass transfer properties as catalyst substrates and simultaneously serve as Joule heating elements for the catalytic conversion of CO₂ via its reaction with methane or hydrogen.

With the proposed system utilizing Joule-heated Rh/Al₂O₃-coated SiSiC foam, CO₂ conversions approaching equilibrium were measured across a wide range of conditions for both eCRM and eRWGS. We further show that such a new reactor concept ensures remarkably low specific energy demand for CO₂ valorization, reaching approx. 0.7 kWh/Nm³CO₂ for eRWGS in an optimized process configuration, assuming an overall adiabaticity of 95% and a recovery of 90% sensible heat. If the feed H₂ is sourced from water electrolysis (3.8 kWh/Nm³H₂) [3], it is possible to achieve an overall specific energy consumption of 4.5 kWh/Nm³CO₂ for CO₂ valorization,

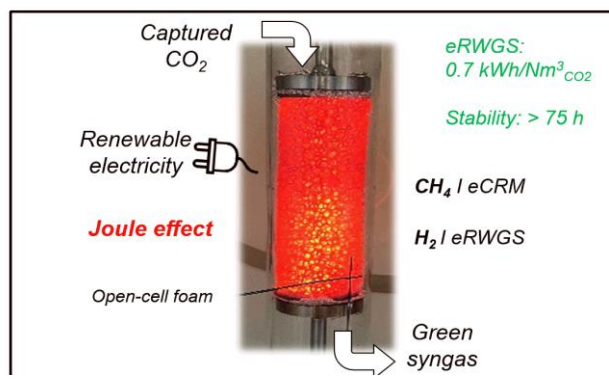


Figure 1. Joule-heated structured catalytic reactor.

which is lower compared to solid oxide electrolyzers for CO₂ reduction to CO (6-8 kWh/Nm³CO₂, [3]). Furthermore, the system demonstrated excellent catalytic and electrical stability for over 75 hours.

By replacing fuel combustion with Joule heating driven by renewable electricity, the electrified CO₂ valorization processes provide an important approach for dealing with the intermittent nature of renewable sources by storing the energy in chemicals with a low carbon footprint.

References:

- [1] S.T. Wismann et al., Science 364 (2019) 756.
- [2] L. Zheng et al., AIChE J. 69 (2023) e17620
- [3] D.J. Jovan et al., Energies 13(24) (2020) 6599.

Electrically Heated Reactor for Steam Methane Reforming

H. Malburg¹, M. Baumgärtl^{1,2}, S. Guffanti², G. Pauletto², J. Lercher¹

¹Technical University of Munich, Garching b. München

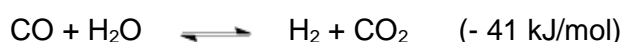
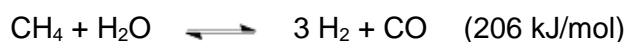
²SYPOX GmbH, Freising

Abstract

In steam-methane reforming (SMR) – the primary method for hydrogen production – gas-fired furnaces account for 40% of CO₂ emissions. Beyond the environmental concerns, these furnaces introduce inefficiencies and complexities, including the need for heat recovery, escalating costs. SYPOX's electrically heated reactor technology offers a compelling alternative for methane-derived hydrogen production. The innovative design integrates a catalytically active ceramic macrostructure with resistive heating elements. It allows for enhanced heat transfer, superior thermal efficiency, and reduced material stress. Utilizing a standard SMR catalyst in this electrically heated reactor, we observed a 92% conversion over 1,000 hours under close to industrial conditions (10 bar, 900°C outlet temperature, with a steam-to-carbon ratio of 2). Notably, the catalyst remained stable, showing no signs of deactivation. The reactor's material durability was further showcased during rapid thermal cycling, oscillating between 350°C and 900°C under a consistent airflow for over 1,500 hours. Cumulatively, these results position the SYPOX design as a viable candidate for industrial adoption.

1. Introduction

Hydrogen is an important chemical building block and energy carrier with approximately 100 megatons annual world production capacity. [1] According to many forecasts, the importance of H₂ as energy vector will increase with the energy transition, and demand is set to increase strongly in the coming decades. [1-3] Around 80% of H₂ is produced by steam-methane reforming, a highly endothermic process, in which natural gas and water react to form H₂, CO, and CO₂ according to the following equations [4]:



Steam-methane reforming is a carbon-intensive process. Around 10 kg of CO₂ are emitted per kilogram of H₂ produced. [1,4,5] This means that 900 million tons of CO₂, or 3% of global CO₂ emissions, are annually emitted by SMR plants. [4] The furnace providing the reaction enthalpy and the temperature to allow for full conversion is responsible for 40% of the total emissions and constitutes the best target for emission reduction. [6]

In existing reformer furnaces, the process heat is generated by burning fresh methane and off-gases coming from the pressure swing absorption (PSA, see Figure 1). Temperatures well over 1200 °C are reached in the furnaces (firebox), while the temperature inside of the reactor varies between 700 °C and 900 °C. [4,5]

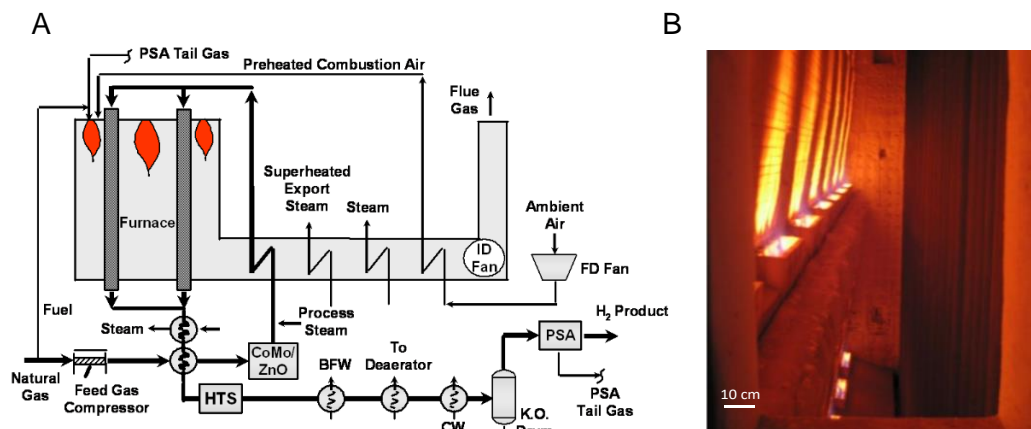
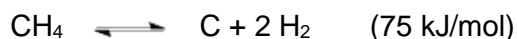


Figure 1: A. Layout of an SMR plant. B. Burners and reformer tubes in a Foster Wheeler wall-fired reformer. [5]

Three main industrial configurations for SMR furnaces exist, i.e., top-fired, side-fired, and bottom-fired. The location of the burners impacts both heat flux and temperature profiles, yet these three configurations achieve very similar results. [7] Existing reformers are limited by heat transfer, which results in steep radial temperature gradients within the reformer tubes. [4] The radial temperature gradients from the tube wall to the center of the catalyst bed may reach 100 K. [6]

Carbon formation is a serious risk factor during operation. Under SMR conditions, carbon is mainly formed by the cracking of methane.



This reaction continuously takes place when a steam reformer is in operation. [7] However,

under optimal conditions carbon removal reactions avoid a net accumulation of carbon on the catalyst. [8] If cracking rates are enhanced and a net laydown of carbon occurs, catalyst particles will be covered by carbon; the heat consumption of the reaction is then suppressed and hot spots may form. The formation of carbon whiskers can also crack the catalyst particles, changing the fluid dynamics of the system, and may even lead to blockage. [7] Carbon formation is suppressed by high molar ratios of steam to methane (S/C ratio), carbon-suppressing promoters such as potassium, but also by increasing the catalytic activity and minimizing radial temperature gradients. High catalytic activity reduces the local temperature and lowers the methane concentration. Improved radial heat transfer allows to move heat from the reactor wall (the hottest point) into the catalyst bed, where it increases the reaction rate and further reduces the methane content of the gas phase. [8]

Controlling the burners in an SMR furnace is made challenging by the high heat capacity of the system (a furnace may measure 30 x 10 x 18 m, with several hundred alloy reformer tubes that affect the thermal dynamics of the system). [6,9] In such an array, catalyst or tube replacement is a challenging process, i.e., hundreds of tubes must be opened and filled with catalyst (possibly up to three different layers) in equal measure to avoid differences in pressure drop. The integration of the reformer into the overall process is equally challenging and requires substantial on-site activities. In order to reach high energy efficiencies, extensive heat integration is indispensable. [4,5]

The chemical industry seeks to abate the emissions generated by reformer furnaces, [10] because CO₂ is or will be costly to emit under carbon taxation systems. Furthermore, the combustion of natural gas leads to lower efficiencies of H₂ produced per amount of methane. Attempts to decarbonize SMR furnaces include carbon capture in existing plants, autothermal reforming (ATR), and heating technologies powered by green electricity, including resistive heating, induction heating, and microwave heating. Carbon capture of low-pressure flue gas in conventional SMR plants is more expensive than in high-pressure process streams. Autothermal reformers, while resolving that issue, only become economical at a very large scale, and are, thus, limited in their application. [11,12]

Electrified SMR (e-SMR) has several advantages over the conventional design. Heating does not emit CO₂ and makes direct use of green electricity, while maximizing efficiency and storing part of the electric power in the H-H bond. The electrified heating designs are significantly more compact, easier to control, and safer than their fired counterparts.

While conceptually several possibilities exist to generate heat for an electrically heated reformer, resistive heating appears to be the most applicable solution for large scale industrial applications. While resistive heating could also be integrated into existing SMR plants as e-furnaces, the challenging heat transfer limits the benefits of electrification. Nevertheless, a similar approach has been taken with respect to steam cracking, a non-catalytic, high-temperature process for ethylene production. Several large chemical companies have recently undertaken the construction of a demonstration unit involving an e-furnace. [13] Other resistive heating technologies provide further advantages, including higher power-per-volume ratios and allowing to operate at higher temperatures and pressures (Table 1).

Table 1: Overview of resistive heating technology for SMR. [14-16]

	e-Furnaces	e-Structures	e-Tubes
Furnace	Electric	No	No
Reformer Tube	Traditional	Pressure vessel housing macrostructure, cold skin	Electrified tube
Catalyst	Pellets in Reformer	Washcoated macrostructure	Pellets in reformer
Advantages	<ul style="list-style-type: none"> minimal modifications required 	<ul style="list-style-type: none"> high energy efficiency optimized heat transfer high temperatures and pressures possible 	<ul style="list-style-type: none"> Use of standard catalyst pellets
Possible Limitations	<ul style="list-style-type: none"> low energy efficiency heat recuperation required heat transfer limitations temperature limitations of tube material 	<ul style="list-style-type: none"> Electricity supply into pressure vessel 	<ul style="list-style-type: none"> low voltage power supplies required expensive materials complicated power rails temperature limitations of tube material

In this paper, we present a new reactor design for highly endothermic thermochemical reactions. A test rig incorporating this design was built and tested for steam reforming of natural gas and biogas. We show that the SYPOX reactor technology will enable easy, fast and inexpensive commercialization of e-SMR technology.

2. Design of the SYPOX Reactor

The SYPOX reactor consists of an electrified catalytic bed inside of a refractory-lined pressure vessel (Figure 2). [17]

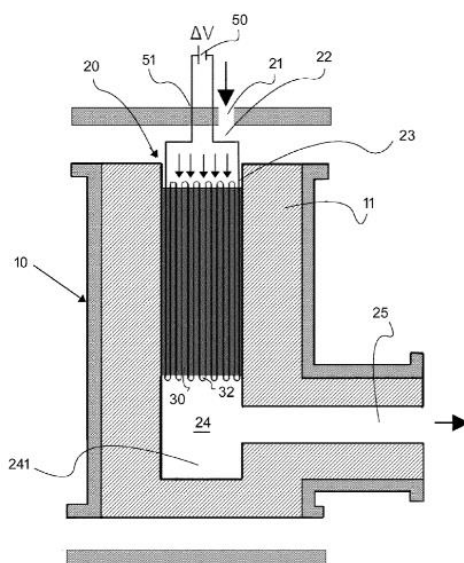


Figure 2: General design of the SYPOX reactor.

The catalytic bed consists of a ceramic macrostructure in which FeCrAl heating elements are installed (Figure 3). The ceramic is coated with a catalyst layer. This configuration creates a millimetric annular gap between heating element and the supported catalyst. Thus, the required reaction heat is generated in close proximity to the catalyst surface. This leads to a uniform heat distribution and a linear temperature profile along the axial coordinate of the reactor.

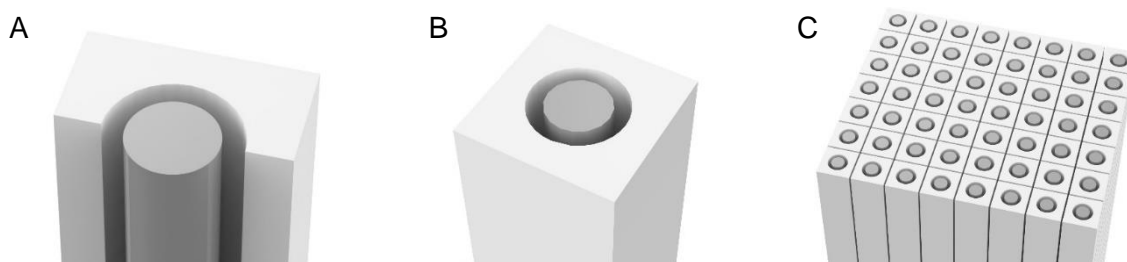


Figure 3: A. Longitudinal section of the ceramic structure supporting the catalyst with the internal heating element. B. Cross section of the ceramic structure and the co-axial heating element. C. Assembly of 56 ceramic structures.

The heating elements, covered by an inert oxide layer, are in direct contact with the reaction gases. The number of channels in the ceramic macrostructure dictates the maximum hydrogen production capacity. Subsequently, we will discuss the unique properties of this design and the implications for the SMR process.

3. Properties of the SYPOX Reactor

3.1 Catalyst

Catalysts in conventional SMR are usually based on nickel. They are installed as pellets in fixed bed reactors. [7] Over the last four decades, continuous improvements have led to an optimization of the pellet geometry and catalyst formulation (Table 2). The catalyst in SYPOX reactors advances these improvements while changing the method of heat supply (see section 4.1).

Table 1: Comparison of SMR catalyst geometries and their effects on performance parameters over the last 40 years. [18-21]





KPI \ Year	1980s	2000s	2014	2020s
Cross section	4-hole 	Improved geometry 	Metal-structured 	SYPOX 
Shape	Pellet	Pellet	Macrostructure	Macrostructure
Steam to carbon ratio, $mol\ mol^{-1}$	3 - 4	2.5	2	1.2
Relative pressure drops	0.62	0.43	0.34	0.05
Relative reactor volume	100	100	90	1
Relative CO ₂ emission	100	100	95	60

Table 1 shows that successive catalyst generations have reduced the pressure drop across the reactor bed. Yet, even when compared to the recently launched catalytic metal-structures (Catacell by Johnson Matthey), the SYPOX reactor exhibits a marked enhancement in this regard. This improvement stems from the SYPOX design, where the gas flows through a structured ceramic bed with a high void fraction, rather than traversing a lengthy catalyst bed.

In a traditional reformer tube, significant radial temperature gradients lead to suboptimal catalyst utilization (usually less than 10%) and a heightened risk of carbon formation. [6,7] In contrast, the thin catalyst coating in the SYPOX design minimizes radial temperature differences across the catalyst.

3.2 Heat transfer

Within conventional fired furnaces, over 90% of the heat transfer primarily occurs through radiation. Inside the reformer pipes, convection and conduction mechanisms dominate. [7] In contrast, the SYPOX electrified reformer uses direct heat transfer through radiation from resistance rods and the ceramic material. Additionally, convection plays a substantial role as the gas flows through the annular gap (between the ceramic tube and the heating rod), in direct contact with the heating elements. This results in a heat transfer surface area that surpasses traditional fired steam reforming furnaces by three orders of magnitude. Our experimental findings have quantified the power per unit volume of the electrically heated catalytic bed to be in the range of 20 - 30 MW/m³ (Table 3).

Table 3: Comparison of fired SMR and SYPOX reactor. [6]

SMR Parameter	SYPOX	Furnace
Power Density [MW/m ³]	> 20	0.03
Heat Flux [W/m ²]	> 80	100
Heat Transfer Surface per Volume [m ² /m ³]	250	0.3

Reformer tubes in furnaces are exposed to temperatures exceeding 1000°C, with their longevity largely dictated by constrained heat transfer. Their lifetime is around 10 years, but an increase of just 20 K in temperature can halve the lifespan of the tube. [9] The SYPOX reactor's innovative design, which generates heat at the reactor's center, employs a cold skin pressure vessel made only of conventional steel. This design not only enhances durability but also considerably reduces capital expenditure (CAPEX).

3.3 Process economics

While this is not a techno-economic analysis, we would like to highlight several some of the economic advantages electrification offers for the SMR process.

First, e-SMR reduces process emissions by up to 40%. Under the carbon taxation imposed by many countries now, this eliminates a significant cost factor. Germany, for example, plans to introduce a carbon fee of at least €55 per kg of CO₂ by 2026. This means that a German SMR unit producing 70,000 tons of hydrogen per year will save €15.4 m in carbon credits annually. [22,23] Second, replacing fired furnaces with e-reactors saves considerable amounts of natural gas. Between 25 – 30% of the natural gas going into SMR is burned to supply the high temperature heat required in the process. Third, the electric heating of the SYPOX reactor has the potential to improve operational flexibility and safety. The high heating/cooling rates (up to 30 °C/min) enable fast modulation of production. Lastly, incorporating electrified equipment like the SYPOX reactor into SMR plants will decrease the extent to which heat recuperation is necessary. Depending on the process configuration, this offers the possibility to avoid steam export, which often is difficult to be commercialized.

4. Experimental

4.1 Experimental Setup

The experimental setup is schematically depicted in Figure 6 and consisted of the following parts:

- Mass-flow controllers for gas supply
- HPLC pump for water supply
- Steam generator
- electrically heated SYPOX reactor with power supply
- cooling and phase separation
- on-line gas chromatograph

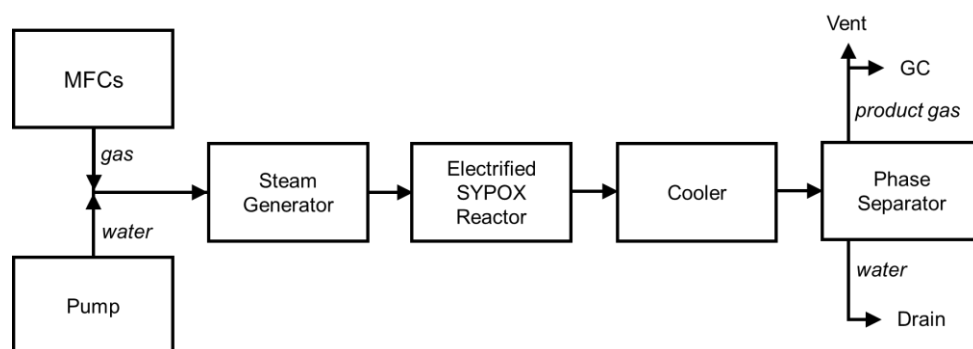


Figure 4: Scheme of the 2 kW e-SMR reactor unit.

For the electrically heated reactor, electricity is supplied to the reformer from a power supply and introduced into the pressure vessel via electricity feedthroughs. The feedthroughs are an important part of the reactor as they electrically insulate the pressure shell from the electrical connection and ensure pressure sealing. In this setup, the electrically heated catalytic bed was tested for catalyst activity and stability under an array of conditions. At 10 bar, steam reforming was performed at temperatures from 700 – 1000 °C and at S/C 1.0 – 2.5, using a variety of feeds (pure methane, natural gas, biogas).

4.2 Catalyst performance and stability

The activity and performance of a commercial Ni-catalyst under industrially relevant reforming conditions were evaluated in a 1,000 h campaign. For this purpose, ceramic macrostructure coated with catalyst and assembled with heating elements (Figure 3) was loaded into a pressure vessel with internal refractory lining. After the electricity supply was connected to the pressure vessel, the vessel was closed. After an initial reduction phase, the reaction was started by adding methane and steam to the feed gas.

At 10 bar and 350 °C inlet temperature, a mixture of steam and methane with a S/C of 2 were fed into the reformer. A high GHSV was chosen to stay under kinetic limitation, as it is impossible to evaluate catalyst stability when operating too close to the thermodynamic equilibrium. The outlet temperature was set to 900 °C. Analysis of the product gas gave a conversion of 92%, and an approach to equilibrium (ATE) of 60 °C (Figure 5). The mass balances were calculated using nitrogen as an internal standard and were 97% closed throughout the campaign.

Across the duration of the 42-day experiment, the approach to equilibrium remained constant at 60°C (no decrease in conversion), indicating no significant sintering or degradation of the catalyst. Additionally, an inspection of the catalytic material after reaction showed no indication of coke formation, or damage of the ceramic support or the heating elements.

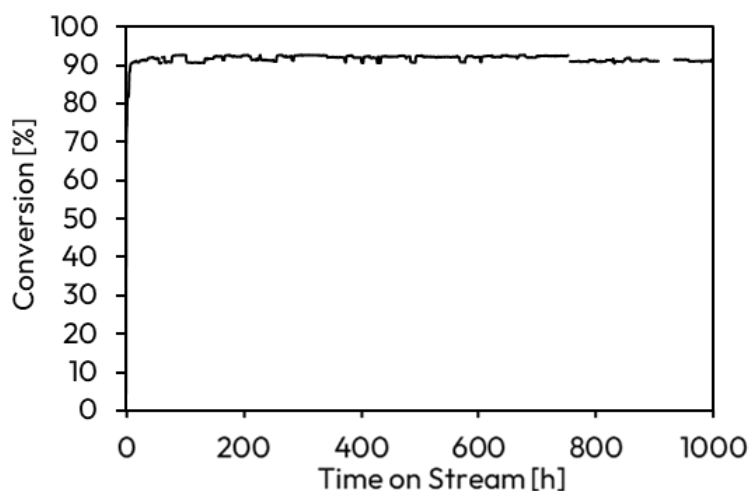


Figure 5: Methane conversion during 1,000 h SMR campaign in the SYPOX reactor.

To test catalyst stability, steaming was used as it tends to enhance sintering of the metal particles. Years of operation can be simulated when steaming for 100 h at 50 °C – 100 °C above the operating temperature.

In a 600-hour-test run at 10 bar and 900°C, two operating conditions were alternatively investigated (Table 4).

Table 4: Conditions used in steaming campaign and respective catalyst performance parameters.

Condition	Feed	S/C [-]	P [bar]	X_{Methane} [%]	ATE [°C]
1	CH ₄	2.5	10	95	10
2	CH ₄ /CO ₂ (1/1)	1.5	10	89	25

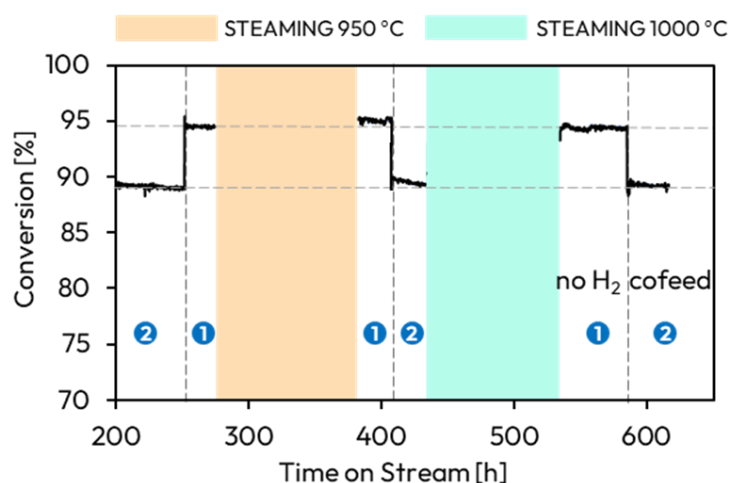


Figure 6: Detailed view on SMR campaign between 200 and 650 h time on stream.

After initial 280 h time on stream under reforming conditions 1 and 2, the feed was switched to pure steam and the temperature was increased to 950 °C. These conditions were kept for 100 h. Then, the previous SMR conditions were reestablished. The rates and conversion levels were identical. After maintaining conditions 1 and 2 for 24 h each, steaming was repeated at 1000 °C for 100 hours. Subsequently, the previous conditions (conditions 1 and 2) were again reestablished. Again the rates and conversions were identical to the steam reforming performance observed before. As the catalyst was active immediately after the steaming procedure and did not require prereduction, we conclude that Ni is rapidly reduced under the used operating conditions.

4.3 Material robustness

While we were able to show the catalyst stability over a large period of time (Figure X and Y), mechanical stress on the ceramic macrostructure and heating element resulting from years of operation would not be apparent in these experiments. Material fatigue is typically the result of large temperature gradients and frequent heating and cooling cycles. Therefore, ceramic and heating elements were tested for their ability to withstand temperature fluctuations and gradients far more extreme than would be expected under regular SMR operation. For this purpose, a catalyst bed was installed in the 2 kW e-SMR rig and air was fed into the reactor at room-temperature.

A thermal cycling protocol was executed as follows: Over a span of 1,500 hours, the temperature was cycled between 350°C and 1050°C with a rate of 50°C/min. Each extreme, minimum and maximum, was maintained for 30 minutes before transitioning again. Figure 7 depicts twelve of these cycles conducted over 20 hours. A clear correlation is evident between temperature and power. An increase in power is instantly reciprocated by a rise in temperature, and conversely, a power decrease leads to an immediate drop in temperature.

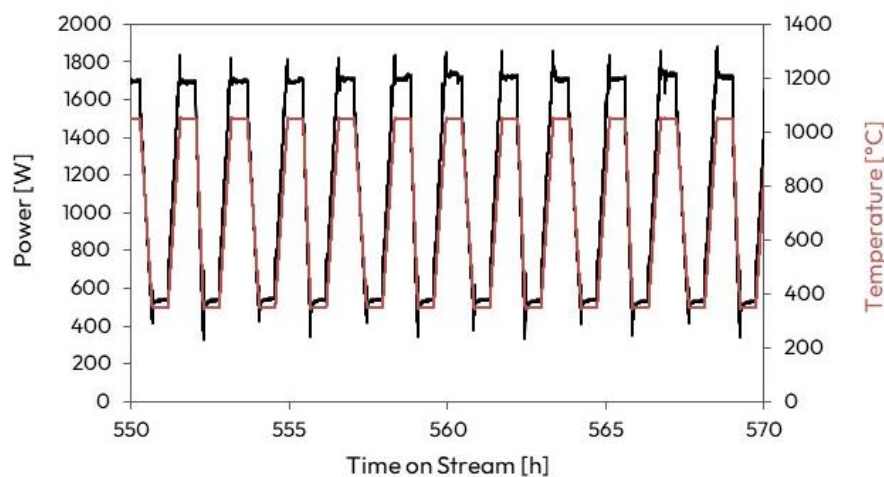


Figure 7: Temperature and power profiles during thermal cycling.

When looking at the entire thermal cycling campaign, different sections can be seen in which the power varies over slightly different ranges (see Figure 8). This is because at regular intervals, the control K-type thermocouple broke and had to be replaced. The positions of these thermocouples were slightly different from one another and measured slightly different temperatures. For a single thermocouple, however, the power range is highly uniform. This indicates that during the cycling, the material properties of the catalyst bed, especially heating wire resistance and ceramic integrity, did not change. Upon removing the module from the pressure vessel, we found ceramic and wire unchanged and intact. Due to an inlet temperature of only 25°C and an outlet temperature of up to 1050°C, a much stronger axial temperature gradient is generated compared to SMR, where typically inlet temperatures of 400 – 600°C are used.

At the same time the surface temperature of the heating element is expected to be much higher for air heating compared to SMR. In SMR much higher contact times are feasible, as the endothermicity of the reaction is consuming a major part of the provided heat.

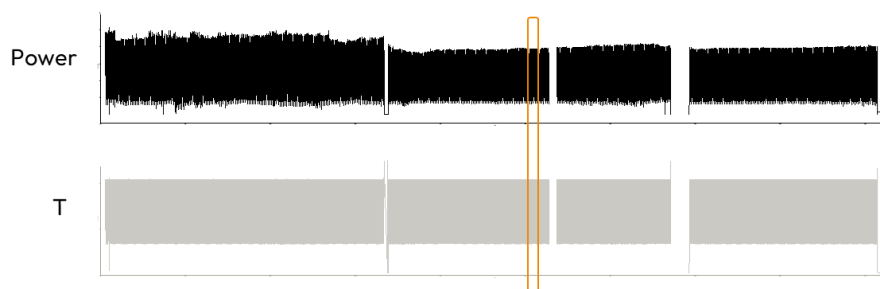


Figure 8: Overview of the thermal cycling and the different power ranges due to control thermocouple replacement.

5. Summary

Electrified reactors are emerging as groundbreaking technologies with the capability to curtail emissions in energy-intensive chemical processes. By replacing fired furnaces in SMR plants, substantial emission reductions can be achieved in a straightforward manner. SYPOX has developed an electric reformer, integrating catalytic ceramic macrostructures that house resistive heating elements. This design surpasses traditional fired reforming in various ways. It mitigates the risk of carbon formation due to optimized heat transfer, ensuring uniform radial temperature profiles. The consequent benefits extend to efficiency, material longevity, and economic viability in industrial contexts. In our experiments, a 2 kW SYPOX reactor, outfitted with a standard Ni catalyst, was operated under close to industrial conditions (10 bar, 900°C outlet temperature, S/C = 2) for 1,000 hours. This resulted in a methane conversion of 92%, with no observed catalyst deactivation. Tests involving recurrent high-temperature steaming and CO₂ co-feed underscored its remarkable stability. Furthermore, the reactor's endurance was evident during thermal cycling between 350°C and 1050°C over 1,500 hours. Throughout this period, the consistent electrical consumption to achieve specific temperatures indicated unaltered wire resistance. While these experiments validate the reactor's prowess under industrial conditions, more extensive-scale trials are in progress to validate its capacity for higher electrical power input while preserving superior reaction attributes.

6. Acknowledgements

The authors gratefully acknowledge the funding of this work via an EXIST Forschungstransfer Grant by the German Ministry of Economy and Climate Protection and the European Project EReTech (Electrified Reactor Technology, grant agreement ID 101058608).

7. References

- [1] International Energy Agency. Global Hydrogen Review 2022. (2022)
- [2] Deloitte. Green Hydrogen: Energizing the Path to Net Zero. (2023)
- [3] The Hydrogen Council, McKinsey & Company. Hydrogen Insights 2023. (2023)
- [4] Wismann, S.T., Engbaek, J.S., Veldelbo, S.B., Eriksen, W.L., Frandsen, C., Mortensen, P.M., Chorkendorff, I. *Ind. Eng. Chem. Res.*, 58, 23380 (2019)
- [5] Bonaquist, D. Analysis of CO₂ Emissions, Reductions, and Capture for Large-Scale Hydrogen Production Plants (White Paper). (2010)
- [6] Wismann S.T., Engbaek J.S., Veldelbo S.B., Benedixen F. B., Aasberg-Peterson, K., Eriksen W.L., Frandsen C., Chorkendorff I., Mortensen P.M., *Science*, 364, 756, (2019)
- [7] Nielsen J. R., Christiansen, L. J. Concepts in Syngas Manufacture. Imperial College Press. London. (2011)
- [8] Carlsson, M. Johnson Matthey Technology Review, 59, 313. (2015)
- [9] Lantham, D. A., McAuley, K. B., Peppley, B. A., Raybold, T. M. *Fuel Processing Technology*, 92, 1574. (2011)
- [10] Collodi, G. *Chemical Engineering Transactions*, 19, 37. (2010)
- [11] Noelker, K., Johanning, J. Autothermal Reforming: A Flexible Syngas Route with Future Potential. Contribution by Thyssenkrupp Uhde to the Nitrogen & Syngas 2010 International Conference. (2010)
- [12] Dahl, P. J., Christensen, T. S., Winter-Madsen, S., King, S. M. Proven Autothermal Reforming Technology for Modern Large-Scale Methanol Plant (White Paper). (2014)
- [13] Nonnast, T, Spengler, U., Kron, M. BASF, SABIC and Linde start construction of the world's first demonstration plant for large-scale electrically heated steam cracker furnaces. (Website Article) <https://www.basf.com/global/en/who-we-are/sustainability/whats-new/sustainability-news/2022/basf-sabic-and-linde-start-construction-of-the-worlds-first-demonstration-plant-for-large-scale-electrically-heated-steam-cracker-furnaces.html> (2022) [accessed 05.09.2023]
- [14] Kochendorfer, K. A., Laib, H., Shustov, A., Kuehn, H.-J., Jenne, E., Jacob, R. *WO 2020035575*. (2019)
- [15] Mortensen, P. M., Klein, R., Aasberg-Petersen, K. *EP 3574991*. (2018)
- [16] Zellhuber, M., Hofstätter, M., Kemper, R., Kochendoerfer, K. A., Shustov, A., Jenne, E., Haurert, A., Stevenson, S. A., Broekhuis, R. R., Ward, A. M. *WO 2022214622*. (2022)
- [17] Pauletto, G. *EP 3981859*. (2020)
- [18] Steam Reforming Catalysts. Natural Gas, Associated Gas and LPG. Johnson Matthey Catalysts. (2019)

- [19] Murkin, C., Brightling, J. Johnson Matthey Technology Review, 60, 263. (2016)
- [20] Catacell SSR. Tailored Catalyst Technology. Johnson Matthey Catalysts. (2018)
- [21] Murkin, C., Brightling, J. Johnson Matthey Technology Review, 60, 263. (2016)
- [22] Merten, F., Scholz, A., Krüger, C., Heck, S., Girard, Y., Mecke, M., Goerge, M. Bewertung der Vor- und Nachteile von Wasserstoffimporten im Vergleich zur heimischen Erzeugung (Studie). Wuppertal Institut. (2020) [in German]
- [23] BGBl. 2022 Teil I Nr. 43 vom 15.10.2022 (2022) [in German]

Syngas Production from Secondary Feedstock as a Key Element for a Circular Carbon Economy – Gasification Performance Enhancement via Plasma Integration

Antonia Helf¹, Florian Keller¹, Martin Gräbner^{1,2,3}

¹ Institute of Energy Process Engineering and Chemical Engineering (IEC), TU Bergakademie Freiberg (TUBAF), Freiberg, Germany

² Fraunhofer Institute for Ceramic Technologies and Systems IKTS, Energy and Process Engineering – Circular Carbon Technologies, Freiberg, Germany

³ Center for Efficient High Temperature Processes and Materials Conversion (ZeHS), TU Bergakademie Freiberg (TUBAF), Freiberg, Germany

Introduction

Plastics are an essential part of our lives due to their unique properties (in terms of weight, price, flexibility) and the wide application possibilities, but are also associated with huge quantities of non-degradable waste. Its handling and the minimization of environmental impacts is a central challenge of our time. The largest fraction of produced plastic is used in packaging thus has very low lifespans and quickly ends up as waste, thus magnifying the issue. Their sustainable application requires the establishment of a circular economy and its key elements, including the utilization of renewable feedstock, the maximization of the product life time and recycling after utilization, while maintaining safe handling and treatment to prevent direct plastic emissions into the environment [1].

Plastic waste treatment in Germany is primarily based on the combination of mechanical recycling and thermal treatment with or without energy recovery. 2.6 of 5.7 Mio t (46%) of occurring plastic waste is considered as recycled in Germany, but only 2.3 of 14 Mio t (12%) used plastics are covered by secondary sources [2], despite one of the most advanced recycling systems globally. According to the waste framework directive and the plastic and plastic waste directive of the EU [3], challenging targets are defined with a re-use or recycling rate of 65% by 2035 Europe-wide and minimum targets for recycled content in plastic products, indicating a real recycling effect.

In terms of practicability, mechanical plastic recycling is limited by its recovery to sortable waste fractions, waste quality and contamination, recycling technologies and the quality of the recovered materials. Recent studies paint a pessimistic picture for the applicability of conventional recycling, with plastic circularity of up to 72% for an optimized system [4], and a true recycling rate of 23% [5]. Table 1 indicates typical yields of a state-of-the-art recycling facility for source-separated packaging waste. At least 50% of the contents of plastics and carbon end up in only partially or non-recycled product fractions in mixed polyolefin waste (MPO), mixed plastic waste (MPW) and sorting residues, leading to high degrees of CO₂ emission.

Table 1: Recovery yields of typical state-of-the-art packaging waste sorting facilities

Output fraction	Mass	Plastics	Carbon
Recycling plastics	16.7%	31.8%	24.8%
Other recycled fractions (incl. liquid cartons, paper, metals)	34.3%	13.8%	21.5%
Mixed polyolefins (MPO)	10.3%	19.5%	16.1%
Mixed plastic waste (MPW)	7.4%	14.1%	11.6%
Sorting residues	31.3%	20.7%	25.9%
Sum	100.0%	100.0%	100.0%

The application of chemical recycling opens up the possibility to improve achievable recycling rates by expansion to non-recyclable fractions. Figure 2 shows an overview of possible pathways for chemical recycling and application of its products. Pyrolysis, depolymerization and solvent-based purification are currently most prominently considered as chemical recycling processes, but gasification provides the largest quantitative feedstock potential, as especially sorting residues and mixed waste fractions are only applicable to gasification.

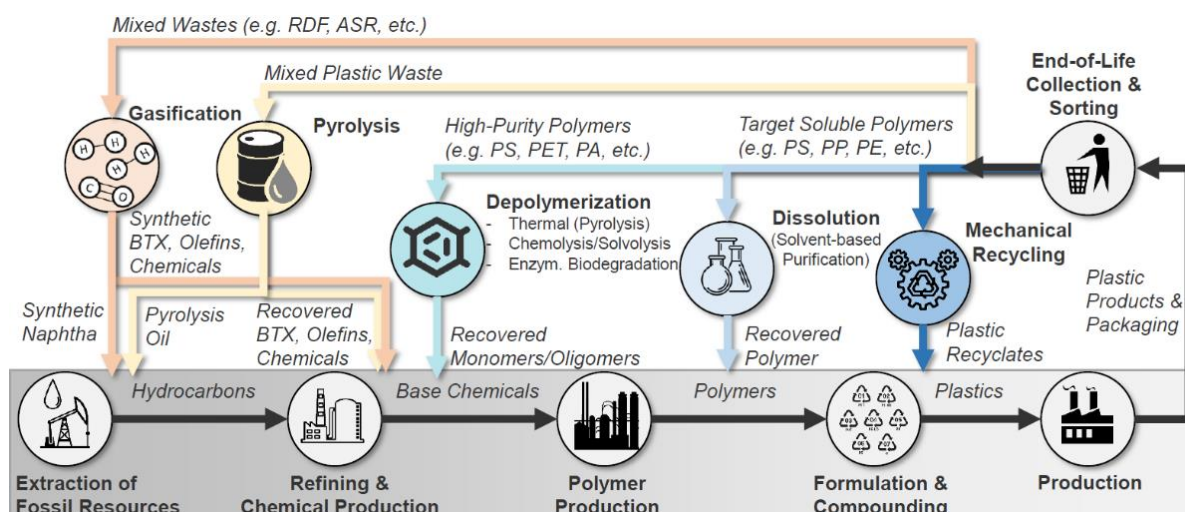
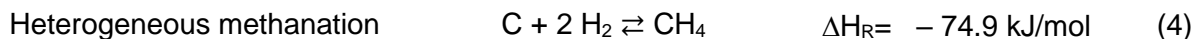
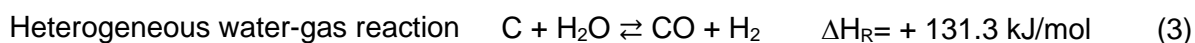
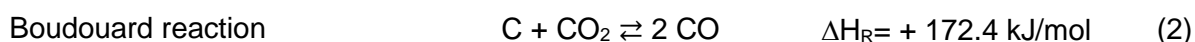
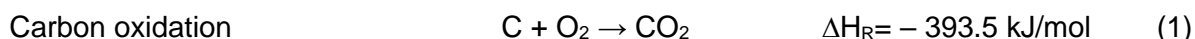


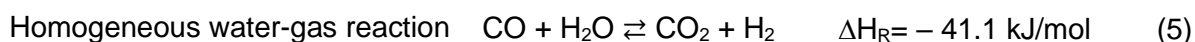
Figure 1: Overview of chemical recycling pathways [6]

Gasification of secondary feedstock for carbon recovery

In a gasification process, a carbon-containing solid material is contacted with a gasification agent to break down the molecules of the feedstock into gaseous species, mainly hydrogen and carbon monoxide. These reactions take place at high temperatures between 800 and 1600 °C. Typical gasification agents are oxygen, air, steam, CO₂ and mixtures thereof. In addition to the main components CO and H₂, the generated gas usually contains significant amounts of steam and carbon dioxide and depending on the process conditions also methane [7]. The chemical process comprises a complex system of numerous chemical reactions, but the essential conversion of carbon to the major product gas components can be described by the following reactions:

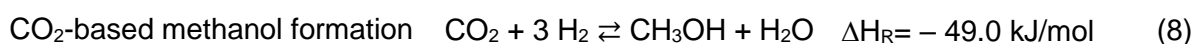
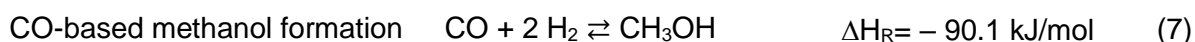


The product gas, usually called syngas, contains a number of impurities or inerts that trace back to the matrix, additives and compounds of the plastic (e.g. fillers, dyes, fibers, flame retardants). They need to be separated to avoid inefficient production or damage to downstream equipment. Subsequently, the gas can be used for a wide range of syntheses to reach products such as methanol and other carbon-based base chemicals, fuels, ammonia or hydrogen. For these syntheses, a defined ratio of hydrogen to carbon monoxide is required. This can be adjusted by the water gas shift reaction:



This therefore presents a pathway from almost any kind of carbon-containing waste to the whole spectrum of carbon products, including plastics. In the following discussion, the production of methanol is exemplarily addressed as a versatile chemical with a wide range of application as chemical intermediate and energy carrier. The necessary syngas composition is described by the syngas modulus (optimum at 2.03), and the chemical synthesis can be pursued via CO or CO₂.

Syngas modulus $SN = \frac{H_2 - CO_2}{CO + CO_2}$ (6)



From a technological point of view, gasification temperature is a decisive factor. Firstly, higher temperatures generally lead to a higher (and faster) conversion which in turn produces higher quality gas with less hydrocarbon content. Secondly, at high temperatures ash components melt and produce a vitrified, non-leachable slag that allows safe encapsulation of most critical waste impurities (e.g. heavy metals) upon withdrawal from the reactor whereas sintered ash output from a lower temperature gasification is difficult to handle.

The gasification reaction system contains oxidizing exothermal as well as reductive endothermal reactions, depending on the heat supply strategy. Temperature is adjusted either by adding more oxidizing gasification agent or supplying external heat. The latter requires an external heat source which is usually an additional fuel combustion while the first leads to more combustion reactions within the gasification process and therefore a higher CO₂ content in the gas especially for oxygen-containing or high-ash feedstocks. Consequently, gasification is associated with a significant amount of intrinsic CO₂ production.

However, gasification is especially interesting in the context of chemical recycling as it has a high tolerance for varying and strongly heterogeneous feed. The wide range of possible feedstock as well as the low requirements regarding waste purity make gasification a potential treatment process for a large quantity of waste streams.

Gasification as a waste treatment technology is currently considered for sewage sludge, MSW and mixed plastic wastes, especially in the USA, UK and Japan [8]. Another upcoming

feedstock is automotive shredder residue. In commercial projects, the product is usually either fuels or hydrogen. So far, plants with an annual feed capacity of about 385 thousand tons of waste are operational, and an additional 4.35 million tons of waste processing capacity has been announced according to internal monitoring of public domain information [9]. Progress is slow on most of the projects as the scale-up of waste gasification faces technological challenges as well as social opposition and administrative and regulatory grey areas.

Concepts for increasing the carbon recovery of waste gasification

As discussed, gasification of waste streams has large application potential but its sustainability is limited by the achievable carbon recovery and consequently, associated intrinsic CO₂ formation. To nonetheless serve as a circular carbon technology, carbon integration along the process chain needs to be improved.

While there is potential room for improvement of the technology itself, reactor designs, etc. that can improve the overall technological and environmental performance of gasification systems, there are also systematic approaches that can be taken to increase the carbon recovery of gasification process chains. These approaches are based on the integration of renewably produced electricity to replace energy supply from the feedstock or external carbon fuels. There are different points in the gasification process chain where the integration of renewable power can improve the carbon recovery of the treatment route. One option is to supply energy to the gasification via direct heating with renewable electricity. This can be done either within or directly after the gasification reactor. Another option is to replace the water gas shift process by integration of renewably produced hydrogen to increase the H₂/CO-ratio without converting CO to CO₂. For both options, the carbon recovery is increased by replacing the combustion-based energy supply to the process by renewably produced power – directly via plasma or indirectly via hydrogen. Alternatively, the CO₂ emissions from this process route can also be reduced by capturing the generated CO₂. However, this does not increase the carbon recovery to products.

In the following subchapters, plasma-assisted gasification as well as hydrogen integration into gasification process chains will be discussed conceptually and subsequently be evaluated from a technical and economical point of view.

Option 1: H₂-integration

Process concept

The indirect integration of renewable power into the gasification process chain is achieved via hydrogen. It is assumed that hydrogen can be produced at scale through electrolysis by means of renewable, net-zero power. This hydrogen is fed to the gasification process chain instead of using a water gas shift unit. Without hydrogen addition, CO is converted to CO₂ here (see equation (5) for reference) in order to increase the hydrogen to CO ratio in the gas since it is usually not high enough coming from the gasifier for the following downstream synthesis. Instead of this reaction, which further increases the CO₂ production from the process, hydrogen from external sources is applied to adjust the syngas modulus. Hence, the quality of the raw syngas in terms of hydrogen fraction is not decisive for the carbon recovery of the process.

In this way, the major reason for CO₂ emissions from the process chain is remedied. On top of that, the air separation unit that produces oxygen for the gasification can be replaced by the electrolysis unit that is used to supply the hydrogen to the shifting step. These two aspects are visualized in Figure 2, that shows the integration of hydrogen and oxygen from an electrolysis unit to a gasification process. Figure 3 furthermore shows the effect of hydrogen integration on product yield, carbon recovery, CO₂ emissions and oxygen demand for an exemplary case for RDF gasification-based methanol production (feed composition shown in Table 3).

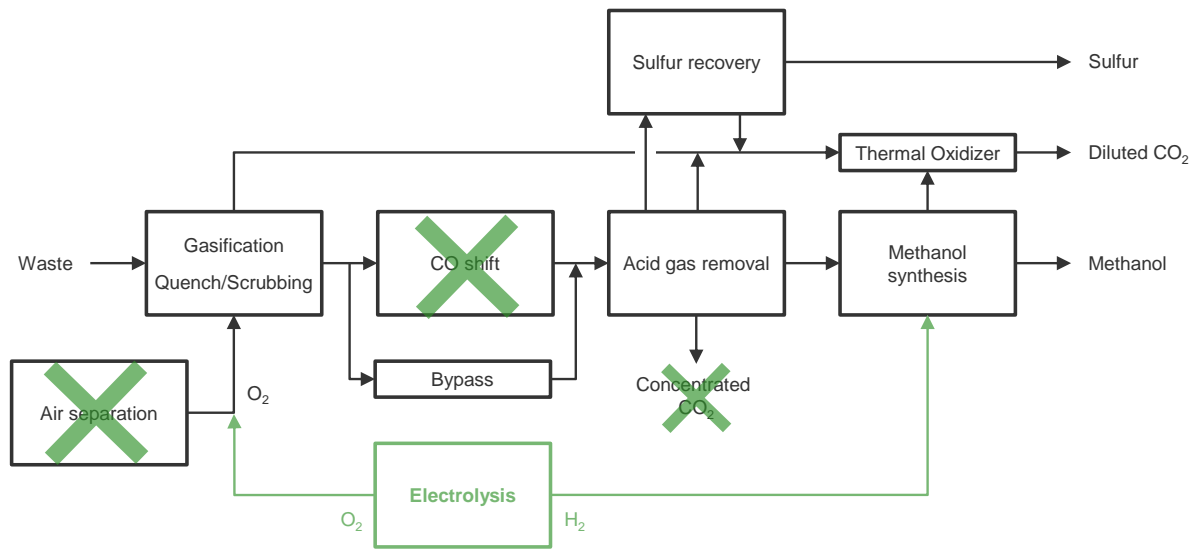


Figure 2: block flow diagram of hydrogen integration

Another advantage of hydrogen integration into the waste gasification process chain is that the process chain adaptation happens after the gasifier. Consequently, technological developments and improvements made to the gasification reactor are not affected by this modification. Instead, hydrogen integration can be retrofitted. This is especially attractive since the hydrogen production from renewable power has a fluctuating output depending on the availability of renewable power, thus varying with the weather conditions. A hydrogen integrated process chain can easily be configured flexibly to integrate as much hydrogen as available and still perform shifting if the H₂ supply is insufficient. The dynamic characteristic of renewable power therefore does not pose a risk to stable gasification operation.

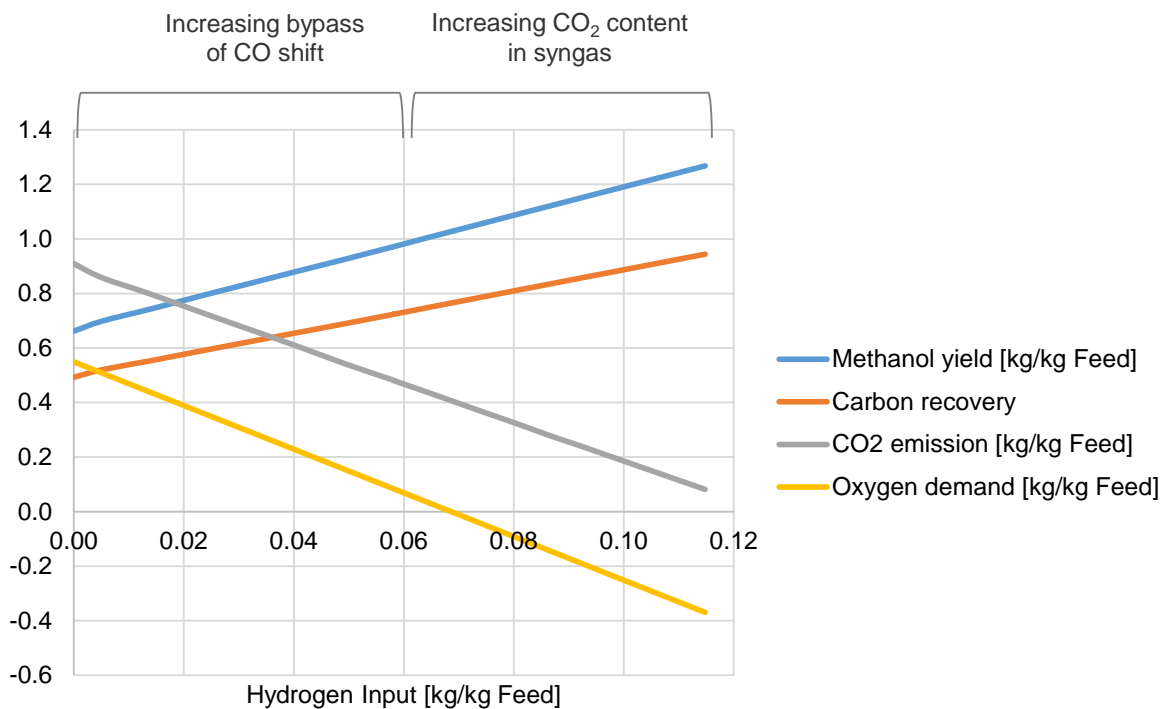


Figure 3: Effect of hydrogen integration on different process performance characteristics for a gasification-based RDF-to-methanol process

Technological limits

On the other hand, two major aspects need to be considered as drawbacks of the hydrogen integration option. Firstly, the electrolysis energy efficiency and development potential are limited which means that significant amounts of power need to be supplied to the electrolysis to reach relevant hydrogen outputs. Figure 4 shows the energy efficiency status and perspective of electrolysis processes (adapted from [10]). Moreover, electrolysis cells are limited in their individual capacity. Consequently, to supply the necessary amount of hydrogen (under the assumption that the power supply is not the bottleneck), a large amount of electrolysis cells/stacks is required. Due to scaling effects of major process components, gasification-based facilities are usually only economically feasible at large scales. The scalability of the adjacent technology, in this case the electrolysis, is therefore a rather decisive factor. Especially concerning the investment costs, scaling electrolysis plants to match the capacity of a gasification unit is a capex-intensive concept.

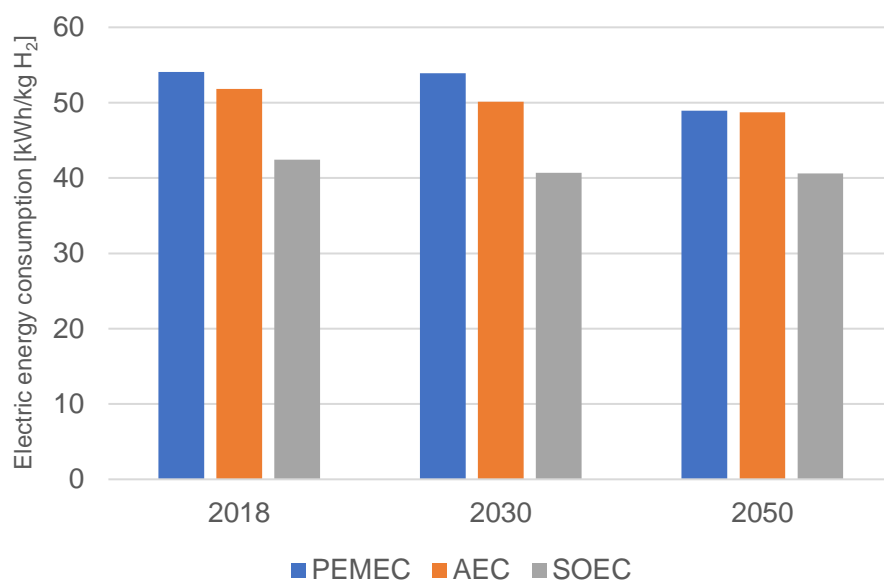


Figure 4: Energy efficiency status and perspective of electrolysis processes [10]

Option 2: Direct heating via plasma

Process concept

Alternatively or additionally to hydrogen integration, the quality of the raw syngas coming from the gasifier can be improved by targeting to decrease CO₂ and increase hydrogen fractions. Since CO₂ in the syngas is attributed to oxidation reactions that provide heat to endothermic conversions and temperature level (Boudouard equilibrium, see equation (2)), heat supply and syngas composition are coupled. To decouple them, external heat supply is necessary. This is usually done by combusting a part of the carbon-containing fuels and providing sufficient area for heat exchange as for example done in steam methane reforming. This also leads to CO₂ emissions and is thus not a viable way of increasing the overall carbon recovery of the process. Therefore, the direct integration of renewable power into the gasification via plasma is alternatively employed to feed energy into the gasifier without an oxidant.

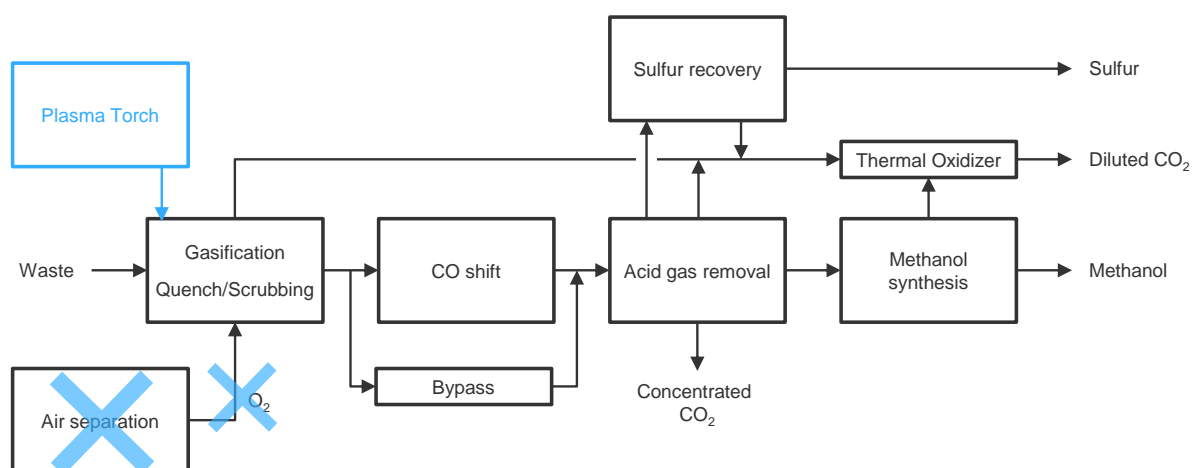


Figure 5: Plasma-assisted gasification process chain

In this way, the oxygen input can be minimized depending on the amount that is fed to the gasifier with the feedstock as heat supply is decoupled from oxygen supply. As Figure 5 shows, the air separation unit (ASU) is replaced by the plasma torch.

Plasma-assisted gasification has traditionally been considered for waste management to neutralize hazardous substances [11]. In recent years, developments have gained traction and now also focus on other waste streams such as MSW, sewage sludge and plastic waste. In the following paragraphs the basics of plasma gasification are briefly explained.

Plasma as a state of matter is defined as an ionized gas and thus is conductive and also contains large amounts of energy [12]. Conceptually, it therefore allows the supply of substantial amounts of heat to a process tied to very limited material input, i.e., a high energy density. Additionally, the use of that heat is not tied to the production of CO_2 directly, as it is with chemically stored energy that is unlocked with oxidation. However, large amounts of electricity are required for generating plasma, which also leads to CO_2 emissions, especially if this power is not generated renewably. On top of that, devices that generate plasma also have attributed losses that is accounted for in a technology-specific generation efficiency.

Possibilities of plasma integration

Fundamentally, plasma can be generated in different ways with electrostatic and electromagnetic methods being the most common forms of plasma generation. Depending on the plasma source, different properties are realizable. In general, plasma streams are described by their pressure (below atmospheric, medium, high pressure), their degree of ionization and whether they are in thermal equilibrium. The thermal equilibrium determines if the plasma stream is at a uniform high temperature (thermal equilibrium), if there are local gradients (local thermal equilibrium) or if the light weight electrons are at a high temperature but the heavy rest of particles is not (no thermal equilibrium, cold plasma). For heat supply to gasification, thermal equilibrium is a decisive factor [12].

In the application, some more relevant properties of the generated plasma within the specific system can be identified. These are the plasma's specific enthalpy and diffusion rate as this governs the heat transfer to other parts of the reactor. The injected power and the thermal efficiency of the torch additionally decide on the plasma system design and its overall efficiency for electricity integration. An important consideration is also the type of gas that is (can be) ionized, for example argon, nitrogen or steam.

Table 2: Plasma generation technologies [11–13]

Plasma generation	Technology mechanism	Advantages	Disadvantages
Thermal arc	Spark between two conducting parts (electrodes) by initial application of high voltages	<ul style="list-style-type: none"> - High temperatures possible - High efficiency possible 	<ul style="list-style-type: none"> - Limited electrode lifetime - Difficult process control
Microwave	Plasma is induced by microwaves, i.e., wavelength similar or smaller to plasma size	<ul style="list-style-type: none"> - No electrode erosion - Variable temperature 	<ul style="list-style-type: none"> - Limited efficiency - Limited treated surface (scale)
Radio frequency (inductive, capacitive)	Induced by magnetic or electric fields that lead to electron scattering	<ul style="list-style-type: none"> - No electrode erosion - Direct feed-plasma interaction possible - High power possible 	<ul style="list-style-type: none"> - Limited efficiency and scale - Difficult operation

Table 2 shows the technological pathways that are used for plasma generation. Literature shows that DC thermal arc plasmas are the most commonly deployed technology due to their ability to be scaled to the needs of the gasification system. The limited lifetime of the electrodes is the decisive factor that technology research and development is addressing. Apart from that, AC arcs and microwave plasma are investigated [11].

Plasma gasification comes in different design concepts depending on the scenario. The two basic approaches are detailed below:

- **Plasma melting:** In these systems, plasma torches bring in energy at the bottom of the reactor to support ash melting into slag, to avoid the production of dry ash as a gasification product as it is difficult to handle and to dispose of. Depending on the nature of the slag, a transferred or a non-transferred arc can be employed. Due to the positioning within the slag bath, the conversion in the gas phase is hardly affected, thus gas composition is not impacted significantly. This approach is especially applicable for feedstock with a high content of ash that leads to a high energy demand for melting. Boson Energy [14] is using this approach by placing plasma torches at the bottom of a counter-current fixed bed gasifier, to support the vitrification of the slag. Another example of this approach is the InEnTec [15] system that has a separate plasma chamber below the main gasification reactor where temperatures are so high that molten metals and slag can be discharged separately. Gas quality improvement is done by a secondary gasification zone that does not utilize plasma. SG H2 Energy [16, 17], a member of the Solena Group also uses this approach for plasma gasification of plastic waste in a counter-current fixed bed gasifier.
- **Plasma gas conversion:** The plasma torch is either positioned in a separate reactor or close to the syngas output where it creates a secondary gasification zone. Secondary cracking and reaction equilibration improve the gas quality, especially by converting higher hydrocarbons and tar components. This requires additional reactor space but allows significant improvement of gas quality. Slagging is not supported so if desired, the necessary heat must be available within the primary gasification chamber. Consequently, this concept is most suitable for feedstocks with low ash content and high organic fraction as the conversion of the organic fraction into high quality syngas components has the bigger impact on the energy demand of the reactor. An example for this is the process by Advanced Biofuel Solutions Ltd. (ABSL) [17], who use a bubbling fluidized bed reactor followed by a DC transferred-arc plasma torch in a secondary reactor that supports ash

melting as well as secondary conversion of tars and yields a refined syngas alongside slag. OMNI Conversion Technologies [18] (formerly Plasco) uses a similar approach but only sends the raw syngas to the plasma conversion reactor, without the ash. Melting of the ash takes place in the primary gasification reactor already.

Overall, the effect of plasma on the gasification process is higher cold gas efficiency, increased syngas yield, less impurities/tars/higher HCs in syngas, better syngas quality and lower CO₂ yield in syngas, which leads to a higher carbon recovery i.e., a higher fraction of feedstock carbon that can be recovered to a chemical product. Plasma-based gasification units can further benefit from the high energy density without heating surfaces and improved kinetics due to reactive species in highly excited states, enabling the construction of compact and less cost-intensive reactors [19].

Despite recent development progress and process demonstration, application of plasma in gasification still faces challenges that need to be addressed to improve the process applicability and sustainability. These include the plasma energy efficiency, the applicable process pressure, the feedstock conversion rate due to contacting limitations of plasma with gasification feedstock, and the unit longevity, especially electrodes in plasma torches [19].

Technological and economical comparison of plasma- vs. H₂-integration

Above the two basic options for improving the carbon balance of waste gasification process chains have been qualitatively discussed and explained on a technology level. In this section, these general tendencies are quantified by comparing three process chains: a conventional one, one with direct and one with indirect power integration for one feedstock. RDF is chosen for this analysis as a representative feedstock for actual waste streams (see Table 3).

Table 3: Exemplary composition of typical waste fractions

	Waste wood	Refuse derived fuel	Polyethylene waste
Proximate analysis [wt.-%, wf.]			
Fixed Carbon	14.89	8.60	1.25
Volatiles	82.76	69.30	98.75
Ash	2.35	22.10	0.00
Sum	100.00	100.00	100.00
Ultimate analysis [wt.-%, wf.]			
Ash	2.35	22.10	0.00
Carbon	50.70	46.80	85.60
Hydrogen	6.15	5.70	14.40
Nitrogen	0.63	1.60	0.00
Chlorine	0.08	0.26	0.00
Sulfur	0.05	1.25	0.00
Oxygen	40.04	22.29	0.00
Sum	100.00	100.00	100.00
Heating value [MJ/kg, wf.]			
LHV	18.75	22.37	44.94
HHV	20.09	23.62	48.10

The comparison is based on thermodynamic process chain modelling using Aspen Plus. The gasification is assumed to reach equilibrium. The plasma input is integrated as thermal input without material input with the plasma efficiency considered as a performance indicator in the

results evaluation. A similar approach is chosen for the electrolysis. The process chain evaluation considers the conversion processes from feedstock up to methanol including syngas compression, the adjacent air separation and electrolysis, the combustion of off gases and basic heat integration. The basic scaling of the three cases is for an LHV-based thermal input of 200 MW of RDF, equaling about 270 thousand tons of waste per year. The plasma and the electrolysis case are adapted to reach a carbon recovery to methanol of 76.6 %, benchmarked by the maximum recovery can be reached by plasma integration. Due to the equilibrium-nature of the gasification reaction system and the oxygen contained in gasifying steam and the feedstock, a certain amount of intrinsic CO₂ is inevitable, thus leading to a certain amount of inevitable carbon dioxide in the syngas. Since the hydrogen process chain uses a downstream modification, the performance of the gasification section is the same as in the conventional process chain. This can be seen exemplarily in the syngas yield, that amounts to around 2 m³ (CO+H₂, STP)/kg, while the plasma gasification produces 2.7 m³ (CO+H₂, STP)/kg. Figure 6 shows the electricity demand for the conventional, the plasma and the hydrogen route, by consumer, along with the carbon recovery. As mentioned before, the carbon recovery was fixed at 76.6 % for both cases with power integration to improve comparability, which is an increase of 18.6 percentage points compared to the conventional case. The power demand shows some general power consumers (including syngas and methanol recycle compressors) that are in a similar range of electricity demand. The demand for the plasma process chain is slightly higher due to the increased syngas flow.

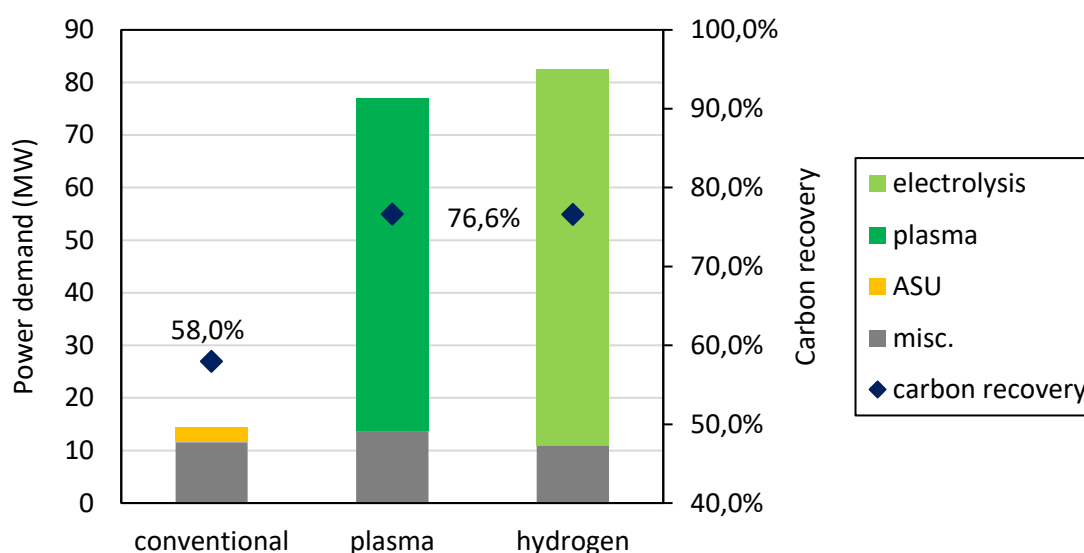


Figure 6: power demand and carbon recovery for all process chains

Figure 6 also shows that plasma as well as hydrogen integration leads to a significant increase in electricity demand, as can be expected. The plasma process chain requires slightly less electricity compared to the hydrogen process chain. Since the carbon recovery is the same for the plasma and the hydrogen process chain, the amount of CO₂ that is saved compared to the conventional process chain is also the same. The increase in power demand can be related to the decrease in CO₂ emissions, which yields about 5.99 kWh of power input per kg of CO₂ that is saved when using plasma. For hydrogen integration the number is slightly higher at 6.54 kWh/kg. This shows the same trend as the electricity demand in Figure 6. This difference can be attributed to the different integration efficiency that is higher for the direct integration of electricity.

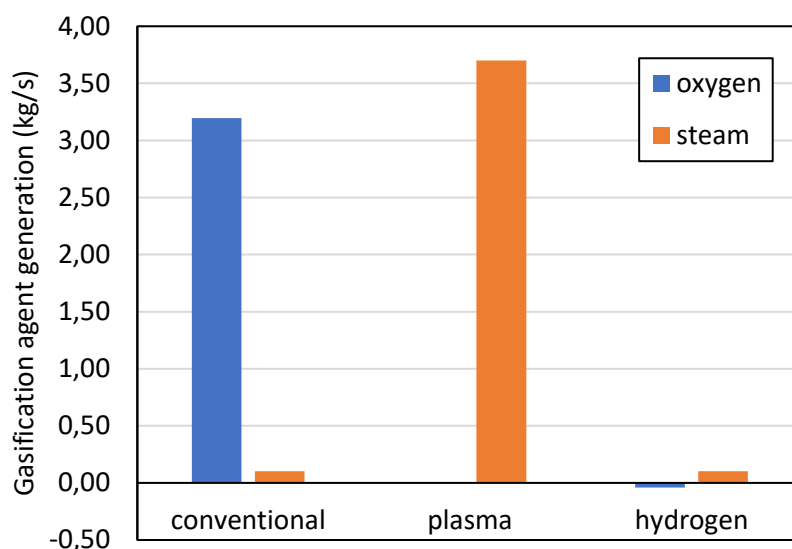


Figure 7: gasification agent demands for all process chains

Another relevant aspect is the gasification agent demand that the different process chains exhibit, as shown in Figure 7. The conventional route consumes large amounts of oxygen that is provided by the cryogenic ASU. Some steam is also injected into the gasifier as moderating agent. The plasma route on the other hand consumes no oxygen but large amounts of steam that consumes the injected plasma energy by endothermic reforming reactions. The hydrogen process chain uses the same amount and ratio of oxygen and steam; however, no ASU is required since it is assumed that the oxygen produced by electrolysis can be used for the gasification step. In fact, as Figure 7 shows, the oxygen production of the electrolyzer is more than enough for the gasifier. Therefore, the hydrogen process chain has an overall rather small gasification agent demand.

This technological performance comparison can be used to estimate capital investment and operating cost of the three process chains. By assigning a price to process CO₂ emissions, a leveled comparison between the different approaches can be drawn. The assumptions for this economical evaluation are shown in the following in Table 4.

Table 4: Assumptions for economic evaluation

Assumption	Value	Unit
Thermal input scale	200	MW
Operating hours	8000	h/y
Electricity cost ¹	0,05	€/kWh
Price for CO ₂ emissions	100	€/t
Gate fee for waste	100	€/t
Methanol revenue	395	€/t
Target year	2025	

¹ This is assumed to be produced renewably i.e., without associated CO₂ emissions.

Table 5: Unit reference cost for CAPEX estimation

	Source	Price reference [Mio. €] (converted to 2025)	Reference capacity	Scaling degression exponent
Gasifier	Estimation	38.15	5.8 kg/s (waf)	0.55
Air separation	[22]	21.02	4.3 kg/s O ₂	0.61
Syngas compressor	[23]	31.30	1.5 kmol/s dry syngas	0.65
AGR & TGT	[23]	14.73	9.6 kg/s CO ₂	0.65
Methanol synthesis	[23]	20.17	11.2 kg/s Methanol	0.65
Electrolyzer	[24]	4.28	5.0 MW(el)	0.88
Plasma system	[25]	0.36	1.2 MW(el)	0.88

These assumptions lead to an estimation of annual operating expenditure as well as revenues. Additionally, capital investment can be estimated from reference costs for the respective equipment by scaling of reference costs (see Table 5) to the required size as well as adapting the reference cost to the target year. Table 6 shows the results of this estimation:

Table 6: Results of economic assessment for RDF gasification

	Conventional	Plasma	Hydrogen
Annual OPEX [Mio. €]	24.46	41.12	43.39
Annual revenues [Mio. €]	100.59	124.28	124.25
CAPEX [Mio. €]	102.85	99.58	129.02

Due to the strong increase in electricity demand, the operating cost of the plasma as well as the hydrogen process chain increase significantly, which cannot be compensated by the reduced cost of CO₂ emissions in the assessed framework. The main difference in the increased methanol yield in the plasma and hydrogen case.

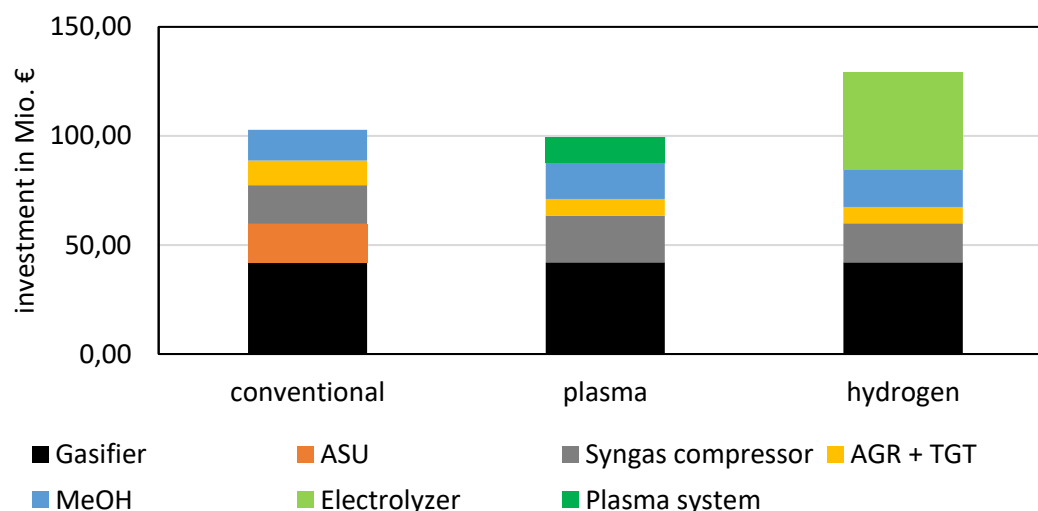


Figure 8: CAPEX composition for gasification-based process chains

When comparing the capital investment, it is evident that the hydrogen case is the most expensive case due to the cost of the electrolysis equipment. The cost of the gasifier is the same in all three cases. Since the cost of the plasma system is lower than the cost of the ASU while the rest of the costs are quite similar between the conventional and the plasma case leading to overall lower investment in the plasma case.

Another perspective on this is to compare the CAPEX in relation to the amount of methanol that the respective plant can produce (product-specific investment). The conventional route requires an investment of 552 € per ton per year methanol produced (€/tpa). The plasma route ranges at 404 €/tpa and the hydrogen route at 524 €/tpa. This clearly shows that the increase in production also has an effect on the overall costing balance. However, comparing annual operating costs versus revenues still reveals that higher revenues from increased methanol sales do not cover the cost of electricity. With 21.16 Mio. € per year vs. 10.50 vs. 8.23 Mio. € per year in operating cost balance for the conventional, the plasma and the hydrogen process chain respectively, the conventional route is still advantageous.

In this context, the scaling of the three process chains for a range of thermal input can be investigated. Figure 9 shows the CAPEX of the process chain as well as the methanol-specific investment for a range of thermal input from 10 MW to 500 MW.

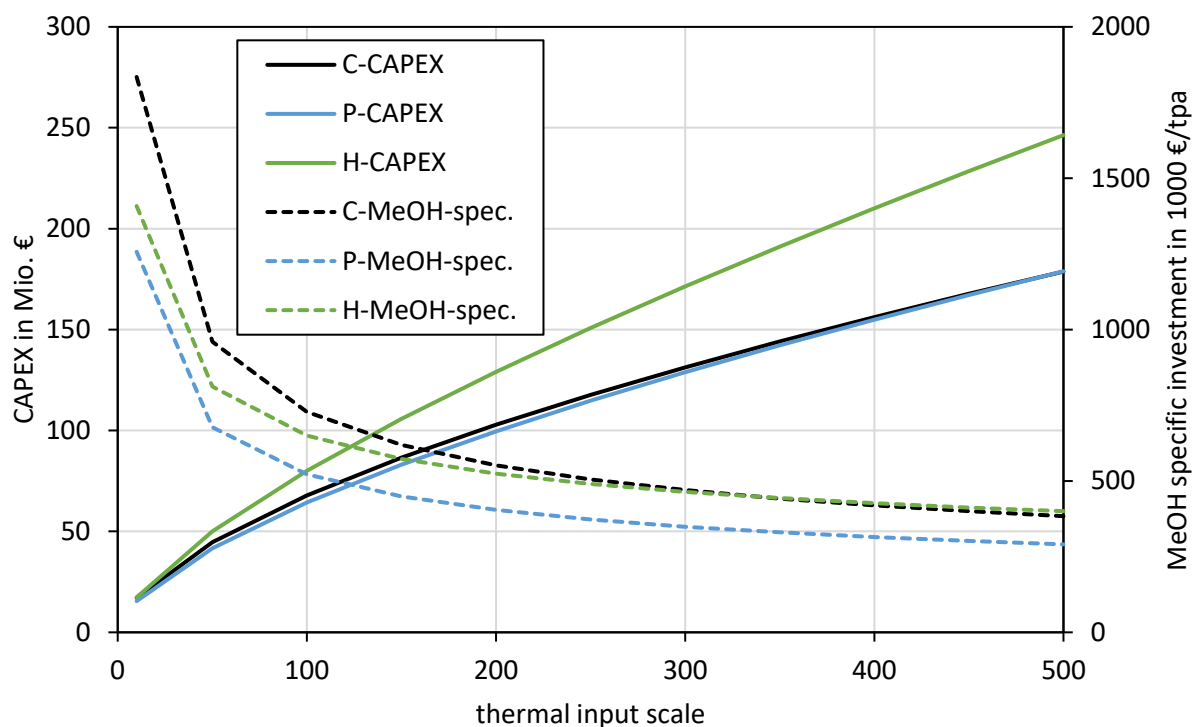


Figure 9: CAPEX and MeOH-specific CAPEX for different scales (cases: C – conventional; H – Hydrogen; P – Plasma)

The graph indicates that a small-scale process chain leads to high methanol-specific investment which consequently drives up the annual cost of the investment and therefore the production cost of methanol within this chain. This shows that small scales are not economically feasible for this kind of process chain. Additionally, Figure 9 also shows the increase of CAPEX with increasing thermal input and the differences for the three configurations. While the conventional and the plasma case show a similar scaling behavior, the hydrogen process chain shows a stronger CAPEX increase for larger scale facilities. This is due to the limited scale of an electrolysis cell as upscaling is only possible by increasing the number of cells and stacks, which leads to a more linear scaling instead of a damped increase as in conventional plants. At large scales this even leads to a lower methanol-specific

investment for the conventional process chain despite the lower methanol yield. For both overall CAPEX as well as methanol-specific investment, the plasma process chain performs best.

Moreover, the behavior of operational costs and revenues can be analyzed. Figure 10 shows the difference between annual cost and revenues i.e., the annual surplus (in disregard of the cost of capital) when the prices of inputs and outputs of the process chains are varied. The prices of electricity, CO₂ emissions and methanol sales are each increased and decreased by 25 % to study their influence.

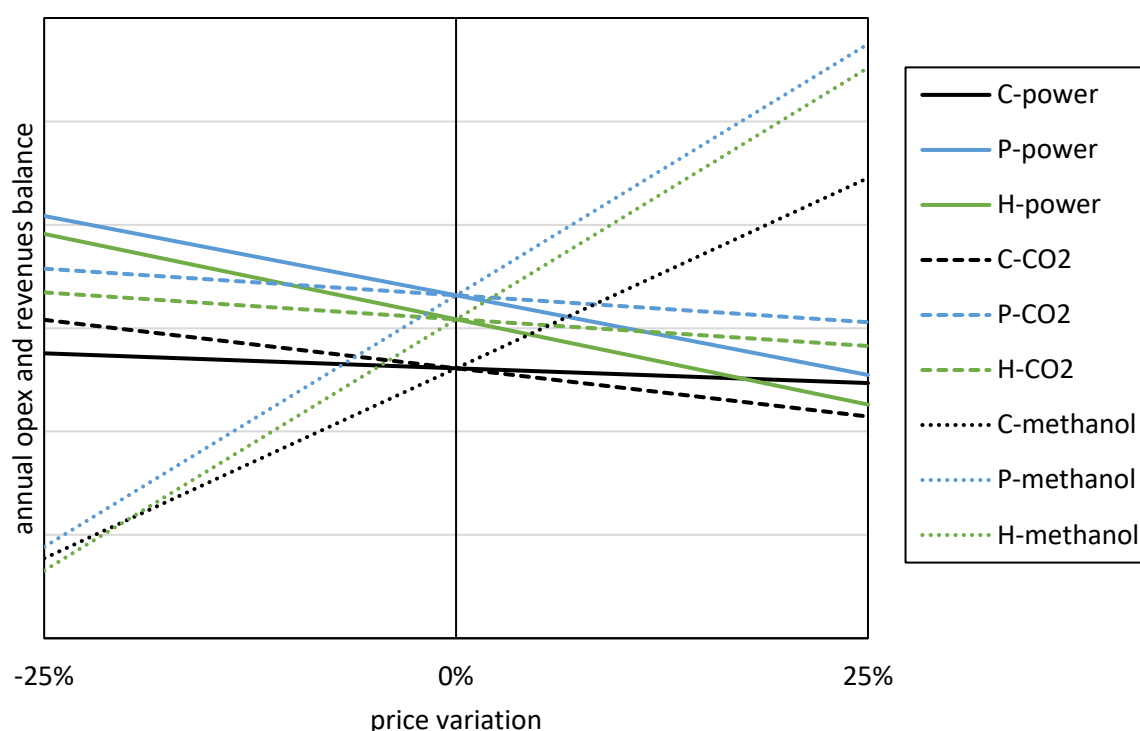


Figure 10: balance of annual cost and revenue for varied prices

First of all, the electricity price is considered. An increase here leads to an increase in OPEX and thus a smaller balance. This effect is stronger for the plasma and hydrogen process chain as their electricity demand is significantly higher. While the cost-revenue-balance is the highest for the plasma case and the lowest for the conventional case in the base scenario, increasing the cost of electricity leads to a crossover between the conventional and the hydrogen process chain and an almost equal balance between the plasma and the conventional process chain. Too high electricity prices therefore endanger the competitiveness of the alternative process chains. A similar but reversed trend can be observed for the methanol price. Since the methanol yield is higher for the non-conventional process chains, their balance shows a higher increase for rising methanol prices than the conventional process chain. A decrease in methanol price leads to a lower balance in all cases that is at very similar values, minimizing the cost performance differences. For the CO₂ emissions, a price increase leads to a decrease in cost-revenue balance for all three process chains, as all three emit CO₂. The decrease is stronger for the conventional process chain as it has the highest emissions. For the full range of price variation, the cost-revenue balance is the lowest for the conventional route. The price of CO₂ would need to go down to around 15 €/t for the conventional route to perform better. Overall, this comparison again shows that the plasma process chains can be an economically attractive option in a framework with low electricity prices and high incentive for carbon emission reduction.

Finally, Table 7 shows a comparison of the processing performance of three feedstock with varying degree of heating value and oxygen content. From an effectiveness perspective, two aspects should be pointed out. For feedstock with high oxygen content (waste wood in this case) in high-temperature gasification, the required oxygen input for heat supply together with the feedstock-bound oxygen already exceeds the minimal demand, with excess oxygen leading to a decreasing syngas yield. This is relevant for conventional and hydrogen-based systems, but can be avoided via plasma application. Second, the achievable carbon recovery via plasma gasification increases with decreasing oxygen content, as more hydrogen can be delivered from steam conversion without limitations from oxygen capacities.

Table 7: Variation of gasification feedstock

Feed Configuration	Waste wood			Refuse derived fuel			Polyethylene waste		
	Conv	Plasma	H ₂	Conv	Plasma	H ₂	Conv	Plasma	H ₂
Oxygen balance [mol/kg feed (waf)]									
Demand	40.57	40.57	40.57	47.78	47.78	47.78	72.34	72.34	72.34
Feedstock	25.63	25.63	25.63	17.88	17.88	17.88	0.00	0.00	0.00
Oxygen	36.15	0.00	36.15	29.07	0.00	29.07	67.92	0.00	67.92
Steam	0.00	14.94	0.00	0.83	29.89	0.83	4.42	72.34	4.42
Net excess	21.20	0.00	21.20	0.00	0.00	0.00	0.00	0.00	0.00
Carbon Recovery	0.42	0.70	0.70	0.58	0.77	0.77	0.67	0.99	0.99
Electricity demand									
[MJ/MJ (LHV feed)]	0.09	0.62	0.74	0.07	0.38	0.41	0.08	0.55	0.61
[MJ/kg MeOH]	2.94	12.26	14.73	2.22	8.99	9.66	2.31	10.97	12.20
OPEX [€ / t MeOH]	230	230	263	131	167	176	99	155	172
CAPEX [€ / (t/y MeOH)]	726	429	619	552	404	524	499	323	473

Conclusions of concept evaluations and outlook

Technological and economical evaluation of direct and indirect integration of renewable power has been conducted. Several conclusions can be drawn from this: Plasma integration is a suitable pathway for decoupling the syngas composition and quality from the energy supply, enabling a more tailored supply of required hydrogen or oxygen depending on the feedstock, and consequently make better material use of feedstock atoms. Plasma heat integration in gasification processes faces similar challenges to electrolysis-based hydrogen production in terms of scaling effects for large-scale facilities, but shows a comparatively small impact on total CAPEX, thereby giving a clear perspective for CAPEX reduction in future low-carbon applications. Further, the shown application advantages for low-value feedstock enable a potentially wide feedstock range. A drawback is the necessity of constant availability of sustainable and low-cost electricity, as flexibility of the heat supply regime in a complex gasification reactor is highly challenging. In this regard, hydrogen integration is advantageous, as it only requires flexibility of downstream processes, which is easier achievable.

A combination of both plasma and electrolysis application could further be promising, combining a high investment efficiency with a potential for near-complete carbon product integration and minimal emissions.

Significant work is necessary on plasma gasification but a lot is already on the way, both in term of technology development as well as identification of optimal pathways and concepts to pursue. Efficiency enhancements in gasification-based application via plasma and hydrogen both appear to be promising pathways to integrate energy for conversion processes from non-fossil sources in order to reduce the consumption of fossil carbon and move towards an anthropogenic carbon cycle.

References

- [1] M. Crippa, B. de Wilde, R. Koopmans, J. Leyssens, J. Muncke, Ritschkoff A-C., K. van Doorselaer, C. Velis, M. Wagner, *A circular economy for plastics: Insights from research and innovation to inform policy and funding decisions*, Brussels 2019.
- [2] Conversio, *Stoffstrombild Kunststoffe in Deutschland 2019*.
- [3] European Commission, *Directive 2008/98/EC of the European Parliament and of the Council of 19 November 2008 on waste and repealing certain Directives: Waste Framework Directive 2018*.
- [4] M. T. Brouwer, E. U. van Thoden Velzen, K. Ragaert, R. ten Klooster, *Sustainability* 2020, 12 (23), 10021. DOI: <https://doi.org/10.3390/su122310021>
- [5] M. Klotz, M. Haupt, S. Hellweg, *Waste management (New York, N.Y.)* 2022, 141, 251 – 270. DOI: <https://doi.org/10.1016/j.wasman.2022.01.002>
- [6] M. Gräbner, *Überblick zu thermochemischen Konversionstechnologien für das chemische Recycling*, Berliner Recycling- and Sekundärrohstoffkonferenz, Berlin 2022.
- [7] M. Gräbner, *Industrial coal gasification technologies covering baseline and high-ash coal*, Wiley-VCH, Weinheim, Germany 2015.
- [8] Nova Institute, *Chemical Recycling – Status, Trends and Challenges: Technologies, Sustainability, Policy and Key Players* 2020.
- [9] A. Helf, A. Baran, M. Gräbner, *Chemical Recycling: Status update and international project developments*, NK2 Workshop “Chemical Recycling”, Leipzig 2023.
- [10] T. Smolinka, N. Wiebe, P. Sterchele, A. Palzer, F. Lehner, M. Jansen, S. Kiemel, R. Miehe, S. Wahren, F. Zimmermann, *Studie IndWEDe. Industrialisierung der Wasserelektrolyse in Deutschland: Chancen und Herausforderungen für nachhaltigen Wasserstoff für Verkehr, Strom und Wärme*, Berlin 2018.
- [11] F. Fabry, C. Rehmet, V. Rohani, L. Fulcheri, *Waste Biomass Valor* 2013, 4 (3), 421 – 439. DOI: <https://doi.org/10.1007/s12649-013-9201-7>
- [12] V. S. Sikarwar, M. Hrabovský, G. van Oost, M. Pohořelý, M. Jeremiáš, *Progress in Energy and Combustion Science* 2020, 81, 100873. DOI: <https://doi.org/10.1016/j.pecs.2020.100873>
- [13] M. Oliveira, A. Ramos, T. M. Ismail, E. Monteiro, A. Rouboa, *Energies* 2022, 15 (4), 1475. DOI: <https://doi.org/10.3390/en15041475>
- [14] Q. Zhang, L. Dor, D. Fenigshtein, W. Yang, W. Blasiak, *Applied Energy* 2012, 90 (1), 106 – 112. DOI: <https://doi.org/10.1016/j.apenergy.2011.01.041>
- [15] <https://inentec.com/pem-technology/deployed-pem-technology/> (Accessed on September 05, 2023).
- [16] <https://www.sgh2energy.com/technology/> (Accessed on September 05, 2023).
- [17] J. Hrbek, *Status report on thermal gasification of biomass and waste* 2022.
- [18] L. Waldheim, *Gasification of waste for energy carriers – a review* 2018.
- [19] M. Gräbner, *Electrification of chemical conversion processes*, NK2 Workshop, Freiberg 2022.

- [20] M. Gräbner, J. Krahl, B. Meyer, *Biomass and Bioenergy* 2014, *64*, 190 – 198.
DOI: <https://doi.org/10.1016/j.biombioe.2014.03.054>
- [21] M. Gräbner, B. Meyer, *Fuel* 2013, *114*, 56 – 63.
DOI: <https://doi.org/10.1016/j.fuel.2012.01.069>
- [22] D. Dave, M. Arné, *Air Separation Unit Update: PEP Review 2016-07* 2016.
- [23] E. C. D. Tan, M. Talmadge, A. Dutta, J. Hensley, J. Schaidle, M. Bidy, D. Humbird, L. J. Snowden-Swan, J. Ross, D. Sexton, R. Yap, J. Lukas, *Process Design and Economics for the Conversion of Lignocellulosic Biomass to Hydrocarbons via Indirect Liquefaction. Thermochemical Research Pathway to High-Octane Gasoline Blendstock Through Methanol/Dimethyl Ether Intermediates*, Golden, CO 2015.
- [24] M. Holst, S. Aschbrenner, T. Smolinka, C. Voglstätter, G. Grimm, *Cost Forecast for Low-Temperature Electrolysis: Technology Driven Bottom-Up Prognosis for PEM and Alkaline Water Electrolysis Systems*, Freiburg 2021.
- [25] W. Peng, H. Chen, J. Liu, X. Zhao, G. Xu, *Energy Conversion and Management* 2021, *245*, 114622. DOI: <https://doi.org/10.1016/j.enconman.2021.114622>

But-1-ene Hydroformylation in a Continuous Gas-phase Membrane Reactor: Road to Industrial Application

A. Al-Shaibani¹, M. Schörner¹, I. Wilson Panjikaran², C. Nentwich², F. Weigelt³, T. Brinkmann³, F. Stenger², R. Franke^{2,4}, M. Haumann¹

¹Friedrich-Alexander-Universität Erlangen-Nürnberg (FAU), Lehrstuhl für Chemische Reaktionstechnik (CRT), Erlangen, Germany

²Evonik Operations GmbH, Marl, Germany

³Helmholtz-Zentrum Hereon GmbH, Geesthacht, Germany

⁴Ruhr-Universität Bochum, Lehrstuhl für Theoretische Chemie, Bochum, Germany

Abstract

Since its discovery by Otto Roelen in 1938, hydroformylation grew to become one of the largest industrial chemical processes utilizing homogeneous catalysts at more than 10 million metric tons of products annually [1]. One of the major challenges for industrial operation is the efficient and complete recycling of the expensive Rh catalyst. Developments in the field of catalysis that allowed the immobilization of a homogeneous catalyst on a solid support gave rise to supported liquid phase (SLP) catalysis. Being a bridge between homogeneous and heterogeneous catalysis, SLP showed great potential in improving current industrial processes significantly. Investigations on this catalytic system demonstrated the employment of rhodium and biphosphos (bpp) ligand with the amine additive sebacate as a liquid phase to catalyze but-1-ene hydroformylation to aldehydes. [2, 3] The catalyst system showed superior performance with selectivities reaching 60% toward n-pentanal and exceptional regioselectivity with linear to total aldehyde ratio of 99%. Given the high reactivity of the formed aldehydes, their consecutive reaction toward aldols must be suppressed for continuous gas-phase SLP catalysis.

Recently, we successfully developed a membrane reactor approach that combined reaction and separation into a single operating unit. A monolithic structure of silicon carbide was coated with polydimethylsiloxane (PDMS) then directly impregnated with the SLP catalyst system. This polymeric membrane layer facilitated the selective separation of the reaction products resulting in n-pentanal rich permeate stream.

In this contribution, we demonstrate this approach with a continuous membrane reactor set-up. The results from kinetic investigations and stability studies were used to implement a membrane reactor model within Aspen Custom Modeler (ACM). This ACM model has been used to scale up the hydroformylation process by a factor of 500. The demonstration reactor will be implemented in a production plant of Evonik in Marl, Germany.

References:

1. Franke, R., et al., Applied hydroformylation. Chemical reviews, 2012, 112(11).
2. Schörner, M., et al., Silicon Carbide Supported Liquid Phase (SLP) Hydroformylation Catalysis - Effective Reaction Kinetics from Continuous Gas-phase Operation. ChemCatChem, 2022. 14(12).
3. Logemann, M., et al., Continuous gas-phase hydroformylation of but-1-ene in a membrane reactor. Green Chemistry 2020. 22(17).

Continuous Processes for the Rh-catalyzed Carbonylation of Olefins and Unsaturated Esters Enabled by Cyclodextrin-mediated Aqueous Biphasic Systems

T. Roth, K. Künnemann, D. Vogt, T. Seidensticker

TU Dortmund University, Department for Biochemical and Chemical Engineering, Laboratory of Industrial Chemistry, Dortmund, Germany

Abstract

Sustainability and efficiency are two crucial values in the chemical industry. One strategy to reach these goals in homogeneous catalysis is the use of environmentally benign solvents in the development of novel, efficient production processes. A successful example is the Rh-catalyzed carbonylation in an aqueous-organic two-phase system. While separation of the aqueous catalyst phase and apolar products is accomplished very effectively, the approach is limited by the solubility of the substrates, which especially holds for long-chain substrates. The resulting need for an intensification technique has long been an area of research that has received great attention. The use of cyclodextrins (CD), cyclic oligosaccharide molecules that form conical cylinders with a hydrophilic surface and a hydrophobic cavity, as mass transfer agents represent a promising avenue for the success of such aqueous biphasic systems (Figure 1, left). Their implementation leads to a potentially economically competitive trade-off between reaction activity and catalyst retention.

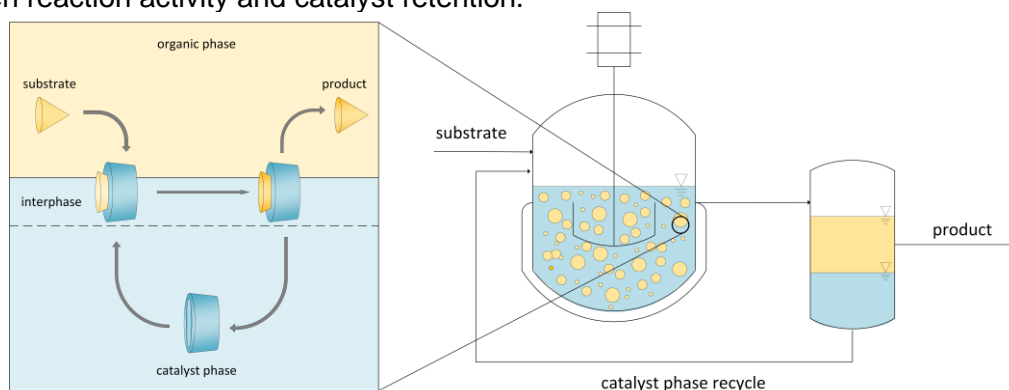


Figure 1: Working principle for cyclodextrin-mediated reaction systems (left). Process design for the recycling of homogeneous catalysts using aqueous biphasic systems (right).

We investigated these reaction systems in a continuous operated miniplant (Figure 1, right) for hydroformylation and hydroaminomethylation (one-pot auto tandem reaction of hydroformylation followed by reductive amination) reactions. After preliminary batch experiments, optimization of different reaction parameters was carried out during continuous operation. At high selectivity's of 80% and yields above 70%, on average only 0.15 mg Rh per kg of main product was lost via the product stream. With such extremely low loss of 0.003 % h⁻¹ of the initial Rh mass (0.24 % overall), being the lowest leaching value ever reported for the HAM at this scale, industrial application comes into reach.

Carbon Chain Building Reactions from Synthesis Gas to Hydrocarbons via a Three-Step Reaction Cycle with Increased Selectivity

Jeroen T. Vossen,^{1,2} Andreas J. Vorholt,¹ Walter Leitner^{1,2}

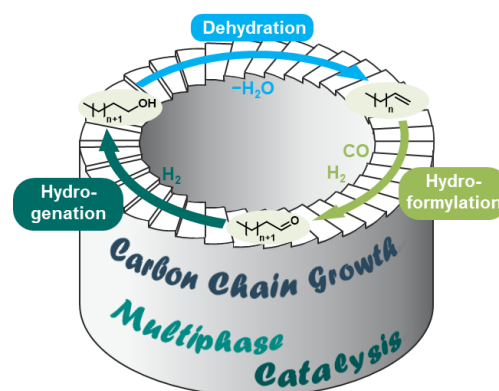
¹ Max Planck Institute for Chemical Energy Conversion, Mühlheim an der Ruhr, Germany

² Institute for Technical and Macromolecular Chemistry, RWTH Aachen University, Aachen, Germany

Abstract

The Fischer-Tropsch process for the conversion of synthesis gas to hydrocarbons currently exceeds a production volume of about 10 million metric tonnes per year as of 2013.^[1-3] As several sectors and product lines such as aviation, heavy duty shipping and polymer production cannot be easily decarbonized, this number is only expected to grow as fossil resources are replaced by renewable feedstocks. The synthesis gas required for Fischer-Tropsch reactions can be derived from renewable and sustainable feed stocks such as biomass gasification and hydrogen produced with green energy.^[4-6] So far, the Fischer-Tropsch reaction yields a broad spectrum of products all the way from methane to long-chain waxes, alcohols and olefins according to an Anderson-Schulz-Flory distribution.^[7] Light gases such as methane in particular cannot be used in further chemical processes and are thus considered waste products.

In this work, we present a synthesis route that improves the carbon chain length selectivity of the hydrocarbons formed from synthesis gas and narrows down the product distribution to selective carbon chain lengths. By a combination of hydroformylation, hydrogenation and dehydration reactions, carbon chains can be elongated to specific value products. The cycle can be ended at one of the desired products: olefins, aldehydes or alcohols. If synthesis gas derived from biomass and bio-ethanol or bio-butanol are used as starting compounds for the cycle, this reaction can be based entirely on renewable resources. A key focus in the development of this system is the catalyst recycling in each of the three steps, reducing waste to a minimum.



References

- [1] P. M. Maitlis, A. de Klerk, *Greener Fischer-Tropsch Processes for Fuels and Feedstock*, Wiley-VCH Verlag & Co. KGaA, Weinheim, **2013**.
- [2] F. Fischer, H. Tropsch, *Brennst. Chem.* **1923**, *4*, 276.
- [3] C. Masters, in *Advances in Organometallic Chemistry*, Vol. 17 (Eds.: F. G. A. Stone, R. West), Academic Press, **1979**, pp. 61-103.
- [4] H. Gruber, P. Groß, R. Rauch, A. Reichhold, R. Zweiler, C. Aichernig, S. Müller, N. Ataimisch, H. Hofbauer, *Biomass Convers. Biorefin.* **2021**, *11*, 2281-2292.
- [5] K.-W. Jun, H.-S. Roh, K.-S. Kim, J.-S. Ryu, K.-W. Lee, *Appl. Catal. A-Gen.* **2004**, *259*, 221-226.
- [6] B. Kamm, *Angew. Chem. Int. Ed.* **2007**, *46*, 5056-5058.
- [7] A. Y. Krylova, *Solid Fuel Chem.* **2014**, *48*, 22-35.

Continuously Operated Hydroaminomethylation in Advanced Multiphase Systems for Efficient Recycling

T. B. Riemer, A. Kampwerth, T. Sinnhoffer, D. Vogt, T. Seidensticker

TU Dortmund University, Department for Biochemical and Chemical Engineering, Laboratory of Industrial Chemistry, Dortmund, Germany.

Abstract

The development of sustainable processes is an ongoing challenge in the chemical industry. In an integrated approach, we combine highly selective homogeneous catalysis with efficient catalyst recycling and product separation and purification. As a means for process intensification, our group developed various thermomorphic multiphase systems (TMS) to reach these objectives. Such a TMS makes use of a temperature-dependent miscibility gap to carry out reactions under monophasic conditions at elevated reaction temperature, avoiding liquid-liquid mass transport limitations. Cooling after reaction leads to the formation of two phases. One phase containing the product and the other phase containing the valuable homogenous catalyst in its active form, which can directly be reused. We successfully applied a TMS consisting of methanol and dodecane for the continuous hydroaminomethylation (HAM) of various longer chain alkenes using molecular hydrogen and CO. We were able to achieve a stable catalyst recycling in a continuously operated miniplant and switch the substrates on stream, highlighting the robustness of this system. However, in these conventional TMS, the apolar product phase contains large amounts of the apolar solvent *n*-dodecane, thus, after decantation still requiring energy-intensive downstream processing.

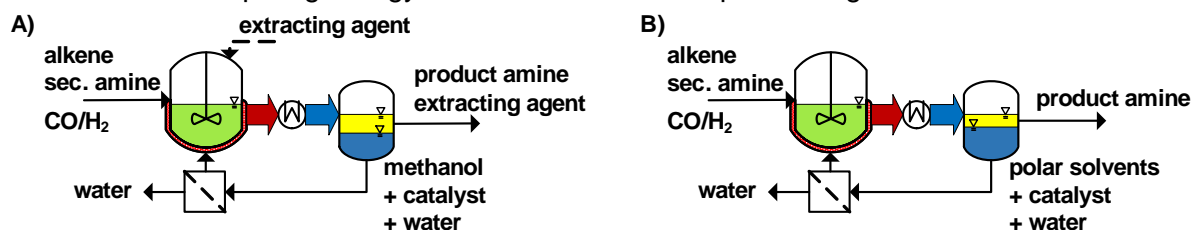


Figure 1: Process flowsheet of continuous hydroaminomethylation in conventional TMS with the nonpolar extracting agent *n*-dodecane **A)** and newly developed TMS without extracting agent **B)**.

Here, we report on a newly developed generation of TMSs that fully omit the use of nonpolar extracting agents to significantly reduce the efforts for product purification. To this end, the composition of green polar solvents is tailored such that the reaction proceeds without mass transport limitation, and an almost solvent-free product phase is formed after cooling. Very successful hydroaminomethylation of 1-decene with diethylamine in a continuously operated miniplant will be presented. In addition, we included an in-situ removal of the by-product water *via* an organic solvent nanofiltration (ONF) membrane. With this approach, we were able to maintain consistent process conditions for over 90 hours with reaction yields to the tertiary amine of up to 79%, providing reliable information about the stability of the novel solvent systems, the homogeneous catalyst and the overall process.

Co-electrolysis and its Integration into Power-to-X Concepts as a Key Step in a Renewable Energy System

E. Reichelt, P. Adam, R. Näke, G. Herz, S. Megel

Fraunhofer IKTS, Fraunhofer Institute for Ceramic Technologies and Systems IKTS, Dresden, Germany

Abstract

Co-electrolysis offers huge potential for increasing achievable efficiencies of Power-to-X processes. Within this work a short overview on co-electrolysis, its advantages and its influence on overall process performance is presented. Experimental results on small-scale co-electrolysis-based plants are given to illustrate the current development status and to demonstrate that the benefits attributed to the technology can actually be shown in technical application.

Introduction

The advantages of high-temperature electrolysis and especially co-electrolysis have been discussed in several publications [1–3]. However, even though high-temperature electrolysis has been demonstrated at a scale close to 1 MW [4], the technology is still often regarded to be on a status somewhere between lab-scale and early demonstration. In this paper a short overview on co-electrolysis technology is presented, highlighting the advantages and the necessary system layout. Own results on small-scale electrolysis-based demonstration plants are given in that context, showing that large-scale application is feasible based on the current development status.

Basics of co-electrolysis

The production of syngas is generally the first step of Power-to-X process concepts. Basically, there are two potential pathways allowing for the electrolysis-based production of syngas (Figure 1).

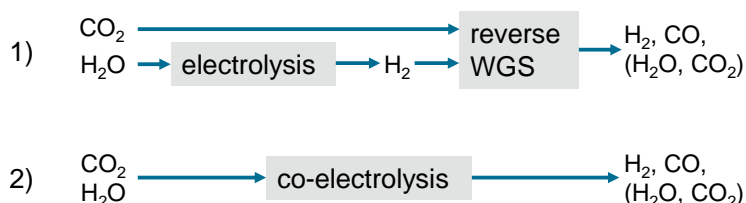


Figure 1: Electrolysis-based pathways for syngas generation.

The first option is the production of hydrogen via



and the subsequent conversion via reverse water-gas shift (rWGS) reaction:



This pathway is the option of choice when applying low-temperature electrolyzers (LTEL). While hydrogen generation in this process concept could generally also be based on high-temperature electrolysis (HTEL), it is more convenient in that case to produce syngas via so-called co-electrolysis, which is presented as the second route in Figure 1. Co-electrolysis is no

independent technology, but rather an operation mode of high-temperature electrolysis (HTEL), which is also known as solid oxide electrolysis (SOEL). A general scheme of a high-temperature co-electrolysis cell is given in Figure 2.

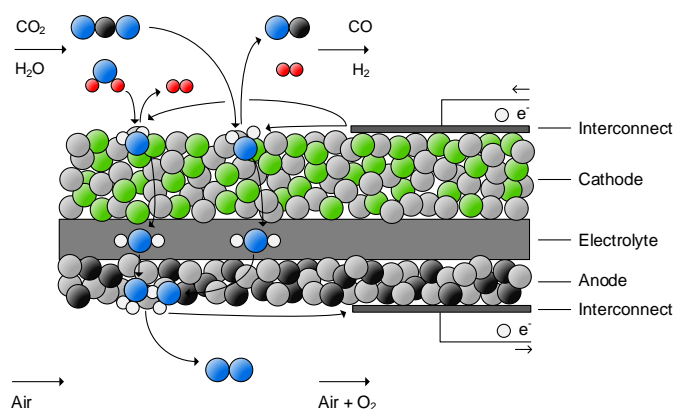


Figure 2: Scheme of a high-temperature co-electrolysis cell.

At temperatures of $\vartheta \approx 700\text{--}900\text{ }^\circ\text{C}$, the active material (Ni) allows not only for the conversion of steam to hydrogen, but also of carbon dioxide (CO_2) into carbon monoxide (CO). In that context CO_2 can be either converted directly via



or via rWGS reaction (Eq. 2) of CO_2 with H_2 , which was formed according to Eq. 1. Even though both options are possible, CO_2 conversion via rWGS has often been found to be prevailing in co-electrolysis operation [3,5–7]. In contrast to pathway 1 from Figure 1, the reactions given in Eqs. 1 and 2 occur in parallel in one apparatus and not subsequently in two. Thus, a higher conversion of CO_2 can be reached applying co-electrolysis in comparison to the two-step low-temperature electrolysis-based approach.

Additionally, co-electrolysis also offers the advantage of a higher energetic efficiency of syngas generation which is offered by the high operating temperatures. While the energy demand of the phase transition from liquid water to gaseous hydrogen has to be provided in form of electric energy for low-temperature electrolyzers, phase transition and reduction can be decoupled with high-temperature electrolyzers. Thus, generating steam by waste heat of an associated process allows to reduce the electric energy demand considerably. As the synthesis step of a Power-to-X process is generally an exothermal, boiling water-cooled process, efficient heat integration of high-temperature co-electrolyzers is possible.

Another advantage of high-temperature co-electrolyzers is the activity of Ni – as the active cathode material – for reforming reactions. Thus, to a certain amount of short-chained hydrocarbons that might be available as by-products, e.g. of a Fischer-Tropsch synthesis, can be converted within the electrolyzer. This might be an interesting option for small-scale systems where the gas phase products of Fischer-Tropsch synthesis cannot be utilized and valorized. To allow for an assessment of co-electrolysis and its potential, a comparison of the two approaches given in Figure 1 is presented in Figure 3. The performance of the syngas production step of a Fischer-Tropsch-based Power-to-X process, as described in Ref. [8], was calculated for the low-temperature electrolysis-based approach and for the one based on co-electrolysis. For the low-temperature electrolysis, a polymer electrolyte membrane electrolysis (PEMEL) was chosen. In order to assess both technological options, the energetic efficiency of the syngas generation step within the Power-to-X process was calculated according to:

$$\eta_{en,syngas} = \frac{P_{ch,syngas}}{P_{el,electrolyzer} + P_{el,compression} + P_{el,pre-heating} + P_{ch,purge\ gas} (+P_{el,evaporation})} \quad \text{Eq. 4}$$

The chemical power was calculated on the basis of the lower heating value (LHV). For the electric energy demand of the electrolyzer losses due to AC/DC conversion were included. Additional assumptions can be derived from Refs. [8,9]. As syngas generation is most often directly coupled with a synthesis step, it is beneficial to integrate both processes as effectively as possible. For the exemplary case presented in Figure 3, combustion of the purge gas of the considered Power-to-X process was integrated into the syngas generation step. The chemical power of the purge gas, which is converted into thermal power, was integrated into the calculation of efficiency according to Eq. 4, as the energy would else have to be provided in form of electric energy.

For the Fischer-Tropsch synthesis an operating pressure (p_{FT}) of 20 bar was assumed. Thus, for the PEMEL-based syngas generation pressurized operation of the electrolyzer was assumed, which leads to a negligible energy demand for water compression and only a comparably small energy demand for CO₂ compression. In case of co-electrolysis the produced syngas has to be compressed, as pressurized operation is technically and economically not feasible [8]. This leads to a higher energy demand for that purpose, as can be seen in Figure 3 a). However, co-electrolysis benefits from the fact that in high-temperature electrolysis the energy demand of evaporation can be decoupled from the electrolysis step, as discussed above. Thus, if waste heat at a temperature level sufficient for steam generation is available, the electric energy demand can be significantly decreased, and energetic efficiency of the syngas production can be increased according to Eq. 4. As especially Fischer-Tropsch synthesis is highly exothermal and generally cooled with boiling water [10,11], steam is frequently available in such a Power-to-X process.

Figure 3 b) highlights that in case of electric evaporation of the necessary water comparable energetic efficiencies for syngas generation of approx. 66 % (PEMEL+rWGS) and 69 % (co-electrolysis) can be reached for both pathways. However, if waste heat from the synthesis reaction is utilized, energetic efficiency ($\eta_{en,syngas}$) of the co-electrolysis approach can be increased to values close to 80 %.

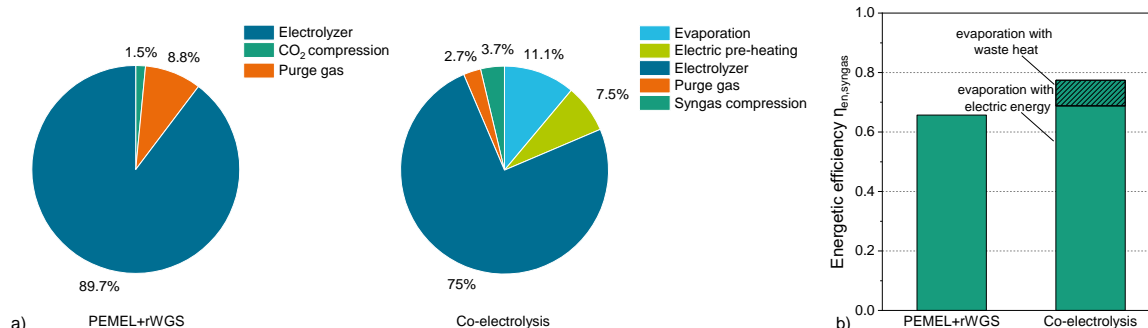


Figure 3: Comparison of PEM electrolysis and subsequent reverse water-gas shift reaction with co-electrolysis for syngas generation within a Fischer-Tropsch-based Power-to-X process: a) energy input to the electrolysis system; b) energetic efficiency.

Co-electrolysis systems

Concepts and process integration

To yield sufficient syngas production capacity co-electrolysis systems have to be built based on the available high-temperature electrolysis cells. As the scales differ considerably, it needs several steps to come from a cell to systems (Figure 4). At first, several cells – generally a number of less than 50 – are stacked with interconnects separating the anode and cathode compartments of different cells but allowing for electric in-series connection along the stack. In order to reach a gas-tight connection, glass sealants between the cells are applied. After assembly of all components, the stacks are joined at high temperatures, generally in the range of $\vartheta > 900$ °C. The joining step is an additional process step in comparison to the manufacturing process of low-temperature electrolyzers, leading to the stack being one single gas-tight

unit. Therefore, in comparison to low-temperature electrolyzers, single cells within a stack cannot be replaced. For the current stack technology, the nominal power input to a co-electrolysis stack is generally less than 10 kW.

In order to reach sufficient system scales to combine the electrolysis with a subsequent synthesis step, it is state of the art to build modules containing several stacks as well as the necessary gas processing apparatuses (heat exchangers, electric heaters). Parallelization of several modules allows for reaching appropriate system sizes (Figure 4).

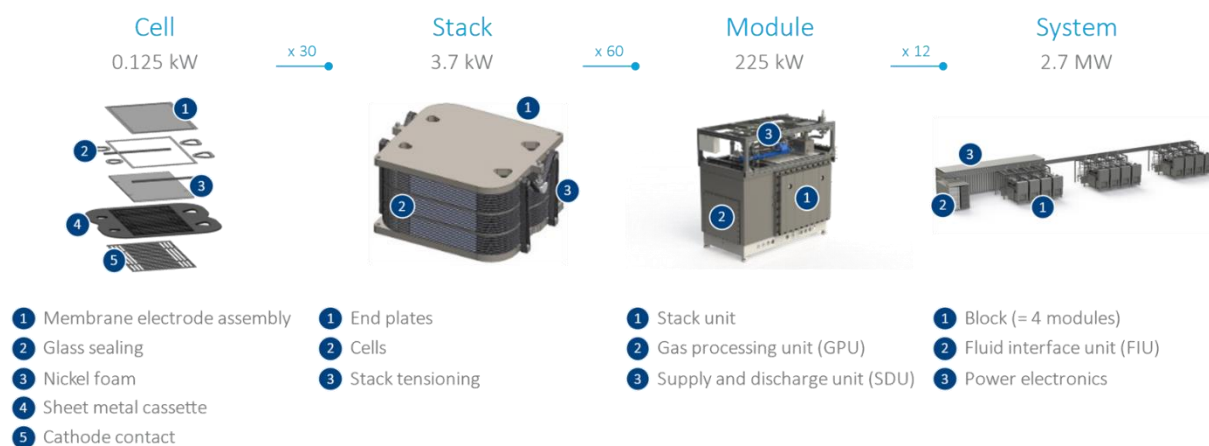


Figure 4: Different scales of co-electrolysis development (© Sunfire).

A flow sheet of a co-electrolysis system consisting of m modules with n stacks each is given in Figure 5. CO_2 and water are fed to the system (1,2). The necessary steam can be produced from waste heat of an associated process or via electric heating (3). As outlined above, the option to utilize waste heat offers a considerable reduction in electric energy demand. Downstream of the evaporation step, the cathode feed gases have to be distributed to the m modules (4–6) of the electrolysis system. Within a specific module, the cathode feed gases are heated against the produced syngas in a counter-current heat exchanger (4). Due to heat losses and limited exchanger efficiency the inlet gases cannot be heated up to the operating temperature of the n stacks. To compensate these losses, an electric pre-heater (5) is often applied downstream of the heat exchanger to heat up the gases to the temperature of the electrolysis stacks or above. The electric heater is also necessary during startup, in order to heat up the system to operation temperature. After conversion of the feed gases on the cathode of the cells within the stack unit (6), the produced syngas is cooled down via a counter-current heat exchanger. The conversion within the cells is limited. This is due to a considerably increasing voltage at high conversion. Additionally, at the resulting high current densities degradation rate increases considerably [12]. Thus, the conversion within the electrolyzer is generally limited to values in the range of approx. 80 %. Unconverted water is condensed in the syngas cooling step (7,8) prior to compression of the produced syngas (10) to the desired operating pressure of the downstream synthesis process. The condensed water can be recycled to increase the utilization of water.

High-temperature electrolyzers in general need a certain amount of reducing gases at the inlet of the cathode to prevent oxidation of the electrode material [5,13,14]. Therefore, part of the produced syngas is recycled (9) to achieve a fraction of reducing gases (H_2 , CO) at the inlet of the cathode, generally in the range of approx. 5 %.

The generation of pure oxygen (O_2) in high-temperature electrolyzers is challenging [12,15–17]. Thus, the anode is often purged with a gaseous medium, most often air. The purge medium is also heated up in a counter-current heat exchanger (4) and an electric pre-heater (5).

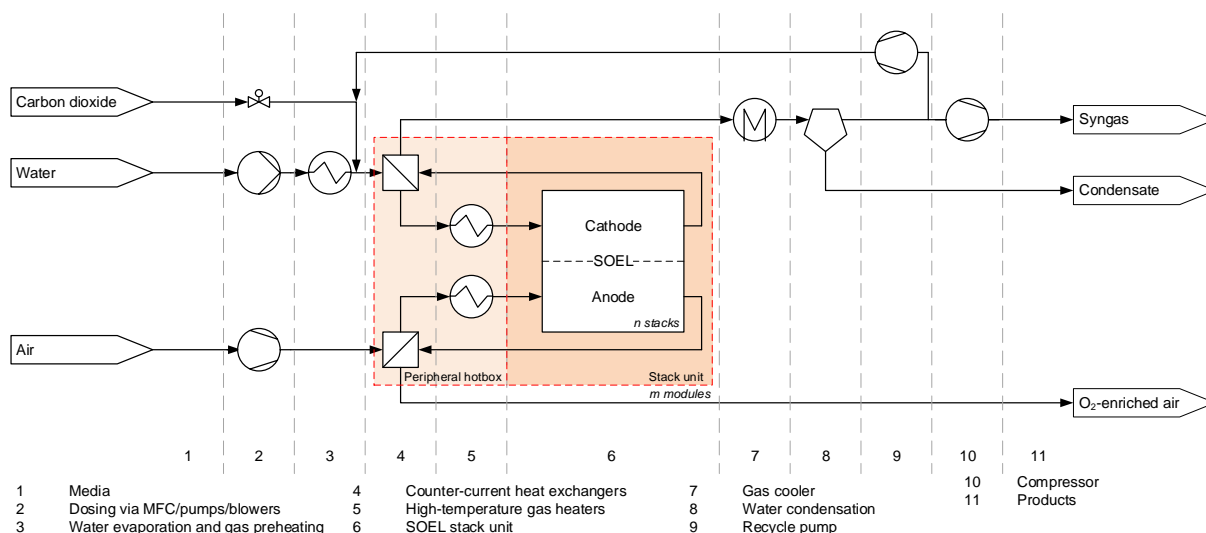


Figure 5: General process scheme of a high-temperature co-electrolysis system (MFC: mass flow controller; SOEL: solid oxide electrolysis).

As outlined above, there are several advantages of a deep integration of the co-electrolysis step into the associated Power-to-X process. A simplified process scheme highlighting these options is given in Figure 6. The most important option – determining the potential for highly efficient syngas production via high-temperature co-electrolysis – is the utilization of waste heat from the exothermal synthesis reaction for water evaporation and, thus, for a decrease in electric energy demand. Another mentioned integration option is the recirculation of less valuable short-chained hydrocarbon products into the co-electrolyzer for internal reforming into syngas.

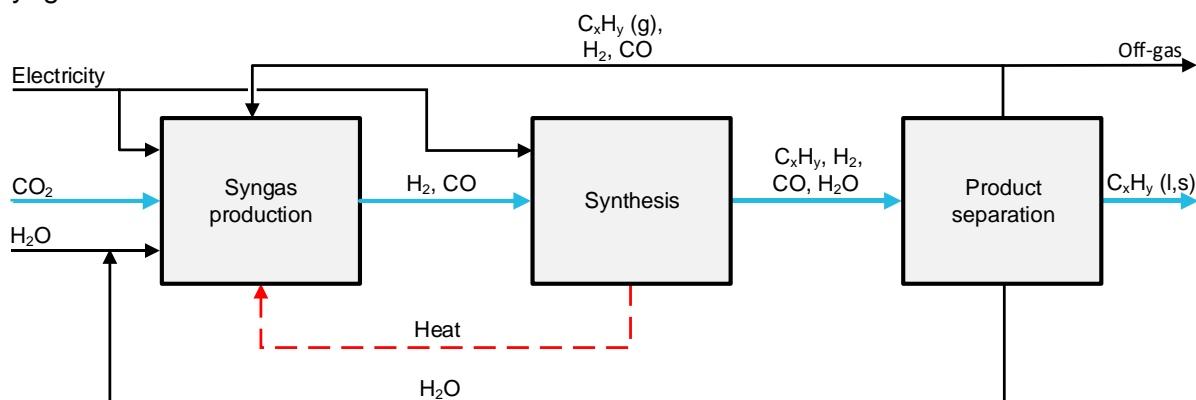


Figure 6: Simplified process scheme of a Fischer-Tropsch-based Power-to-X process highlighting potential means of process integration.

As already shown in Figure 3 there is a huge potential for increasing the efficiency by utilizing waste heat, which also transfers to the overall Power-to-X process applying a co-electrolyzer. In Figure 7, literature data on the overall energetic efficiency of such a process are compared depending on the applied syngas generation technology. The energetic efficiency applied for this comparison is based on the chemical power of the synthesis products (LHV), e.g. methanol or Fischer-Tropsch hydrocarbons, and the electric energy input to the overall process, also including the synthesis step.

The results in Figure 7 depict that the increase in efficiency, when applying a co-electrolyzer, is mainly due to the waste heat integration for steam generation, as concepts based on the two-step approach applying high-temperature water electrolysis and an rWGS step also yield nearly comparable process efficiencies as co-electrolysis-based concepts allow for. However, when it comes to the operational implementation applying co-electrolysis allows to omit one costly process step in the overall process – the rWGS reactor.

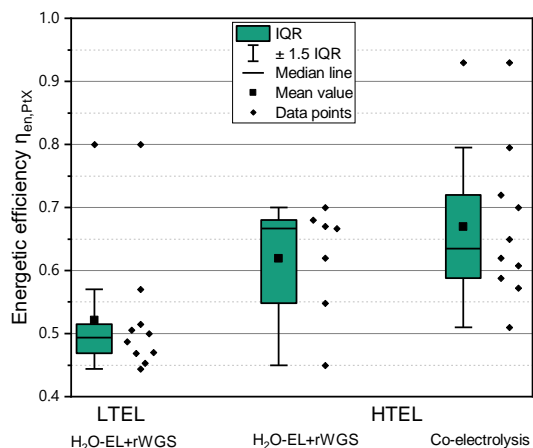


Figure 7: Literature data on the energetic efficiency of Power-to-X processes based on different syngas generation schemes [18–41] (IQR: interquartile range; LTEL: low-temperature electrolysis; HTEL: high-temperature electrolysis).

Thus, there are several advantages of high-temperature co-electrolysis. However, besides technical aspects, for implementation and utilization at industrial scale also economics are of major importance. Currently, cost for high-temperature electrolyzers are considerably higher than for low-temperature electrolyzers (Figure 8). Therefore, the effect of decreased operational expenditures in form of electric energy could be offset by the higher capital expenditures. It is expected that the differences in cost between the technologies decrease in future with increasing maturity of the technology. Improvements in cell technology, increased stack footprints and especially more automation in the manufacturing process are expected to drive the cost degradation.

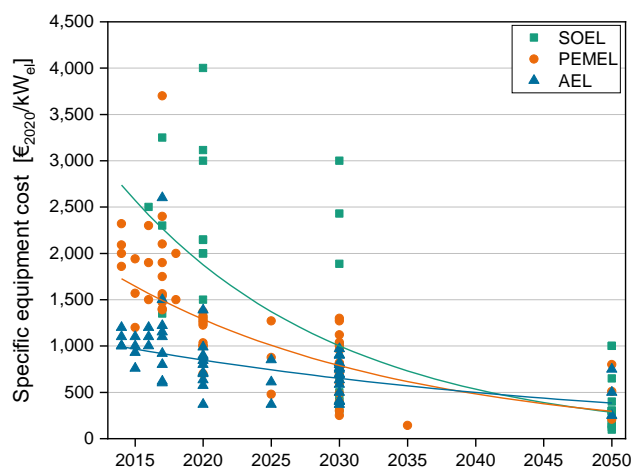


Figure 8: Expected cost degradation for the different electrolysis technologies (AEL: alkaline electrolysis; PEMEL: polymer electrolyte membrane electrolysis; SOEL: solid oxide electrolysis) (adapted from [42]).

Technical realization

Even though co-electrolysis offers huge potential for the application in Power-to-X processes, experimental results on stand-alone plants are rather scarce [43,44]. Therefore, experimental data on a small-scale co-electrolyzer consisting of a single module with four 30-cell stacks and a nominal input power of $P_{el,nom,DC} = 12 \text{ kW}$ have been presented by the authors in Ref. [45]. To give some insights on the performance of co-electrolyzers, a short overview of the results will be given in the following.

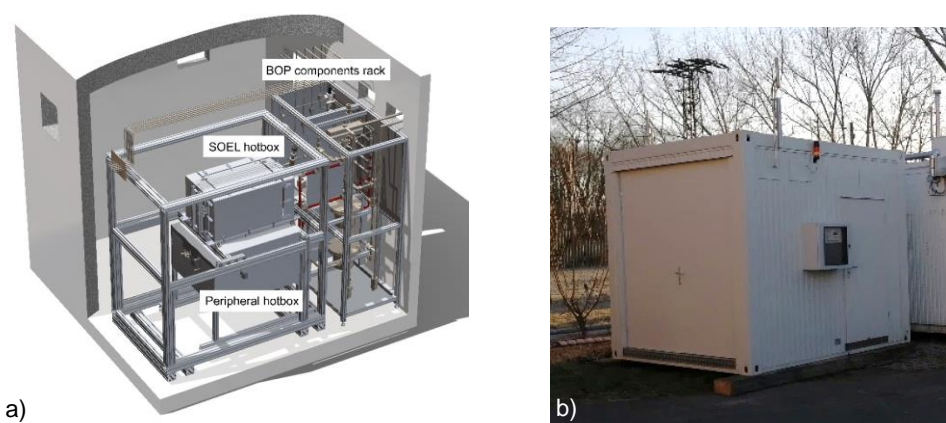


Figure 9: a) CAD model of the containerized electrolysis plant; b) Co-electrolysis container at operational site [45].

In Figure 9 a) a CAD model of the containerized plant is given. The thermally isolated stacks (SOEL hotbox) are placed in close proximity to the peripheral hotbox containing both the necessary heat exchangers as well as the electric heaters. The automated and fully self-sustained plant was operated remote at a biogas facility in Thallwitz, Germany. In Figure 9 b) the co-electrolysis container is shown at its operational site.

The plant was operated in steam electrolysis and co-electrolysis mode under different loads at atmospheric pressure (Figure 10). The small-scale plant could be operated highly dynamic – when at operation temperature – over a wide range of operating conditions. Part-load operation was possible down to approx. 10 % of the nominal load. Given the fact that the system was rather small and, thus, heat losses of the hotbox to the surrounding are more significant than for large-scale systems, smaller values should be achievable for systems of industrially relevant size.

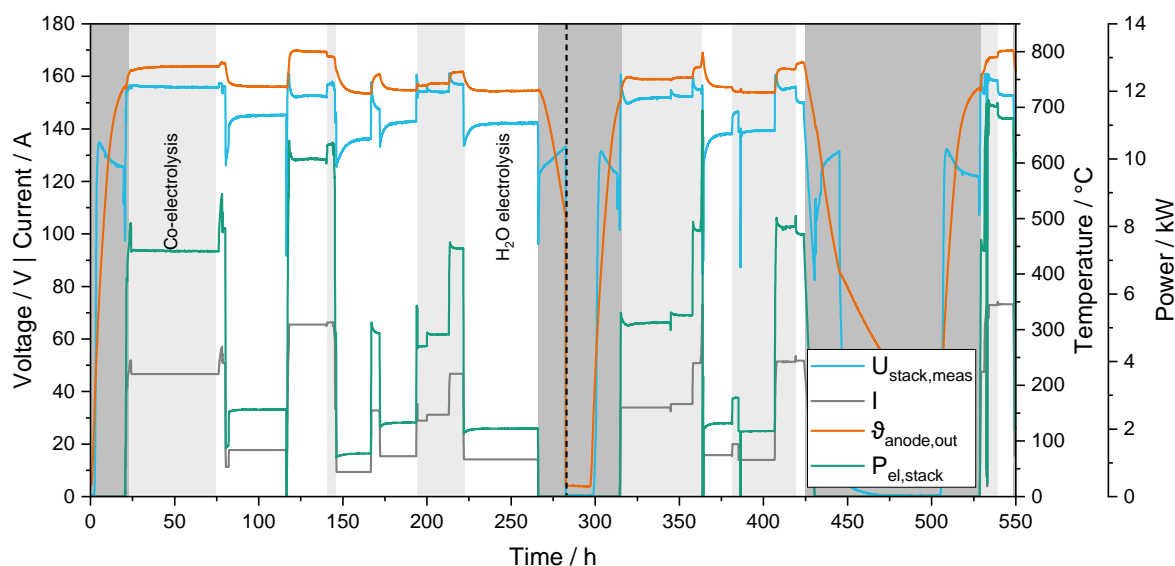


Figure 10: Overview of the trend of key parameters during the conducted tests. Data on stack voltage $U_{stack,meas}$, current I , anode outlet temperature $\vartheta_{anode,out}$ and electric power $P_{el,stack}$ is given. Operation in H_2O electrolysis mode is highlighted by a white background, co-electrolysis mode is represented by light grey. Startup and shutdown operation is highlighted by dark grey. The dotted line at approx. 280 h represents a longer shutdown period due to maintenance work at the site [45].

A Sankey diagram depicting the energy flows within the small-scale co-electrolyzer is given in Figure 11. Due to the high operating temperature large parts of the energy intrinsic to the streams are thermal energy. A significant share of this thermal energy can be reutilized within the system to decrease overall energy demand. The importance of heat recuperation within such a system as well as the high energetic efficiency that can be reached by applying co-electrolysis for syngas generation is highlighted by the data. For operation under full load in

co-electrolysis mode the small-scale electrolyzer reached an energetic efficiency (LHV) of 76.2 % with electric evaporation of the feed water. If the energy for evaporation would have been supplied in form of waste heat, an efficiency (LHV) of 88.1 % would have resulted. However, it has to be mentioned that in comparison to the values given in Figure 3 no losses for AC/DC conversion as well as no compression of the syngas have been considered. Applying valid assumptions for these two energy consumers leads to comparable and, thus, still very high values for energetic efficiency of syngas generation.

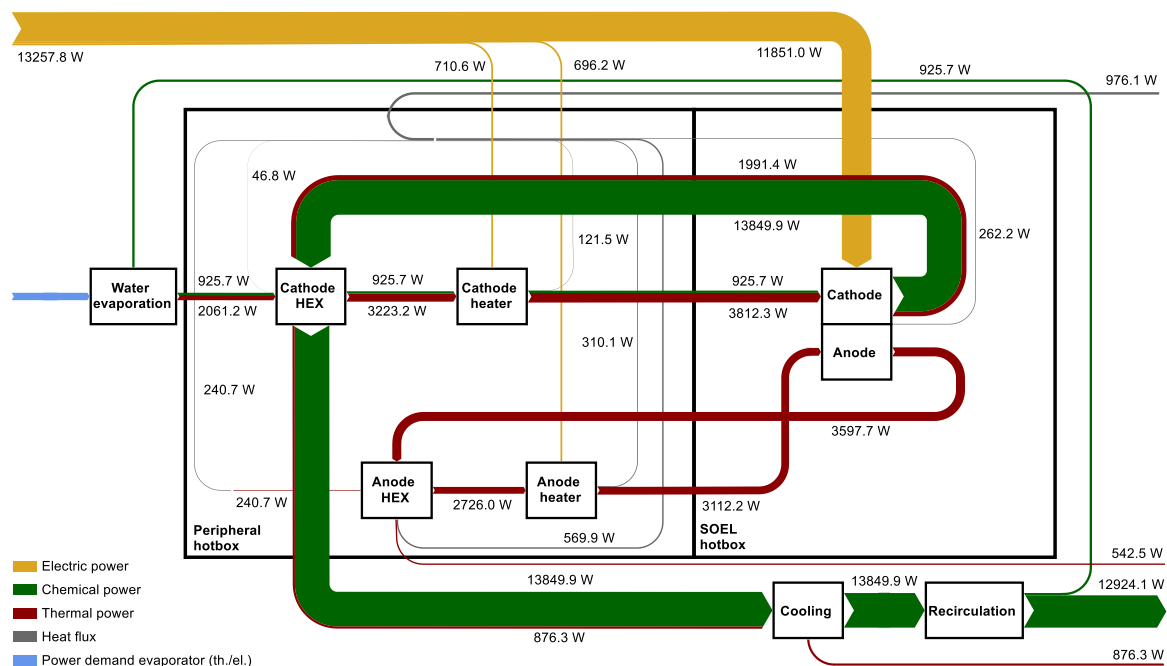


Figure 11: Sankey diagram on the energy balance of the electrolyzer in co-electrolysis mode at $P_{el,stack} \approx 12 \text{ kW}$ [45].

In order to gain insights into system integration, a co-electrolyzer and a small-scale Fischer-Tropsch reactor were coupled on laboratory scale (Figure 12). The results of this work are given in detail in Ref. [46]. Within this plant, a ten-cell stack ($P_{el,nom,DC} = 1 \text{ kW}$) was applied for co-electrolysis. For the Fischer-Tropsch synthesis, a fixed-bed reactor loaded with an industrial Co catalyst was applied.



Figure 12: Lab-scale Power-to-X plant [46].

Focus of the tests was to assess the influence of a recycle of the gaseous hydrocarbons products as well as of the unreacted syngas. During the course of the experiments, the recycle ratio was increased step-wise. In order to hold the syngas composition constant, with every increase in recycle ratio the operating conditions of the electrolyzer were adjusted. The results presented in Figure 13 highlight that this adjustment worked out well as the product composition and the per-pass conversion for the Fischer-Tropsch synthesis were comparable for all tested recycle ratios.

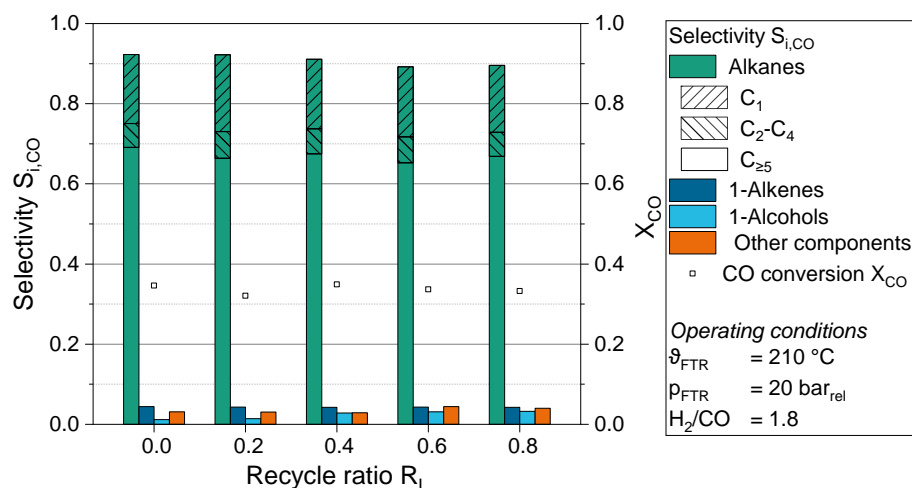


Figure 13: Product composition and per-pass conversion of the Fischer-Tropsch synthesis for varying recycle ratios R_L [46].

However, the recirculation had considerable influence on the performance of the overall system, as can be derived from Figure 14 a). By increasing the recycle ratio the carbon efficiency of the process could be increased, because carbon bound in CO , CO_2 and hydrocarbons could be used again. It has to be noted that the overall values for carbon efficiency, especially in once-through operation were quite low. This is due to the fact that conversion in the Fischer-Tropsch reactor was chosen to be rather low to offer some leeway in the conducted variations. For more information it is referred to Ref. [46].

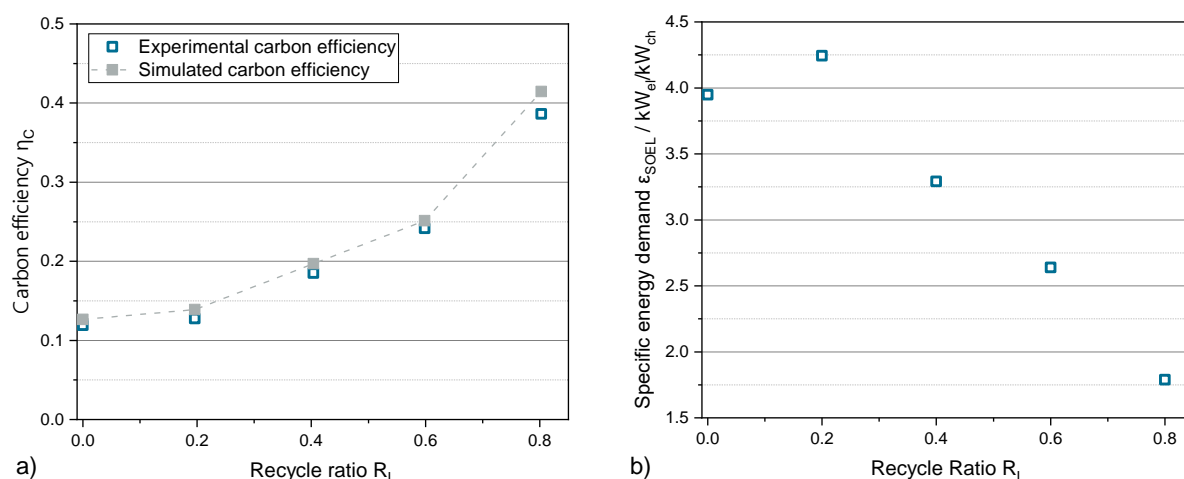


Figure 14: a) Correlation of experimentally and theoretically derived carbon efficiency η_C for varying recycle ratios R_L ; b) Specific energy demand ϵ_{SOEL} for varying recycle ratios R_L [46].

Figure 14 b) highlights how the electric energy demand decreases by increasing the recycle ratio. As not only unreacted H_2 and CO as the relevant components of syngas but also hydrocarbons – that can be converted to syngas within the co-electrolyzer via internal reforming – are recycled and the overall syngas stream is held constant, the electric energy demand for syngas production is reduced considerably.

The results of the two realized small-scale plants highlight that the advantages of high-temperature co-electrolysis cannot only be shown in theoretical works [8,9] but also on a technical scale. A demonstration plant with a nominal input power of $P_{el, nom, DC} = 12$ kW combining co-electrolysis and Fischer-Tropsch synthesis is currently under construction.

Conclusion

The presented results show the advantages of co-electrolysis in high-temperature electrolyzers. The demonstration plants that were applied to generate the presented results were realized on a rather small-scale. However, as the important features for integration into Power-to-X processes were included, it is possible to transfer these concepts to larger scale plants. This upscaling is a current focus of engineering and construction work at Fraunhofer IKTS. This focus is in line with the current efforts of commercial co-electrolyzer manufacturers.

Acknowledgments

The presented research was supported by the Federal Ministry of Economic Affairs and Climate Action (03EWS001A) and the Federal Ministry of Education and Research (03ZZ0741A).

References

- [1] Y. Wang, T. Liu, L. Lei, F. Chen, *Fuel Process. Technol.* 161 (2017) 248.
- [2] A. Hauch, R. Küngas, P. Blennow, A.B. Hansen, J.B. Hansen, B.V. Mathiesen, M.B. Mogenssen, *Science* 370 (2020).
- [3] S.R. Foit, I.C. Vinke, L.G.J. de Haart, R.-A. Eichel, *Angew. Chem. Int. Ed.* 56 (2017) 5402.
- [4] K. Schwarze, P. Meisel, R. Blumentritt, K. Hauptmeier, O. Posdziech, *Meet. Abstr. MA2021-03* (2021) 188.
- [5] S. Diethelm, J. van herle, D. Montinaro, O. Bucheli, *Fuel Cells* 13 (2013) 631.
- [6] S.-W. Kim, H. Kim, K.J. Yoon, J.-H. Lee, B.-K. Kim, W. Choi, J.-H. Lee, J. Hong, *J. Power Sources* 280 (2015) 630.
- [7] S.D. Ebbesen, R. Knibbe, M. Mogensen, *J. Electrochem. Soc.* 159 (2012) F482-F489.
- [8] G. Herz, C. Rix, E. Jacobasch, N. Müller, E. Reichelt, M. Jahn, A. Michaelis, *Appl. Energy* 292 (2021) 116655.
- [9] G. Herz, N. Müller, P. Adam, S. Megel, E. Reichelt, M. Jahn, *Chem. Ing. Tech.* 92 (2020) 1044.
- [10] M. Iglesias Gonzalez, B. Kraushaar-Czarnetzki, G. Schaub, *Biomass Conv. Bioref.* 1 (2011) 229.
- [11] M. Konarova, W. Aslam, G. Perkins, Fischer-Tropsch synthesis to hydrocarbon biofuels: Present status and challenges involved, in: *Hydrocarbon Biorefinery*, Elsevier, 2022, pp. 77–96.
- [12] Y. Wang, W. Li, L. Ma, W. Li, X. Liu, *J. Mater. Sci. Technol.* 55 (2020) 35.
- [13] Q. Cai, E. Luna-Ortiz, C.S. Adjiman, N.P. Brandon, *Fuel Cells* 10 (2010) 1114.
- [14] G. Cinti, G. Discepoli, G. Bidini, A. Lanzini, M. Santarelli, *Int. J. Energy Res.* 40 (2016) 207.
- [15] B.-K. Park, Q. Zhang, P.W. Voorhees, S.A. Barnett, *Energy Environ. Sci.* 12 (2019) 3053.
- [16] M.S. Khan, X. Xu, R. Knibbe, Z. Zhu, *Renewable Sustainable Energy Rev.* 143 (2021) 110918.
- [17] J. Mikkola, K. Couturier, B. Talic, S. Frangini, N. Giacometti, N. Pelissier, B.R. Suredreddy, O. Thomann, *Energies* 15 (2022) 1168.
- [18] F.G. Albrecht, T.-V. Nguyen, *Energy* 192 (2020) 116511.
- [19] M.J. Bos, S. Kersten, D. Brillman, *Appl. Energy* 264 (2020) 114672.
- [20] G. Botta, M. Solimeo, P. Leone, P.V. Aravind, *Fuel Cells* 15 (2015) 669.

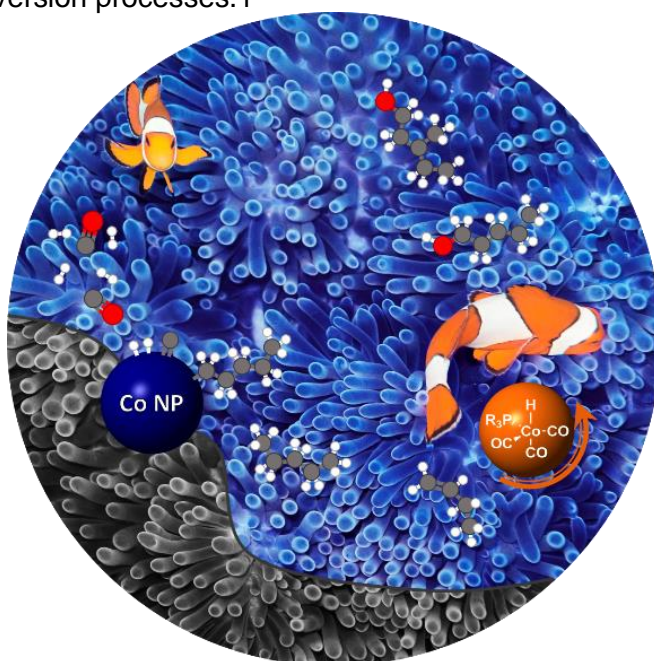
- [21] Q. Fu, J. Dailly, A. Brisse, M. Zahid, *ECS Trans.* 35 (2011) 2949.
- [22] C. Graves, S.D. Ebbesen, M. Mogensen, K.S. Lackner, *Renewable Sustainable Energy Rev.* 15 (2011) 1.
- [23] A. Jess, P. Kaiser, C. Kern, R.B. Unde, C. von Olshausen, *Chem. Ing. Tech.* 83 (2011) 1777.
- [24] S. Michailos, S. McCord, V. Sick, G. Stokes, P. Styring, *Energy Convers. Manage.* 184 (2019) 262.
- [25] J.B. Hansen, N. Christiansen, J.U. Nielsen, *ECS Trans.* 35 (2011) 2941.
- [26] M. Marchese, E. Giglio, M. Santarelli, A. Lanzini, *Energy Convers. Manage.* 6 (2020) 100041.
- [27] D. Mignard, C. Pritchard, *Chem. Eng. Res. Des.* 84 (2006) 828.
- [28] D. Parigi, E. Giglio, A. Soto, M. Santarelli, *J. Cleaner Prod.* 226 (2019) 679.
- [29] R. Rivera-Tinoco, M. Farran, C. Bouallou, F. Auprêtre, S. Valentin, P. Millet, J.R. Ngameni, *Int. J. Hydrogen Energy* 41 (2016) 4546.
- [30] S. Schemme, J.L. Breuer, M. Köller, S. Meschede, F. Walman, R.C. Samsun, R. Peters, D. Stolten, *Int. J. Hydrogen Energy* 45 (2020) 5395.
- [31] A. Tremel, P. Wasserscheid, M. Baldauf, T. Hammer, *Int. J. Hydrogen Energy* 40 (2015) 11457.
- [32] L. Wang, M. Chen, R. Küngas, T.-E. Lin, S. Diethelm, F. Maréchal, J. van herle, *Renewable Sustainable Energy Rev.* 110 (2019) 174.
- [33] H. Zhang, U. Desideri, *Energy* 199 (2020) 117498.
- [34] H. Zhang, L. Wang, J. van herle, F. Maréchal, U. Desideri, *Energies* 12 (2019) 3742.
- [35] F.G. Albrecht, D.H. König, N. Baucks, R.-U. Dietrich, *Fuel* 194 (2017) 511.
- [36] W.L. Becker, R.J. Braun, M. Penev, M. Melaina, *Energy* 47 (2012) 99.
- [37] D.H. König, *Techno-ökonomische Prozessbewertung der Herstellung synthetischen Flugturbinentreibstoffes aus CO₂ und H₂*, Institut für Energiespeicherung der Universität Stuttgart, 2016.
- [38] D.H. König, M. Freiberg, R.-U. Dietrich, A. Wörner, *Fuel* 159 (2015) 289.
- [39] J.P. Stempien, M. Ni, Q. Sun, S.H. Chan, *Energy* 81 (2015) 682.
- [40] G. Cinti, A. Baldinelli, A. Di Michele, U. Desideri, *Appl. Energy* 162 (2016) 308.
- [41] F.V. Vázquez, J. Koponen, V. Ruuskanen, C. Bajamundi, A. Kosonen, P. Simell, J. Ahola, C. Frilund, J. Elfving, M. Reinikainen, N. Heikkinen, J. Kauppinen, P. Piermartini, *J. CO₂ Util.* 28 (2018) 235.
- [42] E. Jacobasch, G. Herz, C. Rix, N. Müller, E. Reichelt, M. Jahn, A. Michaelis, *J. Cleaner Prod.* 328 (2021) 129502.
- [43] R. Blumentritt, A. Surrey, J. Kaufhold, *Verbundvorhaben P2X: Erforschung, Validierung und Implementierung von "Power-to-X" Konzepten - Teilvorhaben Q0.*
- [44] O. Posdziech, T. Geißler, K. Schwarze, R. Blumentritt, *ECS Trans.* 91 (2019) 2537.
- [45] E. Reichelt, P. Adam, R. Näke, G. Herz, S. Megel, *Energy Technol.* 11 (2023) 2300086.
- [46] G. Herz, M. Gallwitz, R. Näke, S. Megel, M. Jahn, E. Reichelt, *Energy Technol.* 11 (2023).

Combining Fischer Tropsch and Hydroformylation for long Chain Alcohols from Syngas

K. Jeske, T. Rösler, M. Belleflamme, W. Leitner, A. J. Vorholt, G. Prieto
Max Planck Institute for chemical energy conversion

Abstract

The selective conversion of syngas to higher alcohols is an attractive albeit elusive route in the quest for effective production of chemicals from alternative carbon resources. We report the tandem integration of solid cobalt Fischer–Tropsch and molecular hydroformylation catalysts in a one-pot slurry-phase process. Unprecedented selectivities (>50 wt%) to C₂ + alcohols are achieved at CO conversion levels >70 %, alongside negligible CO₂ side-production. The efficient overall transformation is enabled by catalyst engineering, bridging gaps in operation temperature and intrinsic selectivity which have classically precluded integration of these reactions in a single conversion step. Swift capture of 1-olefin Fischer–Tropsch primary products by the molecular hydroformylation catalyst, presumably within the pores of the solid catalyst is key for high alcohol selectivity. The results underscore that controlled cooperation between solid aggregate and soluble molecular metal catalysts, which pertain to traditionally dichotomic realms of heterogeneous and homogeneous catalysis, is a promising blueprint toward selective conversion processes.¹



¹ K. Jeske, T. Rösler, M. Belleflamme, T. Rodenas, N. Fischer, M. Claeys, W. Leitner, A. J. Vorholt, G. Prieto, *Angew. Chem.*, 2022, 61, 31, e202201004 DOI: [10.1002/anie.202201004](https://doi.org/10.1002/anie.202201004)

Promotor Effect on Fe-based Catalysts for CO₂-FTS: A XAS Study

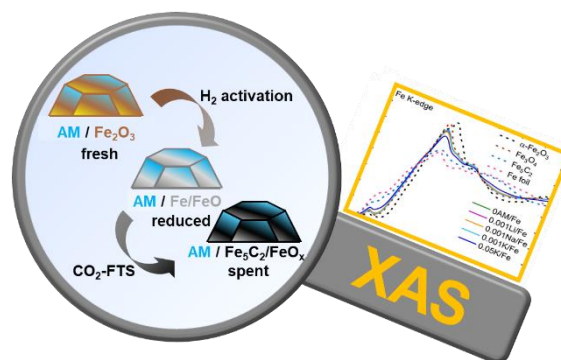
E. Saraçi¹, Q. Yang², E. Fedorova², D. Doronkin¹, E. Kondratenko²

¹Institute for Catalysis Research and Technology (IKFT), Karlsruhe Institute of Technology (KIT), Karlsruhe

²Leibniz Institute for Catalysis e.V. (LIKAT), Rostock

Abstract

Processes that store renewable H₂, from wind and solar power, in energy-dense molecules, like the Fischer-Tropsch synthesis (FTS) are in the core of a successful energy transition.¹ While the classical CO-FTS is more common², the CO₂-FTS that utilizes atmospheric CO₂ and green H₂ is highly desirable and also feasible.³ Fe-based catalysts have the ability to catalyze this reaction and are the most industrially relevant catalysts. Iron carbides, formed *in situ*, are considered the catalytically active species in the CO-FTS.⁴ These catalysts are often modified by alkali metal dopants, which act as electronic and/or structural promoters for improving product selectivity/activity. In addition, these promoters are assumed to enhance catalyst basicity required for CO/CO₂ adsorption and to stabilize iron carbides against oxidants (H₂O and CO₂). However, their function is still under debate and their role remains unclear. Therefore, it is of eminent importance to understand effect of these dopants on the formation of Fe-carbide species during activation and reaction. Therefore, in this collaborative study we used in-situ X-ray absorption spectroscopy (XAS) to identify the structure of alkali-promoted iron catalysts during reduction and under CO₂-FTS reaction conditions⁵. Insights on its reducibility and carbide formation aid the knowledge-based optimization of FTS catalysts as well as other catalytic processes where alkali promoters are used.



Scheme 1. XAS study of alkali metal (AM) promoted Fe-based catalyst in fresh, reduced and spent state.

References

1. G. Prieto, ChemSusChem, **2017**, 10, 1056.
2. M. Loewert, M. A. Serrer, T. Carambia, M. Stehle, A. Zimina, K. F. Kalz, H. Lichtenberg, E. Saraci, P. Pfeifer, J. D. Grunwaldt, React Chem Eng, **2020**, 5.
3. E. V. Kondratenko, G. Mul, J. Baltrusaitis, G. O. Larrazábal, J. Pérez-Ramírez, En. Env. Sci., **2013**, 6, 3112.
4. M. Albrecht, U. Rodemerck, M. Schneider, M. Bröring, D. Baabe, E. V. Kondratenko, Appl. Catal., **2017**, 204, 119.
5. Q. X. Yang, V. A. Kondratenko, S. A. Petrov, D. E. Doronkin, E. Saraci, H. Lund, A. Arinchtin, R. Kraehnert, A. S. Skrypnik, A. A. Matvienko, E. V. Kondratenko, Angew Chem Int Edit, **2022**, e202116517.

Controlling the Complex Reaction Network of the Hydrogenation of CO to Higher Alcohols Using Co-based Catalysts Derived from Prussian Blue Analogues

P. Diehl, P. Telaar, M. Muhler

Laboratory of Industrial Chemistry, Ruhr University Bochum, Bochum, Germany

Abstract

Higher alcohol synthesis (HAS) can play an important role in the development towards reducing CO₂ emissions since the obtained product mixtures containing higher alcohols as well as olefins can be applied as climate-neutral fuels and bulk chemicals, provided that the synthesis gas is obtained using renewable electricity to produce H₂ and industrial exhaust gases as carbon source.^[1] Recently, a new promising class of catalysts derived from prussian blue analogues (PBAs) was reported for the heterogeneously catalyzed CO hydrogenation to higher alcohols.^[2] Pyrolysis of the K-promoted Co- and Mn-containing PBAs resulted in the metal atoms being embedded in a unique functionalized carbon matrix, which enabled a facile carbidization of Co to Co₂C, which is the crucial phase for HAS.^[3,4] In contrast to established HAS catalysts,^[5,6] a rather unusual product spectrum was obtained including primary and secondary alcohols, aldehydes, acids, and olefins. Consequently, a complex reaction network was proposed for this catalyst including the carbide-based mechanism, carbonylation of primary alcohols, reductive hydroformylation of olefins, and hydration of olefins.^[2]

Due to this plethora of occurring reactions, this network offers various opportunities to influence the obtained product spectrum by modification of the catalyst preparation and implementation of suitable promoters. One example is the addition of different amounts of Cu to the PBA-based catalysts aiming at the acceleration of the carbonylation reaction, which was deemed the most important mechanism,^[2] by increasing the amount of methanol. Another example is the adjustment of the K content by intensive washing after the synthesis of the PBA precursor. Besides catalytic long-term testing, the different catalysts were thoroughly characterized by XRD, TG-MS, N₂ physisorption, ICP-MS, TEM-EDX, XPS, and N₂O-RFC, thereby providing comprehensive information about the capabilities of PBA-based HAS catalysts and the reaction network. Finally, the relevance of the choice of the reaction conditions will be addressed taking the dependance of the selectivities on conversion and the strong exothermicity of the involved reactions into account.

Acknowledgements

The research project was funded by the German Federal Ministry of Education and Research (Bundesministerium für Bildung und Forschung, BMBF, Verbundvorhaben Carbon2Chem®, L-4: C₂₊-Alkohole, C₂₊-Olefine, synthetische Kraftstoffkomponenten, FKZ: 03EW0008C).

References

- [1] International Energy Agency, *World Energy Outlook 2021*, **2021**.
- [2] P. Telaar, S. Schmidt, P. Diehl, P. Schwiderowski, M. Muhler, *submitted to ChemCatChem* **2023**.
- [3] V. M. Lebarbier, D. Mei, D. H. Kim, A. Andersen, J. L. Male, J. E. Holladay, R. Rousseau, Y. Wang, *J. Phys. Chem. C* **2011**, *115*, 17440.
- [4] Y.-P. Pei, J.-X. Liu, Y.-H. Zhao, Y.-J. Ding, T. Liu, W.-D. Dong, H.-J. Zhu, H.-Y. Su, L. Yan, J.-L. Li, W.-X. Li, *ACS Catal.* **2015**, *5*, 3620.
- [5] C. Göbel, S. Schmidt, C. Froese, T. Bujara, V. Scherer, M. Muhler, *J. Catal.* **2021**, *394*, 465.
- [6] J. Anton, J. Nebel, C. Göbel, T. Gabrysch, H. Song, C. Froese, H. Ruland, M. Muhler, S. Kaluza, *Top. Catal.* **2016**, *59*, 1361.

About the Art to Prepare Mixed SAPO-CHA/MFI Catalyst Materials for Methanol-to-olefins Reaction

M. Seifert¹, L.A. Haufe¹, R. Shiyanova¹, F. Ahmadi¹, H. Rahimi¹, J.J. Weigand¹

¹Technische Universität Dresden, Faculty of Chemistry and Food Chemistry, Inorganic Molecular Chemistry, Dresden, Germany

Abstract

Since the start of the millennium, efforts to use alternative and sustainable hydrocarbon sources for essential chemical supplies have driven the growing commercialization of the "methanol-to-olefins" (MTO) process. Current research endeavours a predominantly rely on established systems, yet the refinement of catalyst stability and olefin selectivity remains a critical pursuit. Notably, industrially significant materials including SAPO materials featuring the CHA structure (SAPO-34) and aluminosilicates with the MFI structure (ZSM-5), which have emerged as good performing contenders. Depending on the density of the active site, the higher selectivity of SAPO-34 is attributed, among other things, to generally milder acid centers due to framework phosphates. The long-term stability of ZSM-5 is attributed to lower transport limitation despite stronger acid centers.

Consequently, an ideal MTO catalyst amalgamates ZSM-5's transport properties with the mild acid centers of SAPO-34, necessitating a delicate charge balance of framework phosphates, silicates, and aluminates to uphold structural integrity.

The study comprehensively assesses divers synthetic pathways for mixed-phase SAPO-CHA/MFI materials, encompassing (a) distinct hydrothermal crystallization coupled with grinding, (b) a sequential hydrothermal synthesis approach, and (c) a combination through spray crystallization. The results show that the interfaces between both structures and contact points are crucial for flexible tuning the performance in MTO process from the material crystallization perspective, but also from the proximity perspective.

Introduction

The ongoing surge in the commercialization of more sustainable industrial processes within the oil refining, petrochemistry, and the energy sector has spurred the development and advancement of novel catalysts as integral component of the methanol economy. [1] Emerging from diverse carbon sources such as organic waste (biomass), CO₂ from carbon capture and utilization (CCU) strategies,[2] as well as lingering fossil resources (e.g., coal) in the "coal to liquid" (CtL) process [3], the conversion of synthesis gas (a blend of carbon monoxide and (green) hydrogen) *via* Fischer-Tropsch synthesis (FTS),[4] or through the utilization of small alcohols using Mobil alcohol conversion processes, offers a flexible interim technology to establish a sustainable hydrocarbon supply within the existing petrochemistry infrastructure. [5, 6] Presently, industrial facilities and complexes are already capable of producing olefins, with annual capacities reaching 1,600,000 tons through methanol conversion (coal-based) in China (e.g., Baofeng Group), and by employing natural gas (*via* methanol) in United States (e.g., UOP/Hydro). Forecasts predict a doubling of these capacities every two years for the escalating energy, transportation, and basic materials self-reliance.[6-8]

The aim of this research is to unravel the intricacies behind various preparation methodologies employed for crafting mixed-phase catalyst materials. This pursuit seeks to offer a comprehensive overview of prospects and challenges associated with research catalyst

produced *via* hydrothermal synthesis, as well as an industry-oriented catalyst structures showcased in spray crystallization. From distinct perspectives, the synthesis of mixed-phase materials unveil not only added challenges and adaptability within the context of sustainability paradigms, but also unexpected structural elegance that can be seen through microscopy.

Experimental

The chemicals employed for this investigation include sodium silicate solution (Na_2SiO_3 , Supelco), silicic acid (referred to as “heavy”, SiO_2 , Grüssing), sodium aluminate (NaAlO_2 , technical grade, Sigma-Aldrich), aluminium oxide (Al_2O_3 , PURAL SB), orthophosphoric acid (85%, Fisher Scientific), sodium hydroxide (analytical grade, Fisher scientific), tetrapropylammonium bromide (TPAB, > 98.0 %, TCI), sulfuric acid (H_2SO_4 , 95-97 %, VWR), ammonium nitrate (NH_4NO_3 99 %, Grüssing), morpholine (purum, USSR), kaolin (Sigma-Aldrich), aluminium chloride ($\text{AlCl}_3 \cdot 6\text{H}_2\text{O}$, Alfa Aesar), and methanol (CH_3OH 99.9 %, TCI). All chemicals were used as received. Additionally, commercial reference catalysts NH_4 -ZSM-5 (with a Si/Al ratio of 25, designated as CBV-5524G, Zeolyst Inc.) and H-SAPO-34 (from SKU: MSSA3421, ACS Material, LLC) were used as received as well.

Synthesis of Catalyst Materials: The synthesis of **Na-ZSM-5** was performed with sodium silicate solution as the source of silicon, sodium aluminate for aluminum, sodium hydroxide and sulfuric acid for pH and sodium adjustment, deionized water, and TPAB as an organic template. Subsequent to synthesis, calcination was performed in an air flow until reaching 540°C , with a dwell time of 12 hours. To acquire **H-ZSM-5**, ion exchange was performed three times with 0.1 M solution of NH_4NO_3 , followed by calcination after synthesis at 450°C for 12 hours. This procedure was akin to preliminary work.[9] The synthesis of **H-SAPO-34** materials was achieved through the combination of orthophosphoric acid, aluminum oxide, silicic acid, morpholine, and water in the molar ratio 1 Al : 1 P : 0.5 Si : 1.5 morpholine : 30 water.[10] The synthesis was performed by adding all ingredients together, aging at room temperature for 24 hours, and subsequent hydrothermal synthesis conducted at 183°C for 3.5 days, with a stirring rate of 180 rpm. This was executed in a stainless steel autoclave with PTFE inlet (E2500 by Berghof). After washing with water, the materials were subjected to calcination 540°C for 12 h in air. The process of **physically mixing SAPO-34 with ZSM-5** entailed careful balancing and grinding with a mortar, followed by overnight drying at 65°C . For the autoclave synthesis of **mixed-phase SAPO-34 / ZSM-5**, the initially crystallized H-SAPO-34 served as addition to the aged gel of Na-ZSM-5, 10 minutes prior to transferring to the autoclave for hydrothermal crystallization. **Grains of SAPO-34 / ZSM-5** from spray crystallization were prepared by blending 30 wt.% kaolin (dry weight), 20 wt.% aluminum chloride (solid), and 50 wt.% zeolite/zeolite-like material as solid constituents. Additionally, an excess of 230 % water was introduced to form a homogeneous slurry at pH 3 with 8 min of ultrasonication. The materials were subsequently processed using a Büchi B290 spray drying equipped with 2 feed nozzle (slurry and compressed air), operating at 200°C as per recent reports.[11]

Materials Characterization: The morphology of the synthesized samples was analyzed utilizing a **scanning electron microscopy** (SEM) on a SU8020 from Hitachi HTE. For this purpose, samples were mounted on carbon pads affixed to an aluminum sample holder. A coating of gold was applied using rotary-pump coating system Q150R ES from Quorum. The accelerating voltage was set to 2 kV, with magnification varying between $\times 1,000$ and $\times 10,000$. Further analytical methods and catalytic properties will be demonstrated during the oral presentation. Worth mentioning are dynamic **nitrogen physisorption** measurements, conducted to ascertain the specific surfaces of the samples. The measurements were performed using a ThermoScientific specific surface analyser (Surfer). Prior to measurement, samples were pre-dried at 250°C under vacuum for 8 hours to remove all adsorbed molecules. The outcome of the surface analysis, based on physisorption of nitrogen, were assessed using the B.E.T. theory and the B.J.H. method. For examining changes in long-range crystalline order, **X-ray powder diffraction** experiments were undertaken using STADI P X-ray powder diffractometer from STOE. Diffractograms were recorded through transmission measurement

of the solid samples using Cu-K α_1 radiation (1.5406 Å) at room temperature within the range between 5 to 90° 2 θ . **Dynamic laser scattering** was used to deduce particle size distribution, utilizing a **Bettersizer S3 Plus** by 3P Instruments. The wet dispersion procedure involved stirring at 2000 rpm and ultrasonication at 200 W (26 kHz) for 2 min. Data acquisition and processing were done in accordance with ISO 13320:2009, and calculation of particle size distribution was conducted using the Mie theory. For determining the water content of saturated samples, **thermogravimetric analysis** was carried out using the TG50 instrument from Mettler Toledo. For this purpose, 20 to 40 mg of sample were heated from 35°C to 850°C, within a nitrogen stream at a heating rate of 10 K/min.

Results and Discussion

The hydrothermal synthesis of ZSM-5 yielded agglomerated crystals of small but irregular shape (Si/Al = 50), whereas SAPO-34 typically exhibited cubic-shaped crystallites (see *Figure 1*). Apart from the Si : Al : template (TPAB, Na) ratio for ZSM-5 [9] and the P : Si : Al : template (morpholine, triethyl amine) ratio for SAPO-34, [10, 12] the morphology and size of the final product from hydrothermal crystallization were influenced by crystallization parameters as well as the sources of P, Si and Al. An option for producing mixed-phase materials is through physical mixing, which includes grinding and ultrasonication. However, this approach does not result in a stable proximity between the crystals.

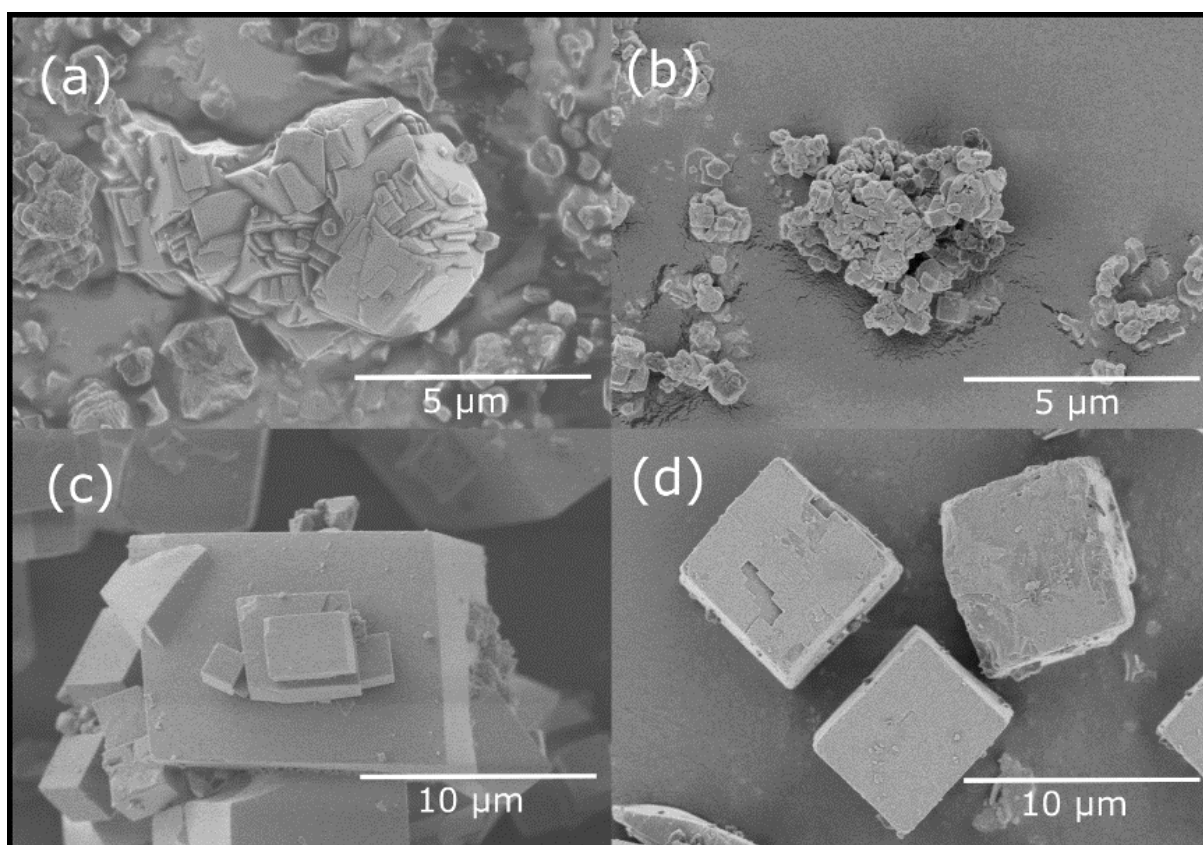


Figure 1. SEM images at magnification of x10,000 of (a, b) **ZSM-5** and x5,000 of (c, d) **SAPO-34** from hydrothermal crystallization and purchased from commercial enterprises (*Zeolyst Inc.* and *ACS Material, LLC*).

In 2017, Liu et al. proposed a method to grow ZSM-5 by impregnating TPAB on a previously grown SAPO-34 material. [5] Although microwave-assisted crystallization is challenging to scale up for industrial purposes, the crucial challenge of step-wise batch-mode hydrothermal crystallization in steel autoclaves is the extended crystallization time required for ZSM-5

(> 4 days) depending on the Si/Al ratio. [9] This often leads to decomposition of the previously formed SAPO-34. Instead of impregnating the organic template TPAB to SAPO-34 while adding other ingredients stepwise, an alternative approach involves introducing H-SAPO-34 to ZSM-5 gel shortly before transferring to the autoclave vessel. This results in a gradual growth of ZSM-5 on the expense of SAPO-34 decomposition and gel transformation (see *Figure 2*). To prevent complete amorphization of SAPO-34 with crystallization time, the crystallization speed of ZSM-5 needs to be enhanced by raising the temperature. This has been previously achieved on small scale using microwave synthesis at 180°C, [5] as opposed to the standard 150°C in autoclave vessels [9]. With the addition of Si and Al sources to the SAPO-34 material, a silica-rich gel readily forms, causing a decrease in SAPO-34 fraction and the initiation of ZSM-5 growth. However, even after 4 days SAPO-34 still exists and crystallization of amorphous gel to ZSM-5 is not complete (see *Figure 2*).

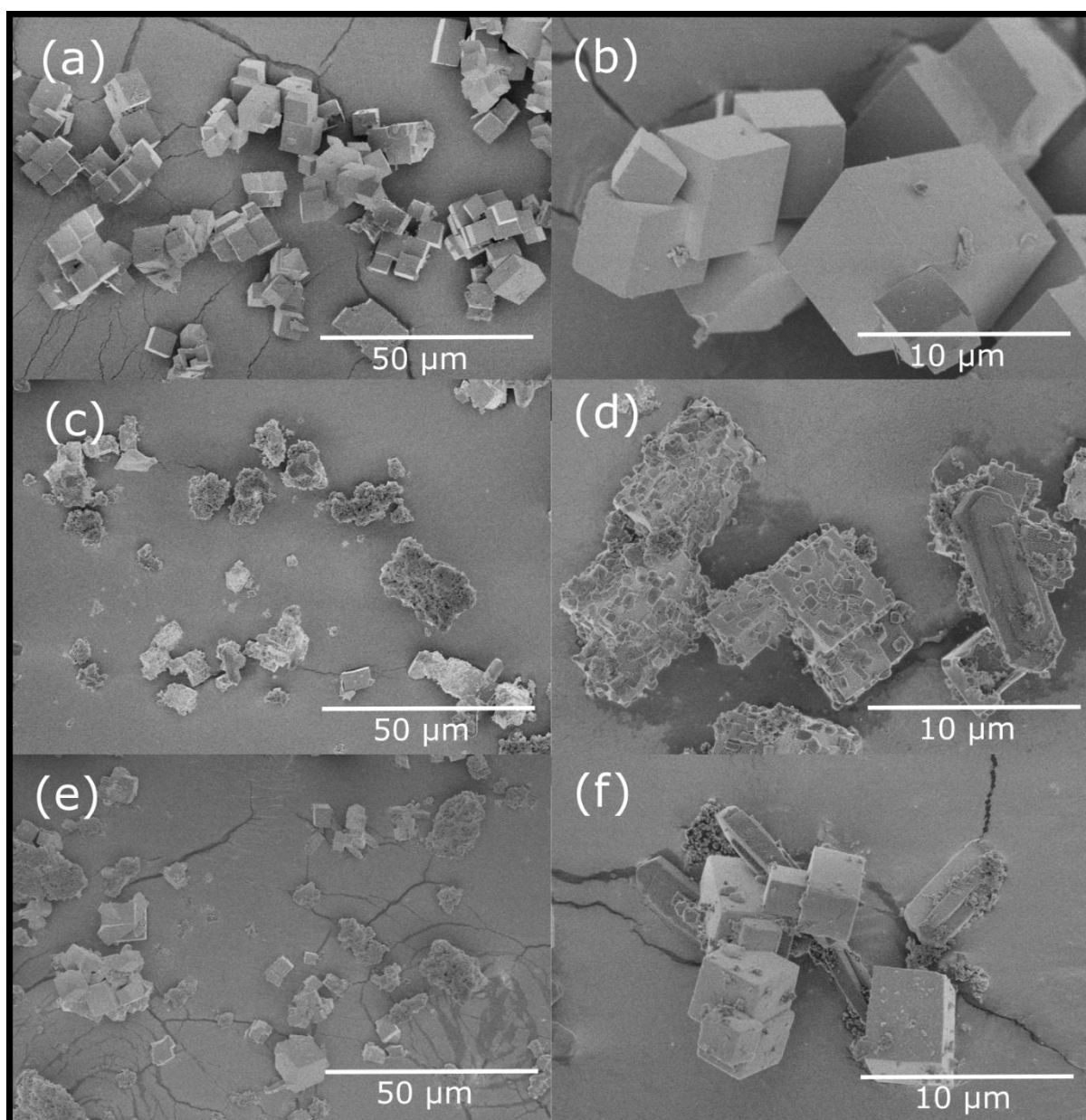


Figure 2. SEM images at magnification of x1,000 (a,c,e) and x5,000 (b,d,f) of two-step mixed-phase synthesis of **SAPO-34 / ZSM-5** (a,b) initially produced SAPO-34, (c,d) subsequently grown ZSM-5 and synthesis gel on SAPO-34 material after 2 days; (e,f) mixed material after 4 days.

However, the zeolite (ZSM-5) and zeolite-like materials (SAPO-34) described earlier are primarily employed as research catalysts due to their limitations. These include their packing density, high pressure drop in fixed-bed reactors, or their unfavorable rheological behavior in fluid bed reactors, as highlighted in the context of the methanol conversion reaction. [13] Consequently, further efforts for industrial-scale applications are hindered. Depending on the deactivation speed in methanol-to-olefins reaction and the necessary regeneration through coke combustion in air, extrudates [14] or pellets for fixed-bed reactor configuration (for slow coking, ~24h) are recommended. Alternatively, spherical grains from spray crystallization [15, 16] are suggested for fast coking scenarios.

For the demonstration of spray drying, akin to the production of FCC catalysts and additives, [11] an additional level of flexibility is achieved the utilization of ZSM-5 and SAPO-34 in well-defined ratio, positioned in close proximity on the surface of a catalyst grain (Figure 3). To harness this inherent flexibility, the materials should be used without undergoing additional destructive preparation steps, such as ion exchanges required to generate the active solid acid sites. During the process of spray crystallization, the inclusion of Al-based, Na-free binder serves a dual purpose: it prevents shelling or undesired surface coverage, while concurrently, reactive porous materials like NH₄-zeolite (or H-zeolite) are employed. This combination enables the amalgamation of thermally induced binding together and the process of deammonization or activation *via* the final calcination in an air atmosphere. Additionally, the size of the porous components (ZSM-5, SAPO-34) resulting from ultrasonication with the spray slurry plays a pivotal role in determining their accessibility within the subsequently formed grain.

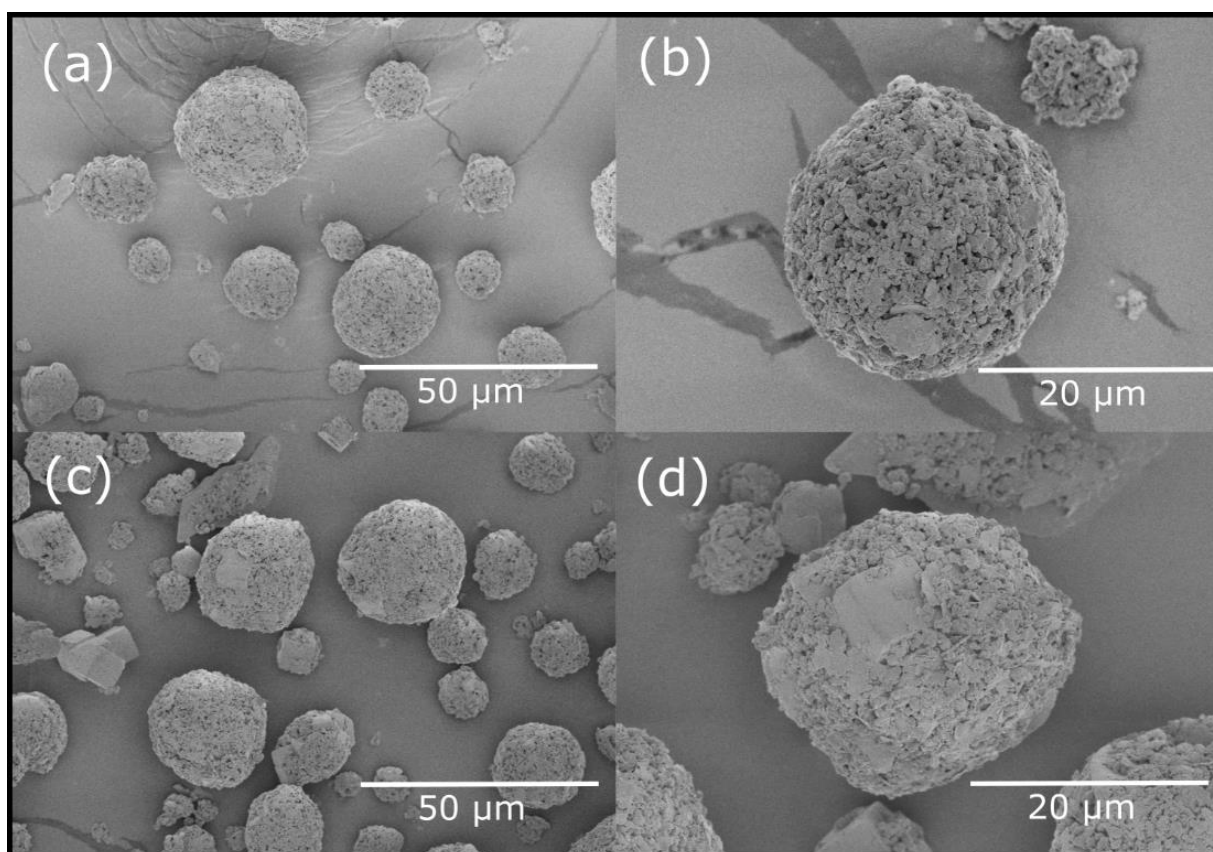


Figure 3. SEM images at magnification of (a,c) x1,000 and (b,d) x2,500 of composite materials from spray crystallization with kaolin as filler material and aluminum chloride binder (ACH binder), i.e. (a,b) grains produced with commercial ZSM-5 and (c,d) grains produced with commercial ZSM-5 and commercial SAPO-34.

Based on their distinct shape-selective properties and varying acid strength, ZSM-5, which favors the generation of aromatics with reduced coking due to its broad 10-ring window pores,[17] can be effectively combined with SAPO-34, known for its propensity to produce preferred olefins and quicker pore blockage *via* its narrow 8-ring CHA pores. [18] The precise ratio between these two materials requires careful calibration. [5]

Addressing Sustainability Aspects and Embracing Structural Elegance

When considering the application of these mixed-phase catalysts in the industrial methanol-to-olefins reaction, it is very important to account for economic feasibility, practicality, and sustainability aspects to guide their development. [19]

- (1) Despite the use of **expensive and toxic** precursors like tetraethyl orthosilicate (TEOS) for silicon, aluminum organyls for aluminum, or organophosphorus compounds for phosphorus, adopting less hazardous alternatives such as silicic acid or water glass, sodium aluminate, or phosphoric acid salts is advised. Moreover, the utilization of methanol, despite its higher water by-product content during olefins production, should be considered over the use of dimethyl ether which forms explosive mixtures in the presence of air.
- (2) Reevaluating or **avoiding** the use of organic templates (TPAB, morpholine) during catalyst synthesis is crucial, particularly in relation to **waste generation** during required air calcination.
- (3) Option for sodium-free binder and ingredients during shaping offers the advantages of **circumventing** additional ion-exchange, materials **separation, and purification steps**, while also expediting catalyst synthesis.
- (4) The concept of continuous-mode production, achieved through **standardized scaling procedures** for zeolite synthesis (e.g., in pulsed pipe reactors), facilitates an **“output pulled” synthesis** approach.
- (5) This approach is facilitated by employing lab-scale equipment (e.g., externally heated, stirred tank reactors, extruders, spray dryers) rather than specialized apparatus (e.g., lab-scale microwave ovens).
- (6) In line with this perspective, the synthesis route has been intentionally **designed to be straightforward, relying on readily available materials** instead of exotic porous catalysts.
- (7) While the ultimate aim of combining materials is to enhance **durability and selectivity**,
- (8) a strategy for recycling spent materials should align with well-established FCC catalyst **recycling strategies**.
- (9) Limited **reliance on compounds** (excluding heavy or rare earth metals)
- (10) **sourced from comparable** FCC catalyst and oil refining catalyst production can facilitate rapid development and subsequent recycling.
- (11) Similar to how today’s oil refining catalyst residues become **urban resources** for rare earth elements in electronics, alumina and silica for construction, and catalyst re-synthesis, these catalyst materials hold potential for a comparable **afterlife**,
- (12) rendering them (almost) **renewable** products.

While the inherent materials themselves possess a certain degree of structural beauty (see Figures 1-3), the true artistry lies in the **amalgamation of synthesis attributes** to sidestep interim synthesis steps (such as additional ion-exchange), sidetrack **costly and hazardous reactants** (considering template-free synthesis as a possibility), and **circumvent undesirable catalyst characteristics** by combining beneficial properties of distinct materials in close proximity to each other.

Conclusion

Individually synthesizing the frequently referenced active materials, ZSM-5 and SAPO-34 – recognized as pivotal catalyst in the methanol to olefins reaction (MTO) – unveils a remarkable degree of adaptability contingent upon diverse ingredient sources, types, and crystallization parameters. [9, 10]

Nonetheless, the combination of both materials has demonstrated advantages pertaining to olefins selectivity and catalyst stability, attributed to their close proximity stemming from stepwise hydrothermal crystallization. [5]

Building upon this approach, the subsequent phase of this study entails the pursuit of a development trajectory that underscores scalable hydrothermal crystallization processes, alongside different catalyst shaping techniques such as spray crystallization. This effort may result in catalyst manufacture for large-scale application. [20] Importantly, the principles of Green Chemistry [21] and Green Engineering [19, 22] can aptly serve as guiding principles for further advancements.

Acknowledgment

This work has been supported by Fond der Chemischen Industrie (SK 209/05) and funded by German Research Foundation (WE 4621/8-1 (498384863) and SE 2450/2-1 (507997100)). Our sincere appreciation extends to Prof. M. Ruck and Prof. T. Doert, for their generosity in granting access to the SEM imaging and XRD infrastructure.

References

- [1] Olah, G.A., *Angew. Chem. Int. Ed.* **44**, 2636-2639 (2005)
- [2] Gabrielli, P., Gazzani, M., Mazzotti, M., *Ind. Eng. Chem. Res.* **59**, 7033-7045 (2020)
- [3] Yang, S., Xiao, Z., Deng, C., Liu, Z., Zhou, H., Ren, J., Zhou, T., *J. Clean. Prod.* **253**, 120006 (2020)
- [4] de Smit, E., Weckhuysen, B.M., *Chem. Soc. Rev.* **37**, 2758 (2008).
- [5] Liu, F., Wang, X., Xu, F., Lin, Q., Pan, H., Wu, H., Cao, J., *Microporous Mesoporous Mater.* **252**, 197-206 (2017)
- [6] Gogate, M.R., *Petroleum Science and Technology* **37**, 559-565 (2019)
- [7] Foster, K. *ExxonMobil's China Petrochemical Project Inches Forward*. April 13, 2021.
- [8] Retka Schill, S. Braskem Starts up Ethanol-to-Ethylene Plant
<https://Ethanolproducer.Com/Articles/7022/Braskem-Starts-up-Ethanol-to-Ethylene-Plant> (Accessed Feb 08, 2023).
- [9] Jonscher C., Seifert, M., Kretzschmar, N., Marschall, M.S., Le-Anh, M., Doert, T., Busse, O., Weigand, J.J., *ChemCatChem* **14**, e202101248 (2022)
- [10] Askari, S., Rouein, H., Sohrabi, M., *Rev. Adv. Sci.* **32**, 83-93 (2012)
- [11] Haufe, L.A., Timoshev, V., Seifert, M., Busse, O., Weigand, J.J., *ACS Omega* **7**, 44892-44902 (2022)
- [12] Bahrami, H., Darian, J. T., Sedighi, M., *Microporous Mesoporous Mater.* **261**, 111-118 (2018)
- [13] Sie, S.T., *Appl. Catal. A: Gen.* **212**, 129-151 (2001)
- [14] Lee, Y.J., Kim, Y.W., Viswanadham, N., Jun, K.W., Bae, J.W., *Appl. Catal. A: Gen.* **374**, 18-25 (2010)
- [15] Kim, M., Chae, H.J., Kim, T.W., Jeong, K.E., Kim, C.U., Jeong, S.Y., *J. Ind. Eng. Chem.* **17**, 621-627 (2011)
- [16] Shoinkhorova, T., Dikhtiarenko, A., Ramirez, A., Chowdhury, A.D., Caglayan, M., Vittenet, J., Bendjeriou-Sedjerari, A., Ali, O.S., Morales-Osorio, I., Xu, W., Gascon, J., *ACS Appl. Mater. Interfaces* **11**, 44133-44143 (2019)
- [17] Schulz, H., Wei, M., *Top Catal* **57**, 683-692 (2014)
- [18] Yang, L., Wang, C., Zhang, L., Chu, Y., Xu, J., Wu, G., Gao, M., Liu, W., Xu, Z., Wang, P., Guan, N., Dyballa, M., Ye, M., Deng, F., Fan, W., Li, L., *Nat Commun* **12**, 4661

- (2021)
- [19] Anastas, P., Zimmerman, J.B., *Environ. Sci. Technol.* **37**, 94-101 (2003)
- [20] Regalbuto, J., *Catalyst Preparation – Science and Engineering*, CRC Press, Vol.1, 139-465 (2007)
- [21] Anastas, P., Eghbali, N., *Chem. Soc. Rev.* **39**, 301-312 (2010)
- [22] Zimmerman, J.B., Anastas, P.T., Erythropel, H.C., Leitner, W., *Science* **367**, 397-400 (2020)

Process Intensification Strategy Demonstrated by Innovative DME Synthesis

M. Semmel, O. Salem, A. Schaadt

Fraunhofer Institute for Solar Energy Systems ISE, Freiburg

Abstract

Dimethyl ether (DME) is a promising PtX energy vector with multiple applications in different sectors. Its thermophysical properties promote DME as an additive and replacement for fossil LPG. DME is also an outstanding and environmentally benign hydrogen carrier with an excellent hydrogen capacity of 26.1 wt.-%. The conventional DME production process has the disadvantage of a large number of process steps and high external heat demand. A promising alternative is DME synthesis via reactive distillation, where DME is removed in-situ from the chemical equilibrium, allowing complete conversion of the feedstock and product purification in a single process step [1]. This process alternative results in fewer unit operations and lower maintenance requirements and can also enable an energy self-sufficient process without external heat requirements [2]. The DME reactive distillation implies a reaction in liquid phase at significantly lower reaction temperatures than in the conventional gas phase synthesis. Consequently, in a previous publication of our group several catalysts for the liquid phase DME synthesis were screened and a kinetic model of DME synthesis on two different ion exchange resins was derived based on fixed bed profile reactor measurements [3].

The target of this work was the transfer of the reaction kinetics from a laboratory scale reactor to the actual process conditions in a reactive distillation column on a more industrially relevant scale in a DN50 pressure distillation column. Starting from both pure and crude methanol feed, the production of purified DME in a single unit operation was successfully demonstrated. Multiple experiments were carried out, examining the influence of reflux ratio and WHSV and the gas phase composition was determined on multiple positions along the column using FT-IR spectroscopy. By modeling the system and comparing the theoretical reaction rate according to kinetic models with the actual measured distillate stream, the transfer of the kinetic model from the laboratory reactor towards the process conditions of a reactive distillation column could be successfully validated.

With the validated kinetic model, industrial-scale reactive distillation process configurations were simulated in Aspen Plus V12. Besides the stand-alone reactive distillation column, process configurations with a complementing side- or pre-reactor were analyzed and optimized with regard to minimum total production cost and it was shown that the best reactive distillation process can reduce the production cost by 40 % compared to the conventional DME process.

References

- [1] M. Semmel, R.E. Ali, M. Ouda, A. Schaadt, J. Sauer, C. Hebling, Power-to-DME: a cornerstone towards a sustainable energy system, in: Giuseppe Spazzafumo (Ed.), Power to Fuel: How to Speed Up a Hydrogen Economy, Elsevier, 2021, pp. 123–151.
- [2] T. Cholewa, M. Semmel, F. Mantei, R. Güttel, O. Salem, Process Intensification Strategies for Power-to-X Technologies, ChemEngineering 6 (2022) 13. <https://doi.org/10.3390/chemengineering6010013>.
- [3] M. Semmel, L. Steiner, M. Bontrup, J. Sauer, O. Salem, Catalyst screening and reaction kinetics of liquid phase DME synthesis under reactive distillation conditions, Chem. Eng. J. (2022) 140525. <https://doi.org/10.1016/j.cej.2022.140525>.

Directly Coupled Production of Methanol and Formaldehyde Based on CO₂

P. Münzer, U. Arnold, J. Sauer

Karlsruhe Institute of Technology (KIT), Institute of Catalysis Research and Technology (IKFT),
 Eggenstein-Leopoldshafen

Abstract

In order to enable the implementation of a circular economy, the use of CO₂ as chemical feedstock is inevitable. Key element of this endeavor is H₂, which is needed for a number of CO₂-based processes. Since the utilized H₂ should preferably be generated sustainably, e.g. via electrolysis, the correlated production costs of CO₂-based products are estimated to be much higher than those of their fossil equivalents. Hence, it is essential to optimize not only H₂-production technologies but also the subsequent process chains to maximize overall H₂-efficiency. This goal then leads to the necessity to modify established industrial processes so that any arising H₂-rich waste gas streams that are currently only thermally exploited may be used for chemical syntheses instead.

One example of an industrial process, which releases a H₂-rich flue gas, is the silver catalyzed oxidative dehydrogenation of methanol (CH₃OH) for the production of formaldehyde (CH₂O). Considering that the manufacture of CH₃OH itself requires a large amount of H₂, especially when CO₂ is deployed as carbon source, it is reasonable to recycle H₂ that is released during CH₂O production to the preceding CH₃OH synthesis.

This study therefore focuses on the concept of the directly coupled production of CH₃OH and CH₂O based on CO₂. The direct connection of the two processes is realized by returning the waste gas of CH₂O production to the feed stream of CH₃OH manufacture. For that purpose, the silver catalyst process has to be modified, so that the N₂ introduced to the system along with atmospheric O₂ is eliminated and cannot accumulate. Thus, it is suggested to substitute N₂ with CO₂, which can easily be fed to the input stream of CH₃OH production together with H₂. This is of particular interest when considering the CO₂-based synthesis route. The schematic flow diagram of the directly coupled processes is shown in Fig.1.

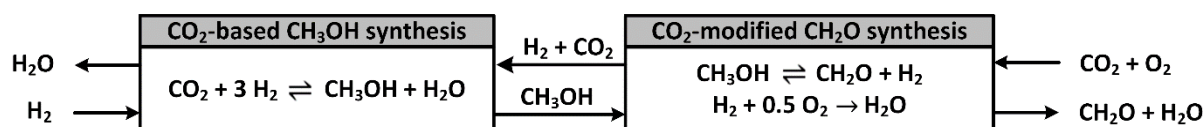


Fig.1: Schematic flow diagram of the directly coupled production of CH₃OH and CH₂O.

In a detailed evaluation of the concept it is shown that directly coupling the manufacture of CH₃OH and CH₂O does not only lead to an increase in overall H₂-efficiency and CO₂ conversion but also results in a reduction of the related CO₂ abatement costs of the process chain. In addition, experimental investigations of the modified silver catalyst process will be discussed.

Mobile Small-Scale Methanol Synthesis Pilot-Plant with Internal Recycle Operated with CO_x from Waste Gasification

J. Reisch¹, T. Nowak¹, M. Siodlaczek², B. Epple², A. Drochner¹, B. J.M. Etzold¹

¹Technische Universität Darmstadt, Ernst-Berl-Institut für Technische und Makromolekulare Chemie

²Energy Systems and Technology, Technische Universität Darmstadt

Abstract

For the reduction of CO₂ emissions chemical recycling of carbon-containing residuals is of increasing interest. The gasification of non-recyclable waste streams offers a way to convert carbon into valuable base chemicals. One particular example is CO_x based methanol which can be utilized in various ways as an energy storage, clean fuel and building block for chemical industry.

At TU Darmstadt a mobile small-scale methanol pilot-plant was realized, with the aim to study the methanol synthesis process from CO_x including a reactant/product separation through condensation, high-pressure gas recycles and purge as well as different connection possibility of two fixed bed reactors, the separation and recycle. Furthermore, the scale is this small that catalysts can be tested on a pre commercial production scale and lower amount and that approx. 50 mL h⁻¹ of liquid product mixture are produced, allowing detailed product characterization but avoiding huge amounts of storage and disposal. Through the small scale the pilot-plant is also mobile and easy to transport to real CO_x sources. The composition of the streams before and after each reactor can be analyzed by a gas chromatograph which detects the permanent gases via TCD and the larger carbon compounds and oxygenates via FID. As a part of the BMWi project VERENA real syngas is obtained from Hochtemperatur-Winkler-gasification (HTW). The 500 kW pilot plant at TU Darmstadt operates at temperatures of up to 1000°C. A subsequent raw gas cleaning removes impurities such as dust, strong acids and organic compounds. One part of the cleaned syngas is afterwards used for methanol synthesis to study the full chain process.

First experiments were carried out with 30 g of commercially available CZA-catalyst (copper zinc oxide on aluminum oxide), a reaction temperature of 230 °C and a pressure of 30 bar. The stoichiometric feed stream of CO₂ and H₂ with 30 g h⁻¹ was mixed from bottled gas. The results show that a full conversion of the reactants is possible when increasing the recycle ratio. At the same time a small accumulation of byproducts can be observed in the recycle stream. Nevertheless, no detectable purge stream was necessary. Moreover, the start-up process of the reaction including the recycle can be recorded. When increasing the reactor temperature from RT to 230 °C a first decrease of the off-gas mass flow can be observed at a reaction temperature of about 180 °C. Full conversion is reached at a specific combination of reaction temperature and recycle ratio for the given point of operation. Investigation of dynamic plant behavior shows a pressure dependence for the time until a new stationary point is reached. Further experiments are planned with real CO_x mixtures from the HTW-gasifier to investigate the influence of real syngas on the recycle ratio, the catalyst stability and the spectra and accumulation of byproducts.

An In-Depth Investigation: Surprising Effect of the Second Liquid Phase in Homogeneously Ru-Catalyzed CO₂ Hydrogenation to Formic Acid

K. R. Ehmman^{1,2}, K. Dinsing^{1,3}, C. Ribeiro Maier^{1,3}, A. J. Vorholt¹, W. Leitner^{1,2}

¹Max Planck Institute for Chemical Energy Conversion, Mülheim an der Ruhr, Germany

²RWTH Aachen University, Aachen, Germany

³TU Dortmund University, Germany

Abstract

Carbon dioxide is an attractive C₁ building block for future chemistry, as it reduces the carbon footprint not only by using the greenhouse gas itself as a raw material, but also primarily by substituting fossil raw materials. Accordingly, the area has an increased focus in (academic) research. In the field of homogeneously catalyzed conversion of CO₂, academic research often focuses on showing a proof of concept with the selected substrates or catalysts initially. Aspects such as catalyst recycling or product separation often only play a subordinate role at first and are mostly considered in the further process development. A frequently used strategy for catalyst recycling in homogeneous catalysis is the use of liquid-liquid biphasic systems. However, many monophasic gas-liquid reaction systems are barely understood before going into multiphase systems. For this reason, we investigated the behavior of the homogeneously catalyzed hydrogenation of CO₂ to formic acid in-depth. This understanding will aid the transition to a multiphase reaction system for catalyst recycling approaches.

The model reaction system includes the organic solvent 4-methyl-2-pentanol, the additive triethylamine (needed to stabilize the formed formic acid), a Ru dppm complex (dppm: bis(diphenyl-phosphino)-methane) as a precursor for the homogeneous catalyst, and the gaseous substrates CO₂ and H₂. The addition of water as second, immiscible solvent transfers the monophasic to a biphasic system.

The study was carried out in a miniplant with a 300 mL stirred tank reactor in batch mode. The miniplant is equipped with mass flow meters for the substrates CO₂ and H₂ and an ATR-IR probe for online detection of the product formic acid and the substrate CO₂.

The recorded concentration-time profiles of the monophasic reaction show an expected influence of the parameter total pressure as well as an unexpected inhibition of the catalyst depending on the composition of the liquid phase. The inhibitory effect can be overcome by using the second, immiscible solvent water, making the biphasic reaction system more productive than the monophasic one.

This shows, that the understanding of the monophasic reaction system is essential for identifying improvements in multiphase systems.

A Review of the Fischer-Tropsch and Methanol Pathways for the Production of Jet Fuel

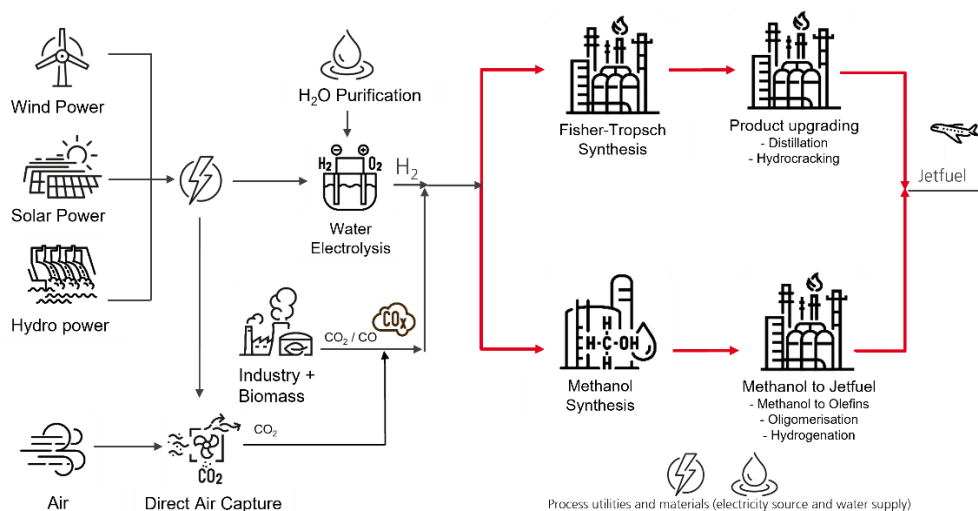
R. Ali, L. Edenhofer, A. Schaadt, O. Salem

Fraunhofer Institute for Solar Energy Systems ISE, Freiburg, Germany

Abstract

Around 300 Mio. tons of kerosene are consumed for aviation each year. By 2050, the demand is expected to reach 450 Mio. tons. While the use of renewable-based fuels is still being discussed in other sectors, the decision has already been made in the hard-to-abate sectors such as aviation. By 2050, the global demand for kerosene is expected to come from sustainable and regenerative sources. On the one hand, in the *Fischer-Tropsch* pathway, the production of jet fuel from water and air is powered by renewable electricity, where the H_2 and CO_2 reactants are first heated and converted into *syngas*, followed by Fischer-Tropsch synthesis to produce multifunctional hydrocarbons that can be further processed into chemicals, oils and gas, subsequent product separation takes place in the distillation column. On the other hand, the *MeOH-to-jet* pathway involves the conversion of methanol to light olefins followed by oligomerization of the light olefins with hydrogenation. The process yields products in both the distillate and gasoline ranges and can be adjusted to shift the yield to the desired fraction range.

The focus is on presenting a comprehensive knowledge base on the pathways and in particular on the evaluation under the criteria of process design, material and energy efficiency. Last but not least, a potential assessment on the technology pathways in terms of technology bottlenecks, advantages and disadvantages and technology readiness level.



Liquid-phase Co-Reagent Free Hydrogenation of Carbon Monoxide to Methanol Using Molecular Manganese Catalysts

S. Stahl^{1,2}, A. J. Vorholt¹, W. Leitner^{1,2}

¹Max Planck Institute for Chemical Energy Conversion, Mülheim an der Ruhr, Germany.

²Institute for Technical and Macromolecular Chemistry, RWTH Aachen University, Aachen, Germany

Abstract

Methanol is a central component in the chemical value chain and an important compound for energy storage either as a combustion fuel or as a hydrogen/syngas carrier.^[1,2] Global methanol production

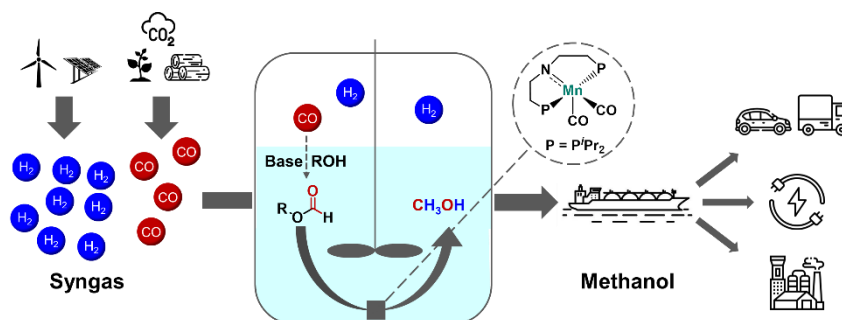
is mainly based on coal and natural gas as primary feedstocks. Syngas from renewable carbon sources as the raw material can make methanol a central pivot point of a sustainable chemical value. The syngas conversion to methanol over heterogeneous catalysts is well established.^[3] While these processes benefit strongly from the economies of scale they are not ideal for a decentralized small scale methanol production. Homogeneous molecular complexes in contrary, offer the possibility of small scale production. Unfortunately, the direct CO hydrogenation by homogenous catalysts has proven inefficient until the groups of Prakash and Beller employed the use of amines as co-reagents.^[4-5] These systems, however suffer from incomplete conversion of the formamide intermediates and trace amounts of *N*-methylated products leading to undesired side products.

Recently, a system to produce methanol from CO alcohol-assisted catalysed by a manganese pincer complex in an effective and clean way was developed at our institute.^[6] This process yields only methanol and formate ester as detected products in the liquid phase with an high activity (TON>4000) under relatively mild conditions (150°C, 60 bar). However, this system still comprises of ethanol as a co-reagent and lacks the possibility for easy product separation.

In this work, we present a co-reagent free system using the product methanol itself as the activating agent. By optimizing of various process parameters, the catalytic activity was improved while the complexity of the system was reduced. Additionally, it enables facile product separation opening the possibility for continuous operations.

References

- [1] Olah, G. A., Goepfert, A., Prakash, G. K. S. *Beyond Oil and Gas: The Methanol Economy*; Wiley-VCH Verlag GmbH & Co. KGaA: Weinheim, **2009**.
- [2] Bertau, M., Offermanns, H., Plass, L., Schmidt, F., Wernicke, H.-J. *Methanol: The Basic Chemical and Energy Feedstock of the Future*, Springer-Verlag: Berlin, Heidelberg, **2014**.
- [3] Waugh, K. C., *Catal. Lett.* **2012**, *142*, 1153–1166.
- [4] Kar, S.; Goepfert, A.; Prakash, G. K. S., *J. Am. Chem. Soc.* **2019**, *141*, 12518–12521..
- [5] Ryabchuk, P., Stier, K., Junge, K., Chęcinski, M. P., Beller, M., *J. Am. Chem. Soc.* **2019**, *141*, 16923–16929.
- [6] Kaithal, A., Werlé, C., Leitner, W., *JACS Au.* **2021**, *1*, 130-136.



Biogenic Residues as Potential Feedstock for Green Energy Carriers in Urban Areas – Gasification and Synthesis Demonstration in Vienna

T. Schubert, P. Krobath, S. Egger, M. Höller
Wien Energie GmbH, Vienna, Austria

Abstract

Wien Energie is Austria's leading energy supplier, providing 2 million people with power, gas as well as district heating and cooling energy in the urban area of Vienna. Furthermore, Wien Energie thermally utilizes 1 million tons of waste (MSW, sewage sludge and hazardous) each year.

The successful energy transition is one of the main challenges to reach climate neutrality. Especially in urban areas, since cities with their high population density pose a particular challenge for renewable and CO₂-free energy supply for all sectors. To achieve the CO₂ net zero 2040 target of the City of Vienna, new technological options and pathways have to be developed and implemented into the energy system and the existing infrastructure. For this purpose, close cooperation and a shoulder-to-shoulder approach with mutual understanding of the different points of view between research and industry is required. This includes for the example of green energy different carriers like hydrogen and sustainable methane, as well as CO₂ utilization and energy storage.

One example for such an application-oriented collaboration is the multi-firm research project Waste2Value, a consortium led by BEST – Bioenergy and Sustainable Technologies. The ambition is to develop and demonstrate an innovative process chain, converting biomass and waste via gasification into syngas and subsequently into green liquid fuels and platform chemicals.

The first pathway to be demonstrated is the gasification of different biogenic residues like waste wood, sewage sludge or rejects from wastepaper recycling in a 1 MW dual fluidized bed gasification unit. The gasification is followed by a multi-step syngas cleaning process, a Fischer-Tropsch synthesis in a slurry reactor and finally a product separation into a wax, a middle distillate and a naphtha fraction. Since commissioning of the demonstration plant in early 2022 several testing campaigns have been performed, providing numerous data for balancing and simulation purposes of the gasifier as well as the whole process chain. Main research aspects, from the point of view of Wien Energie, are generating know-how, especially regarding the challenges of continuous process operation like ash handling or syngas cleaning as well as obtaining data for techno-economic assessment for future upscaling considerations. The mid-term perspective of Wien Energie is the commercialization of this innovative technology for different synthesis product applications – for example green fuels, methane and methanol – which can be used in the energy and mobility sector.

Introduction

Climate protection has a long history in Vienna. In 1999, the City of Vienna adopted its first Climate Protection Program [1]. 21 years later, in 2020, Vienna as first federal province in Austria set its goal to become climate-neutral by 2040 [2]. Therefor the Smart City Wien Strategy [3] and the Vienna Climate Guide [2] together provide the necessary framework and show the way towards reaching that objective.

In Vienna, as a population-dense and large city with a well-developed public transport network, modern buildings and significantly lower heating demands due to many apartment buildings, per capita energy consumption (18.140 kWh) is only 55% of the average for all of Austria [4]. Nevertheless, in 2022, Vienna's gross inland consumption amounted 40 TWh, whereas 19.2 TWh stem from natural gas and 11.3 TWh are provided by (almost exclusively) liquid and solid fossil fuels [4]. The share of renewable energy was below 15 % and up to 88 % of the energy had to be imported from outside the city borders [4].

A recent study [5], conducted in 2021, modelled how the energy system of Vienna has to be redesigned to reach the ambitious goal of climate neutrality by 2040. Following major changes contribute to the drastic decrease of CO₂ emissions:

- Energy for mobility purposes is provided by electricity almost exclusively;
- District heating and electricity-based systems (heat pumps) supply space heating and hot water;
- Geothermal energy and large heat pumps to harvest off-heat from various sources feed the district heating system instead of gas-powered CHP plants;
- The increased electricity demand is covered by an increased renewable electricity production within the area of Vienna but mainly depends on imports from outside the city.

As illustrated in Figure 1, the total energy consumption will decrease due to increases in energy efficiency and the contribution of energy generation which will shift towards renewable electricity. Nevertheless, 0.8 TWh of hydrogen and synfuels as well as 1.7 TWh of heat from gas-CHP and peak load boilers require chemically bounded energy in form of green gases and fuels. The modelled overall demand of green energy carriers in 2040 is estimated to be 4.0 TWh. This is much lower than the 30 TWh fossil fuel and natural gas consumption in Vienna in 2019, but still has to be covered. [5]

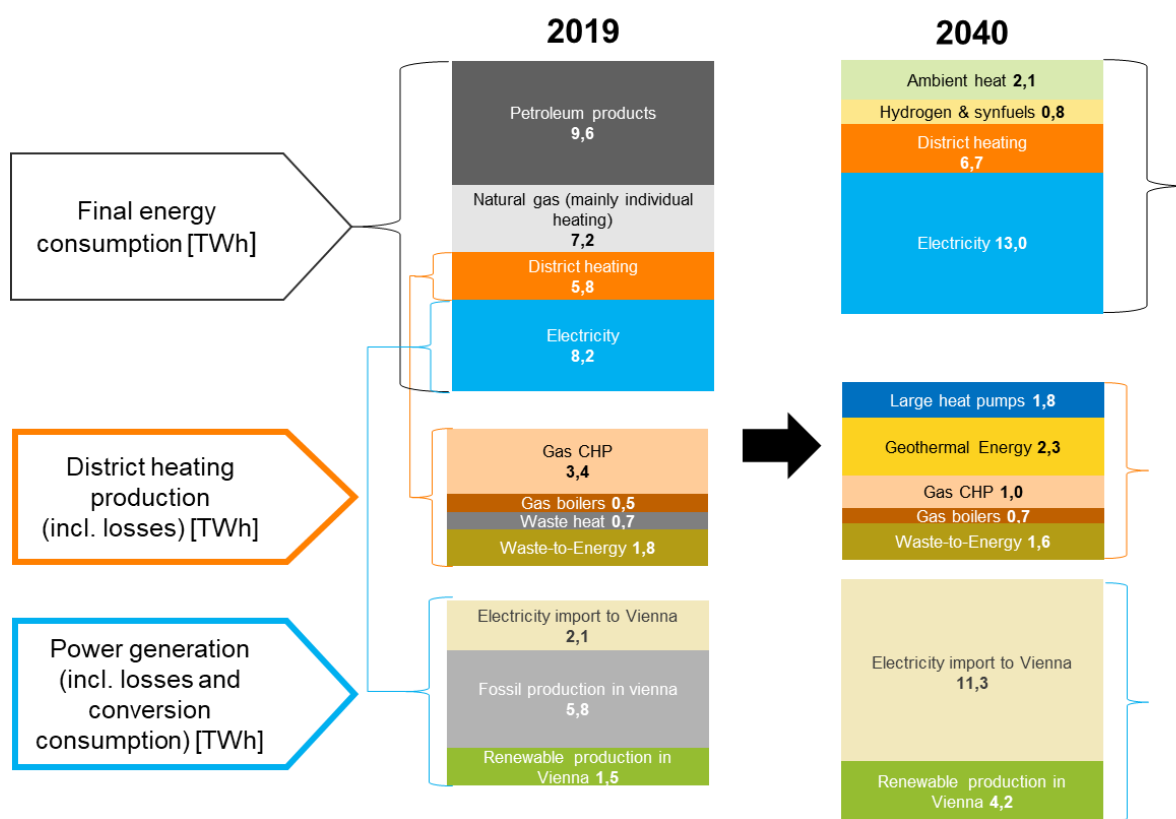


Figure 1: Changes in the final energy consumption, district heating and electricity production in Vienna 2019-2040 (adapted from [5]).

One of the major challenges, which is addressed by flexible energy provision by green energy carriers, is the flexibilization of energy production in the heating sector. Geothermal energy sources, as well as waste-to-energy plants and certain shares of off-heat utilization, provide constant heat amounts all year, whereas the heating demand during winter is much higher than in summer. This leads to an excess heat production in summer and a gap to cover the heat demand in cold months. To close this gap between need and coverage, large storage capacities are needed as well as new, more flexible solutions, which enable the seasonal shift of heating energy.

One technological approach, which offers an alternative to incineration and bears the opportunity to shift energy supply seasonally is the pathway via gasification and subsequent syntheses. This means transforming chemical energy of residual biogenic materials into storable carriers. By converting waste fractions from municipal waste management systems and forestry into syngas (mainly CO, H₂, CH₄, CO₂) instead of heat and power offers the opportunity to add a subsequent synthesis to produce standardized hydrocarbons. This bears different advantages for a sustainable and reliable energy system of the future like illustrated below in Figure 2. On the one hand a broad range of various hydrocarbons as well as hydrogen can be produced for different applications in energy resource supply as well as material recovery. On the other hand, time-independent sector coupling between waste management and energy provision is possible.

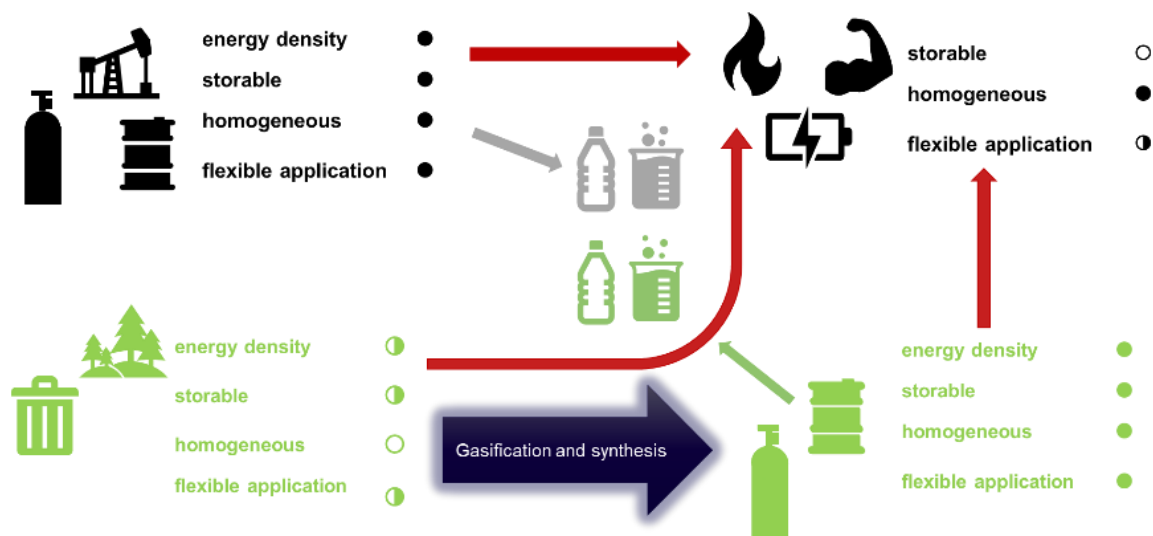


Figure 2: Gasification and synthesis offer a great opportunity to obtain energy carriers and resources from residual materials.

Although this approach is not entirely new, there are no commercially available technologies, processes or equipment yet. Increased urgency to reduce CO₂ emissions from utilizing fossil fuels and eagerness to promote circular material utilization, as well as recent attention to ensure local energy provision opens social tailwinds and economic opportunities for such emerging technologies.

Waste2Value – The technology and the research project

Within the course of the research project Waste2Value a revolutionary research infrastructure was erected at Simmeringer Haide, a site of Wien Energie. The research project has received funding from BMK, BMDW and the Federal States Vienna, Lower Austria and Styria within the scope of the Austrian COMET Programme (Competence Centers for Excellent Technologies - Grant Agreement no 892426). The COMET Programme is managed by the Austrian Research Promotion Agency (FFG).

The consortium, led by BEST – Bioenergy and Sustainable Technologies [6, 7], set up resources and expertise to build the Syngas Platform Vienna (Figure 3). A demo site to investigate the potential of gasification of residues and waste materials and subsequent synthesis as an essential building block of the energy system and circular resource utilization was realized within the framework of the project.



Figure 3: Syngas Platform Vienna at Wien Energie's site Simmeringer Haide.

The site Simmeringer Haide offers a unique location for such a research facility. At this site, Wien Energie operates Austria's only hazardous waste incineration plant as well as several lines for the thermal utilization of municipal and commercial waste and sewage sludge. Due to the existing infrastructure, several synergies can be exploited, for example media supply, usage of the off-gas treatment system and permits for the treatment of waste of different types.

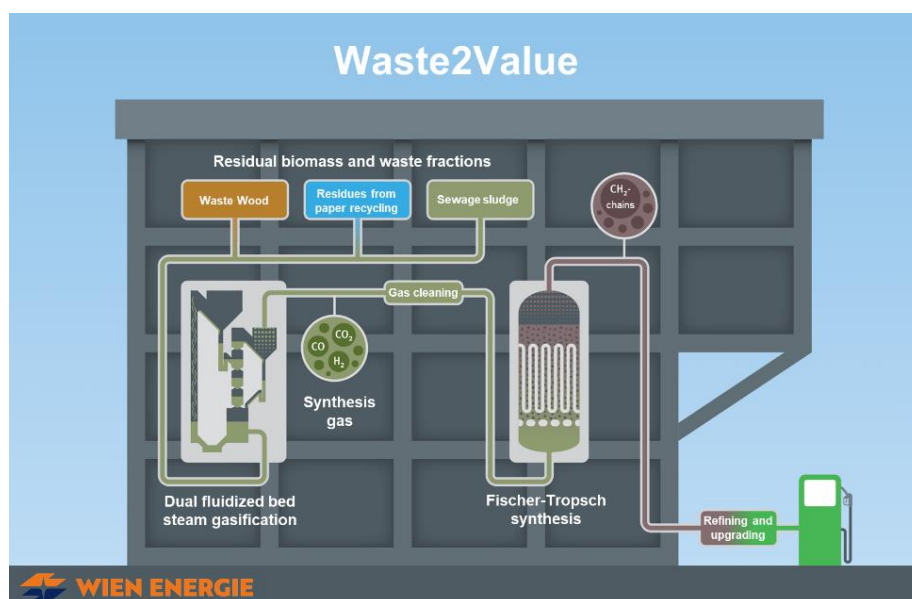


Figure 4: Schematic illustration of the Waste2Value process chain (demonstrated at the Syngas Platform Vienna).

The research facility consists of a 1 MW dual fluidized bed (DFB) steam gasification unit, several gas cleaning steps (coarse gas cleaning and fine gas cleaning) and a 250 kW Fischer-Tropsch synthesis based on a slurry reactor. The DFB gasifier represents one of the core technology equipment for research activities at the Syngas Platform Vienna. Its advanced DFB design (schematically illustrated in Figure 5), which was developed and implemented in pilot-scale at TU Wien [8], consists of two fluidized bed reactors, which are interconnected via a circulating bed material. In a bubbling fluidized bed reactor, the fuel is dried, pyrolyzed and gasified with steam and thereby converted to product gas. The product gas leaves the system

by passing a counter current column on top of the gasification reactor. The bed material and fixed carbon contents of the fuel are transported to a second, fast moving fluidized bed reactor, where the combustion of the remaining char heats up the bed material. The hot bed material, which is separated from the flue gas via a cyclone, moves back to the gasification reactor and provides the necessary energy for the drying, pyrolysis and gasification reactions.

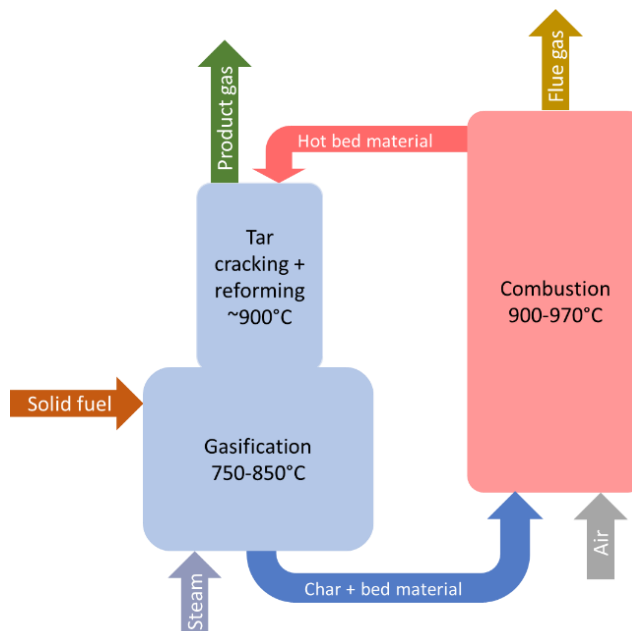


Figure 5: Principle of the advanced dual fluidized bed steam gasification (adapted from [8, 9]).

The applied steam gasification leads to a product gas without additional nitrogen from air, which is highly beneficial in subsequent syngas utilization via catalytic syntheses. Furthermore, also its high hydrogen content is advantageous in subsequent conversion processes to hydrocarbons as well. A typical syngas composition of the DFB system can be found in Table 1. [8, 10]

Table 1: Typical syngas composition from DFB steam gasification (wood pellets as fuel, olivine as bed material) [10].

Component	Unit	Typical range
H ₂	vol.% _{db}	36-42
CO	vol.% _{db}	19-24
CO ₂	vol.% _{db}	20-25
CH ₄	vol.% _{db}	9-12
C ₂ H ₄	vol.% _{db}	2.0-2.6
C ₂ H ₆	vol.% _{db}	1.3-1.8
C ₃ -fraction	vol.% _{db}	0.3-0.6
H ₂ O	vol.%	30-45

The product gas from gasification contains several contaminants and impurities, which have to be removed before utilizing the syngas. For this reason different gas cleaning steps are installed to ensure that the necessary gas quality is achieved at the Syngas Platform Vienna. The coarse gas cleaning, which provides a gas quality sufficient for gas motors, is illustrated in Figure 6, which also illustrates the flue gas treatment system. After product gas cooling in a radiation cooler, dust and the particulate matter in the product gas are removed via cyclone and hot gas filter. Filtration at a higher temperature is necessary to prevent tar condensation in the product gas stream. In A two-stage liquid scrubber, the product gas is afterwards

quenched, and finally tars are removed by absorption in rapeseed oil methyl ester (RME). Flue gas on the other hand can be cooled down without the risk of tar condensation before removing dust via a fabric filter.

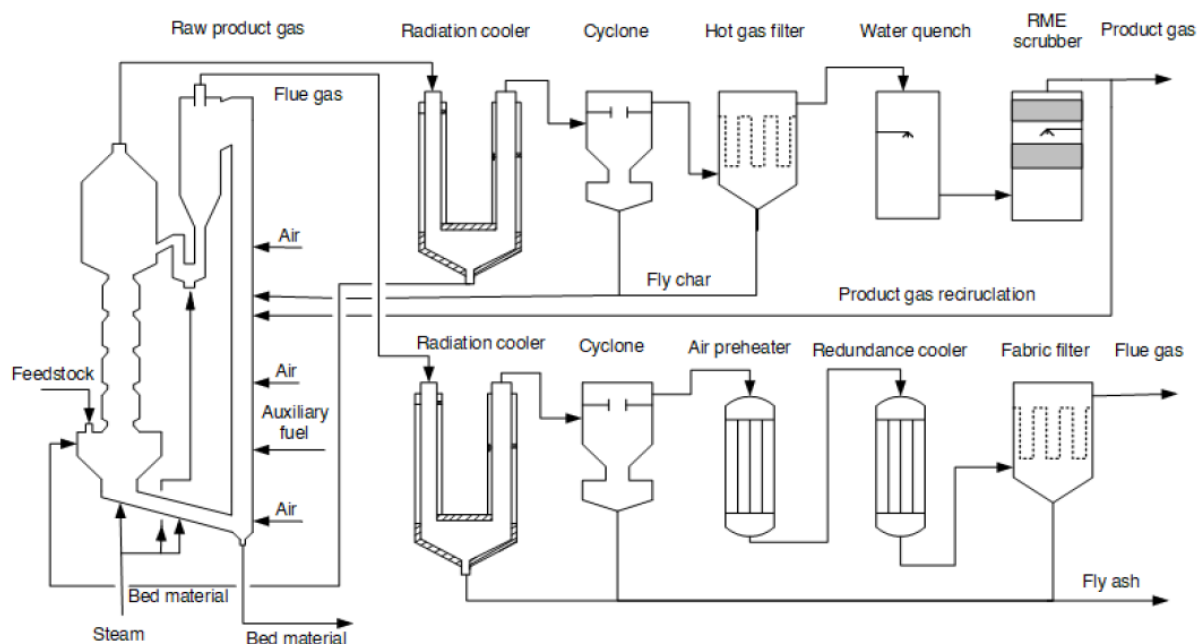


Figure 6: Basic flow sheet of the gasification and coarse gas and flue gas cleaning infrastructure [11].

Further gas cleaning and conditioning is necessary to provide a syngas quality which is applicable for catalytic synthesis. For this purpose, a fine gas cleaning system similar to the process chain illustrated in [12], is used. It's consisting of a cold RME scrubber to reduce further tars, a NH_3 scrubber and activated carbon adsorbers as well as a ZnO adsorber to remove catalyst poisons.

In the final step, a slurry bubble column reactor for Fischer-Tropsch synthesis with a capacity of one barrel per day is utilized to convert a part of the conditioned syngas into syncrude. This liquid hydrocarbon mixture with similar properties like crude oil is separated into fractions (wax, middle distillate and naphtha) and can be processed further to obtain green fuels and chemicals.

Next to the demonstration plant, BEST implemented a technicum and lab infrastructure for accompanying research activities like alternative gas cleaning steps, water treatment and synthesis optimization in smaller scale [12, 13, 14] and to perform necessary process analytics.

With an overall project budget of about 9 Mio. EUR, the Syngas Platform Vienna was erected and commissioned in March 2022 within the Waste2Value project. A strong consortium from science and industry (among others BEST, Wien Energie GmbH, SMS Group, Heinzl Paper, Wiener Linien GmbH, Wiener Netze GmbH, Österreichische Bundesforste, OMV Downstream GmbH, TU Wien, Luleå University of Technology) bundled its competencies to drive technology development forward [6]

This unique research infrastructure provides the basis for detailed experimental investigations on the performance, flexibility as well as long-term behaviour in close-to-industrial scale. Fundamental questions about the further commercialisation of the technology are now being answered within the framework of in-depth and continuing research projects.

Wien Energie's interests in the research project

From the perspective of Wien Energie, relevant information towards a commercial, large-scale implementation will be generated. As a potential technology adopter and future plant operator, the behaviour and performance of different feedstocks from waste materials (fractions from municipal and commercial wastes, sewage sludge, waste wood, plastic rejects from paper industry) need to be tested in detail to identify technically and economically feasible fuel inputs. In this context, it is particularly interesting to determine experimentally, where the optimum lies between lowest-quality fuels possible, which are available on the market and can be obtained by low prices or even gate-fees, and lowest possible effort (CAPEX, OPEX) for operation, especially gas conditioning. For this purpose, the selection according to technical criteria and economic perspectives like market prices and availabilities will be complemented by systemic considerations, for example available alternative material recovery pathways, which should not be in competition with each other.

A reliable data base and in-depth knowledge on optimal plant design and process operation are crucial for a successful technology rollout. To gain this information for future plant engineering and process operation, experimental investigations are accomplished on the 1 MW demonstration plant. This should provide a solid data base over a broad spectrum of operating parameters and potential fuels. Future technology deployment always necessitates deep understanding of how core components. The scale-up of components like the DFB system, the gas cleaning process chain or single equipment parts is relying on a valid data base for engineering. Wien Energie as energy provider will not engineer and build the necessary plant and equipment by itself but will enable companies from engineering industry to do so. The project details are highly valuable to Wien Energie to enable technically qualified tendering and contracting for commercial implementation.

It is not only the process chain that needs to be engineered and developed considerably, also technology integration in existing infrastructure plays an important role, which will be facilitated by the results of the project. Due to its nature as high-temperature process, heat integration like for example coupling with existing district heating systems will be considered based on experiences with the demonstration plant. Furthermore, valuable data and requirements for potential sites can be identified to promote technology development and deployment. This includes for example auxiliary electricity and water demand, possible synergies with other waste management facilities like existing flue gas treatment units or sorting plants.

Besides engineering and design for the technology scale-up, substantiated experiences how to operate and maintain such a novel technology chain can be gathered during the experimental test runs of the 1 MW demonstration plant. This knowledge is essential to provide staff with a deep process understanding of the future industrial plant and estimate the operation and maintenance effort, that can be used to develop sufficient operation and maintenance strategies.

Finally, based on the generated experimental results, it is possible to determine or estimate necessary equipment parts like requirements in fuel preparation and gas cleaning steps. This also allows to predict the consumption of utilities as well as realistic yields and product qualities for different fuels on a larger scale. These insights provide a reliable basis for capital and operational cost estimations, informed techno-economic assessments and subsequent business case development, which enables data-based invest decisions for further scale-up steps and commercialization.

First experiences and preliminary results

The gasification and coarse gas cleaning subsystems of the demonstration plant were successfully commissioned with wood chips as reference fuel in March 2022. Valuable

information and insights were already gained during these commissioning tests. First experiences in partial load operation, which can be found in more detailed in literature [15, 16], helped to identify crucial points to ensure stable test runs and showed several optimization potentials of the research infrastructure. One was the identification of necessary equipment adaptations at the research site including continuous trace heating, stronger motors for the bed material outlet system, replacement of temperature sensors and additional gas cleaning before inserting it into analysis equipment. Furthermore, several crucial factors during operation were identified, which include stable and low fuel water contents as well as reliable fuel calibration. Due to an operating point not congruent with design values, especially in regard of too low temperatures and too high steam-to-fuel ratios, a lower cold gas efficiency (65.3%) and product gas yield ($0.98 \text{ Nm}^3_{\text{db}}/\text{kg}_{\text{fuel,daf}}$) than expected were obtained.

After commissioning, the plant was operated within several test campaigns for several weeks with different fuels, as indicated in [17]. The adaptations and recalibrations, which were deduced from commissioning, led to a stable operation point with the reference fuel, which met the performance expectations in the first test campaign after the commissioning. Fuel input of 1 MW produced 765 kW, leading to a cold gas efficiency of 76.5 % and a product gas yield of $1.18 \text{ Nm}^3_{\text{db}}/\text{kg}_{\text{fuel,daf}}$.

Besides the evaluation of the general performance of the DFB system, different fuels already were tested in the gasification and coarse gas cleaning subsystem. For example, as discussed in detail in [11], a mixture of wood chips with 50 wt.%, plastics reject with high content of volatiles and a lower heating value of $26.9 \text{ MJ/kg}_{\text{db}}$ was successfully converted into syngas. During this test campaign, detailed measurements along the coarse gas cleaning chain were performed, tracking the succession of tars and inorganic impurities like H_2S , NH_3 , HCl and HF in the product gas. The results showed that the presented coarse gas cleaning was capable to reduce GCMS without BTEX tars down by 90 % (11 g/Nm^3 initial concentration after the reactor), HCl by 97 % (37 ppm initial concentration after the reactor) and NH_3 by 70 % (293 ppm initial concentration after the reactor). In addition, a detailed analysis of the flue gas provided information on how flue gas is composed, and which components need to be removed further in order to meet the legal requirement for waste incineration plants. Other fuel tests with biogenic residues from forestry in different categories and bark were performed successfully as well.

At the end of 2022, extensive refining and upgrading of the obtained syncrude by OMV Downstream GmbH yielded the first litres of renewable, wood-based diesel fuel. To investigate the performance under realistic conditions, two test runs with a bus from Wiener Linien GmbH were carried out on a vehicle roller dynamometer in Graz. Two different blends, 15 and 25 % of Fischer-Tropsch diesel, were tested by measuring engine emissions and fuel consumption [18].

Conclusion and outlook

The FFG-funded research project Waste2Value enabled the erection and commissioning of a unique demonstration facility at the Syngas Platform Vienna. Within the framework of the project, the consortium was able to gain valuable know-how in design and engineering as well as first operation experiences. The implemented research infrastructure is a major achievement to promote the technology development and future deployment of DFB gasification, gas cleaning and subsequent synthesis.

From technology user's perspective, Wien Energie gathered first insights in the engineering, construction, and operation as well as performance of the demonstrated process chain. The stable operation of the DFB system as core element of the project with the reference fuel as well as already tested alternative feedstocks convinced that the technology is viable, fuel-flexible and promising for future, industrial applications. Furthermore, first experiences showed the significance of fuel properties and operating parameters on the syngas quality and quantity

but also on the process handling. Due to the quite complex nature of this system, profound understanding of the occurring effects and interdependencies is essential and has to be deepened further with additional research activities.

For more detailed investigations, and the exploitation of the full potential of installed research infrastructure, further projects and ongoing complementary commercialization activities will be performed, following Waste2Value. For this purpose, the FFG-funded the follow-up projects "Waste2Value-LevelUp" and "Green Fuel and Chemicals" to continue research work. The two projects enable Wien Energie to work on further essential research aspects like in-depth investigations of the gasification of different fuels, the optimization of gas cleaning and Fischer-Tropsch synthesis units and alternative syngas utilization routes like alcohol synthesis and hydrogen production. The research program is complemented with additional projects. For example, is the research project "KLAR", which is funded by the Vienna Business Agency [19], aims at investigating the conversion of sewage sludge into syngas and simultaneous recovery of inorganic nutrients of the residues from the process.

The major aim of Wien Energie in the next steps is to identify the most suitable fuel and product combinations from all possible options (see Figure 7), regarding technical, economic and strategic aspects.

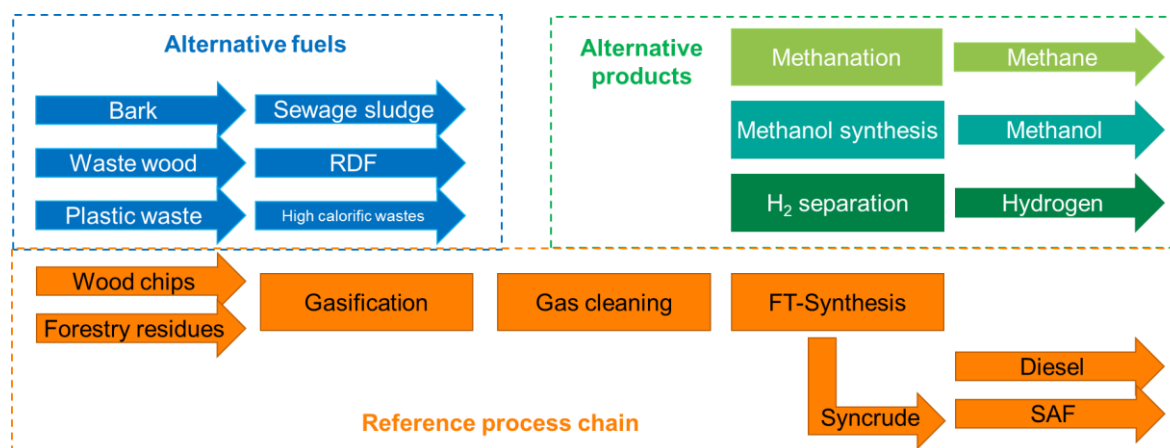


Figure 7: Gasification and subsequent synthesis gas utilization offer different fuel-product combinations for further commercialization steps.

More extensive and broad fuel conversion experiments in the future will provide necessary information to enable modelling of potential large-scale implementations. Data-driven estimation of cost structures, risk and ecological assessments and the deduction of further research and development demands should guarantee a successful scale-up and comparison of the different fuel options. To enable continuous commercial operation in the future, this knowledge is essential. Additional research infrastructure in form of alternative syntheses and hydrogen separation plants will be implemented in the future between lab-and demo-scale to evaluate alternative product options and assess the syngas' suitability for these utilization routes.

Furthermore, long-term operation of the whole process chain with promising fuels is necessary to make long-term effects visible. The obtained knowledge is essential to understand, which technical challenges can arise during stationary long-term operation. Constructional and operational requirements as well as maintenance routines, reliable utility consumption and lifetimes for continuous operation in a commercial plant are investigated and evaluated.

Within the research project "Waste2Value", a major step already was accomplished to advance the technology. Continuing work will build on it to ensure successful technology development and obtain a reliable basis for decision making. These research activities will enable the production of residual-based energy carriers and resources for the future's urban energy system of Vienna and generate higher value from waste.

References

- [1] Vienna City Administration, „Wiener Klimaschutzprogramm (KliP I),“ 1999.
- [2] Vienna City Administration, “Vienna Climate Guide,” 2022.
- [3] Vienna City Administration, “Smart City Strategy Vienna,” 2022.
- [4] Stadt Wien - MA 20, “Energie! voraus - Energiebericht der Stadt Wien,” 2022.
- [5] G. Aue und A. Burger, „Wärme & Kälte, Mobilität, Strom: Szenarien für die Dekarbonisierung des Wiener Energiesystems bis 2040,“ <https://positionen.wienenergie.at/wp-content/uploads/2021/10/WE-DECARB21-Studie.pdf>, 2021.
- [6] BEST, “Waste2Value,” [Online]. Available: https://best-research.eu/en/competence_areas/all_projects/view/611. [Accessed 21 07 2023].
- [7] Wiener Stadtwerke GmbH, „Waste2Value: Grüner Treibstoff aus Abfall,“ [Online]. Available: <https://www.wienerstadtwerke.at/waste2value-gr%C3%BCner-treibstoff-aus-abfall#!>. [Accessed 26 07 2023].
- [8] J. C. Schmid, F. Benedikt, Fuchs, Josef, A. M. Mauerhofer, S. Müller and H. Hofbauer, “Syngas for biorefineries from thermochemical gasification of lignocellulosic fuels and residues—5 years` experience with an advanced dual fluidized bed gasifier design,” *Biomass Conversion and Biorefinery*, no. 11, pp. 2405-2442, 2021.
- [9] S. Rusch-Fazekas and T. Schubert, „Stand der thermischen Abfallbehandlung in Österreich,“ in *Energie aus Abfall - Band 20*, Stephanie Thiel, Elisabeth Thomé-Kozmiensky, Peter Quicker, Alexander Gosten, 2023.
- [10] C. Pfeifer, S. Koppatz and H. Hofbauer, „Steam gasification of various feedstocks at a dual fluidised bed gasifier: Impacts of operation conditions and bed materials,“ *Biomass Conv. Bioref.*, Nr. 1, pp. 39-53, 2011.
- [11] M. Huber, D. Hochstöger, T. Karel, A. Egger, M. Binder, D. Kadlez, T. Pröll, H. Hofbauer and M. Kuba, „Syngas from plastic rejects: Evaluation of gas impurities from dual fluidized bed steam gasification and an integrated gas conditioning unit,“ in *31st European Biomass Conference & Exhibition*, Bologna, Italy, 2023.
- [12] H. Gruber, L. Lindner, S. Arlt, A. Reichhold, R. Rauch, G. Weber, J. Trimbach and H. Hofbauer, „A novel production route and process optimization of biomass-derived paraffin wax for pharmaceutical applications,“ *Journal of Cleaner Production*, Bd. 275, Nr. doi:10.1016/j.jclepro.2020.124135, 2020.
- [13] J. Loipersböck, G. Weber, R. Rauch and H. Hofbauer, „Developing an adsorption-based gas cleaning system for a dual,“ *Biomass Conversion and Biorefinery*, Nr. 11, pp. 85-94, 2021.
- [14] G. Zoppi, G. Pipitone, H. Gruber, G. Weber, A. Reichhold, R. Pirone and S. Bensaid, „Aqueous phase reforming of pilot-scale Fischer-Tropsch water effluent for sustainable hydrogen production,“ *Catalysis Today*, Nr. 367, pp. 239-247, 2021.
- [15] D. Hochstöger, T. Karel, M. Binder, K. Fürsatz, M. Huber, D. Kadlez, H. Hofbauer and M. Kuba, „Experiences from commissioning and first operation of a 1 MW demonstration-scale dual fluidized bed gasification plant,“ in *31st European Conference & Exhibition*, Bologna, Italy, 2023.
- [16] D. Hochstöger, „Performance evaluation of DFB gas generation based on a comparison of two research plants with 100 kW and 1 MW,“ *Master's Thesis - TU Wien*, Vienna, 2023.
- [17] D. Kadlez, F. Benedikt, K. Fürsatz, S. Müller and H. Hofbauer, „Technology

development of advanced dual fluidized bed steam gasification from pilot to demonstration scale," in 31st European Biomass Conference & Exhibition, Bologna, Italy, 2023.

[18] Österreichische Bundesforste AG, „Forschung Jahresbericht,“ Purkersdorf, 2022.

[19] BEST - Bioenergy and Sustainable Technologies GmbH, „KLAR: Sewage sludge inorganic recycling,“ [Online]. Available: https://best-research.eu/en/competence_areas/supplychain/supplychain_projects/view/850. [Accessed 18 08 2023].

The Influence of the Support on Pd-based Catalysts in direct DME Synthesis

B. Wang, M. Zimmermann, S. Behrens

Institute for Catalysis Research and Technology, Karlsruhe Institute of Technology

Abstract

The syngas to dimethyl ether (STD) process on bifunctional catalysts is of great interest for the valorization of CO₂ and syngas from biomass gasification. Dimethyl ether (DME) economics (conventionally based on fuel use) is attracting growing interest, in parallel with the development of various pathways for conversion to hydrocarbons (fuels and chemicals such as olefins, oxygenates, aromatics, and liquefied petroleum gas) and H₂ production. DME is commercially produced from syngas (CO / H₂) in a two-step process *via* dehydration of methanol. This two-step process typically employs Cu/ZnO/Al₂O₃ catalysts for methanol synthesis in combination with a solid acid (for example, γ -Al₂O₃ or zeolites) for its dehydration. Taking advantage of favorable thermodynamics, the single-step STD process leads to higher syngas conversions and entails further economic and technical advantages. This necessitates the design of specific bifunctional catalysts with high methanol synthesis and dehydration activity as well as high stability against deactivation. Recently, Pd-based compounds have emerged as interesting alternatives providing improved reaction rates, methanol selectivity or thermal stability [1, 2, 3]. For example, Pd/ZnO in combination with a solid acid was shown to be a suitable catalyst for hydrogenation of CO or CO₂ to DME [3]. The activity of these catalysts was ascribed to the formation of an intermetallic PdZn phase during reductive catalyst pretreatment [3].

In this study, a series of Pd/Zn nanoparticles with different Pd/Zn ratio were obtained by reductive stabilization [3] and anchored on a hierarchical H-ZSM-5 zeolite for bifunctional PdZn/ZnO-based STD catalysts. We demonstrate the influence of the Pd/Zn ratio and the dehydration catalyst on the catalytic performance in the hydrogenation of CO to DME. Alternatively, Pd/CeO₂ was obtained by colloidal, liquid-phase synthesis providing a catalyst with high reaction rates in the STD process when combined with γ -Al₂O₃. The reaction rates were highly dependent on the preparation procedure and catalysts supported on commercial ceria revealed much lower reaction rates. Nanoparticles and catalysts were characterized by various analytical tools including powder X-ray diffraction, inductively coupled plasma optical emission spectroscopy, electron microscopy (SEM/EDS, STEM-HAADF/EDS), and N₂ physisorption. Catalytic tests were carried out in a continuous, fixed-bed laboratory reactor employing CO-rich syngas (CO/H₂ 1 : 1).

[1] T. Pinheiro Araújo, C. Mondelli, M. Agrachev, T. Zou, P. Willli, K. Engel, R. Grass, W. Stark, O. Safonova, G. Jeschke, S. Mitchell, J Pérez-Ramírez, *Nature Commun.* 13, 5610 (2022) 13; [2] M. Gentzen, D. Doronkin, T. Sheppard, J.-D. Grunwaldt, J. Sauer, S. Behrens, *Applied Catalysis A* 562, 206 (2018); [3] M. Gentzen, D. Doronkin, T. Sheppard, A. Zimina, H. Li, J. Jelic, F. Studt, J.-D. Grunwaldt, J. Sauer, S. Behrens, *Angew. Chem. Int. Ed.* 58, 15655 (2019).

Multiphasic Hydroformylations of long Chain Alkenes and the Liquid-liquid Interface

K. E. Naße,¹ M. Schrimpf,¹ F. S. Heinen,¹ N. Pawlowsky,¹ Andreas J. Vorholt,¹ W. Leitner^{1,2}

¹Max Planck Institute for Chemical Energy Conversion, Mülheim an der Ruhr, Germany

²Institute of Technical and Macromolecular Chemistry, RWTH Aachen University, Aachen, Germany

Abstract

Multiphase catalysis in hydroformylation are well known by the Ruhrchemie/Rhône-Poulenc process. In here the water-soluble catalyst is dissolved in the polar aqueous phase. The product forms a second organic, non-polar phase, which allows an easy separation of both phases. Nevertheless, the substrate in the Ruhrchemie/Rhône-Poulenc process is quite water soluble. In contrast, for long chain alkenes this easy separation technique is accompanied with transport limitations during the reaction and still the exact steps for the reaction are discussed.

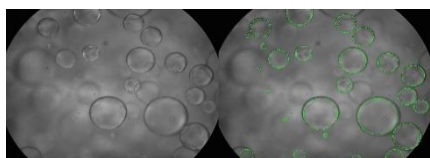


Figure 1: Emulsion of the biphasic reaction mixture recorded and analysed by the SOPAT borescopy technique

With borescope measurements we investigated the steps for multiphase hydroformylation of long chain substrates. This technique allows us to investigate interfaces during the reaction in situ, even with enhanced pressures. It takes pictures of the reaction solution under reaction conditions. Afterwards, an algorithm evaluates these pictures for calculating the liquid-liquid interface size or the Sauter diameter and is able to distinguish between liquid droplets and gaseous bubbles.

We investigated the liquid-liquid interface of the hydroformylation of 1-octene with the water soluble Rh/TPPTS. In artificial samples TPPTS concentration from 0 mol m_{aq}⁻³ to 100 mol m_{aq}⁻³ in the aqueous phase lead to an increase of the liquid-liquid interface of 48%. An addition of 40 mol% nonanal into the organic phase resulted in an increase of the interfacial area of 322%. Of more significance is the relationship between catalytic activity and the interfacial area during the reaction. Opposing the assumption that the catalyst accumulates in the liquid-liquid interface, our results show that this is unlikely. A non-linear relationship between the interface and the catalytic activity was observed. On basis of these results, the effective available interface for the catalyst seems to be reduced by the amphiphilic nonanal.

In actually research projects we investigate the liquid-liquid interfaces by assisted hydroformylation with cyclodextrins and the interfacial area in multiphasic enzymatic systems.

References:

- [1] M. Schrimpf, P. A. Graefe, A. E. Kaczyna, A. J. Vorholt, W. Leitner, *Ind. Eng. Chem. Res.* 2022, 61, 2701–2713.
 [2] M. Schrimpf, P. A. Graefe, A. Holl, A. J. Vorholt, W. Leitner, *ACS Catal.* 2022, 12, 7850–7861.

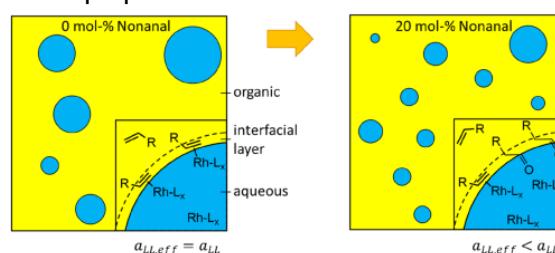


Figure 2: Proposed effect of the accumulation of nonanal with the reduction of the available interfacial area for the catalyst.

Different Exfoliation Procedure of Carbon Nitride-Based Catalysts for CO₂ Photoreduction

I. Rossetti^{1,2}, Simge Naz Degerli², M. Tommasi¹, G. Ramis^{3*},

¹Chemical Plants and Industrial Chemistry Group, Dip. Chimica, Università degli Studi di Milano, Milan, Italy, ²INSTM Unit Milano-Università, Milan, Italy, ³Dip. Ing. Chimica, Civile ed Ambientale, Università degli Studi di Genova and INSTM Unit Genova, Genoa, Italy

Abstract

In this work we focus on the comparison of different approaches for the preparation of g-C₃N₄ photocatalysts for the photoreduction of CO₂. After preparation of the bulk material by thermal condensation, exfoliation has been realised by thermal treatment or by ultrasound sonication at tuneable power. The metal-free polymeric catalyst, graphitic carbon nitride (g-C₃N₄), is a relatively novel material, characterized by a wide absorbance in the visible region and demonstrating a superior performance compared to the commercial titania P25 benchmark, the most used photocatalyst for this application. We used an innovative photoreactor operating at high pressures of up to 20 bar, which is unprecedented in photocatalytic applications where transparent windows are needed. This enabled a boost in the solubility of CO₂ in water when operating the reactor as a tri-phase liquid/gas/solid device and improved the surface adsorption over the catalyst. The materials were characterised to correlate the main textural, structural and optical properties with the activity. The best productivity for HCOOH was observed at 18 bar, with 6 h of irradiation, while the better energy storage capacity after 2 h of irradiation at 8 bar using a sample exfoliated by ultrasound.

Introduction

Artificial photosynthesis is a process that aims to mimic the natural photosynthesis process by harnessing sunlight to convert carbon dioxide (CO₂) into useful fuels such as hydrogen and carbon-based compounds. Although artificial photosynthesis is still in its early stages and large-scale implementation is not yet feasible, ongoing research focuses on developing artificial leaves and photoelectrochemical cells that efficiently convert solar energy into various fuels and chemicals. By replicating the natural processes of photosynthesis, artificial photosynthesis has the potential to reduce anthropogenic CO₂ emissions, enhance fuel security and contribute to a sustainable global economy. Further advancements and research are necessary to optimize efficiency, cost-effectiveness and scalability.

Various materials can efficiently convert CO₂ into valuable chemicals using solar energy. Among these TiO₂ is the most studied but allows only limited efficiency under solar light since it exploits the UV portion of the spectrum, only [1]. Alternative visible responsive materials are made on chalcogenides, but they are poorly stable due to photocorrosion. Alternatively, single or mixed transition metal oxides (e.g. In₂O₃, BiVO₄, WO₃, Cu₂O) or ordered mesoporous materials (OMMs) can be used [2–6].

The efficiency and performance of these semiconductors can be further enhanced through various strategies, including structural modifications, surface modifications, and co-catalyst integration [7,8].

Among the different options, graphitic carbon nitride (g-C₃N₄) is a two-dimensional rather inexpensive nanomaterial that has gained significant attention as a semiconductor photocatalyst. It is an earth-abundant metal-free semiconductor with tuneable optical and electronic properties, making it suitable for harvesting visible light. The unique properties of g-C₃N₄, such as its bandgap energy of 2.7 eV (460 nm), good visible-light harvesting capabilities, and appropriate conduction band and valence band edge positions, make it a promising material for CO₂ photoreduction.

The synthesis of g-C₃N₄ typically involves the polymerization of precursors such as melamine, cyanamide, urea, thiourea, or dicyandiamide using techniques like chemical vapor deposition,

solid-state reaction, or thermal nitridation. However, bulk $g\text{-C}_3\text{N}_4$ tends to exhibit poor optoelectronic properties. To overcome this limitation, nanostructured forms of $g\text{-C}_3\text{N}_4$, such as ultrathin nanosheets, hollows, nanorods, or nano-leaves, have been developed with improved optical and electronic properties.

Nanocomposites and nanostructured $g\text{-C}_3\text{N}_4$ have shown enhanced properties like low electron-hole recombination rate and large surface area, which are beneficial for the target reaction [9].

$g\text{-C}_3\text{N}_4$ can be synthesized through various methods. Here are summarised the most common synthetic approaches [10]:

1. Thermal Polymerization of a precursor. The polymerization process involves heating the precursor at temperatures ranging from 400°C to 700°C in air for a specific duration. This method allows for the controlled formation of graphitic carbon nitride [11];
2. Electrodeposition of $g\text{-C}_3\text{N}_4$ on a substrate from a saturated acetone solution of cyanuric trichloride and melamine at room temperature.
3. Solid-State Reaction. In this method, a mixture of melamine and cyanuric acid, or melamine and urea, is heated to high temperature (often above 550°C) under an inert atmosphere [12].

The exfoliation of $g\text{-C}_3\text{N}_4$ is a relatively novel area of research compared to other 2D materials. One possible approach involves the intercalation of organic molecules, such as alkylamines or solvents like dimethylformamide, into layered carbon nitride structures, followed by sonication or other mechanical agitation methods to promote exfoliation. This method aims to disrupt the weak van der Waals forces between the carbon nitride layers and achieve exfoliation into nanosheets [13–18].

The aim of this work is the comparison of different approaches for the preparation of $g\text{-C}_3\text{N}_4$ photocatalysts for the photoreduction of CO_2 . After preparation of the bulk material, exfoliation has been realised by thermal treatment (TE) and by ultrasound (US) sonication at tuneable power.

The materials were characterised to correlate the main textural, structural and optical properties with the activity. They were tested for the photoreduction of CO_2 through an innovative high pressure photoreactor using a UVA lamp (365 nm, 250 W, irradiance ca. 150 W/m^2), at 80°C and up to 20 bar pressure. These unconventional operating conditions allowed us to improve CO_2 absorption in liquid phase even by using high temperature, which in turn speeds up the kinetics of transport and of some possibly limiting non-photocatalytic steps.

Materials

The $g\text{-C}_3\text{N}_4$ bulk catalyst was prepared in a tubular furnace by thermal condensation of melamine over the continuous flow of air at desired temperature according to [19,20]. In a typical procedure, melamine was placed in a covered ceramic crucible and heated to the target temperature. After cooling down the furnace to ambient temperature, the sample was removed and crushed to powder.

The resulting yellow powder was then exfoliated by successive thermal (TE) or ultrasound (US) treatments in order to obtain the exfoliated material. In particular, for the thermal exfoliation, the yellow $g\text{-C}_3\text{N}_4$ was heated by 3°C min^{-1} in a static air atmosphere at 550°C, maintained for 2 h before cooling down. The US treatment was performed at different input power for a fixed time of 3 h (5 h with 3 sec on and 2 sec off). We have applied US energy in the range of 0.32-1.3 MJ which corresponds (at fixed time) to an input power of 30W-120W, by keeping 3 hours sonication time constant. The data reported in this work refers to sonication power of 120W for the sake of brevity.

Characterization

X-ray diffraction (XRD) analyses were performed with Rigaku Miniflex-600 horizontal-scan powder diffractometer (Tokyo, Japan) using $\text{Cu-K}\alpha$ radiation with a graphite monochromator on the diffracted beam. Crystallite size was calculated according to the Scherrer equation (1).

$$D = (K \cdot \lambda) / (\beta \cdot \cos\theta) \quad (1)$$

where D is the crystal size, λ is the X-ray wavelength (0.154 nm with Cu $K\alpha$ generator), K is the shape factor (0.9), β is the width at half maximum of the peak (*i.e.*, FWHM) and θ is the Bragg angle.

N_2 adsorption and desorption isotherms of samples were measured with a Micromeritics ASAP2020 apparatus (Norcross, GA, USA). The BET SSA (Brunauer-Emmett-Teller Specific Surface Area) and pore volume have been calculated from N_2 adsorption/desorption isotherms, collected at -196 °C for the samples previously outgassed at 150 °C for 4 h. Micropore volume was calculated according to the t-plot method [21]. BET linearization was used in the range 0.05–0.30 P/P° to calculate the specific surface area (SSA). Barrett-Joyner-Halenda model (BJH) was used to determine pore-size distribution from the adsorption branch.

Scanning Electron Microscopy (SEM) images and Energy Dispersive X-ray Analysis (EDX) were obtained using a JSM-7900F Schottky Field Emission Scanning Electron Microscope (JEOL, Tokyo, Japan) operating at an accelerating potential of 20 kV. The 3D analysis of the surface has been elaborated by using the Image J software.

Diffuse Reflectance (DR) UV-Vis spectra of samples were recorded on a Shimadzu UV-3600 Plus (Kyoto, Japan), using an integrating sphere and $BaSO_4$ as reference standard. Measurements were recorded between 190 and 800 nm with 1 nm intervals and spectral bandwidth of 20 nm. The results were processed according to the Kubelka-Munk elaboration and with the equation (2, 3), using the reflectance spectra as input data.

$$(F(R)hv)^{\frac{1}{n}} = B(hv - E_g) \quad (2)$$

Where, h represents the Planck constant, ν the light frequency, n is a coefficient that is considered equal to $\frac{1}{2}$ when referring to the direct transition and equal to 2 when referred to the indirect transition [22,23]. E_g is the band gap expressed in eV and B represents the absorption constant corrected for a proportional factor between $F(R)$ and the molar extinction coefficient.

$$F(R_\infty) = (1 - R_\infty)^2 / 2R_\infty \quad (3)$$

Tauc plot method was applied to evaluate band gap energy (E_g) of the samples. The calculated $(F(R)hv)^{1/r}$ (with $r = 2$ or $\frac{1}{2}$ for direct and indirect band gap) was plotted versus hv to obtain the band gap of each sample [24]. Due to the strong absorption of the materials, the $g-C_3N_4$ was mixed with $BaSO_4$ (50 wt%) with a mortar-pestle prior to recording the spectra in order to prevent saturation in the case of samples absorbing strongly. Therefore, the shape of the curves was not affected by the blending, but the absolute value of reflectance cannot be compared.

Photocatalytic tests

Photocatalytic studies were performed according to our previous report [25–27], All the tests were performed using an innovative pressurized batch photoreactor (Figure 1), whose detailed description has been reported elsewhere [19]. Briefly, it has a cylinder shape and it is surrounded by a cooling/heating jacket where circulates water. The temperature is regulated thanks to a thermostatic system. The reactor is provided with an axial quartz window which allows the introduction of a lamp. The apparatus is designed to work under pressure up to 20 bar and temperatures not higher than 90 °C. The internal volume (with the cap secured) is about 1.3 L and 1.2 L of liquid was used for each experiment. A magnetic stirrer set at 400 rpm and placed under the reactor ensures the catalysts dispersion and mixing.

The photons are supplied by means of a 125 W medium pressure Hg vapour lamp made of two bulbs which emits in the range of 254-364 nm. The average irradiance during the reported tests was 152.63 W/m^2 as measured in the UVA range by a delta OHM HD 2102.2 photoradiometer. The optimal catalyst and hole scavenger (HS) concentration were 31 mg L^{-1} of photocatalyst and 1.67 g L^{-1} of HS. Each test lasted for 24 h if not specified differently. The productivity was expressed as $\text{mmol/h kg}_{\text{cat}}$ dividing the whole amount of product produced by the duration of the test.

Na_2SO_3 was used as inorganic HS and no products of any type were detected without its addition. The suspension containing both HS and the photocatalyst was saturated overnight with CO_2 at the desired pressure and room temperature. Hence, the resulting pressure is taken as the starting value. The reaction starts when the lamp is switched on and the temperature into the reactor reaches 80°C (measured with a thermocouple). In order to determine the composition of the reacting suspension, 3 aliquots of 10 ml each are taken at the beginning and the end of the reaction, centrifuged in order to remove the catalyst and analysed with an HPLC (LC-4000 series, Jasco) The latter was equipped with both UV (UV-4074, Jasco) and refractive index (RI-4030, Jasco) detectors. The column was a 2000-0 BP-OA, Benson Polymeric and the eluent an aqueous H_2SO_4 solution (0.5 mmol L^{-1}). Multiple injections of the same sample gave reproducible results, given that the maximum error on chromatographic analysis was ca. 5% and repetition of the same test under identical conditions led to an experimental error up to 10%. The residual HS amount has been evaluated via iodometric titration. To a precise volume of sample excess acid was added (1 M HCl) and potassium iodide (0.02 M) and the proper amount of potassium iodate solution (0.002 M). Then, the mixture was titrated with sodium thiosulfate (0.002 M) until discoloration.

The gas products were collected in the headspace of the photoreactor and analysed by a gas chromatograph (Agilent 7890, Palo Alto, CA, USA) equipped with a TCD detector and a two columns in series (HPplot Q and HP Molsieves), with the proper set of configurations for the quantification of H_2 , CH_4 and both polar/non-polar light gases.

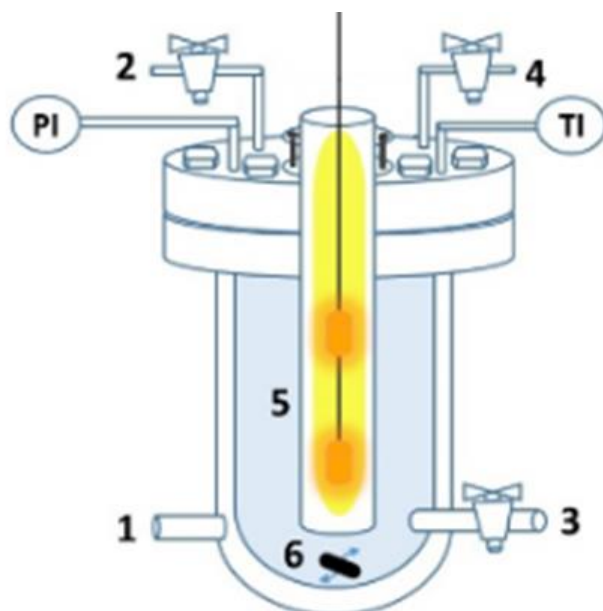


Figure 1. Scheme of high-pressure photo-reactor, reproduced from [19].

Proper blank tests in absence of catalyst, or irradiation and of hole scavenger evidenced negligible products formation.

Results and discussion

The XRD patterns of powder g-C₃N₄ showed the characteristic diffraction peaks of conjugated aromatic system at ~28° and ~13° which correspond to (002) and (100) crystal planes, respectively [28,29]. The observed low intensity peak at 13.1° was attributed to the in-plane structural packing motif. Moreover, is very evident a significant decrement in the intensity of (002) peak after exfoliation, which is remarkable to demonstrate successful exfoliation of layered carbon nitride [29]. Moreover, the two consistent reflections with exfoliated g-C₃N₄ suggest that the nanosheets essentially have the same crystal structure as their parent bulk counterpart, i.e. the layers of g-C₃N₄ phase. Such diffraction peaks were observed with all the samples, irrespective of the calcination temperature, which only affected the intensity of the reflection. They have become less pronounced, but most of all widened, in the nanosheets mainly due to concurrently reduced plane size of the layers following the exfoliation treatment [30].

In order to determine the textural properties and physical-chemical features, N₂ adsorption-desorption technique was applied. All the samples returned a type IV isotherm, which corresponds to mesoporous materials. Brunauer–Emmett–Teller (BET) elaboration for specific surface area resulted in <10 m²/g for the as-synthesized g-C₃N₄ and ca. triple values for the exfoliated samples at the highest US power tested. The BET surface area and BJH pore size have been detailed in Table 1. US input power showed a direct correlation with the surface area of the materials. Increasing the probe ultrasound power led to an increase of specific surface area, indicating more accessible layers structure with reduced thickness with respect to the bulk precursor. Furthermore, separation efficiency of photogenerated electrons and holes can be improved upon exfoliation, limiting recombination phenomena between stacked layers and favouring the interaction of charge carriers with more abundant adsorbed reactants rather than with recombination sites.

The sample G550US had higher surface area and pore size with respect to G600US, which correlates well with the XRD pattern (broader and less intense reflections for the sample calcined at lower temperature, i.e. smaller crystallites). The higher surface and porosity provide more active sites for adsorption of the reactant, as a result, higher performance is expected.

Sample	BET Surface Area (m ² /g)	Total pore volume (cm ³ /g)	BJH Adsorption pore width (nm)	Band gap (eV)
G550	9.0	0.032	47.1	2.65
G600	6.1	0.027	32.2	2.66
G550US	27.7	0.166	29.3	2.78
G600US	19.8	0.083	15.7	2.69
G550TE	113	0.019	26.8	2.80

Table 1. Textural properties and physical-chemical features of different g-C₃N₄.

The morphology of the G550TE material deduced from SEM images showed the appearance of nanosheets with a thickness of few nanometers, partially twisted on themselves.

The FE-SEM images of G550US and G600US depict an overlap of multiple nanosheets which demonstrate exfoliation of the material into thin pseudo-lamellar form. The 3D analysis of the surface has been elaborated by using the Image J software. The sample G550US showed a slit-shaped surface, with 30 nm deep valleys, while the sample G600US evidenced a rougher surface with ca. 30% lower valley depth (ca. 20 nm). We also observed a few layers thin sheet-like morphology [31].

The band gap, as measured by diffuse reflectance UV-Vis, was 2.65-2.80 eV, compatible with visible light harvesting. This parameter was smaller for the bulk as synthesised sample and

increased upon exfoliation, likely due to nanostructuring which is known to induce blue-shift in the absorption edge.

Photocatalytic Activity

Activity tests for the photoreduction of CO₂ have been carried out on the prepared samples to check the effect of the exfoliation procedure on the performance of the catalysts. On the most interesting samples we also checked the effect of reaction time and operating pressure. The results are reported in Table 2.

Sample	Time (h)	P (bar)	H ₂	CO	HCOOH	Energy stored (J)	Eff. on lamp (%)	Eff. on irradiance (%)
G550	24	8	1587	43	5121	1260	0.0058	0.17
G600	24	8	1254	51	5527	1278	0.0059	0.17
G550US	24	8	3518	28	7930	2132	0.0099	0.28
G600US	24	8	1243	62	8203	1784	0.0083	0.24
G550US	24	20	864	16	10005	2047	0.0095	0.27
G550US	2	8	3776		25798	462	0.0257	0.73
G550US	5	8			24664	970	0.0216	0.62
G550US	6	8			24167	1141	0.0211	0.60
G550US	24	8	3518	28	7930	2132	0.0099	0.28
G550US	6	18	2287		39297	1957	0.0362	1.04
G550TE	24	8	1300		7500	1648	0.0076	0.22
G550TE	24	18	4000		6000	1847	0.0086	0.24
G550TE	6	18	500		16000	778	0.0144	0.41

Table 2. Productivity to the main products expressed in mmol/h kg_{cat}, energy stored (calculated on the LHV of the compounds produced), efficiency based on the lamp power consumption (250 W) and efficiency calculated based on the measured irradiance and the mean exposed surface.

The samples prepared of g-C₃N₄ showed promising for the selected application, compared to literature data. The selected main product was HCOOH, whose formation is favoured under basic conditions. Productivity ranges between 5 and 40 mol/h kg_{cat}, which correspond to 0.23-1.85 kg HCOOH per h per kg of catalyst or 5-45 kg per day per kg_{cat}. Since depending on the reaction conditions and duration, different products distribution can be expected, additional quantitative parameters may be used. For instance the energy stored can be calculated from the moles of product overall obtained during the tests multiplied by the Lower Heating Value (LHV) of each of them. This amount of energy chemically stored into the products can be compared with the energy supplied by the lamp (η_{lamp}) or to the energy effectively reaching the sample (η_{irrad}), quantified by multiplying the measured irradiance and the mean exposed surface (equations 4 and 5).

$$\eta_{lamp} [\%] = (E_{prod} [J]) / (E_{lamp} [W] \cdot time [s]) \cdot 100 \quad (4)$$

$$\eta_{irrad} [\%] = (E_{prod} [J]) / (E_{irradiance} [J h^{-1} m^{-2}]) \cdot time [h] \cdot mean irradiated surface [m^2]) \cdot 100 \quad (5)$$

Due to extinction of the radiation and dissipative phenomena, only a portion of the consumed energy is available for the reaction, as measured through a photoradiometer. Overall, the η_{lamp} values range from 0.0058% and 0.036%, which demonstrates that the use on purpose of lamps for this application is not feasible, even in the case of renewable energy supply for their

functioning. When calculating the efficiency on the available radiation, instead, higher values are achieved, reaching 1% efficiency in the best case. This allows to conclude that there is room for improvement of the materials and the process, but the availability of a free direct irradiation source, e.g. solar power, is the only effective route for this application.

The comparison between the samples evidenced negligible difference between the bulk samples prepared by thermal polymerisation at 550 or 600°C, therefore the former lower temperature was selected. The exfoliation procedure positively affected the catalytic performance (Figure 2). In spite of the much higher surface area, the thermally exfoliated sample GC550TE was slightly less active with respect to the samples delaminated with ultrasounds (Figure 3).

The increase of pressure from 8 to 18 bar further improved the performance, boosting the amount of HCOOH or H₂ for the samples G550US and G550TE, respectively (Figure 4 and 5). η_{irrad} increased from 0.24% to 0.27% for sample G550US and from 0.22% to 0.24% for sample G550TE (Table 2). This is explained with the higher solubility of CO₂ at increasing pressure and the higher adsorption over the catalyst surface.

The effect of reaction time was also deepened for the most interesting sample, i.e. GC550US. At the beginning of the reaction much higher productivity of HCOOH was observed, declining after 24 h. This was explained based on the consumption of the hole scavenger: when the scavenger is present in the reaction medium, the reaction product is predominantly HCOOH. When the hole scavenger is consumed, the photoreforming of the produced HCOOH, which produces significant amounts of H₂ becomes competitive with the main reaction. By looking at the activity data it is evident that the productivity of HCOOH is ca. 25 mol/h kg_{cat} during the first hours of reaction, while it drops to ca. 8000 mol/h kg_{cat} after 24 h, when the conversion of the sodium sulphite (used as hole scavenger) is complete (Figures 4 and 5).

Overall the highest HCOOH productivity has been achieved with G550US, leading to 40 mol/h kg_{cat} with an efficiency over the available irradiance of ca. 1%.

These results open the way to a further application of solar light to drive the reaction so to exploit a free and widely available light source.

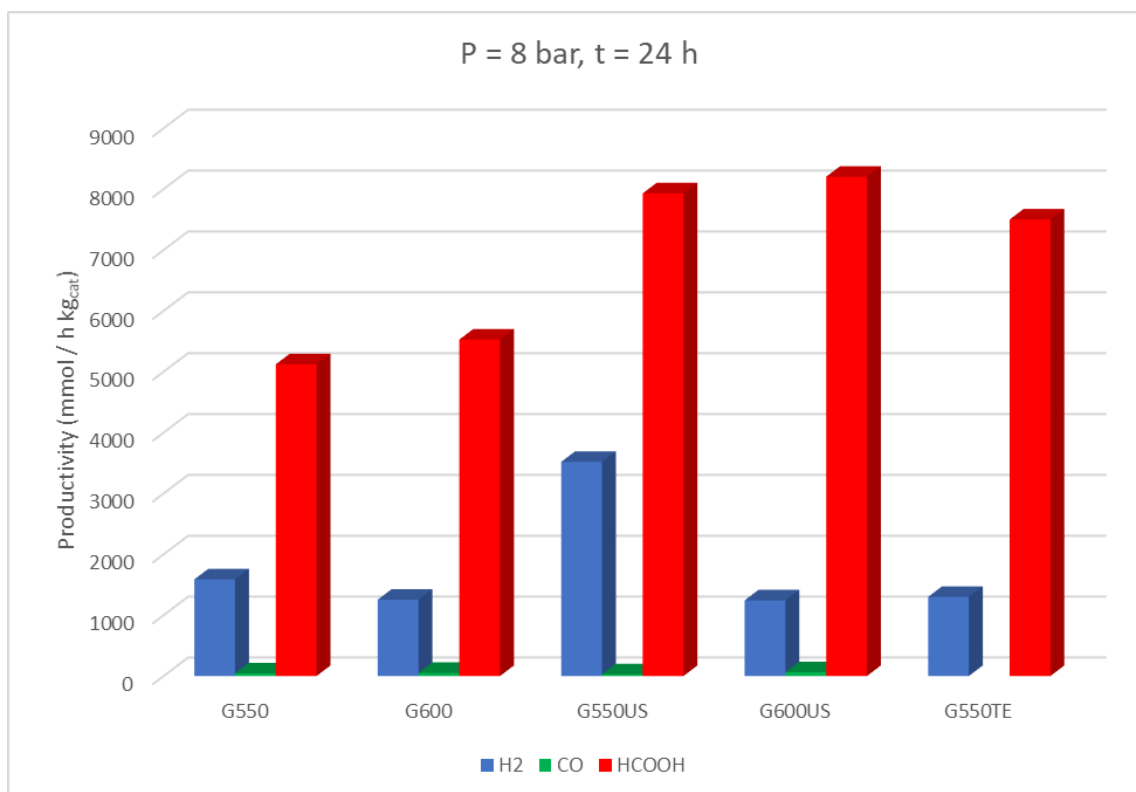


Figure 2. Productivity of H₂, CO and HCOOH for the prepared samples tested at 80°C, 8 bar, for 24 h reaction time.

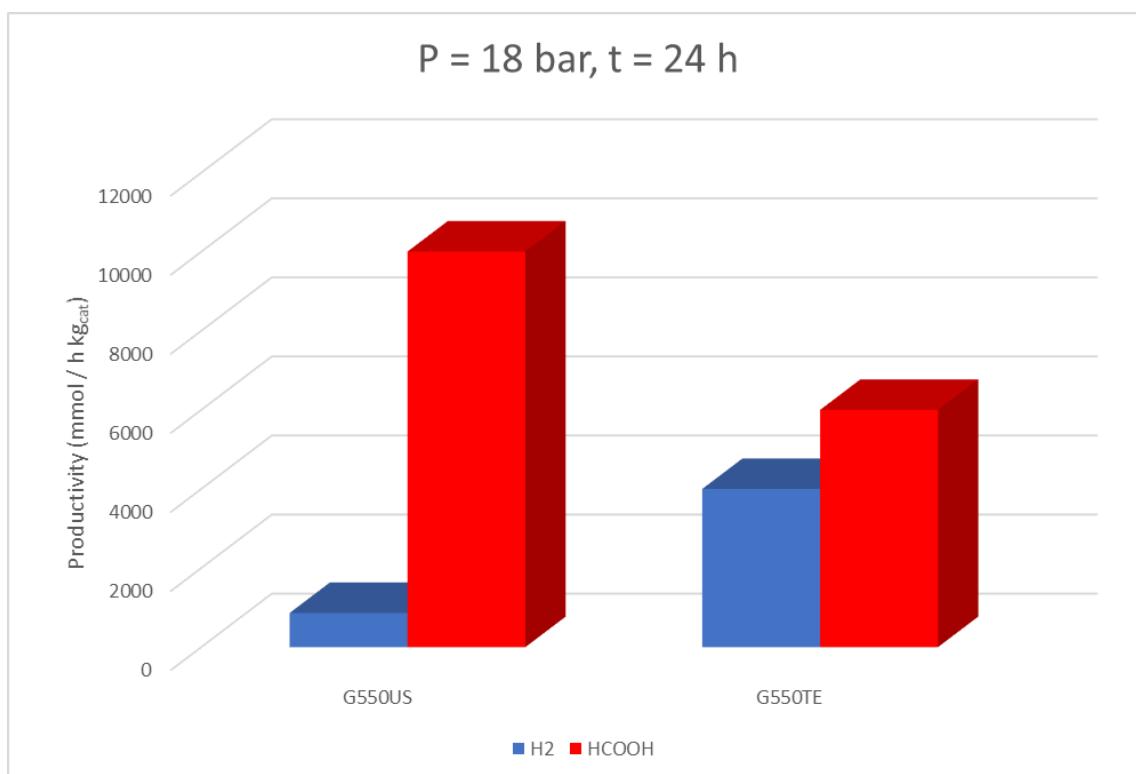


Figure 3. Productivity of H₂, CO and HCOOH for the prepared samples tested at 80°C, 18 bar, for 24 h reaction time.

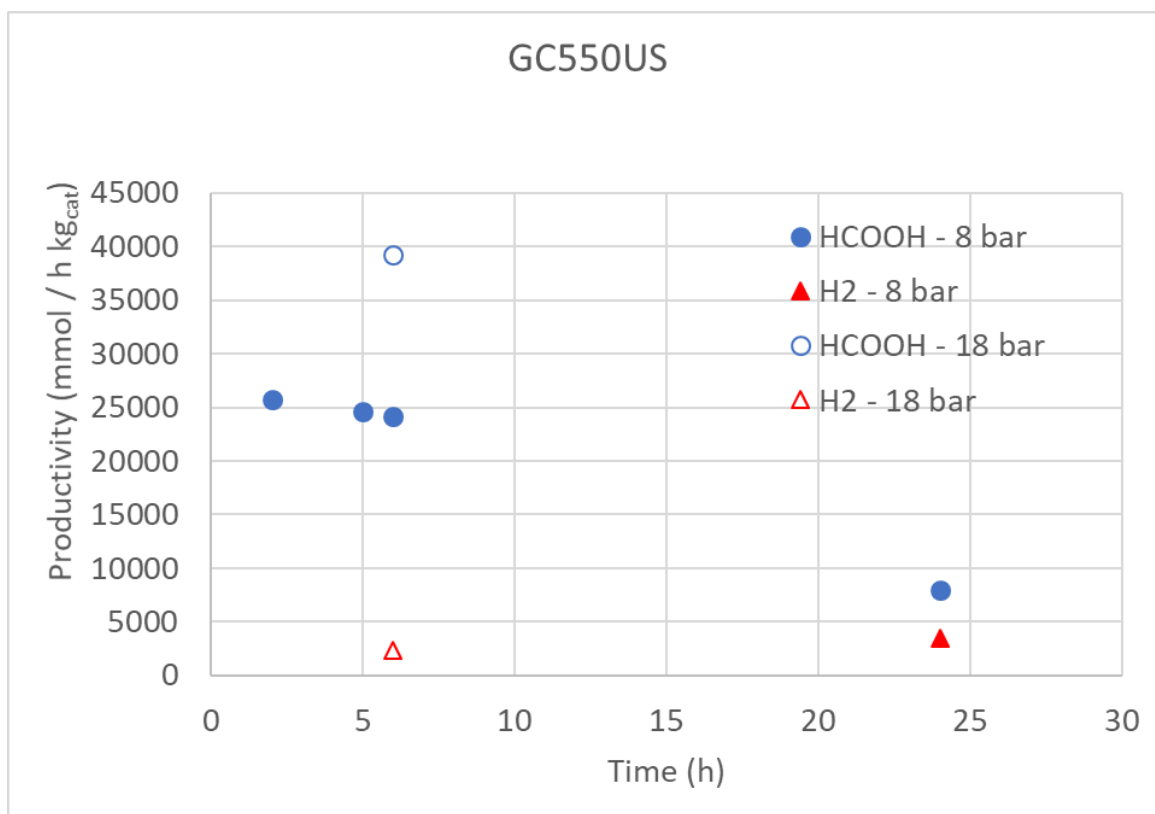


Figure 4. Productivity of H₂ and HCOOH for G550US tested at 80°C, 8 or 18 bar as a function of reaction time.

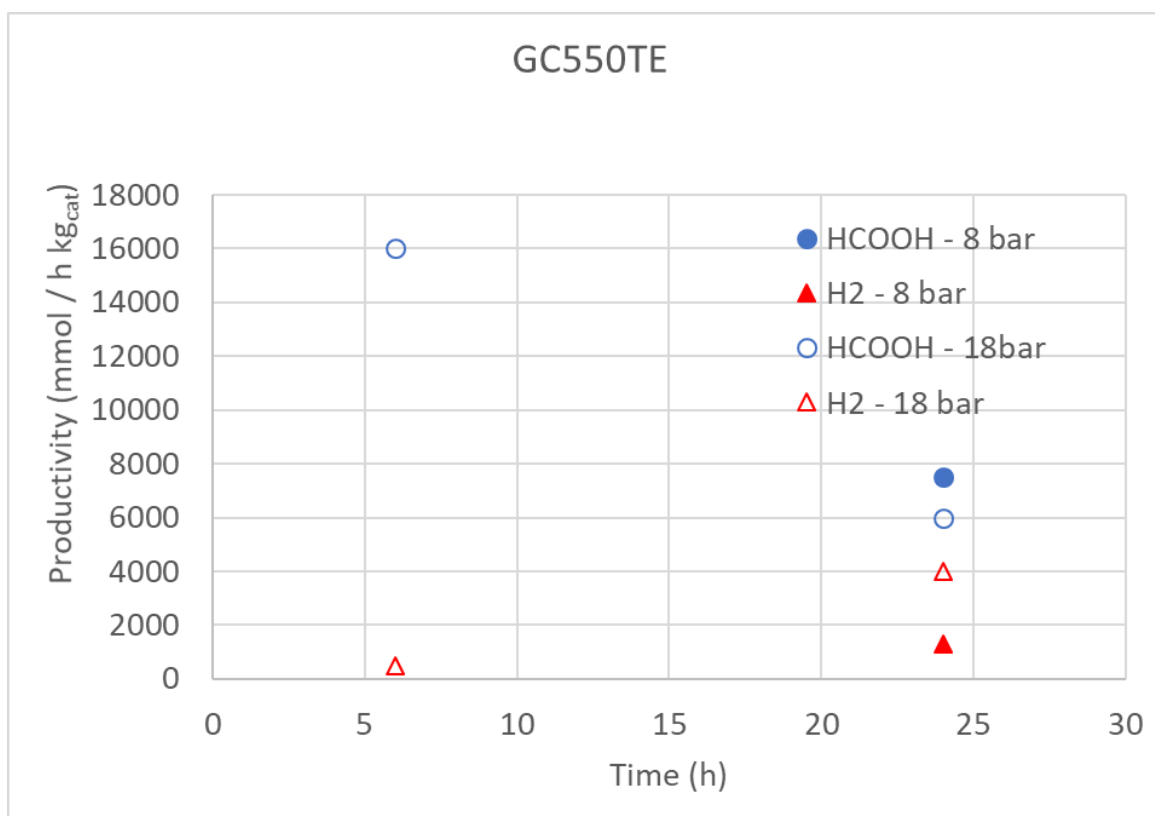


Figure 5. Productivity of H₂ and HCOOH for G550TE tested at 80°C, 8 or 18 bar as a function of reaction time.

Conclusions

In the present work, samples of g-C₃N₄ have been produced as candidate solar harvesting materials for the photoreduction of CO₂. In order to improve the surface area of the materials, bulk synthesised samples from thermal polymerisation of melamine at 550 or 600°C were exfoliated by using thermal treatment or by applying 120W US power.

The physical chemical characterisation confirmed that exfoliation took place with increase of surface area and of the band gap.

Activity testing was carried out using an innovative high temperature and high pressure apparatus fed with UVA lamps, with a 1.2 L volume which is significant with respect to most literature. Exfoliation proved effective to boost the reactivity of the samples and operation at high pressure (18 bar) confirmed useful to achieve practically relevant productivity of the main product, i.e. formic acid. The highest productivity was 40 mol HCOOH/h kg_{cat}, corresponding to an efficiency over the measured irradiance of ca. 1%. Therefore, this application is amenable for improvement, but it makes sense if direct solar irradiance (free) is available for the reaction.

Acknowledgements

The authors gratefully acknowledge the financial contribution of Fondazione Cariplo through the grant 2021-0855 – “SCORE - Solar Energy for Circular CO₂ Photoconversion and Chemicals Regeneration”, funded in the frame of the Circular Economy call 2021.

I. Rossetti acknowledges Università degli Studi di Milano for support through the grant PSR 2021 - GSA - Linea 6 “One Health Action Hub: University Task Force for the resilience of territorial ecosystems”.

This study was carried out within the Agritech National Research Center and received funding from the European Union Next-Generation EU (PIANO NAZIONALE DI RIPRESA E RESILIENZA (PNRR) – MISSIONE 4 COMPONENTE 2, INVESTIMENTO 1.4 – D.D. 1032 17/06/2022, CN00000022). This manuscript reflects only the authors' views and opinions, neither the European Union nor the European Commission can be considered responsible for them. I. Rossetti and M. Tommasi acknowledge specifically the participation and funding of Tasks 8.2.3, 8.3.2 and 8.4.1.

References

- [1] <https://www.iea.org/data-and-statistics/charts/current-limits-on-hydrogen-blending-in-natural-gas-networks-and-gas-demand-per-capita-in-selected-locations>, (n.d.).
- [2] A.-Y. Lo, F. Taghipour, Ordered mesoporous photocatalysts for CO₂ photoreduction, *J. Mater. Chem. A*. 9 (2021) 26430–26453. <https://doi.org/10.1039/D1TA05643C>.
- [3] Y. Zhang, G. Zhang, J. Di, J. Xia, Bismuth-based materials for CO₂ photoreduction, *Curr. Opin. Green Sustain. Chem.* 39 (2023) 100718. <https://doi.org/10.1016/j.cogsc.2022.100718>.
- [4] D. Li, M. Kassymova, X. Cai, S.-Q. Zang, H.-L. Jiang, Photocatalytic CO₂ reduction over metal-organic framework-based materials, *Coord. Chem. Rev.* 412 (2020)

213262. <https://doi.org/10.1016/j.ccr.2020.213262>.
- [5] X. Li, Y. Sun, J. Xu, Y. Shao, J. Wu, X. Xu, Y. Pan, H. Ju, J. Zhu, Y. Xie, Selective visible-light-driven photocatalytic CO₂ reduction to CH₄ mediated by atomically thin CuIn₅S₈ layers, *Nat. Energy*. 4 (2019) 690–699. <https://doi.org/10.1038/s41560-019-0431-1>.
- [6] Q. Mou, Z. Guo, Y. Chai, B. Liu, C. Liu, Visible-light assisted photoreduction of CO₂ using CdS-decorated Bi₂₄O₃₁Br₁₀, *Mater. Sci. Semicond. Process.* 134 (2021) 106011. <https://doi.org/10.1016/j.mssp.2021.106011>.
- [7] E. Bahadori, A. Tripodi, A. Villa, C. Pirola, L. Prati, G. Ramis, N. Dimitratos, D. Wang, I. Rossetti, High pressure CO₂ photoreduction using Au/TiO₂: Unravelling the effect of co-catalysts and of titania polymorphs, *Catal. Sci. Technol.* 9 (2019) 2253–2265. <https://doi.org/10.1039/c9cy00286c>.
- [8] E. Bahadori, A. Tripodi, A. Villa, C. Pirola, L. Prati, G. Ramis, I. Rossetti, High pressure photoreduction of CO₂: Effect of catalyst formulation, hole scavenger addition and operating conditions, *Catalysts*. 8 (2018) 430. <https://doi.org/10.3390/catal8100430>.
- [9] N. Lakshmana Reddy, V.S. Kumbhar, K. Lee, M.V. Shankar, Graphitic carbon nitride–based nanocomposite materials for photocatalytic hydrogen generation, in: *Nanostructured, Funct. Flex. Mater. Energy Convers. Storage Syst.*, Elsevier, 2020: pp. 293–324. <https://doi.org/10.1016/B978-0-12-819552-9.00009-9>.
- [10] P. V. Sarma, Synthesis, structure, and properties of graphitic carbon nitride, in: *Synth. Charact. Appl. Graph. Carbon Nitride*, Elsevier, 2023: pp. 15–41. <https://doi.org/10.1016/B978-0-12-823038-1.00006-4>.
- [11] Z. Zhao, Y. Ma, J. Fan, Y. Xue, H. Chang, Y. Masubuchi, S. Yin, Synthesis of graphitic carbon nitride from different precursors by fractional thermal polymerization method and their visible light induced photocatalytic activities, *J. Alloys Compd.* 735 (2018) 1297–1305. <https://doi.org/10.1016/j.jallcom.2017.11.033>.
- [12] P. Praus, L. Svoboda, M. Ritz, I. Troppová, M. Šihor, K. Kočí, Graphitic carbon nitride: Synthesis, characterization and photocatalytic decomposition of nitrous oxide, *Mater. Chem. Phys.* 193 (2017) 438–446. <https://doi.org/10.1016/j.matchemphys.2017.03.008>.
- [13] X. Gao, J. Feng, D. Su, Y. Ma, G. Wang, H. Ma, J. Zhang, In-situ exfoliation of porous carbon nitride nanosheets for enhanced hydrogen evolution, *Nano Energy*. 59 (2019) 598–609. <https://doi.org/10.1016/j.nanoen.2019.03.016>.
- [14] Z. Wang, X. Yan, Q. Hou, Y. Liu, X. Zeng, Y. Kang, W. Zhao, X. Li, S. Yuan, R. Qiu, M.H. Uddin, R. Wang, Y. Xia, M. Jian, Y. Kang, L. Gao, S. Liang, J.Z. Liu, H. Wang, X. Zhang, Scalable high yield exfoliation for monolayer nanosheets, *Nat. Commun.* 14 (2023) 236. <https://doi.org/10.1038/s41467-022-35569-8>.
- [15] J. Xu, L. Zhang, R. Shi, Y. Zhu, Chemical exfoliation of graphitic carbon nitride for efficient heterogeneous photocatalysis, *J. Mater. Chem. A*. 1 (2013) 14766. <https://doi.org/10.1039/c3ta13188b>.
- [16] J. Zhu, P. Xiao, H. Li, S.A.C. Carabineiro, Graphitic Carbon Nitride: Synthesis, Properties, and Applications in Catalysis, *ACS Appl. Mater. Interfaces*. 6 (2014) 16449–16465. <https://doi.org/10.1021/am502925j>.
- [17] F.K. Kessler, Y. Zheng, D. Schwarz, C. Merschjann, W. Schnick, X. Wang, M.J. Bojdys, Functional carbon nitride materials — design strategies for electrochemical devices, *Nat. Rev. Mater.* 2 (2017) 17030. <https://doi.org/10.1038/natrevmats.2017.30>.
- [18] Y. Li, Z. He, L. Liu, Y. Jiang, W.-J. Ong, Y. Duan, W. Ho, F. Dong, Inside-and-out modification of graphitic carbon nitride (g-C₃N₄) photocatalysts via defect engineering for energy and environmental science, *Nano Energy*. 105 (2023) 108032. <https://doi.org/10.1016/j.nanoen.2022.108032>.
- [19] F. Conte, E.I. García-López, G. Marci, C.L.M. Bianchi, G. Ramis, I. Rossetti, Carbon Nitride-Based Catalysts for High Pressure CO₂ Photoreduction, *Catalysts*. 12 (2022) 1628. <https://doi.org/10.3390/catal12121628>.
- [20] I. Krivtsov, E.I. García-López, G. Marci, L. Palmisano, Z. Amghouz, J.R. García, S. Ordóñez, E. Díaz, Selective photocatalytic oxidation of 5-hydroxymethyl-2-furfural to

- 2,5-furandicarboxyaldehyde in aqueous suspension of g-C₃N₄, *Appl. Catal. B Environ.* 204 (2017) 430–439. <https://doi.org/10.1016/j.apcatb.2016.11.049>.
- [21] H. Marsh, F. Rodríguez-Reinoso, Characterization of Activated Carbon, in: *Act. Carbon*, Elsevier, 2006: pp. 143–242. <https://doi.org/10.1016/B978-008044463-5/50018-2>.
- [22] T. Wang, B. Daiber, J.M. Frost, S.A. Mann, E.C. Garnett, A. Walsh, B. Ehrler, Indirect to direct bandgap transition in methylammonium lead halide perovskite, *Energy Environ. Sci.* 10 (2017) 509–515. <https://doi.org/10.1039/c6ee03474h>.
- [23] M. Bedendi, I. Rossetti, G. Ramis, Design of photocatalytic processes for solar fuels production through CO₂ photoreduction, University of Milan, 2019.
- [24] J. Tauc, R. Grigorovici, A. Vancu, Optical Properties and Electronic Structure of Amorphous Germanium, *Phys. Status Solidi.* 15 (1966) 627–637. <https://doi.org/10.1002/pssb.19660150224>.
- [25] M. Compagnoni, G. Ramis, F.S. Freyria, M. Armandi, B. Bonelli, I. Rossetti, Innovative photoreactors for unconventional photocatalytic processes: the photoreduction of CO₂ and the photo-oxidation of ammonia, *Rend. Lincei.* 28 (2017) S151. <https://doi.org/10.1007/s12210-017-0617-z>.
- [26] F. Conte, A. Villa, L. Prati, C. Pirola, S. Bennici, G. Ramis, I. Rossetti, Effect of Metal Cocatalysts and Operating Conditions on the Product Distribution and the Productivity of the CO₂ Photoreduction, *Ind. Eng. Chem. Res.* 61 (2022) 2963–2972. <https://doi.org/10.1021/acs.iecr.1c02514>.
- [27] F. Galli, M. Compagnoni, D. Vitali, C. Pirola, C.L. Bianchi, A. Villa, L. Prati, I. Rossetti, CO₂ photoreduction at high pressure to both gas and liquid products over titanium dioxide, *Appl. Catal. B Environ.* 200 (2017) 386–391. <https://doi.org/10.1016/j.apcatb.2016.07.038>.
- [28] V.M. Gowri, A. Ajith, S.A. John, Systematic Study on Morphological, Electrochemical Impedance, and Electrocatalytic Activity of Graphitic Carbon Nitride Modified on a Glassy Carbon Substrate from Sequential Exfoliation in Water, *Langmuir.* 37 (2021) 10538–10546. <https://doi.org/10.1021/acs.langmuir.1c01550>.
- [29] S. Yang, Y. Gong, J. Zhang, L. Zhan, L. Ma, Z. Fang, R. Vajtai, X. Wang, P.M. Ajayan, Exfoliated graphitic carbon nitride nanosheets as efficient catalysts for hydrogen evolution under visible light, *Adv. Mater.* 25 (2013) 2452–2456. <https://doi.org/10.1002/adma.201204453>.
- [30] P. Niu, L. Zhang, G. Liu, H.M. Cheng, Graphene-like carbon nitride nanosheets for improved photocatalytic activities, *Adv. Funct. Mater.* 22 (2012) 4763–4770. <https://doi.org/10.1002/adfm.201200922>.
- [31] Y.J. Yuan, Z. Shen, S. Wu, Y. Su, L. Pei, Z. Ji, M. Ding, W. Bai, Y. Chen, Z.T. Yu, Z. Zou, Liquid exfoliation of g-C₃N₄ nanosheets to construct 2D-2D MoS₂/g-C₃N₄ photocatalyst for enhanced photocatalytic H₂ production activity, *Appl. Catal. B Environ.* 246 (2019) 120–128. <https://doi.org/10.1016/j.apcatb.2019.01.043>.

The Change of Product Selectivity in the Electrochemical Methanol Oxidation Reaction with Decreasing Water Content in the Nafion Membrane

S. Lechler, M. Deitermann, Z. Huang, W. Schuhmann, M. Muhler
Ruhr University Bochum

Abstract

The electrochemical methanol oxidation to valuable products like formaldehyde (FA) or dimethoxymethane (DMM) offers several advantages compared with the established thermal production routes such as the opportunity to use renewable energy sources and to produce hydrogen in a separated cathode compartment.

Already in 1992 Fedkiw et al.^[1] presented a gas-phase electrolyzer system that selectively oxidized methanol to products like DMM, FA and methylformate at the anode. The anode consisted of a porous Pt film, which penetrated 0.5 μm deep into in a Nafion 117 membrane.^[1,2] The cathode was filled with 85 wt.% H_3PO_4 to achieve high FA and DMM selectivities. In this cell methanol vapor entered the anode through a gas diffusion layer, and the products and unreacted methanol also left the anode compartment in the gas phase. At the cathode hydrogen evolution reaction occurred: $2 \text{H}^+ + 2 \text{e}^- \rightarrow \text{H}_2$, while the electrochemical reactions at the anode were assumed to be: (1) $\text{CH}_3\text{OH} \rightarrow \text{CH}_2\text{O} + 2 \text{e}^- + 2 \text{H}^+$, (2) $\text{CH}_2\text{O} + \text{H}_2\text{O} \rightarrow \text{HCOOH} + 2 \text{e}^- + 2 \text{H}^+$, (3) $\text{HCOOH} \rightarrow \text{CO}_2 + 2 \text{e}^- + 2 \text{H}^+$ and additionally the following reversible thermal side reactions at the anode were assumed: (4) $\text{CH}_3\text{OH} + \text{HCOOH} \leftrightarrow \text{H}_2\text{O} + \text{HCOOCH}_3$, (5) $2 \text{CH}_3\text{OH} + \text{CH}_2\text{O} \leftrightarrow \text{H}_2\text{O} + \text{CH}_2(\text{OCH}_3)_2$, (6) $\text{CH}_3\text{OH} + \text{CH}_3\text{OH} \leftrightarrow \text{H}_2\text{O} + \text{CH}_3\text{OCH}_3$.

The electrolyzer design was claimed to have the advantage of having FA production with low water content and therefor low energy input for the subsequent separation of water and FA. In our work we adapted the cell design by Fedkiw et al.^[1] and initially planned to increase the production rate of FA. The FA production rate and the applied current were limited for high FA selectivities, as low methanol mole fractions of 1 % in the anode gas stream had to be used.^[1] Upon using the same conditions as Fedkiw et al.^[1] for high FA selectivity, which included 100 °C cell temperature and a potential of 1 V vs RHE, a dilemma was identified regarding FA production with low water content. When keeping the cell temperature for many hours at 100 °C, the amount of gas-phase water leaving the anode decreased from initially around 5 % to 0.25 % after ca. 95 h of heating. This gas-phase water originated from water diffusing through the membrane and evaporating. Therefore, a decrease in the amount of gas-phase water indicated a decrease in the water content in the membrane. With the water vapor content in the anode effluent decreasing from 0.71 to 0.32 %, the product distribution towards FA decreased from 40 % to 25 %, while the product distribution towards DMM increased from 7 % to 41 %. DMM is formed from methanol and formaldehyde with water as coupled product (see anode reaction (5)) in the presence of an acid catalyst in a reversible condensation reaction. Therefore, at the desired low water content in the membrane for FA production the equilibrium is shifted towards the DMM formation rather than FA formation.

These insights can help to improve the conditions for high DMM selectivity and also show that the synthesis of water-free FA is not possible electrochemically in the used electrolyzer with a Nafion membrane.

[1] R. Liu, P. Fedkiw, *J. Electrochem. Soc.*, **1992**, 139, 3514

[2] R. Liu, W.-H. Her, P. Fedkiw, *J. Electrochem. Soc.*, **1992**, 139, 15

[3] R. Sun, I. Delidovich, R. Palkovits, *ACS Catal.* **2019**, 9, 1298

Operando ATR-IR Assisted Mechanistic Study of the Electrocatalytic Methanol Oxidation over a Platinum Catalyst in Acidic Medium

Z. Huang, S. Lechler, S. Cychy, M. Muhler

Lehrstuhl für Technische Chemie, Ruhr-Universität Bochum

Abstract

The advantage of methanol as fuel lies in the high energy density (15.6 MJ/L) and the readily used infrastructure for transportation and storage.^[1,2] Possessing the highest catalytic activity among all the pure metals and outstanding resistance against harsh reaction conditions that are typically used in industry, platinum is still one of the most important catalysts applied in direct methanol fuel cells (DMFCs).^[3-5] However, oxidation of methanol to CO₂ (CH₃OH + H₂O → CO₂ + 6 H⁺ + 6 e⁻) to fully release the energy cannot be achieved, rather intermediates like formate and CO are formed, which could poison the catalyst. The role of these intermediates remains disputable, and the limited understanding of the mechanism impedes the broader application of the catalyst. Therefore, studies regarding the mechanism of the methanol oxidation reaction (MOR) still need to be carried out to uncover the performance-determining factors. The project aims to shed light on the reaction mechanism of the MOR over Pt in acidic media by means of *operando* attenuated total reflection infrared (ATR-IR) spectroscopy, which allows fast product identification similar to differential electrochemical mass spectrometry. Downstream HPLC is also to be applied for the quantitative analysis of the species involved in the effluent of the applied borehole ring electrode (BHE).

The ATR-IR spectrometer cell adopts an Otto configuration, which features approaching the working electrode (WE) perpendicular to the internal reflection unit (IRE) and forming a thin electrolyte layer at the interface. A z-approach micrometer screw allows the fine adjustment of the thin layer thickness. Furthermore, a three-microelectrode-assisted tilt-correction system is integrated in the spectrometer cell so that the WE moves parallelly relative to the IRE thus securing the homogeneity of the electrolyte in the thin layer. Moreover, to overcome the limited mass transport, a BHE connected to a peristaltic pump is adopted, which supplies the fresh electrolyte to the thin layer and simultaneously withdraws the reacted electrolyte from the center of the thin layer for HPLC analysis.

Though successful design of the spectrometer and application for the MOR in alkaline medium, some challenges still remain such as the instable condition in the spectrometer cell in acidic medium impeding the acquisition of reproducible and high-quality spectra.

- [1] F. Schorn, J. L. Breuer, R. C. Samsun, T. Schnorbus, B. Heuser, R. Peters, D. Stolten, *Advances in Applied Energy* **2021**, 3, 100050.
- [2] S. Sarp, S. Gonzalez Hernandez, C. Chen, S. W. Sheehan, *Joule* **2021**, 5, 59.
- [3] A. Kloke, F. von Stetten, R. Zengerle, S. Kerzenmacher, *Adv. Mater.* **2011**, 23, 4976.
- [4] H. Tian, Y. Yu, Q. Wang, J. Li, P. Rao, R. Li, Y. Du, C. Jia, J. Luo, P. Deng et al., *Int. J. Hydrog. Energy* **2021**, 46, 31202.
- [5] P. C. Meenu, S. Roy, C. Chakraborty, S. Roy, *Adv Powder Technol* **2021**, 32, 2663

Improving the Selectivity to Liquefied Petroleum Gas by Combining Fischer-Tropsch Synthesis with Zeolite Cracking

N. Oppmann, A. Jess
Universität Bayreuth

Abstract

The Fischer-Tropsch synthesis (FTS) plays a major role in the large-scale production of hydrocarbons (HCs) from syngas ($\text{CO} + \text{H}_2$) in the so-called gas-to-liquid process. By the use of renewable hydrogen by water electrolysis and CO_2 , such a process can help to reduce anthropogenic greenhouse gas emissions and thus mitigate the effects of climate change. In Wunsiedel, a small city in Upper Franconia (Bavaria), one of the largest water electrolyzers in Europe was put into operation in Sept. 2022. In addition to direct use, the produced hydrogen can be converted to HCs, especially liquefied petroleum gas (LPG) which is needed as fuel in households or small businesses in this rural areas.

The kinetics of the FTS results in a statistical distribution of hydrocarbons, known as Anderson-Schulz-Flory distribution, which limits the use of the reaction, since it is impossible to selectively produce one hydrocarbon or a hydrocarbon cut with a narrow carbon number distribution. For instance, the selectivity towards LPG ($\text{C}_3 + \text{C}_4$ fraction) is therefore limited to a theoretical maximum of $\approx 32 \text{ wt}_\text{C}\%$. To overcome the limitations of FTS and increase the selectivity to LPG, downstream processing of the primary longer-chain FT compounds by means of cracking on an acidic zeolite is an option.

In this project, the optimal process parameters for the production of LPG by a FTS/hydrocracking tandem process were determined. Furthermore, the influence of the gas composition of FTS on the downstream hydrocracking reaction was investigated, i.e. non-reacted carbon monoxide as well as the FT by-product water are present during hydrocracking.

The tested operation configurations and process parameters delivered the best results for a separated two stage operation of FTS and hydrocracking, since both catalysts can operate under optimal conditions. The FT reaction parameters ought to be selected in a way that the lowest possible selectivity to C_1 and C_2 compounds prevails, as these compounds cannot be further converted to LPG at the zeolite. Hydrocracking should be performed at a bifunctional platinum doped H-ZSM-5 zeolite at a maximum of $350 \text{ }^\circ\text{C}$, since a further temperature increase leads to the formation of undesired short chain HCs ($\text{C}_1 + \text{C}_2$).

The product gas of FTS was deliberately simulated by using different mixtures of n-hexadecane (model substance for C_{5+} -HCs typically formed by FTS), H_2 , CO and H_2O in order to study the effect of each compound separately, independent of the upstream FTS. The results showed that it is useful to modify the two stage process of FTS and subsequent hydrocracking by the installation of a product separation downstream of FTS, since CO and water from FT reaction negatively influences the cracking reaction to LPG components.

Development and Enhancement of Iron-Based Catalysts to Boost the Conversion of CO₂ via Fischer-Tropsch-Synthesis

F. Mai, A. Jess

Universität Bayreuth

Abstract

Major challenges for climate change are the sustainable production of liquid fuels from renewable resources. One option is the use of CO₂ from various sources (power plants, chemical industry, and potentially separated from air) and the subsequent conversion with renewable hydrogen to higher hydrocarbons (HCs). For the activation and conversion of CO₂ into higher hydrocarbons (HCs), conventional power-to-liquid (PTL) plants may be used. But current PTL-systems include a two-stage system at which in the first step, CO₂ and H₂ are converted into CO and H₂O by the reverse-water-gas-shift reaction (RWGS). Only subsequently, higher HCs are synthesized via Fischer-Tropsch-synthesis (FTS).

At moderate temperatures (about 220 °C) the conversion of CO₂ is limited to 10 to 20 % by the endothermic RWGS reaction by thermodynamic limitations, depending on the H₂/CO₂-ratio. Since the FTS reaction is strongly exothermic and may substantially convert CO from the RWGS reaction, higher conversions of CO₂ are in principle possible. A suitable catalyst should therefore have reaction rates high enough for RWGS and an even higher rate for the FTS reaction. Furthermore, the catalyst should in general also have a low selectivity to methane.

Many studies have shown that one potential way to directly convert CO₂ with H₂ to higher HCs is by the use of iron-based catalysts. These catalysts contain different active sites (iron oxides + iron carbides) which perform the two catalytic reactions (RWGS+FTS) simultaneously. The FTS reaction takes place on the iron carbides and leads to the formation of a variety of hydrocarbons following the Anderson-Schulz-Flory distribution (ASF).

In this study, iron-based sinter-catalysts were investigated for their activity and selectivity to higher hydrocarbons. The catalysts were tested under Fischer-Tropsch conditions (T = 220 °C, p = 20 bar, H₂/CO₂ = 2). The results showed that iron-sintered catalysts are potentially able to convert CO₂ at moderate reaction conditions to higher hydrocarbons with still a low selectivity to methane. Further studies on the modification of the catalyst composition as well as the variation of the H₂/CO₂-ratios showed that the effectiveness of iron-sintered catalysts can be selectively enhanced by the appropriate choice of promoters and reaction conditions.

Hydrogen Production from Biomass via Formic Acid and Methyl Formate: An Economic Comparison of Different Process Routes

F. Kroll¹, M. Schörner¹, P. Schühle²

¹Chemical Hydrogen Storage, Helmholtz Institute Erlangen-Nürnberg for Renewable Energy (IEK-11), Fürth, Germany

²Lehrstuhl für Chemische Reaktionstechnik, Friedrich-Alexander-Universität Erlangen-Nürnberg, Erlangen, Germany

Abstract

In recent years, hydrogen has gained increasing importance as a key component in the fight against climate change. One strategy to obtain sustainable hydrogen is its production from diverse biomass wastes. In this study, we propose a new approach, that generates hydrogen from waste wet biomass via the intermediate formic acid (FA) or its derivative methyl formate (MF) under milder operating conditions. In the first catalytic step, wet waste biomass streams, such as algae, beech wood or sewage sludge are selectively oxidized in aqueous solution to form formic acid. Recent studies on this so-called OxFA-Process, have revealed that the introduction of methanol as co-solvent effectively suppresses the formation of undesired CO₂, resulting in minimal carbon loss. Nevertheless, the incorporation of methanol triggers the subsequent transformation of FA into MF. The FA/MF ratio is determined by the methanol/water solvent ratio and the equilibrium of the esterification reaction. To extract hydrogen from the intermediates, individual process pathways are required, depending on the MF/FA-ratio. Figure 1 demonstrates the diverse process pathways through which the resulting products, FA and MF, can be further converted into hydrogen. In this study, we conducted simulations in Aspen Plus[®] V12 to explore the impact of three different methanol proportions in the OxFA-Process on the efficiency of the overall hydrogen production route. Our goal was to optimize the process routes to achieve the highest possible hydrogen yield. Subsequently, we performed an economic analysis by considering current data and compared the different routes based on various characteristics. To further investigate the most promising route (OxFA-Process with 10 wt-% methanol), a sensitivity analysis was performed, and the obtained results were compared with alternative sustainable hydrogen production routes, such as biomass gasification. The research findings indicate that the proposed approach can lead to a competitive price for hydrogen production, given the underlying assumptions. Furthermore, this method holds considerable appeal as it can directly apply wet biomass wastes, requires mild operation conditions and generates hydrogen in high selectivity.

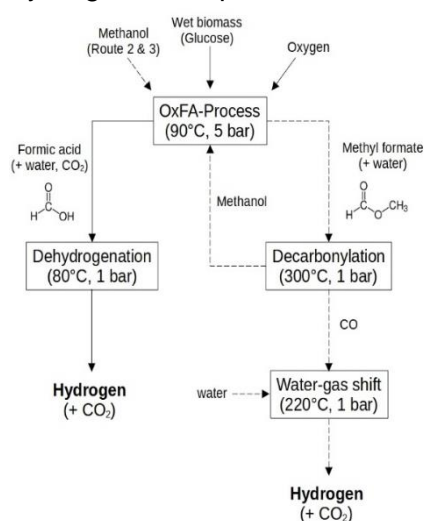


Figure 1: Schematic representation of the production of hydrogen via FA/MF from the OxFA-process.

Efficient Long Distance Hydrogen Transport Including DME as Hydrogen Vector and CO₂ Back-shipping

P. Schühle¹, R. Stöber¹, M. Semmel³, A. Schaadt³, R. Szolak³, S. Thill², M. Alders², C. Hebling³, P. Wasserscheid^{1,2}, O. Salem³

¹Lehrstuhl für Chemische Reaktionstechnik, FAU Erlangen-Nürnberg

²Forschungszentrum Jülich, Institute for a Sustainable Hydrogen Economy

³Fraunhofer-Institute for Solar Energy Systems ISE

Abstract

This contribution introduces the DME/CO₂ hydrogen storage cycle, designed for efficient long-distance transport of renewable hydrogen between specific harbor points. The process involves bonding renewable hydrogen with CO₂ to produce DME and water at a location rich in renewable energy (e.g. Australia). The liquefied DME holds excellent transport properties, making it easily feasible to use existing tanker and port technologies for shipment and handling. Upon arrival at the destination harbor in a rather energy scarce region (e.g. Europe), DME steam reforming is employed to release H₂ and CO₂. These two components are then separated, with H₂ being distributed through a domestic pipeline infrastructure, while the CO₂ is liquefied and transported back to the energy-rich location. This approach significantly reduces the need for costly DAC (Direct Air Capture) technology, as it is only required to make up for CO₂ losses that occur within the transport cycle.

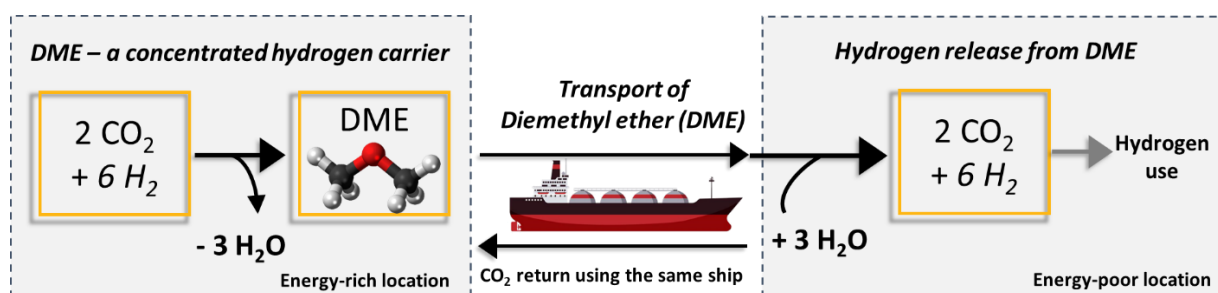


Figure 1: Sketch of the proposed hydrogen transport cycle using DME as vector and including CO₂ back-shipping.

The back-shipping of CO₂ is made possible due to the similarity in physico-chemical properties between DME and CO₂, which significantly enhances the economic competitiveness of this hydrogen logistics technology. Additionally, the DME/CO₂-cycle offers the advantage of efficient water management. The poster will explain that by utilizing DME as a hydrogen carrier, the need for costly and environmentally harmful seawater desalination at the hydrogen generation site can be reduced.

In a direct comparison with ammonia and methanol, which are currently among the most discussed hydrogen carrier molecules, DME exhibits superior technical hydrogen capacity, higher gravimetric energy density, and lower toxicity. The proposed DME/CO₂ cycle also stands out for its high energetic efficiency, as well as its relatively low heat demand and temperature level required for H₂ release, further solidifying the advantages of this new concept.

Photo-selective Methanol Synthesis over Supported Cu Catalysts

J. Huang¹, M. Klahn¹, J. Strunk^{1,2}

¹ Leibniz Institute for Catalysis, Rostock, Germany

² Industrial Chemistry and Heterogeneous Catalysis, Technical University of Munich, Garching, Germany

Abstract

Increasing global CO₂ emissions have resulted in more and more severe greenhouse effects, causing environmental problems and climate changes, especially since CO₂ concentration will continuously grow.^[1] One appealing solution is to upconvert CO₂ into methanol (MeOH).^[2] MeOH is a highly valuable chemical with a worldwide demand of more than 110 million metric tons in 2023.^[3] It can be considered a clean fuel, an excellent liquid energy carrier for fuel cells, and an crucial building block for about 30% of other commodity chemicals, such as dimethyl ether, formaldehyde, methyl formate, acetic acid, methyl tert-butyl ether, or lower olefins.^[4] Cu-based catalysts have been widely used in MeOH synthesis due to the high activity of a Cu surface. Recently, various “photo-enhanced effects” over Cu-based catalysts have proven to be beneficial for CO₂ conversion and product yields, which makes photothermal catalysis an attractive alternative to thermal catalysis.^[5] Here we report a finding that the light wavelength governs the selectivity and reactivity of an unmodified commercial Cu catalyst in MeOH synthesis. It is found that visible light irradiation (400-500 nm) could lead to the promotion of carbon monoxide (CO) production. Conversely, a significant photo-enhancement for production of MeOH was found under the UV light irradiation (365 nm). This work provides hints for understanding of the key elementary processes occurring on the surface of the Cu-based catalyst under light-heat synergistic activation.

Reference

- [1] G. Luderer, Z. Vrontisi, C. Bertram, O. Y. Edelenbosch, R. C. Pietzcker, J. Rogelj, H. S. De Boer, L. Drouet, J. Emmerling, O. Fricko, S. Fujimori, P. Havlík, G. Iyer, K. Keramidias, A. Kitous, M. Pehl, V. Krey, K. Riahi, B. Saveyn, M. Tavoni, D. P. Van Vuuren, E. Kriegler, *Nature Climate Change* **2018**, *8*, 626-633.
- [2] G. A. Olah, *Angew Chem Int Ed Engl* **2005**, *44*, 2636-2639.
- [3] J. Sehested, *Journal of Catalysis* **2019**, *371*, 368-375.
- [4] K. Natte, H. Neumann, M. Beller, R. V. Jagadeesh, *Angew Chem Int Ed Engl* **2017**, *56*, 6384-6394.
- [5] aB. Xie, R. J. Wong, T. H. Tan, M. Higham, E. K. Gibson, D. Decarolis, J. Callison, K. F. Aguey-Zinsou, M. Bowker, C. R. A. Catlow, J. Scott, R. Amal, *Nat Commun* **2020**, *11*, 1615; bB. Xie, P. Kumar, T. H. Tan, A. A. Esmailpour, K.-F. Aguey-Zinsou, J. Scott, R. Amal, *ACS Catalysis* **2021**, *11*, 5818-5828.

Fine-Tuning Texture of Highly Acidic HZSM-5 Zeolite for Efficient Ethanol Dehydration

P. Pornsetmetakul, S. Klinyod, C. Rodaum, S. Salakhum, P. Iadrat, E. J. M. Hensen, C. Wattanakit

School of Energy Science and Engineering, School of Molecular Science and Engineering, Vidyasirimedhi Institute of Science and Technology, 21210 Rayong, Thailand
Laboratory of Inorganic Materials and Catalysis, Department of Chemical Engineering and Chemistry, Eindhoven University of Technology, 5600 MB Eindhoven, The Netherlands

Abstract

Converting carbon-consuming biomass and its derived-compounds into fine chemicals is a promising solution for decarbonization. One of the promising strategy for the conversion of biomass-derived compounds is dehydration of (bio)ethanol to produce ethylene – the largest consumed chemical for plastics manufacturing.^[1] Typically, a high acidic zeolite offers excellent ethylene yield from (bio)ethanol dehydration; however, maintaining stable ethylene production remains challenging due to undesired side-reactions. To overcome this issue, the fine-tuned textural property of the highly acidic HZSM-5 catalyst with a hierarchical structure is crucial to improve diffusion restrictions and prevent undesired side-reactions. Herein, tetrabutylammonium hydroxide as a meso- and micropore directing agent and the controlled molar ratio of NaF-to- Al_2O_3 were employed to fine-tune the texture of high acid catalysts using the hydrothermal synthesis.^[2] The hierarchically designed HZSM-5 with the tiny nanosheet size of 6.5 nm exhibits a high external surface area and mesoporosity, eventually enhancing the catalytic performance of ethanol dehydration up to 95 % ethylene yield as well as inhibiting the formation of heavy hydrocarbons. Insights into the mechanistic points of view by the *in-situ* DRIFTS study revealed that ethylene could be produced through ethoxy-mediated mechanism or decomposition of diethyl ether (DEE). The catalyst deactivation caused by polyaromatics obtained from side-reactions is the main reason for low ethanol conversion and high DEE selectivity. Reducing the crystal size of highly acidic zeolite to ultra-thin nanosheet can shorten the residence time of ethanol, intermediates, and products in porous structures, substantially suppressing the transformation of coke precursors into heavy hydrocarbons to achieve high and stable ethylene yield. These findings open up perspectives for the development of a heterogeneous catalyst for the alternative way of monomer production without CO_2 emission.

References

- [1] IEA, Paris, **2018**.
- [2] P. Pornsetmetakul, S. Klinyod, C. Rodaum, S. Salakhum, P. Iadrat, E. J. M. Hensen, C. Wattanakit, *ChemCatChem* **2023**, *15*, e202201387.

Photocatalytic Conversion of Methanol to Formaldehyde in a Continuous Laboratory Plant

F. Stubenrauch¹; M. Schörner¹; Y. Mahayni¹; A. Bösmann²; P. Schühle²; P. Wasserscheid^{1,2}

¹Forschungszentrum Jülich GmbH, Helmholtz-Institut Erlangen-Nürnberg for renewable Energy (IEK-11)

²Lehrstuhl für chemische Reaktionstechnik, Friedrich-Alexander-Universität Erlangen-Nürnberg

Abstract

In this work we present the highlights of two approaches for the photocatalytic conversion of methanol into formaldehyde under mild conditions using a narrow peak UV-A LED light source in a continuously operated reactor set-up (Figure 1). In the first study, we selectively oxidized methanol to formaldehyde under aerobic conditions using Titanium (IV) oxide (TiO₂) Aeroxide® P25 as photocatalyst. Next to the formation of formaldehyde also methyl formate and CO₂ could be observed as by-products. We evaluated the influence of the catalyst temperature, the residence time, the catalyst load and the irradiation intensity on the reaction selectivity and activity. As a result, the formaldehyde selectivity increased with higher temperature and lower residence time, while the catalyst amount and the irradiation strength did not affect the selectivity significantly. A maximum formaldehyde selectivity of 80% could be achieved. The methanol conversion increased with an increase of all varied parameters. In the second part we added Pt nanoparticles as co-catalyst to the photocatalyst Aeroxide® P25 and conducted methanol dehydrogenation experiments. In this process, methanol is converted into an equimolar amount of formaldehyde and hydrogen. In a consecutive reaction methyl formate is formed as the only by-product in small amounts. As a result, no CO₂ is formed in this process. In this study we varied the irradiation strength, the residence time and the temperature. The formaldehyde selectivity increased with increasing temperature and decreased with increasing residence time. Again, the irradiation strength did not affect the selectivity significantly. At a temperature of 120 °C a carbon-based formaldehyde selectivity of 95% could be achieved showing the high potential of this promising approach for the formation of formaldehyde from methanol.

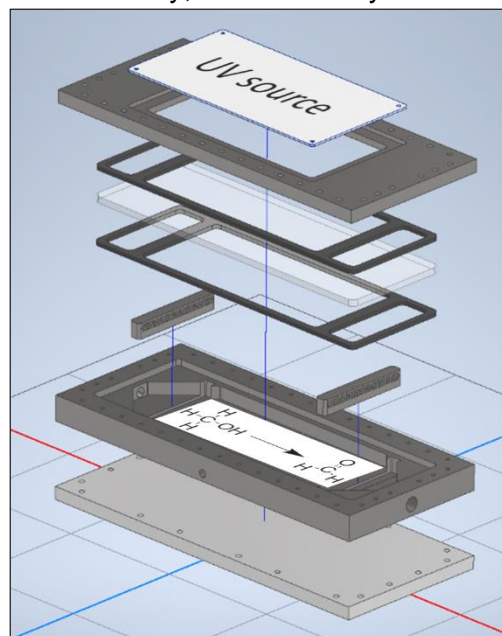


Figure 1: Explosion view of the continuous photoreactor used in this work.

About the Dehydrogenation of Diformamides to Diisocyanates – A Greener Pathway for the Production of Polyurethanes

P. P. Kossmann^{1,2}, A. J. Vorholt¹, W. Leitner^{1,2}

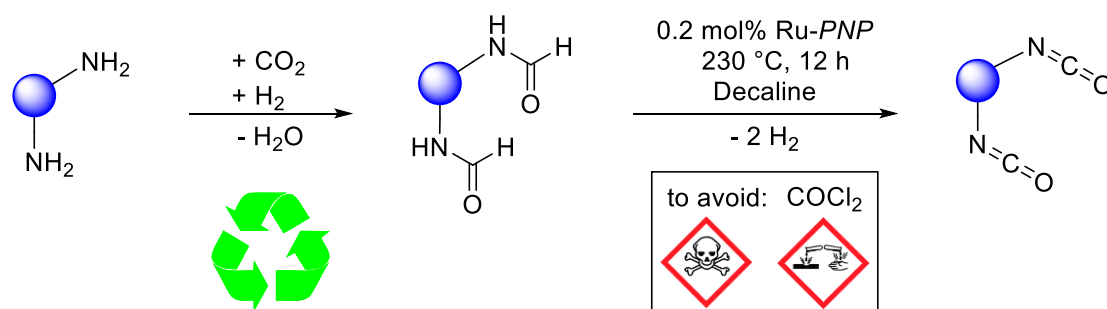
¹Max Planck Institute for Chemical Energy Conversion,
Mülheim an der Ruhr, Germany;

²Institute for Technical and Macromolecular Chemistry, RWTH Aachen University, Aachen,
Germany

Abstract

The synthesis of isocyanates, which are essential building blocks for the production of polyurethanes, has traditionally relied on the use of hazardous and environmentally unfriendly reagents such as phosgene.^[1] However, recent advancements in catalysis and sustainable chemistry have opened up new pathways for the production of isocyanates through more eco-friendly means. In 2021, approximately 1,300,000 tons of polyurethane were produced in Germany alone, underlining the immense demand for these materials.^[2]

To date, there no research has been published on the dehydrogenation of formamides to isocyanates via homogeneous transition metal catalysis. Herein, we address this gap by employing homogeneous ruthenium-pincer catalyst systems to facilitate the direct conversion of formamides into isocyanates.^[3] This ground-breaking approach not only eliminates the use of toxic phosgene but also offers a sustainable alternative to conventional diisocyanate synthesis.^[4] By utilizing fermentation processes, amines can be accessed from biomass sources, providing an eco-friendly source for the production.^[5] Furthermore, an incorporation of an oxidative carbonylation method for the formamide formation using CO₂-derived methyl formate as a feedstock, aligning with the principles of carbon neutrality and a potential circular economy.^[6] This research contributes to a new field in the synthesis of isocyanates by formamide dehydrogenation, offering a cleaner and safer approach. Within this work, we manage to synthesize isocyanates with a yield up to 48% and a selectivity up to 99%.



References

- [1] C. Six, F. Richter, *Isocyanates, Organic*, Wiley-VCH Verlag GmbH & Co. KGaA, Weinheim, Germany, **2003**.
- [2] VCI, *Chemiewirtschaft in Zahlen*, **2022**.
- [3] A. J. Vorholt, T. Faßbach, P. P. Kossmann, W. Leitner, PCT/EP2021/067662, **2021**.
- [4] S. T. Hobson, R. A. Richieri, M. H. Parseghian, *Toxicol. Mech. Methods* **2021**, 31, 293-307.
- [5] A. M. Niziolek, O. Onel, Y. A. Guzman, C. A. Floudas, *Energy Fuels* **2016**, 30, 4970-4998.
- [6] C. Hussong, J. Langanke, W. Leitner, *Green Chem.* **2020**, 22, 8260-8270.